On-line parameter updating as an optimisation tool for Decision Support Systems

Jelmar Schellingerhout

Master of Science Thesis

TU Delft Delft University of Technology

Challenge the future

On-line parameter updating as an optimisation tool for Decision Support Systems

Master of Science Thesis

For the degree of Master of Science in Water Resources Management at Delft University of Technology

Jelmar Schellingerhout

November 6, 2014

Faculty of Civil Engineering and Geosciences (CEG) · Delft University of Technology

The work in this thesis was supported by Witteveen+Bos. Their cooperation is hereby gratefully acknowledged.

Delft University of Technology
Department of
Water Management

The undersigned hereby certify that they have read and recommend to the Faculty of Civil Engineering and Geosciences (CEG) for acceptance a thesis entitled

On-line parameter updating as an optimisation tool for Decision Support Systems

by

Jelmar Schellingerhout

in partial fulfillment of the requirements for the degree of

Master of Science Water Resources Management

Dated: November 6, 2014

Supervisor(s):

prof.dr.ir. N.C. van de Giesen (TU Delft)

dr.ir. P.J.A.T.M. van Overloop (TU Delft)

dr.ir. A.D. Sadowska (TU Delft)

ir. H.J. Mondeel (Witteveen+Bos)

ir. S. Hummel (Deltares)

Abstract

Decision Support Systems (DSSs) that are used nowadays by water managers often predict states that do not correspond with the observed states. This is caused by changing parameters in the real systems, while the parameters used in the current DSSs are kept at a fixed level or follow a temporal pattern that does not always represents reality. Usually, these parameters are calibrated in an off-line setting, but when utilising in an on-line system there is a significant drift in performance. Therefore, there is a high need to some form of on-line parameter estimation that reduces the differences between the modelled and observed states.

The objectives of this study, in order to reduce the differences between the modelled and observed states, read: (1) defining the state-of-the-art knowledge on optimisation of DSSs regarding on-line parameter updating and optimisation techniques for modelling of large-scale river networks; (2) determining whether automatic parameter updating is possible with reasonable results in a twin experiment set-up for different normative scenarios, with respect to parameter identifiability, model bias and model performance; (3) determining whether automatic parameter updating is possible with real measurement data, with respect to the same performance indicators; and (4) determining how much the performance does improve when implementing some form of parameter updating.

The first objective is addressed by former studies (e.g.[2],[4],[7],[9]), which have confirmed On-line Parameter Estimation (OPE) can be applied successfully as a tool to decrease model discrepancies. Both the Doesn't Use Derivatives (DuD) algorithm, [1], and the Shuffled Complex Evolution (SCE) algorithm, [2], have proved to be robust and effective methods for parameter estimation in multiple fields of expertise, e.g. [3],[4],[5],[6],[7]. The DuD algorithm is utilised in this study, since initial model results have illustrated that the high robustness level of the DuD algorithm.

The second objective is addressed by constructively up-scaling the amount of calibration parameters by using several scenarios. The optimisation results are analysed extensively regarding the model performance in terms of robustness, effectiveness, efficiency and model bias. Prior to the OPE, an initial model analysis is performed to determine the model sensitivity to parameter perturbations and identifiability and uniqueness of the optimisation parameters. The analyses of the scenarios' results demonstrate a high level of model performance, in terms

of the performance indicators, in a twin experiment set-up. However, coincidentally the bias follows the temporal pattern in model states, which is probably a numerical error induced by the OPE tool. Nonetheless, the level of bias is sufficiently low to neglect this effect.

Third objective is addressed by following the same procedure as for the second objective. However now, the observational data is assigned with white noise in order to facilitate up-scaling of the twin experiment set-up to field conditions. The analyses of the results illustrate that up-scaling to field condition is very well possible, since the results show high levels of robustness, effectiveness and efficiency while suppressing the model bias.

The fourth objective is addressed by implementing OPE in an existing DSS. Assignment of practical real scenarios, like river maintenance programmes, illustrates the necessity of the OPE tool to accurately estimate the correct parameter values, thereby improving the model performance of the original DSS. The transition zone between two parameter values in time, however, is not predicted, as sharp transitions cannot be predicted well as result of the used calibration window with the assumptions of this study. Moreover, local transitions in parameter values are difficult to predict by the OPE tool.

Concluding, this study demonstrates that it is essential to use some form of OPE to predict the actual parameter values accurately for highly varied scenarios. This statement is grounded by the high level of performance indicators that have been observed in the results of the OPE tool. The computation time is sufficiently low that it is applicable in real-time systems. However, more research on discretisation of the transition phase, on inclusion of control actions and on other types of additive noise is required before implementing the tool in a real system. Furthermore, the added value to the model performance of using more observation locations and more parameters should be investigated.

Contents

List of Figures

List of Tables

Acknowledgements

This thesis is the end product of my MSc thesis project started in January 2014 at Delft University of Technology and Witteveen+Bos. The past nine months were very interesting where I faced a lot of challenges. Luckily, I had a great team of supervisors that helped me a lot in times when I got stuck. I would like to thank these supervisors for their help and support. Firstly, I would like to thank my daily supervisor Peter-Jules for his comments, advice and enthusiastic encouragement. Thanks for all your advice and assistance during the meetings and quick chats. Thanks also for having confidence in me when I started to work at new fields of expertise and had to learn coding in both Java and Python. Secondly, thanks to my company supervisor Herman for introducing me into the subject, as well into the Witteveen+Bos community. Thanks also for your advice and your assistance during these months. Thirdly, many thanks to my coding supervisor Stef, who helped me a lot with introducing me into OpenDA and Java coding. Fourthly, many thanks to my external supervisor Anna for your comments and advice during the meetings. Finally, thanks to professor Nick for providing the opportunity of executing the thesis outside of the Civil Engineering faculty.

Furthermore, many thanks to all people of Witteveen+Bos who helped me feeling home at the office in Rotterdam. Finally, many thank to my girlfriend Nathalie and my family for their unconditional support during my complete study.

Jelmar Schellingerhout October 31, 2014

Chapter 1

Introduction

In this document, the MSc graduation thesis of the author is reported. In this chapter, an introduction is provided based on the initial written research proposal. The structure of this proposal follows the design approach proposed by [8].

1-1 Background

The research topic described below is the result of an interactive discussion held during a meeting with Peter-Jules van Overloop of Delft University of Technology (TU Delft), Herman Mondeel of Witteveen+Bos (W+B) and the author of this document. In this meeting, the performance of prediction and control systems used by water managers was discussed extensively.

Prediction and control systems, also called Decision Support System (DSS), are becoming more and more popular as they give water managers an insight into the most probable near-future states (i.e. water levels and discharges) of their water system. Information on these near-future states is valuable, as this can help water managers to decide which measures have to be taken in order to e.g. prevent flooding or guarantee sufficient water supply. Various computer systems that support the decision making in anticipation to and during a storm event have been built in The Netherlands. These systems utilise a model of the water system to predict the future states. Usually these models are calibrated properly in an off-line setting, but when used in an *on-line system* there is a significant drift in the performance. The reason is that the parameter values used in *on-line systems*, which are (mathematical) systems that simulate and predict processes in real-time, are currently at a fixed value or are only changed according to a fixed schedule (e.g. seasonable varying parameters). Parameter in the real system, however, are constantly changing. Moreover, these changes in the real system are not always the same and can vary from time to time. This results in an offset between the modelled and actual occurring inflows, as the fixed or scheduled parameter values do represent the real parameter values. This leads to structural differences between modelled and actual states that cannot be corrected with a Kalman filter, which is commonly used as a correctional

method. Instead, an adaptive method should be employed that enables accurate parameter estimation in order to improve the performance of on-line systems.

Recently, an optimisation method (used for updating model states and parameters) has been published that strongly resembles the optimisation method Model Predictive Control (MPC), [3]. The reason to select an optimisation method that is often used in MPC is that the model update needs to be executed in real-time, since it is an on-line system. This implies that the model parameters have to be update frequently, e.g. once every week, in order to remain an accurate representation of the current real system. In other words, the optimisation method has to have a high *efficiency*, which means that the computation time required by the optimisation method to obtain an accurate solution needs to be smaller than the required update frequency. In this optimisation method, the actual state of parameters can be determined by comparing actual measurements with the modelled states. This observational data has already been measured and is used to feed the MPC and DSS.

Also, other studies confirmed on-line parameter estimation (OPE) can be applied to decrease the model discrepancies by updating the parameter values, e.g.[4],[9],[10],[11],[12]. Most studies on on-line parameter estimation in environment studies consider gradual changes in parameter values. The innovation of this study, however, is that it considers *sharp*, sudden transitions in parameter values as result of sudden human interference with the river system. Examples of such parameters are the bed friction and crest levels of weirs. In the fall of the year, [13],[14], water managers prune the vegetation in the river system and lower the crest levels of weirs in order to remain a sufficient level of conveyance capacity. This form of maintenance in the river system causes the sharp transitions in parameter values, which eventually leads to differences between the observed and modelled states. Iterative adjustment of the parameters minimises the differences between measured states and modelled states. This method can be combined with Kalman filtering in order to arrive at an improved initial condition of both states and model.

The method is tested on the case of the 'Brabantse Waterschappen' (project BOS 2.0), where presently W+B is building a prediction and control system. The work is supervised by Nick van de Giesen (chairman), Peter-Jules van Overloop (daily supervisor) and Anna Sadowska (external supervisor) of TU Delft, Herman Mondeel (company supervisor) of W+B and Stef Hummel (implementation supervisor) of Deltares.

1-2 Research objective

The main objective in this master's thesis is to improve the performance of DSS by making an assessment of the applicability of data assimilation regarding on-line updating of model parameters, based on effectiveness, efficiency, robustness and practical implications for water resources management.

1-3 Research framework

In Figure 1-1, the research framework used in this graduation project is visualised. (a) A study on scientific literature, regarding information and theory on prediction and control

systems, on data assimilation and on numerical modelling of large-scale river networks and on project BOS 2.0, the DSS developed by W+B yields the assessment applicability criteria, (b) by means of which the inclusion of parameter updating into the conventional MPC-DSS is evaluated. (c) A confrontation of the evaluation results concludes with (d) recommendations for developing DSS with improved performances.

In Phase 1 (a), a study on project BOS 2.0 provides all information concerning the study area (i.e. the water network and key locations), the DSS (i.e. the prediction and control system), measurement data and model requirements. The (scientific) literature study provides knowledge for the implementation of the proposed optimisation method, such as theory on optimising algorithms, performance indicators, etcetera. Moreover, in this phase the assessment methodology is determined.

Phase 2 (b) consists of two subphases: the actual implementation of data assimilation into the DSS (Phase 2A) and the evaluation on the addition of this optimisation method (Phase 2B). In the first subphase, different calibration techniques and algorithms are applied to the DSS. For the second subphase, key locations (bottleneck, measurement, decision and measure locations), different normative scenarios and the obtained operational assessment criteria are used. The numerical DSS model serves as a reference model to investigate the influences of the inclusion of parameter updating. The influences regarding the model performance, which is determined by *performance indicators*, is evaluated by comparison with both artificial and actual occurring physical states, i.e. observational data. The performance indicators are the effectiveness, efficiency, robustness and bias. *Effectiveness* refers to the rate at which the objective function is minimised, i.e. the rate of how accurate the parameters and states are predicted. *Efficiency* refers to the computation time required by the optimisation tool to obtain accurate predictions of the parameter values and modelled states. *Robustness* refers to the number of successful approaches of the global minimum, i.e the number of successful approaches of the actual parameter values. Finally, the *bias* is considered as a measure for the existence of systematic errors, [9],[15]. The bias is determined by the sum of the variation and the estimation of the errors in the predicted states over a certain time window.

In Phase 3A (c), results of the evaluation phase are compared with each other. From this confrontation the possible improvement on DSS is determined. Furthermore, a brief overview of the practical implications, induced by e.g. pruning of vegetation and lowering crest levels of weirs, is provided. Based on the information obtained in Phase 3B (d), recommendations are made for the improvement of DSS.

Elaboration on the framework

For the optimisation problem of minimising the differences between the modelled states and the actual states by estimation of the parameter values, an objective function is used. This objective function, which attempts to minimise the weighted squared errors, is subject to certain physical boundary constraints. First, a local algorithm is applied at the optimisation problem. Depending on outcome of the performance indicators by utilisation of the local algorithm, it is determined whether this algorithm is selected for further research or that a global algorithm is used for further research.

The algorithm is coupled to the hydrodynamic model by use of an generic optimisation toolbox. Prior to solving the optimisation problem, an initial model analyses is executed in order

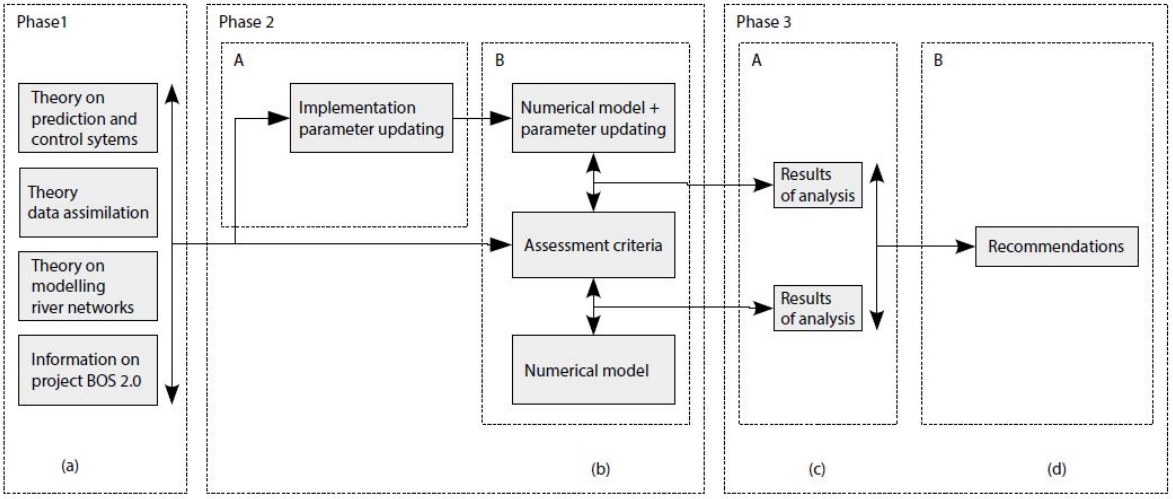

Figure 1-1: The research framework.

to determine the model response as result of various parameter perturbations. From these results, the identifiability and uniqueness of the parameters is determined by use of a singular value decomposition and a correlation matrix. The *identifiability* refers to the ability to estimate parameters in terms of model response, [4],[9]. *Uniqueness* refers to the ability to estimate parameter individually, regardless of the model response, [9]. The outcome of the parameter identifiability and uniqueness determines which parameters or which group of clustered parameters are selected to minimise the objective function. Note that using more parameter gives a more realistic representation of the real system. Nevertheless, introduction of more parameters decreases the efficiency significantly, as the computation time increases exponentially with the number of calibration parameters. Moreover, the optimisation problem becomes less distinct when assigning more parameters to the optimisation method. *Distinctness* refers to the level of how distinctive the shape of the optimisation problem is defined. Usually, an optimisation problem becomes less distinct, when additional parameters are introduced. Eventually, a decrease in distinctness of the optimisation problem can result in longer computation times, which makes the optimisation method less efficient. In on-line system, however, long computation times are far from desirable, since in this time parameter changes can occur which leads to a lower performance. Furthermore, from these results an appropriate calibration window is selected that is large enough to capture the transition of the parameter values, but that is small enough to suppress the computation time.

The observation locations used in this thesis correspond with real measurement locations. The main reason for this is that is useful to get an indication of how the On-line Parameter Estimation (OPE) tool performs in the real river system. This is especially useful, when the OPE tool is applied at the existing DSS. In this thesis, twin experiments are used in order to solely test the influence of the different scenarios on the performance of the OPE tool. In *twin experiments*, the observational data is created artificially in order to remove possible systematic modelling errors. In other words, the outcome of model simulations serves as observational data.

Multiple scenarios are assigned to the selected optimisation method and the selected (clustered) parameters. These scenarios consist of perturbations in individual parameters and in

combination of parameters. The results are evaluated by use of the model indicators that are described in the previous section. These indicators read: the *effectiveness*, the *efficiency*, the *robustness* and the *bias*. Other scenarios determine the influence of the precipitation rate and additive noise on the performance of the OPE tool. For the precipitation rate, a moderate and an extreme rainfall event are selected, as the OPE needs to improve the performance of current DSS is various conditions. For the additive noise, *white noise* is assigned to the observational data. White noise refers to a random signal with a constant power spectral density, [16]. Noise is presented as a random signal that is uniform distributed in a prescribed interval. The colour of the noise, i.e. white, means that the distribution of the power of the noise is equal for each frequency of occurrence, i.e. the power of the noise is the same regardless of the rate of the observed state.

Finally, the practical implications of implementing the OPE tool in an existing DSS are determined by assigning practical real scenarios. The scenarios consist of both global and local transitions in parameter values. The global transitions refer to changes in parameter values for the whole river system. The local transitions refer to changes in parameter values for a single component, such as a single river section or a single hydraulic structure.

1-4 Research questions

In this section, research questions are determined to clarify the research framework and illustrate its contribution to the research objective.

1. What is the state-of-the-art knowledge on optimisation of DSS regarding MPC of large-scale river networks, data assimilation, parameter updating and optimisation techniques?
2. With use of what algorithms and what software can parameter updating be implemented and coupled to existing hydrodynamic models?
3. Is automatic parameter updating possible with reasonable results in a twin experiment set-up, with respect to model sensitivity, parameter identifiability, model bias and model performance? And what is the model response to different normative scenarios?
4. Is automatic parameter updating possible with reasonable results when using real measurement data?
5. How much does the performance improve when implementing some form of parameter updating?

1-5 Outline thesis

In Chapter 2, the first research question is elaborated. Chapter 3 provides a brief, but comprehensive description of the hydrodynamic model and the coupling with the algorithm (research question 2). In Chapter 4, both research question 3 and 4 are answered by applying the optimisation algorithm to an already existing DSS. In Chapter 5, research question 5 is

addressed by investigating the practical implications of introducing the OPE tool in water resources management. Chapter 6 serves to draw conclusions from the results, in order to come up with a list of recommendations that satisfies the research objective.

In the Glossary, an overview of all used nomenclature is provided, i.e. all acronyms, definitions and symbols are listed. Definitions are presented in italics, in order to emphasise the importance of correctly interpreting these definitions.

Chapter 2

On-line calibration

In management of river networks, both models and measurements can provide insight in the hydrodynamic behaviour of those networks. Nonetheless, both contain inherent differences with reality, as not all details of reality can be expressed in a model or data, [9]. This implies there has to be dealt with the simplifications that are included in (hydrodynamic) models, which meet the demands (e.g. fast simulation and high accuracy) of end users (e.g. water board). In turn, this results in modelling errors that can have negative consequences for e.g. operation of control devices, which leads to inadequate water management and possible flooding during heavy storm events.

To minimise these discrepancies, models usually are calibrated. Clemens [9] defines calibration as follows:

> *The process in which a set of model parameters is defined which, combined with a validated process model, reproduces a specific measured situation as good as possible. This implies that in the calibration process the model is adjusted in such a manner that the model result 'fits' as closely as possible to a specific observed reality. It should be noted that the model consists of many different types of parameters.*

In other words, during calibration, the field measurements are used to improve the internal model by tuning certain key parameters. The use of data to improve the model outcomes is a form of data assimilation, [3],[4]. Usually, calibration of these models is executed in an off-line setting, e.g. [17],[18]. In other words, there is no continuous evaluation of the model performance and thereby revising the model parameters. However, when off-line calibration is applied to an on-line system (e.g. several Decision Support System (DSS) used by water boards, see Chapter 3), there is a significant drift in the performance. Initial off-line calibration cannot correct for these discrepancies, since some parameters that contribute to model discrepancies are time-varying. Therefore, on-line calibration is proposed, which continuously processes real-time measurement data and so provides an estimation of the parameters during each iteration, [10],[19]. On-line calibration, also called On-line Parameter

Estimation (OPE), has been applied several times with success in different fields of experience, [10],[11],[12],[20],[21].

A critical requirement for calibration is availability of measurement data. Currently, monitoring networks are used in operational water management to e.g. control the water levels in river systems, [22]. The main goal of this study is to use (only) this data to decrease the model discrepancies by continuous parameter updating. To accomplish this, first a description of the mathematical model is provided, followed by a section of non-linear optimisation. Finally, a section is elaborating on the evaluation of the simulation results.

2-1 Mathematical model

2-1-1 State-space model

The model can be described in a basic mathematical form, which is similar to [23]:

$$\dot{x}(t) = f(x(t), u(t), \theta(t), t) \tag{2-1}$$

$$\hat{y}(t) = g(x(t)) \tag{2-2}$$

where $x(t)$ is an n-dimensional state vector with time-varying variables, $u(t)$ is an n_u-dimensional input vector and $\theta(t)$ is an p-dimensional parameter vector. $\hat{y}(t)$ is the output vector of measured response variables with an n_y-dimension. The functions f and g are non-linear functions that describe the transformation of the corresponding input vectors.

This state space model has been applied successfully in several studies to optimisation of parameter estimation, [23],[24],[25].

2-1-2 Objective function

The aim of the OPE tool is described mathematically by an objective function (or cost function) $S(\theta)$. The main goal of the OPE tool is to reproduce the measured states by estimation of the calibration parameters. This goal consists of several subgoals, of which each subgoal attempts to reproduce the measured states for a specific location.

The objective function tries to minimise the different, sometimes conflicting (sub)goals of the parameter updating tool by quantification of the trade-off between these goals, [26]. In the objective function, the model discrepancies with the actual states, which are penalised and summed up, are minimised by help of an optimisation algorithm. This results in the 'best', 'most optimal' solution of the objective function, which is summed over total number of measurements $i = 1, \ldots, m$:

$$S(\theta) = \sum_{i=1}^{m} \Delta\hat{y}_i(\theta, t)^T W_{ii} \Delta\hat{y}_i(\theta, t) \tag{2-3}$$

where $\Delta\hat{y}_i(\theta, t)$ is described as the difference between measured response variables and modelled output:

$$\Delta\hat{y}_i(\theta, t) = y_i(t) - \hat{y}_i(\theta, t) \tag{2-4}$$

$\Delta\theta$ describes the difference between the actual θ_0 and estimated parameter set $\hat{\theta}$:

$$\Delta\hat{\theta} = \theta_0 - \hat{\theta} \tag{2-5}$$

W_{ii} is a $m \cdot m$-dimensional diagonal matrix that is used to tune the OPE tool. Nevertheless, it is very likely that the ratio between the components of this matrix follows the uncertainty of the measurement data. Therefore, the penalty factor is linked to the maximum squared difference within the prior information, according:

$$W_{ii} = \frac{1}{\Delta\hat{y}_{i,max}{}^2} \tag{2-6}$$

Note that, in general, the relative penalty on discharge data is lower compared to the penalty on water level data, since discharge measurement data is known to have a lower accuracy in general, [27].

2-1-3 Constraints

The objective function Eq. (2-3) is subject to the system dynamics, Eq. (2-1)-Eq. (2-2), and to p physical boundary constraints, which represent the minimum and maximum values of the corresponding parameters:

$$\theta_{min} \leq \theta \leq \theta_{max} \tag{2-7}$$

The constraints applied in this thesis are listed in Section 4-3.

2-2 Non-linear optimisation

2-2-1 Convexity

The main goal of the OPE tool is to solve the optimisation problem Eq. (2-3). In order to find the overall minimum value for this problem, the shape of the objective function has to be evaluated. In other words, the objective function has to be investigated on (non-)convexity [26]. If the function is convex, then every local minimum has to be a global minimum, [28]. An example of a convex function is illustrated in Figure 2-1. Otherwise, the solver of the OPE tool is not ensured to obtain the global minimum when the objective function is non-convex. The latter situation is illustrated in Figure 2-2, [29]. This implies that different starting points (i.e. different initial parameter estimations) by the OPE tool might result in different local minima and thus not the most optimal solution.

The successfulness of the OPE tool to find the global minimum therefore highly depends on the convexity of the objective function. However, since the OPE tool has a non-linear

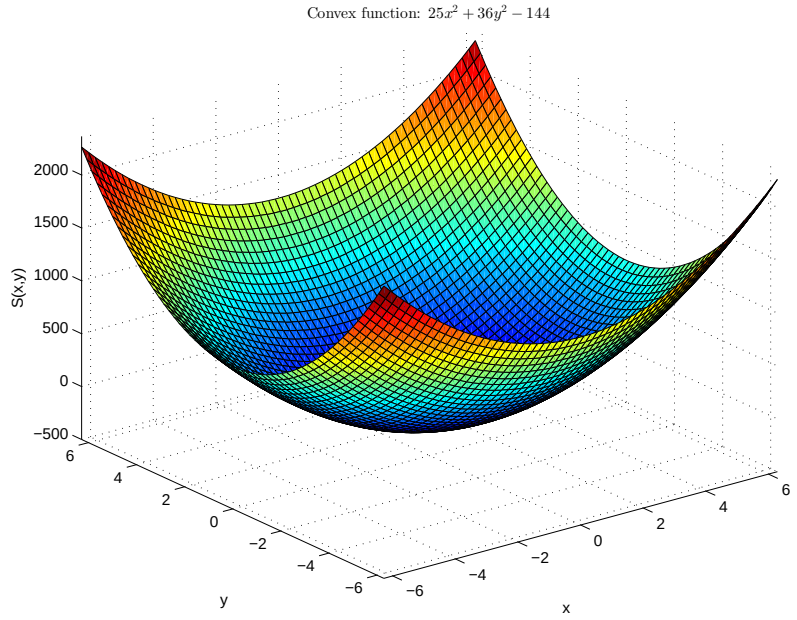

Figure 2-1: An example of a convex objective function S as function of two instances x and y with weights 25 and 36, respectively.

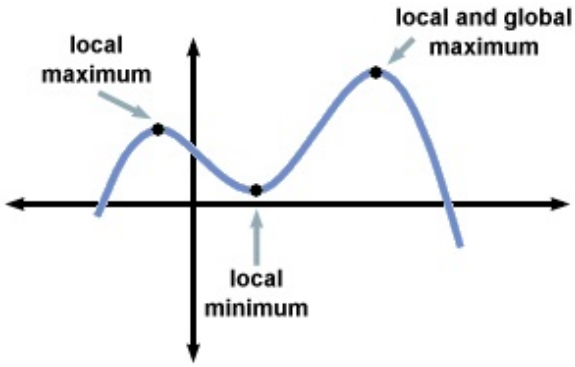

Figure 2-2: An example of a function that contains global and local maxima/minima.

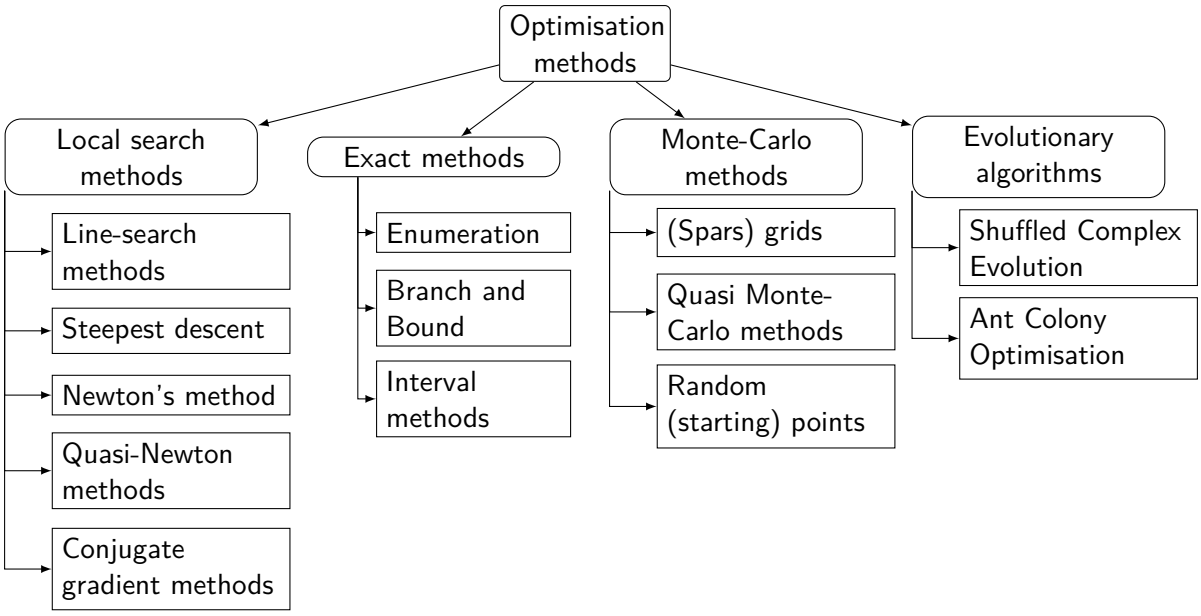

Figure 2-3: Frequently used optimisation techniques, both local and global methods, based on information of [31].

behaviour (see Section 2-1), some degree of non-convexity is introduced according to [30]. Therefore, influence of different optimisation approaches on the final result is investigated.

Some characteristics of local and global optimisation approaches are described in Sections 2-2-2 and 2-2-4. In Figure 2-3, an overview of frequently used optimisation methods are shown, [28],[31]. Furthermore, a detailed description of the optimisation methods that are used is provided.

2-2-2 Local optimisation

Local optimisers are often fast optimisation approaches that are widely applicable on large-scale problems, [28]. This optimisation approach has to deal, however, with the fact that it cannot guarantee the global optimal solution. Moreover, an initial estimate of the optimisation problem is required. This estimate is the starting point of the approach and can influence the solution for the optimisation problem significantly. Another drawback in comparison with global optimisation methods is the sensitivity of local optimisation to parameter values of the used algorithm, [28].

Many local optimisation methods make use of the gradient of the objective function, known as the Jacobian. However, no exact solution of the Jacobian can be provided for the algorithm, since the optimisation problem is non-linear and no analytical expression of the Jacobian can be derived. Therefore, an algorithm that does not use derivatives (abbreviated as DuD) is used as a local optimiser in this thesis.

2-2-3 DuD

The Doesn't Use Derivatives (DuD) algorithm solves the weighted non-linear least square problem of Eq. (2-3) by providing a linear approximation l, [1],[4],[32]. The linearisation agrees with the vector valued response function $\hat{y}(\theta)$ at $p+1$ previous estimates of the parameter vector θ. The new least square problem is solved, resulting in a new estimate for the parameter vector θ. This process is part of the outer iterations. If the cost of the new estimate is not smaller than the costs of the previous estimates, then a line-search, known as inner iterations, is executed till a better estimate is produced. Then, the worst estimate is replaced by the new estimate. These steps are repeated until the moment one of the stopping criteria is satisfied.

With each new iteration the uncertainty (or offset) of the parameters is determined according to one of the two following methods:

$$\text{for } i = 1, \ldots, p: \ \theta_i(j) = \begin{cases} \theta_0(j) & j \neq i \\ \theta_0(j) + \lambda_j & j = i \end{cases} \tag{2-8}$$

or

$$\text{for } i = 1, \ldots, p: \ \theta_i(j) = \begin{cases} \theta_0(j) & j \neq i \\ \theta_0(j) + \lambda_j \theta_0(j) & j = i \end{cases} \tag{2-9}$$

where λ is the transformation of the initial parameter vector. This transformation can represent the offset value itself or an offset factor, depending on the choice of transformation (see Table B-2). In this thesis, the former method of transformation is applied for both parameters.

The following stopping criteria are applied to the DuD algorithm:

- When the maximum number of outer and inner iterations is reached.
- When the maximum absolute difference between the costs of two best parameter estimates approaches T_1: $|Q(\theta_{new}) - Q(\theta_0)| \leq T_1$.
- When the maximum relative difference between the costs of two best parameter estimates approaches T_2: $\dfrac{|Q(\theta_{new}) - Q(\theta_0)|}{Q(\theta_0)} \leq T_2$.
- When the maximum relative difference between the linearised costs $\widetilde{Q}$ of two best parameter estimates approaches T_3: $\dfrac{\left|\widetilde{Q}(\theta_{new}) - \widetilde{Q}(\theta_0)\right|}{\widetilde{Q}(\theta_0)} \leq T_3$.
- When the maximum size of the relative step is reached.

The stopping criteria need to be defined by the user. In Section 4-3, the actual stopping criteria that are used are defined.

2-2-4 Global optimisation

Global optimisers guarantee, in contrast with local optimisation, that the true overall solution of the optimisation problem is obtained, [28]. Nevertheless, a major disadvantage of global optimisation is that it compensates on efficiency, which is of great importance in on-line model optimisation. Boyd and Vandenberghe [28] state that the optimisation complexity rises exponentially with the problem size. Therefore, global optimisers have to be utilised with the greatest care.

To overcome this issue, the convexity of the objective function can be determined. A global solution is guaranteed when the objective function is convex, [28]. This can be done by calculating the Hessian of the objective function. More information on this is provided in [26].

The objective function, however, is non-linear, so an analytical determination of the Hessian is not possible as the model loses convexity, [30]. A possible solution to obtain the derivatives is by evaluation of the objective function. This is, however, very expensive with respect to the computation time needed for performing this evaluation. Furthermore, a new evaluation is required, if the river system changes (e.g. when hydraulic structures are installed or removed). This is not desirable, when applying optimisation methods in an on-line system where computation time is valuable. Therefore, it is essential to apply derivative-free algorithms in such on-line systems.

In Figure 2-3, multiple types of global optimisation methods are listed, including some derivative-free algorithms. Dekens [26] proposed a multi-start method, which uses different initial starting points by following a search pattern. This method, however, is not desired as the dimensions of the optimisation problem grow with the many function evaluations, [26].

Evolutionary algorithms, like genetic algorithms, are known to result in even more function evaluations, [33]. Nevertheless, these algorithms are very functional because of the sometimes discrete nature of water networks, [33]. When combining evolutionary algorithms with local algorithms, the amount of function evaluations can be reduced significantly. An example of a successfully applied evolutionary algorithm is the Shuffled Complex Evolution (SCE), [5],[6],[7],[34],[35].

In this thesis, different scenarios were tested with varying initial parameter predictions and actual parameter values. From these analyses, it was observed that the DuD algorithm was very robust (see Section 2-3-3), i.e. it was able to find the global minimum regardless of the initial parameter prediction and the actual parameter value (see Section 4-5). Therefore, the DuD was applied for all experiments in this thesis as it equals the SCE method with respect to effectiveness and robustness (see Section 2-3-3), but it outperforms the SCE method in terms of efficiency. Nonetheless, more detailed information about the SCE method can be found in Appendix A.

2-3 Results evaluation

After the model parameters are optimised by one of the above algorithms, the model outcomes are evaluated. The parameters and residuals are assessed with three methods: 1) sensitivity

analysis, 2) identifiability and uniqueness analysis, and 3) bias analysis. The first two methods are performed for parameter analysis and the latter refers to residual analysis.

In the next sections, the above discussed analysis methods are described into more detail.

2-3-1 Parameter analysis

2-3-1-1 Sensitivity analysis

The sensitivity analysis looks at the model response initiated by a certain disturbance, in this case a change in model parameters. The main reason for a sensitivity analysis prior to the calibration process is the identification of important parameters for efficient model calibration, [36]. After the one parameter is perturbed, the model response is evaluated in terms of the objective function for both the total model and per location.

2-3-1-2 Identifiability and uniqueness analyisis

For successful parameter updating by the OPE tool, it is important to evaluate the identifiability and uniqueness of the parameters, [4],[9]. In other words, identifiability and uniqueness provides the user with information whether a parameter, or a set of parameters are identifiable. A well-known form of identifiability analysis is based on the singular value decomposition of the Jacobian, [4]. The Jacobian J $(n \cdot p)$ is a sort of sensitivity matrix that gives the model response as result of perturbed parameters:

$$J(\theta) = \begin{bmatrix} \frac{dS_1}{d\theta_1} & \cdots & \frac{dS_1}{d\theta_p} \\ \vdots & \ddots & \vdots \\ \frac{dS_n}{d\theta_1} & \cdots & \frac{dS_n}{d\theta_p} \end{bmatrix} \tag{2-10}$$

In the singular value decomposition, the Jacobian is expressed in three different matrices. The $n \cdot n$-matrix U and the $p \cdot p$-matrix V contain the left and right singular vectors, respectively, [9]. The $n \cdot p$ pseudo-diagonal matrix Σ contain all singular values. The matrices V and Σ hold the most important information for the identifiability analysis. While the matrix V represents the eigenvectors of $J^T J$, it contains all information about which parameter or parameter sets is the most influential. The matrix Σ tells something about how strong the influence is of these eigenvectors on the model response. Σ is determined by the eigenvalues of $J^T J$, [4],[9].

$$J(\theta) = U \Sigma V \tag{2-11}$$

With the Jacobian the correlation between parameters can be determined. First, the covariance matrix needs to be calculated. Then the correlation matrix is obtained according to [4],[9],[37]:

$$cov = (J^T J)^{-1} \tag{2-12}$$

$$cor(i,j) = \frac{cov(i,j)}{\sqrt{cov(i,i)cov(j,j)}} \tag{2-13}$$

2-3-2 Residual analysis

The residuals of the calibrated results are analysed by examining the *bias*. This is an important step in evaluation of the calibration process, as bias is considered as a measure for the existence of systematic errors, [9],[15]. In other words, the results can only be trusted when the bias is insignificant. This means that bias should be negligible in both the time and space domain. So, no pattern as function of time and space may be observed.

The bias is calculated over a moving window T, [9],[15],[21], and is determined by the variation $\sigma^2_{e_w}$ and the estimation of the model discrepancy $\left(\frac{1}{n_w}\sum \Delta\hat{y}^2\right)_{n_w}$:

$$Bias = \frac{1}{T}\int_0^T \left(\left(\frac{1}{n_w}\sum \Delta\hat{y}^2\right)_{n_w} - \sigma^2_{e_w}\right) \mathrm{d}x. \tag{2-14}$$

where n_w is the number of observations in the moving window T. The bias is assumed to be insignificant, when overall bias is smaller than a factor 10^{-1} of the variation of the model discrepancy $\sigma^2_{e_w}$, [9].

2-3-3 Performance indicators

As described in the beginning of this chapter, operational water managers highly rely on the correctness of the internal model in order to have confidence in the calculated control actions. These control actions, like gate settings and pumping operations, are often based on the offset of actual water levels with the set point. Consequently, accurate water level predictions are leading in determining the model performance. In this study, instead of using the deviation of the actual water levels with the set point, the simulated water levels are compared with the observed water levels to determine the model performance. Nevertheless, accurate water level predictions are still of equal importance.

Several performance indicators are used to determine the OPE tool performance. Three performance indicators were used to investigate the model performance, [38]: *effectiveness*, *efficiency* and *robustness*. *Effectiveness* refers to the rate at which the objective function is minimised, i.e. the rate of how accurate the parameters and states are predicted. *Efficiency* refers to the computation time required by the OPE tool to obtain a solution that satisfies the stopping criteria.*Robustness* refers to the number of successful approaches of the global minimum, i.e the number of successful approaches of the actual parameter values.

Chapter 3

Model description

This chapter describes the conceptual structure of the computational sources that are used during this thesis. Section 3-1 elaborates on the hydrodynamic model from the software package SOBEK 3, [39] , while Section 3-2 deals with the structure of the optimisation software OpenDA, [32]. Also, the coupling between these two software packages by a blackbox wrapper is discussed in Section 3-3.

3-1 SOBEK

The SOBEK suite is a powerful software package for simulation of complex flows and water related processes in both time and space. The suite is a useful tool for modelling of integrated water systems for water management, design, planning and policy making. Several modules are available that simulate physical phenomena and processes, and which are connected to and integrated with one-another, [39]. In this section, only the utilised modules of SOBEK are considered. A complete overview of functionality and properties of SOBEK and other details can be found in [39].

3-1-1 Hydraulic model

3-1-1-1 Open channel flow

In this thesis, only the D-FLOW 1D module of SOBEK 3 is used, which simulates water flows in open channels, [39]. The software module calculates one-dimensional flow for shallow water by solving the complete De Saint-Venant (SV) equations. In the case of one-dimensional flow, the following equations are solved, [39]:

Continuity equation (1D):

$$\frac{\partial A_f}{\partial t} + \frac{\partial Q}{\partial x} = q_{lat} \tag{3-1}$$

Momentum equation (1D):

$$\frac{\partial Q}{\partial t} + \frac{\partial}{\partial x}\left(\frac{Q^2}{A_f}\right) + gA_f\frac{\partial h}{\partial x} + \frac{gQ\,|Q|}{C^2 R A_f} - w_f\frac{\tau_{wind}}{\rho_w} + gA_f\frac{\xi Q\,|Q|}{L_x} = 0 \tag{3-2}$$

where Q is the discharge [$m^3\,s^{-1}$], A_f is the cross-sectional flow area [m^2], q_{lat} is the lateral discharge per unit length [$m^2\,s^{-1}$], h is the water level [m], g is the gravitational acceleration [$m\,s^{-2}$], C is the Chézy roughness value [$m^{1/2}\,s^{-1}$], R is the hydraulic radius [m], τ_{wind} is the wind shear stress [$N\,m^{-2}$], w_f is the water surface width [m], ρ_w is the density of water [$kg\,m^{-3}$], ξ is the extra resistance coefficient [$s^2\,m^{-5}$], L_x is the length of the reach segment that holds extra resistance node [m], x is the distance along the channel axis [m] and t is the time [s].

The first term in the momentum equations describes the inertia. The second term is the convection term. The third term is the water level gradient term, which tries to achieve a flat water surface as a result of gravitational acceleration. The fourth term describes the bed-friction term. The fifth term describes the influence of the wind force on the water. The sixth and last term describes the influence of extra resistance, [39].

In the fourth term, the Chézy coefficient C is determined by use of the Strickler's coefficient k_s [$m^{1/3}\,s^{-1}$]:

$$C = k_s R^{1/6} \tag{3-3}$$

3-1-1-2 Hydraulic structures

The D-FLOW 1D module allows the simulation of hydrodynamic behaviour of a water network consisting of rivers and channels. So, it deals with open channel flow, but is also capable of simulating interaction of flow with structures, vegetation and other forms of friction, [39]. The study area (Section 4-2) contains two types of structures: weirs and culverts. Culverts connect two open channels by means of an underground structure. Weirs are overflow structures used for water storage and control of water level and discharge, thereby serving several purposes like irrigation and flood prevention (see Figure 3-1), [22],[40]. Furthermore, these structures can be utilised for monitoring the flow characteristics (e.g. water level and discharge). In this thesis, only changes at the settings of the weirs are applied. Therefore, the culverts are left out of consideration. More information on the flow-culvert interactions are provided in [39].

The flow-structure interactions depend on the flow conditions. The flow-structure interactions are derived from the structure dimensions and user-defined parameters, [39]. Structure dimensions are e.g. the crest width and crest level. User-defined parameters are for instance the entrance loss coefficient and reduction factor. Flow over a weir or through a culvert can be categorised as free flow or submerged flow, depending on the downstream water level, [41]. Typical flow situations over a weir are illustrated in Figure 3-1. In case of submerged flow, the upstream water level is influenced by the downstream water level, according to [39]. On the other hand, the downstream water level does not affect the upstream water level in case of free flow. Submerged and free flow over a weir are defined as, respectively:

$$Q = \begin{cases} c_e c_w W_s \sqrt{2g\,(h_1 - h_2)}\,(h_2 - z_s) & \text{if } h_1 - z_s \leq \frac{3}{2}\,(h_2 - z_s) \\ c_e c_w W_s \frac{2}{3}\sqrt{\frac{2}{3}g}(h_1 - z_s)^{3/2} & \text{if } h_1 - z_s > \frac{3}{2}\,(h_2 - z_s) \end{cases} \tag{3-4}$$

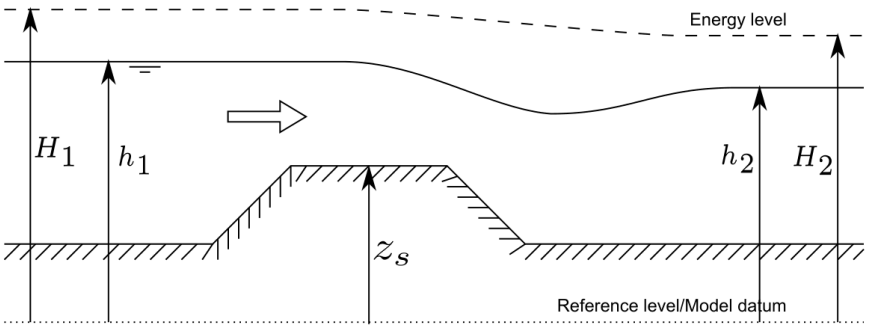

Figure 3-1: Side view of a weir, [39].

where c_e is the discharge coefficient [-], c_w is the lateral contraction coefficient [-], W_s is the crest width [m] and z_s is the crest level [m]. h_1 and h_2 are the upstream and downstream water level [m], respectively.

3-1-1-3 Discretisation

The SV equations are solved numerically, as the equations cannot be solved analytically in real geometry, [42]. The SV equations are discretised on a staggered grid in time (Δt) and space (Δx), [43],[44]. The SV equations are solved numerically by the so-called Delft-scheme. The result is a grid consisting of water level points (h-points) and velocity points (u-points). A graphical representation of the staggered grid is given in Figure 3-2.

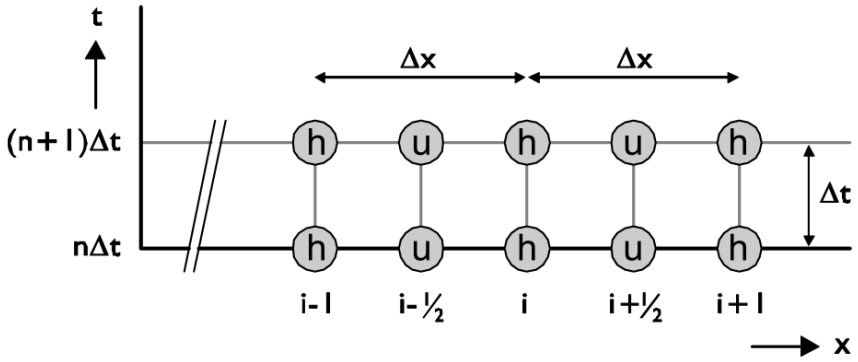

Figure 3-2: Staggered grid used in the hydrodynamic numerical model SOBEK, [39].

3-1-2 Conceptual rainfall-runoff (RR) model

The rainfall-runoff (RR) relations utilised in this thesis are defined before the optimisation is started. In this way, the RR relations do not have to be determined each iteration and computation time is saved. This simplification is valid, because it is assumed that during the optimisation runs only parameters of the D-FLOW 1D module are changed. This means that the RR discharges do not vary within one optimisation cycle and stay equal for each iteration.

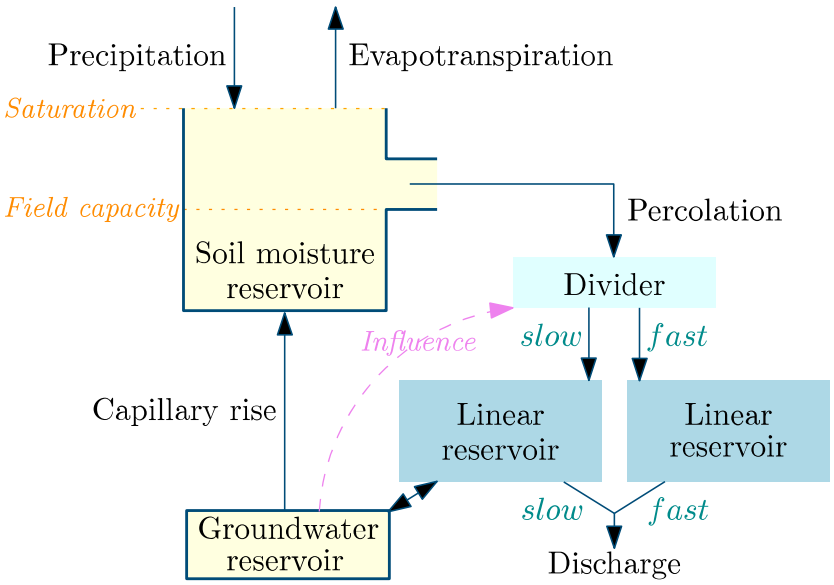

Figure 3-3: A graphical conceptualisation of the Wageningen model introduced by [45] (source: [49]).

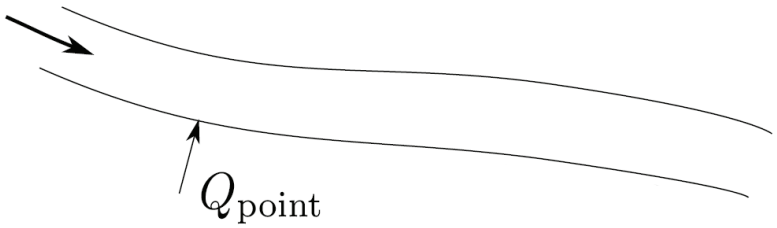

Figure 3-4: Lateral point discharges used in SOBEK in order to route the hydrological flows, [39].

The RR relations are predefined by using the so-called Wageningen model, which is a conceptual hydrological model that takes into account certain lowland-specific processes [45],[46]. These processes represent capillary rise and dynamic division between fast and slow discharge as a function of the wetness of the groundwater reservoir. In this way, the model attempts to describe the non-linear behaviour of the hydrological system, [47],[48]. The Wageningen model is illustrated in Figure 3-3.

The Wageningen model consumes low amounts of computation time and is, therefore, suitable for determining the RR relations prior to the on-line optimisation process. The predefined RR relations are then routed into the channel-river network as lateral discharges. These discharges are defined as point lateral discharges (see Figure 3-4) and tabulated as function of time [$m^3\,s^{-1}$].

3-2 OpenDA

To improve the performance and reliability of hydrodynamic models, like SOBEK 3, observed data could be used. An important step in this, is to reduce the discrepancies between model simulations and measured data. This can be done by means of parameter calibration or data assimilation. In parameter calibration, the model parameters are adjusted in such way that the simulation discrepancies decrease. In data assimilation, model predictions and measurements are combined in order to create a new state estimate, [4],[32],[50],[51].

The necessity for a generic framework that allows data assimilation and parameter estimation of numerical models increases, as more numerical models are developed and more measured data becomes available, [4],[32],[50],[51]. OpenDA is such a generic, open source toolbox for data assimilation and parameter calibration/estimation of numerical models, [4],[32],[51]. In this framework, several methods for parameter estimation and data assimilation are included. The focus of this thesis is on estimation of certain model parameters. Therefore, only the methods for parameter calibration are discussed.

3-2-1 Available optimisation methods

In OpenDA, several methods for parameter estimation are available. An overview of these methods with a brief description is listed in Table 3-1. In this thesis, the Doesn't Use Derivatives (DuD) algorithm was applied in the On-line Parameter Estimation (OPE) tool, for the reason described in Section 2-2. Several studies demonstrated the efficiency and robustness of the DuD algorithm ([3],[4],[52]) compared to other methods. Moreover, no additional information is required to initialise the optimisation when using the DuD algorithm. A more detailed description of this method is provided in Section 2-2.

3-2-2 Blackbox setup

In order to make use of OpenDA, a number of configuration files (XML schema) are required, which contain all essential information for the OpenDA application. A main configuration file refers to the configuration files of three components:

- Stochastic observer.
- Algorithm.
- Stochastic model, the outer layer.

In case of a blackbox setup (described later on in this section), two additional configuration files of the following components are required:

- Model, the middle layer.
- Wrapper, the inner layer.

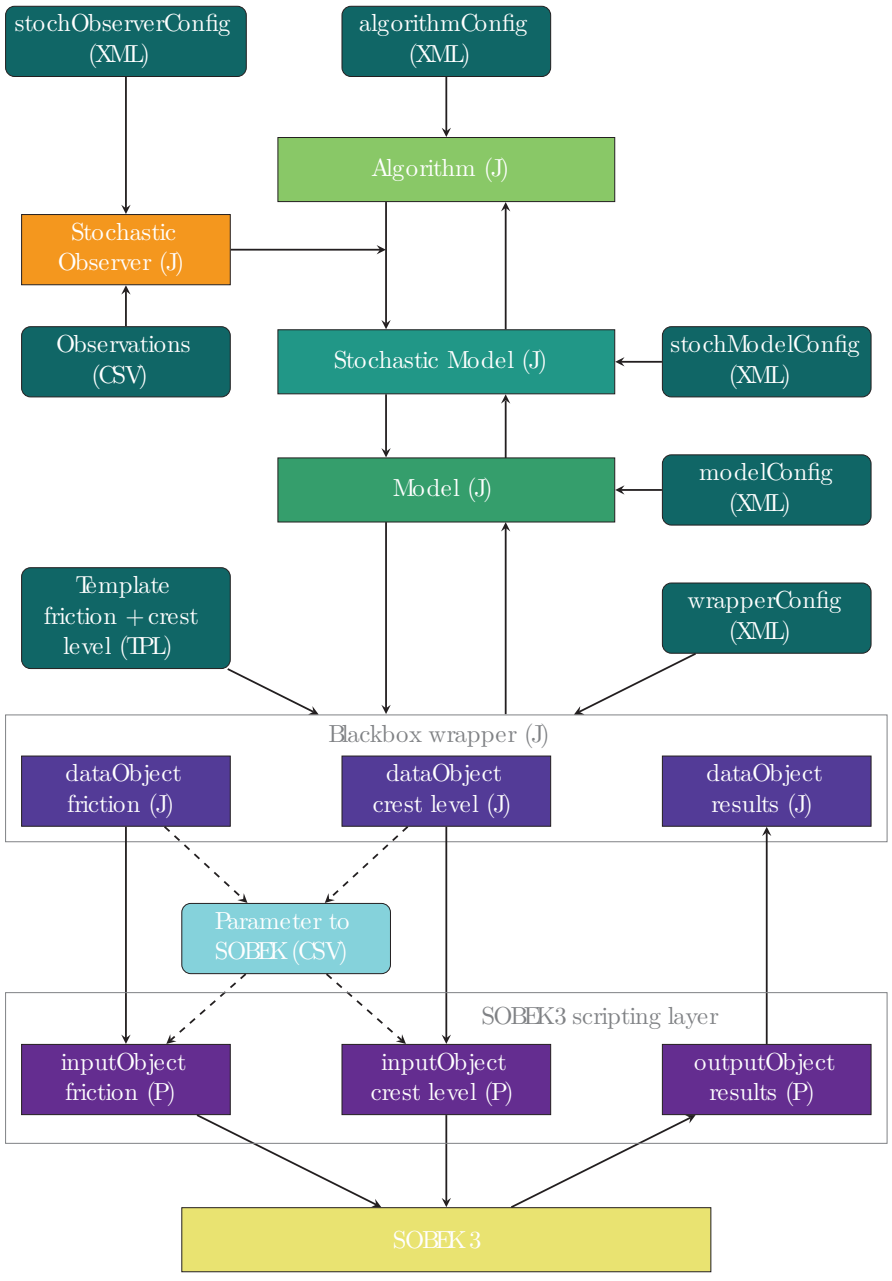

Figure 3-5: Flowchart of the coupling between OpenDA and SOBEK 3, where Java (J) files are used for the actual model description (i.e. all classes, objects, methods, instances, etcetera), XML Schemas describe the model configuration, Python (P) files introduce the actual internal model changes, CSV files are used for data exchange and TPL files provide the OPE tool with templates for the CSV files. The colours used correspond with the colours of Figure 3-6 and Figure 3-7.

The stochastic observer configuration file defines which measurement observations are used and its uncertainties. The algorithm configuration file defines all necessary input parameters (e.g. constraints, stopping criteria) for the calibration algorithm. In the stochastic model, model related information is defined. The stochastic model contains information about vector specifications and holds references to the model and wrapper configurations, when a blackbox setup is applied. The model configuration defines information of the particular model that is used. The wrapper configuration file specifies generic information about the model (e.g. aliases), the executions steps of the model's executable and input-output OpenDA Java classes to communicate with this model, [32]. In Figure 3-5, a graphical overview of all OpenDA components and the communication between them is presented. A list of all used elements in these OpenDA components is provided in Table B-2.

The different OpenDA components communicate by means of interfaces. For the modelling component, two interfaces are required: a model instance interface and a stochastic model instance interface, [4],[32]. The model instance interface specifies the functions for a deterministic model. The stochastic model instance interface specifies the functionalities for the stochastic extension of the deterministic model.

In order to utilise OpenDA in combination with SOBEK, or any other model, the model has to be wrapped, [32]. This is done by extending the model by implementing the two interfaces. In the next section, the coupling is described into more detail.

3-3 Coupling OpenDA and SOBEK

As described in the previous section, SOBEK has to be wrapped to make use of the optimisation techniques of OpenDA. The first method is to implement the model from scratch in Java, [32]. The second way is to combine native model code with a wrapping Java extension. In the third way, the model is written in Java, which implements only parts of these interfaces, while a blackbox setup is used for the other parts. The fourth method is similar to the third method, apart from that it executes its computations with use of the native code. A fully blackbox wrapper is the last possible wrapping method. A general overview of the structure of OpenDA, when the fully blackbox wrapper is applied, is presented in Figure 3-6. In Figure 3-7, the stochastic model utilities layer and the black box model layer are illustrated in more detail. For a complete overview, the reader is referred to [4],[32].

In this thesis, the fully blackbox wrapper setup has been applied. An important reason to choose this setup, is that in this wrapper only several functions, which read and write input and output files of the model, have to be written, [4],[32]. Moreover, the structural design for this wrapper setup already existed, of which the test results were rather satisfying, [3],[4],[52]. A number of small changes had to be implemented in order to implement the functionalities of OpenDA in SOBEK 3. An overview of all changes is listed in Table B-1 (see Appendix B).

There are several reasons to opt for this setup. First, the most convenient approach to apply certain changes into the internal configuration of the hydrodynamic model is by using the built-in Python scripting module of SOBEK 3. A major advantage of this setup is that all desirable modifications can be executed in a straightforward way[1]. The benefits of using different layers of components in the OPE tool are threefold: 1) every action or operation by

[1]For a lot of operations in SOBEK 3, specific functions have been written that make certain modifications

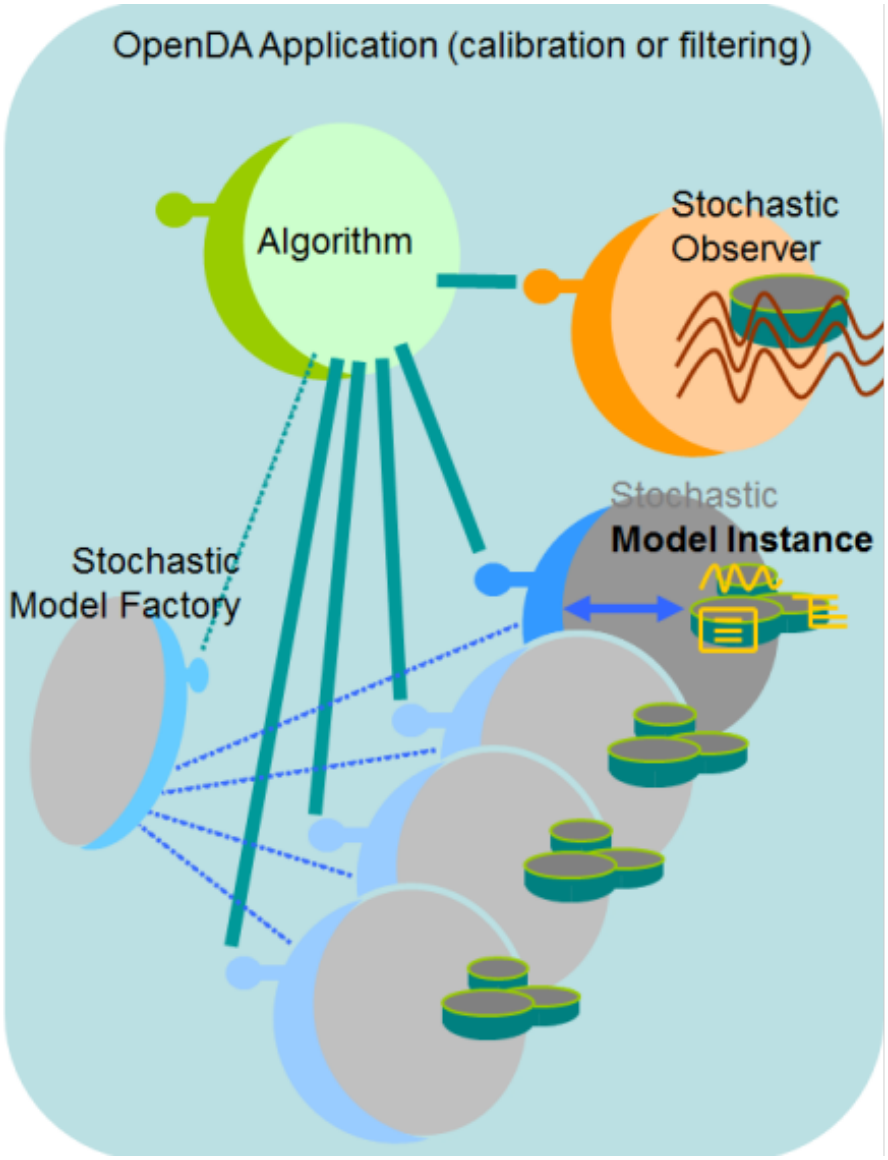

Figure 3-6: The general structure of OpenDA when the fully blackbox wrapper is applied, [32].

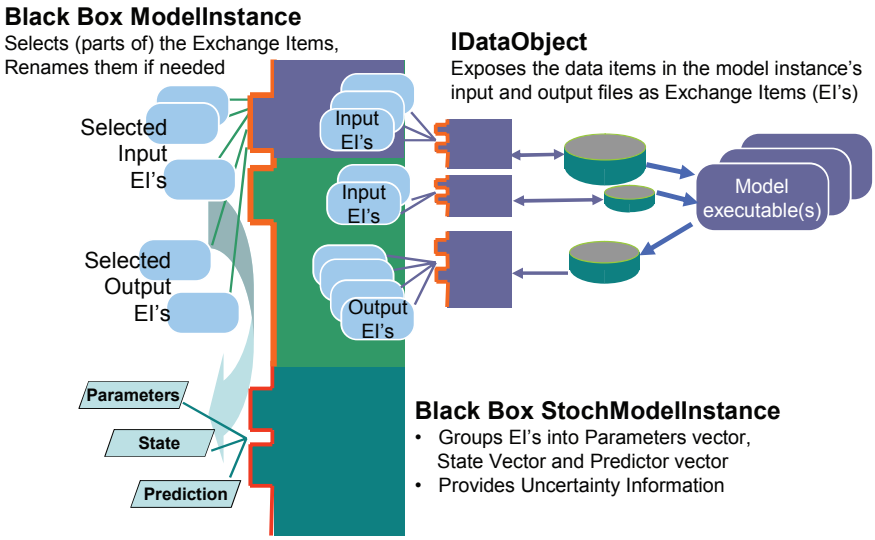

Figure 3-7: The stochastic model utilities layer and the black box model layer of OpenDA when the fully blackbox wrapper is applied, [32].

the algorithm is traceable and therefore reproducible; 2) the chosen model structure enhances the debugging of errors in the OPE tool, as all the components can be tested separately; 3) the OPE tool can be applied to other test cases easily, as only the wrapper components change significantly (Table B-1). The optimisation core of OpenDA can, therefore, be utilised for other test cases, and even completely different models, without large changes.

less complicated. These functions can be used by importing them from the application programming interface (API).

Table 3-1: Optional methods for parameter calibration, [32].

Algorithm	Description	Local/global	Initial information
DuD	DuD transforms the nonlinear least square problem into the well-known linear square problem and solves this linear problem. If this is an improvement, then the linearisation is updated with new point. Else, a line-search is performed until one of the stopping criteria is fulfilled.	L	
Sparse DuD	Sparse DuD is a refinement of DuD. It makes use of independecies between parameters and observations to determine search directions in the optimisation process.	L	Independencies between parameters and observations
Simplex	This method is also called the Nelder-Mead or Downhill Simplex Method. The cost function is minimised with use of vertices, which represent possible sets of parameters and its cost values. During the minimisation the vertices are reflected, expended, contracted and reduced until no more improvement is observed.	L	
Powell	This method transforms the multi-dimensional minimisation problem into multiple one-dimensional minimisation problems. A line-search, also called the Brent's method, is applied to minimise the problem.	L	Initial parameter predictions; search vectors
Conjugate Gradient	This method is based on the second order Taylor approximation of the cost function. It reduces the multi-dimensional problem into a sequence of line minimisations (Brent's method). The search direction is determined by the Fletcher-Reeves method (method 1), the Polak-Ribieri method (method 2) or the Steepest Descent (method 3) until one of the stopping criteria is fulfilled.	L	Initial parameter predictions
BFGS	This algorithm reduces the multi-dimensional problem into a sequence of line minimisations (Brent's method).	L	Initial parameter predictions; if possible initial approximation of inverse of the Hessian
Gridded Full Search	This method applies user defined parameter combinations for evaluation of the cost function. The parameter combination with the smallest cost value is provided as the optimisation output.	L	Range of calibration parameters (min, max, step).
SCE	i) This algorithm randomly draws a set of points based on the defined parameter distributions. ii) The points, which each consist of a set of parameter values, are ordered and grouped into complexes according to their cost. iii) Then, the complexes are split into simplexes and minimised by applying the Simplex method. This procedure is repeated from step i until the global minimum is found.	G	Parameter distribution
GLUE	This method randomly draws parameter sets from the distributions. For each parameter set, it runs the model and determines the likelyhood of each set. The most probable parameters sets are selected by the user based on these likelyhoods.	G	The user needs to analyze the likelyhoods and to select manually the most probable parameter sets.

Chapter 4

Application of the OPE-model

4-1 Introduction

To test the influence of the optimisation method, as proposed in Section 2-1, the algorithm is applied on an existing hydrodynamic model. The model is a product configured by the engineering company Witteveen+Bos (W+B) in the hydrodynamic modelling package SOBEK (see Section 3-1). This river network model has already been used as a Decision Support System (DSS) for operational water management by three water boards. These water boards are located in the southern province Noord-Brabant of the Netherlands (see Figure 4-1). Some adjustments are made to the model so that solely the influence by the On-line Parameter Estimation (OPE) tool can be analysed. However, the overall goal is that the OPE tool can be applied in the DSS. Therefore, after the first analyses, most adjustments are reversed to investigate the robustness of the OPE tool in different environments.

The river network model used throughout this thesis includes many parameters, of which some are constant in time and some are time-varying. The parameters that are calibrated in this thesis solely consist of those that are influenced strongly by an unknown disturbance and, thus, vary in time. These parameters affect the model states and, therefore, can lead to significant deviations with the actual real states. In other words, incorrect parameter estimation is likely to cause a drop in the model performance, as the model itself cannot compensate for these deviations. Therefore, there is a strong need for estimation of these unknown, time-varying parameters. Note that the other parameters, which show a slow varying or more or less constant behaviour in time, are usually compensated by a Kalman Filter. This, however, is not comprehended by the scope of this thesis. Consequently, only parameters that show strong temporal variations are considered. As discussed in the previous sections, these strong variations are often caused by human interaction with the water system. In thesis, the focus is on the parameters that show strong temporal alterations caused by these anthropogenic interactions, i.e. the bed friction roughness parameter and the crest levels of adjustable weirs.

In this chapter, first an overview of the study case is provided. Then, the optimisation problem and the methodology of the experiments is specified. In the last section the results of these experiments are presented.

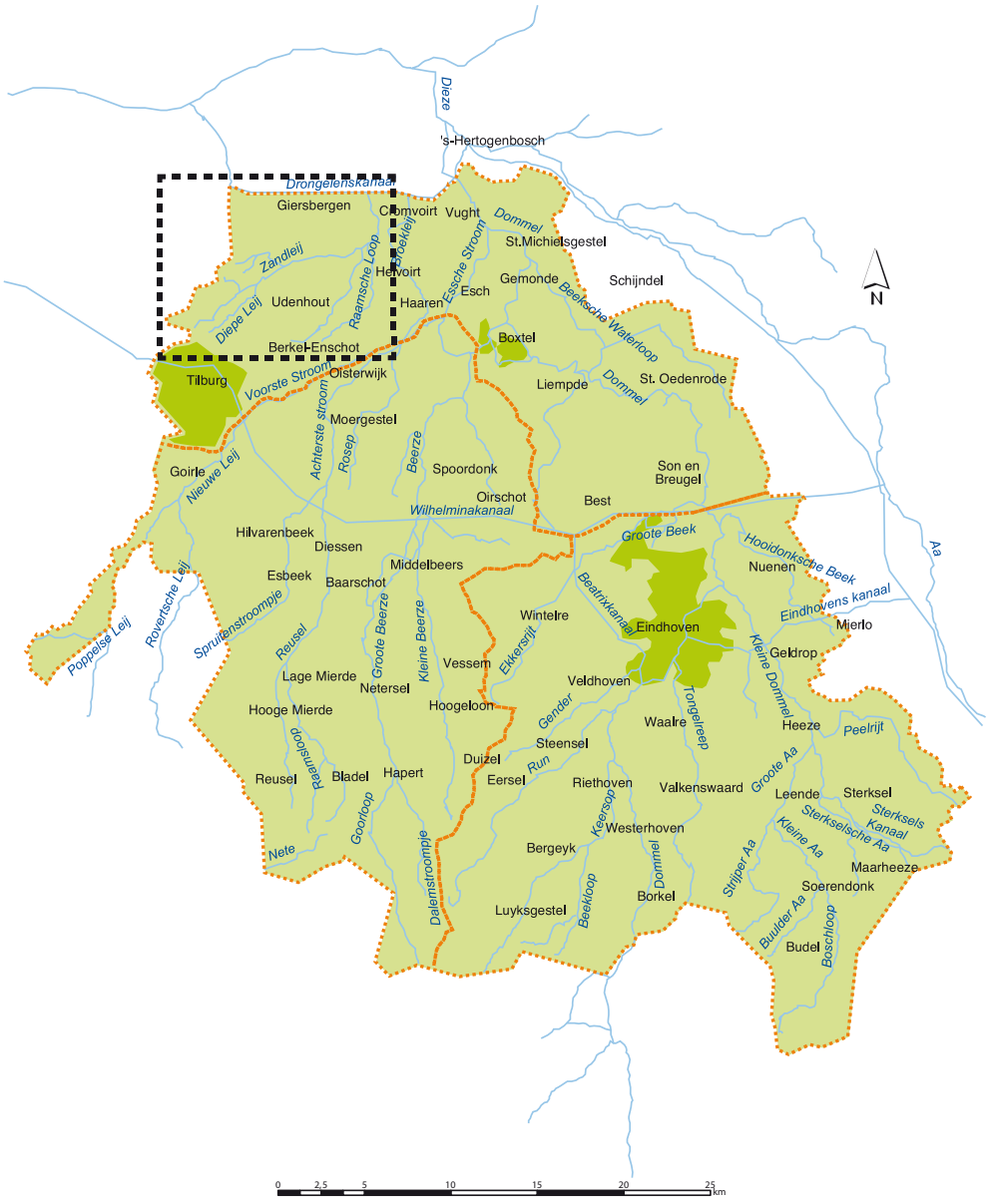

Figure 4-1: A map of the province Noord-Brabant (the Netherlands), wherein the study area is located (indicated with the dashed black border).

4-2 Case description

4-2-1 Calibration parameters

In Table 4-1, an overview of all used parameters in the hydrodynamic model is presented. Some of these parameters show time-varying behaviour. The parameters affected by anthropogenic interaction with the water network are recognised as the most highly time-varying parameters. In other words, these parameters could have a significant influence on the model performance of DSS, once the parameters are changed by human activities. Therefore, there is a high need to estimate these parameters correctly. These parameters (marked with asterisks) are the bed roughness and the crest level of adjustable weirs in the river network.

Table 4-1: An overview of the model parameters in SOBEK, where the most highly time-varying parameters are indicated with asterisks.

Module	Nodes	Parameters				
Flow	Connection Node with Storage and Lateral Flow	Type	Type of well storage	Bottom Level [m AD]	Storage Area [m^2]	Type of street storage
		Street Storage [m^2]	Street Level [m AD]			
	Boundary	Type	Value			
	Lateral Flow	Type of Discharge	Runoff Area [ha]	Seepage/Infiltration [l/s.ha]	Type of Intensity	Source of Intensity
	Cross Section	Type of Profile	Cross section	Friction Type	Value* [depends on type]	
	Weir	Crest Level* [m AD]	Crest Widht [m AD]	Discharge Coeff. [-]	Lateral Contr. Coeff. [-]	Flow directions [-]
	Universal Weir	Type of Profile	Cross section	Discharge Coeff. [-]	Flow directions [-]	
	Culvert	Type	Length [m]	Left Bed Level [m AD]	Right Bed Level [m AD]	Cross Section
		Inlet loss Coeff. [-]	Outlet loss Coeff. [-]	Valve	Flow directions [-]	Friction Type
		Value [$m^{1/3}.s^{-1}$]				

The bed roughness of the river network is the first parameter that is calibrated. According to the maintenance plan of the water boards, the vegetation in river network is pruned on a frequent basis, [13]. This type of maintenance is, however, not always fed back into the numerical model by means of an adjustment of bed roughness. Following the physical description of bed friction, this would lead to large discrepancies in the modelled states (i.e. water levels and discharges).

The second type of parameter that is calibrated is the crest level of the weirs. In order to obtain the desired behaviour of the water system, the water board operates various sluices, pump stations, power stations and other operational devices, [22]. The operations of the most important structures are monitored by the water board, [13]. Small, 'less important' structures can have a significant influence on the model performance as well. Examples of such structures in the study area are weirs with a movable crest level. Despite of the influence of these weirs, the crest levels are not always monitored. Therefore, a correct estimation of the crest levels needs to be made in order to have a realistic representation of the actual water system.

4-2-2 Model schematisation

As stated above, the DSS is modified in such way that improvement in performance by the OPE tool can be monitored relatively straightforward. First, a small area, north of the city Tilburg and Oisterwijk (see Figure 4-1), is selected as the study area of this thesis. One reason for this choice (another reason in given in Section 4-2-4) is the number of available measurement locations compared to the number of calibration parameters in this area. In total, eleven measurement locations are available where both water levels and discharges are monitored Figure 4-2.

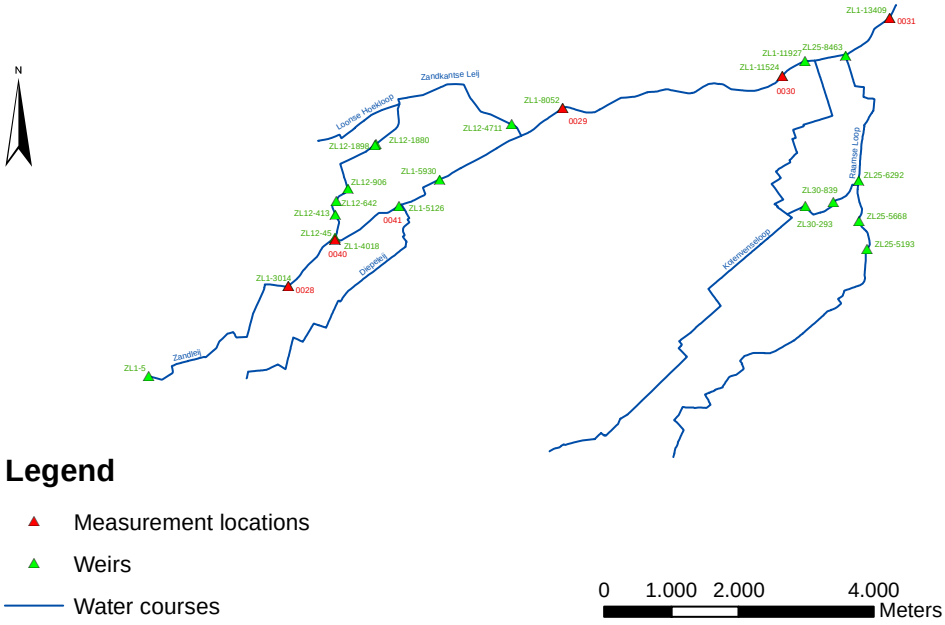

Figure 4-2: A graphical interpretation of the water courses, measurement stations and weirs of the study area. Observation stations 0028, 0029, 0030, 0031, 0040 are used for the optimisation process, since for these station observational data is available. The weirs listed in Table 4-4 are calibrated on their crest levels.

The number of measurement locations is a reference point for the number of calibration parameters that are allowed. According to [9], [37] and [52], the number of optimisation parameters should be significantly less than the observation measurements. In time scale, each measurement station contains 168 observational values, which correspond with the number of hours within the calibration window of a week. In spatial scale, however, the limiting number of measurement locations restricts the number of optimisation parameters not to exceed that number. Therefore, the bed roughness is assumed to be equal for all reaches, i.e. global friction is assumed. The crest levels are optimised separately in the initial model analysis. However, the outcomes of the identifiability analysis of the parameters have to point whether some parameters should be clustered. In short, the calibration parameters are: the crest levels W1, . . . , W9 and the overall friction parameter FA.

The other adjustments that are made to the original river network model are assuming only one-dimensional flow and removing (automatic) control actions by the operational devices. The latter adjustment means that controllers are switched off, but in a later phase are switched on again. In this way, influence of automatic controlled operational devices on the performance of the OPE tool can be determined. The former adjustment implies that two-dimensional overland flow is not taken into account. The rainfall-runoff (RR) model is switched off, since all the rainfall-runoff relations are determined prior to the optimisation. This is done by an alternative RR model to decrease the simulation time for multiple calibration loops, as the RR relations are equal for all calibration loops. A more detailed description of this RR model is provided in Section 3-1-2.

4-2-3 Twin experiment

The above described adjustments are assigned to make the analysis of the calibration results more straightforward. However, these simplifications introduce certain discrepancies with the real world. In other words, the real measurement data is not representative for the results of the adjusted model. Therefore, new measurement data has to be created that corresponds with the model behaviour. The new measurement data, also called artificial data, is created during *twin experiments* by running the model with the original input, [4],[52]. These twin experiments form the starting point for investigating the calibration of the parameters.

Twin experiments can be described briefly by four steps, [4]. First, observational data is created by running the model with the original input like parameter values and initial conditions. The observational data is used during the optimisation for calibration of the parameters. Then, several parameters are perturbed resulting in the initial parameters for the calibration. After calibration of these parameters, a comparison between the state and parameter results of the original run and those of the calibration run is made. The steps are illustrated in Figure 3-5. A major advantage of performing twin experiments is that there is (almost) no noise or uncertainty in the observational data and, thus, a very controlled environment is created for the calibration, [4].

Additive noise

For all experiments, twin experiment set-up is used to create artificial observation data. Most of these data is noise-free. Nevertheless, experiments with noise appended observations are executed as well, in order to simulate situations more closely related to reality. The noise is introduced by assigning so-called *white noise* to the observational data. *White noise* is a random signal with a constant power spectral density, [16]. Noise is presented as a random signal that is uniform distributed in a prescribed interval of ± 2.5 cm and ± 0.1 $m^3 s^{-1}$ for the water levels and discharges, respectively. The colour of the noise, i.e. white, means that the distribution of the power of the noise is equal for each frequency of occurrence, i.e. the power of the noise is the same regardless of the rate of the observed state.

4-2-4 Precipitation events

Next to the disturbance in parameters that is initiated, a disturbance in form of a precipitation event is introduced. Note that the former disturbance, in contrast with the latter, is unknown to the model. Reason for this rainfall event is the requirement of the OPE tool to perform well under all (or most) circumstances. Nonetheless, the most important task of the OPE tool is to obtain a correct representation of the actual river network before an extreme rainfall event, in order to prevent flooding during the rainfall event. Therefore, a moderate rainfall event is selected that was preceding an extreme event.

A recent event that followed this pattern was in the last months of the year 2010. During the months September and October the precipitation was average, while in the first two weeks of November the rainfall was excessive (see Figure 4-3). In the study area, this extreme precipitation event caused a lot of problems related to flooding at multiple locations in the province

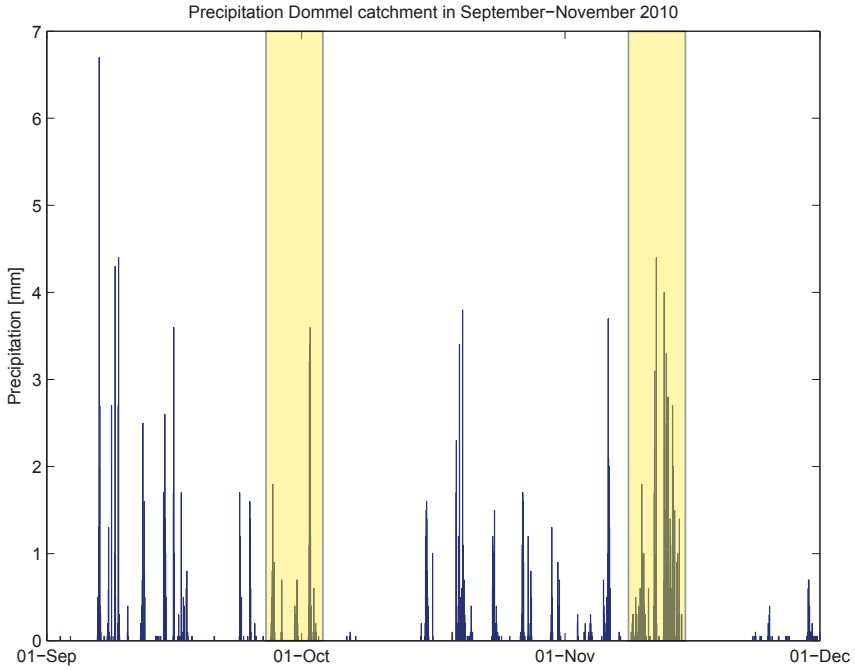

Figure 4-3: The hourly precipitation [mm h^{-1}] of September the 1st till December the 1st in 2010 at observational station 370 in Eindhoven, [53]. The highlighted boxes indicate the calibration window for different scenarios. The left box is from September the 29th till October the 4th and represents moderate precipitation levels. The right box is from November the 8th till November the 15th and stands for more extreme precipitation levels.

(Figure 4-4). Therefore, the OPE tool has to be able to deal with extreme precipitation events as well.

The moderate and extreme precipitation events that have been selected for this study are presented by the highlighted areas in Figure 4-3.

4-2-5 Observation locations

In Figure 4-2, the measurement stations used during this thesis, which currently also provide the water board from real data, are illustrated. These locations are selected, since it is useful to get an indication of how the OPE tool performs in the real river system. This is especially useful, when the OPE tool is applied at the existing DSS. Observation stations 0028, 0030, 0031 and 0040 monitor the up- and downstream water level on an hourly basis at the weirs ZL1-3014, ZL1-11524, ZL1-13409 and ZL1-4018, respectively. Observation station 0029 monitors next to the up- and downstream water levels also the hourly discharge levels over weir ZL1-8052.

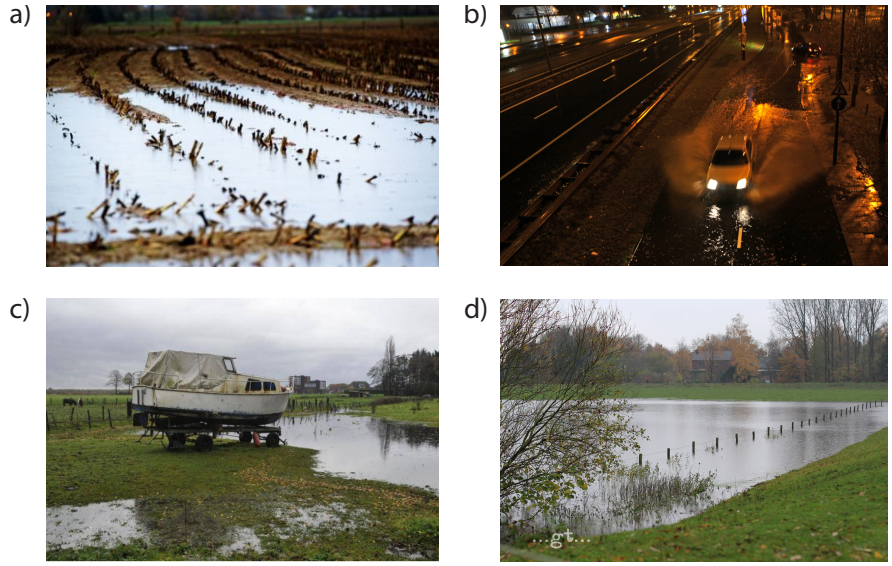

Figure 4-4: Four locations that suffered from flooding as result of long-term precipitation in November 2010: a), c) and d) show a flooded agricultural areas, [54],[55],[56], respectively; b) illustrates flooded roads, [57].

4-3 Optimisation problem

In this thesis, an OPE tool is developed that solves the optimisation problem stated by Eq. (2-3). The optimisation problem is subject to physical boundary constraints. The constraints used during this thesis are specified for the crest levels of the weirs in Table 4-2. The stopping criteria applied at the Doesn't Use Derivatives (DuD) algorithm are listed in Table 4-3.

Table 4-2: The minimum and maximum boundary constraints for the crest levels of the weirs.

Parameter	ID	$z_{s,min}$ [m]	$z_{s,max}$ [m]
W1	ZL1-5	9.90	11.74
W2	ZL1-3014	9.80	11.10
W3	ZL1-5126	7.39	8.80
W4	ZL1-5930	6.84	7.45
W5	ZL12-45	8.66	9.80
W6	ZL12-1880	6.73	8.00
W7	ZL12-4711	5.87	7.30
W8	ZL25-6292	5.16	6.53
W9	ZL25-8463	4.13	5.40

4-4 Experiment

Fifty scenarios are designed to test the sensitivity of the river network model to certain parameter changes. For each parameter, five realistic scenarios are created. The crest levels of the weirs are within the range of the possible crest levels for the corresponding weir. The

Table 4-3: The stopping criteria assigned to the DuD algorithm. The criteria correspond with those listed in Section 2-1-3.

Algorithm	Stopping criteria	Value [-]
DuD	Maximum outer iterations	20
	Maximum inner iterations	5
	T_1	0.001
	T_2	0.0001
	T_3	0.0001
	Maximum size of relative step size	10.0

bed roughness is based on literature, [58], and information of water board De Dommel, [13]. An overview of all scenarios is listed in Table 4-4. The outcome of this initial model analysis is used as a starting point for calibration of the parameters by the OPE tool. The initial model analysis is executed by means of a parameter analysis that consists of a sensitivity analysis and an identifiability and uniqueness analysis.

After the initial model analyses, the development OPE tool is described by use of several scenarios. In the first base scenario F1W0, only the friction of the cross-sections just downstream of weir ZL1-3014 is calibrated, while all other friction values and the weirs' crest levels remain the unchanged. In this scenario, solely the downstream water level of observation location 0028 is used for parameter optimisation, since a downstream water level is more sensitive to friction variations than an upstream water level. In this first base scenario F1W0, six scenarios with the following IDs are optimised: H1, H2, M1, M2, L1 and L2. In the scenario IDs, the letters correspond with 'actual' parameter values in either a high (H), medium (M) or low (L) scenario. The *actual parameter values* are the parameter values that were used to obtain the observational data, i.e. the *actual parameter values* can be recognised as the true parameter values.

The numbers in the IDs represent the initial parameter prediction and, thus, the starting parameter for the optimisation process by the OPE tool. By following this approach, the possibility of finding a local minimum instead of the global minimum is investigated, i.e. the robustness of the OPE tool is tested. The scenarios with their corresponding values are listed in Table 4-5.

The second base scenario F0W1 focusses on the optimisation of only the crest level of weir ZL1-3014. The other weirs' crest levels and friction values are not perturbed. This base scenario the same scenarios (H1,...,L2) are executed. However, in this case, the upstream water level of weir ZL1-3014 is used, as an upstream water level is most sensitive to changes in the crest level of the nearby located weir. All scenarios with their accompanying crest levels are listed in Table 4-5.

The third base scenario FaWc optimises both the friction of all cross-sections and the weirs' crest levels. These crest levels are *clustered* in one parameter Wc, since the initial model analysis demonstrated only one crest level is identifiable. Therefore, it is assumed that the crest levels of all weir follow the same seasonal pattern: in summer, the water level retained high, while the water is drained in the winter. The main reason behind this assumption is that the agricultural function of the water in the study area is rather important. The crest levels are clustered such that they can vary within their physical boundary constraints (see

Table 4-2). In other words, the range in which the crest level can vary is determined by the physical boundary constraints. Thus, a variation in the *clustered* weir parameter is rather a rather an *offset factor* (see Eq. (2-9)) than the offset itself. The latter, described by Eq. 2-8, is used for transformations in the global friction parameter.
In this base scenario, the same six scenarios are applied for both the friction parameter Fa and the clustered weir parameter Wc. Overall, this results in 36 scenarios. The parameter values of all scenarios are listed in Table 4-7.

In the fourth base scenario FaWcP, extreme precipitation (P) is used to determine the influence of high discharge rates on the performance of the OPE tool. For this base scenario, only high (H) and low (L) parameter values are used. In total, 16 scenarios (listed in Table 4-9) were applied in this base scenario.

In the fifth base scenario FaWcN, noise (N) is added to the observational data. In this way, the OPE tool is tested whether it is able to optimise the parameters accurately in an environment where the observational data is uncertain. For this base scenario, high (H) and low (L) parameter values are used. This results in 16 scenarios that are listed in Table 4-11.

4-5 Results and discussion

4-5-1 Initial model analysis

Parameter analysis

As described in Section 2-3, the parameters are analysed prior to the calibration phase. The model sensitivity and parameter identifiability are be determined by following this approach. The results are visualised by using the equations in Section 2-3. The methods can be used to group parameters and reduce number of parameters to be calibrated, [9],[52]. Moreover, the identifiability analysis can be used to give confidence in the parameter values that are calibrated, [4],[9],[15].

Sensitivity analysis

The parameter set that is evaluated is mentioned in Section 4-2-1. In this set, ten parameters are slightly changed according to the scenarios listed in Table 4-4. The model response as result of the perturbed parameters is determined by the cost function, Eq. (2-3).

The total response of the hydrodynamic model is illustrated in Figure 4-5. From this figure it can be observed that parameters W2, FA, W3 and W5 have the strongest influence on the objective function values. The results agree with the intuitive reasoning, when evaluating the model and its measurement locations. The parameter FA changes the bed roughness of the complete river network and, therefore, influences the model behaviour (i.e. water levels and discharges) of each river reach. The influence of weir on the model behaviour, however, is more local compared to the overall bed roughness. Nonetheless, the crest level parameters W2, W3 and W5 are closely located to measurement stations and, thus, have a significant effect on the objective function.

Table 4-4: The parameter scenarios for the initial parameter analysis.

PARAMETER	CREST_LEVEL_WEIR									ROUGHNESS
ID	ZL1-5	ZL1-3014	ZL1-5126	ZL1-5930	ZL12-45	ZL12-1880	ZL12-4711	ZL25-6292	ZL25-8463	ALL (k_s)
UNIT	m	m	m	m	m	m	m	m	m	$m^{1/3}.s^{-1}$
CASE_SCENARIO										
AVG	10.82	10.45	8.4	7.145	9.15	7.2	6.75	5.78	4.6	16
W1-1	10.52	10.45	8.4	7.145	9.15	7.2	6.75	5.78	4.6	16
W1-2	10.67	10.45	8.4	7.145	9.15	7.2	6.75	5.78	4.6	16
W1-3	10.82	10.45	8.4	7.145	9.15	7.2	6.75	5.78	4.6	16
W1-4	10.97	10.45	8.4	7.145	9.15	7.2	6.75	5.78	4.6	16
W1-5	11.12	10.45	8.4	7.145	9.15	7.2	6.75	5.78	4.6	16
W2-1	10.82	10.15	8.4	7.145	9.15	7.2	6.75	5.78	4.6	16
W2-2	10.82	10.3	8.4	7.145	9.15	7.2	6.75	5.78	4.6	16
W2-3	10.82	10.45	8.4	7.145	9.15	7.2	6.75	5.78	4.6	16
W2-4	10.82	10.6	8.4	7.145	9.15	7.2	6.75	5.78	4.6	16
W2-5	10.82	10.75	8.4	7.145	9.15	7.2	6.75	5.78	4.6	16
W3-1	10.82	10.45	8.1	7.145	9.15	7.2	6.75	5.78	4.6	16
W3-2	10.82	10.45	8.25	7.145	9.15	7.2	6.75	5.78	4.6	16
W3-3	10.82	10.45	8.4	7.145	9.15	7.2	6.75	5.78	4.6	16
W3-4	10.82	10.45	8.55	7.145	9.15	7.2	6.75	5.78	4.6	16
W3-5	10.82	10.45	8.7	7.145	9.15	7.2	6.75	5.78	4.6	16
W4-1	10.82	10.45	8.4	6.845	9.15	7.2	6.75	5.78	4.6	16
W4-2	10.82	10.45	8.4	6.995	9.15	7.2	6.75	5.78	4.6	16
W4-3	10.82	10.45	8.4	7.145	9.15	7.2	6.75	5.78	4.6	16
W4-4	10.82	10.45	8.4	7.295	9.15	7.2	6.75	5.78	4.6	16
W4-5	10.82	10.45	8.4	7.445	9.15	7.2	6.75	5.78	4.6	16
W5-1	10.82	10.45	8.4	7.145	8.85	7.2	6.75	5.78	4.6	16
W5-2	10.82	10.45	8.4	7.145	9	7.2	6.75	5.78	4.6	16
W5-3	10.82	10.45	8.4	7.145	9.15	7.2	6.75	5.78	4.6	16
W5-4	10.82	10.45	8.4	7.145	9.3	7.2	6.75	5.78	4.6	16
W5-5	10.82	10.45	8.4	7.145	9.45	7.2	6.75	5.78	4.6	16
W6-1	10.82	10.45	8.4	7.145	9.15	6.9	6.75	5.78	4.6	16
W6-2	10.82	10.45	8.4	7.145	9.15	7.05	6.75	5.78	4.6	16
W6-3	10.82	10.45	8.4	7.145	9.15	7.2	6.75	5.78	4.6	16
W6-4	10.82	10.45	8.4	7.145	9.15	7.35	6.75	5.78	4.6	16
W6-5	10.82	10.45	8.4	7.145	9.15	7.5	6.75	5.78	4.6	16
W7-1	10.82	10.45	8.4	7.145	9.15	7.2	6.45	5.78	4.6	16
W7-2	10.82	10.45	8.4	7.145	9.15	7.2	6.6	5.78	4.6	16
W7-3	10.82	10.45	8.4	7.145	9.15	7.2	6.75	5.78	4.6	16
W7-4	10.82	10.45	8.4	7.145	9.15	7.2	6.9	5.78	4.6	16
W7-5	10.82	10.45	8.4	7.145	9.15	7.2	7.05	5.78	4.6	16
W8-1	10.82	10.45	8.4	7.145	9.15	7.2	6.75	5.48	4.6	16
W8-2	10.82	10.45	8.4	7.145	9.15	7.2	6.75	5.63	4.6	16
W8-3	10.82	10.45	8.4	7.145	9.15	7.2	6.75	5.78	4.6	16
W8-4	10.82	10.45	8.4	7.145	9.15	7.2	6.75	5.93	4.6	16
W8-5	10.82	10.45	8.4	7.145	9.15	7.2	6.75	6.08	4.6	16
W9-1	10.82	10.45	8.4	7.145	9.15	7.2	6.75	5.78	4.3	16
W9-2	10.82	10.45	8.4	7.145	9.15	7.2	6.75	5.78	4.45	16
W9-3	10.82	10.45	8.4	7.145	9.15	7.2	6.75	5.78	4.6	16
W9-4	10.82	10.45	8.4	7.145	9.15	7.2	6.75	5.78	4.75	16
W9-5	10.82	10.45	8.4	7.145	9.15	7.2	6.75	5.78	4.9	16
FA1	10.82	10.45	8.4	7.145	9.15	7.2	6.75	5.78	4.6	20
FA2	10.82	10.45	8.4	7.145	9.15	7.2	6.75	5.78	4.6	18
FA3	10.82	10.45	8.4	7.145	9.15	7.2	6.75	5.78	4.6	16
FA4	10.82	10.45	8.4	7.145	9.15	7.2	6.75	5.78	4.6	14
FA5	10.82	10.45	8.4	7.145	9.15	7.2	6.75	5.78	4.6	12

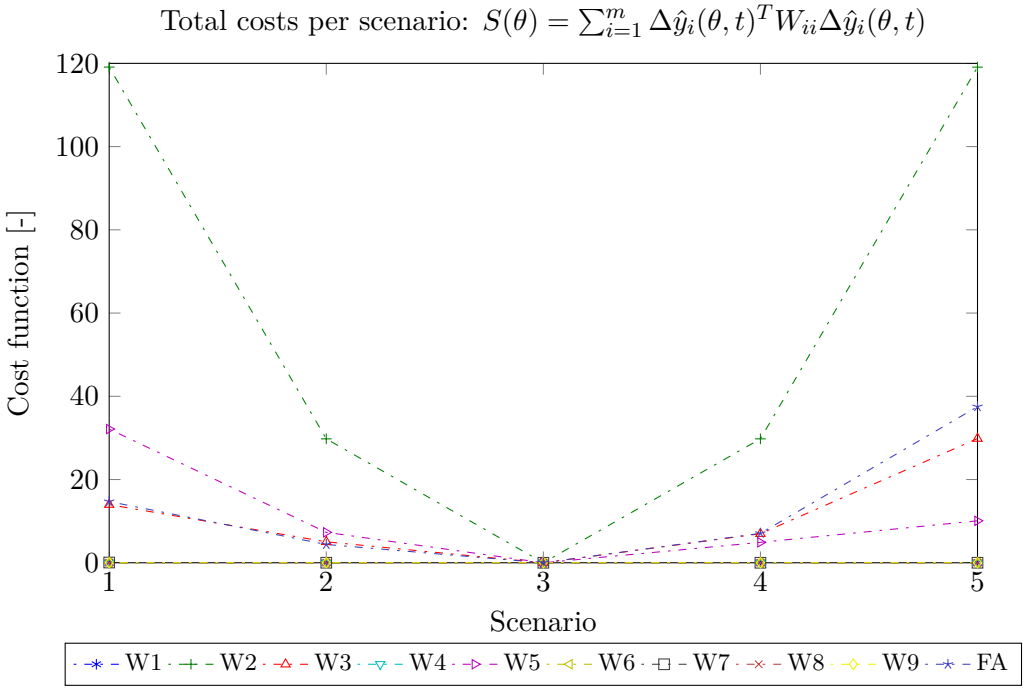

Figure 4-5: The total cost caused by perturbations in parameter values.

When analysing the objective function for each measurement location, only location 0028 and 0040 seems to be influenced by a change in the crest level height of weirs (see Figure C-1 and Figure C-5). At location 0030, 0031 and 0040 the objective function is most affected by the overall bed roughness change (Figure C-3, Figure C-4 and Figure C-5, respectively). The explanation for these differences holds the same as for differences observed for the total cost Figure 4-5. Interesting to see is that for location 0040 the lower scenarios 1 and 2 the cost function is most affected by parameter W5, while for the higher scenarios parameter W3 is most influential. This reason for this is that weir W5 is located upstream in a parallel river branch and weir W3 downstream of location 0040.

A decrease in crest level for W5 (illustrated by scenario 1 and 2) causes an decrease in discharge at location 0040. The reason for this is that the weir at location 0040 and the weir W5 are both located just downstream of a bifurcation point and, thus, in fact regulate the water discharge distribution in the two parallel breaches. This results in lower water levels up- and downstream of location 0040. An increase of the crest level for W5 (scenario 4 and 5) has the opposite, but less powerful influence on the water levels at 0040. The latter is the effect of that the decrease in crest level has a relatively stronger influence on the water distribution. Consequently, the effect on the cost function is larger for scenario 1 and 2.

Weir W3 is located downstream of the weir at location 0040. For moderate conditions, the weir has free flow conditions. This implies that a change in the crest level of weir W3 only affects the downstream level of the weir at 0040. Moreover, an increase of the crest level W3 has a relative stronger influence on this downstream level than a decrease of the crest level, since the backwater curve of weir W3 has stronger effect for a larger crest level.

Overall, from this sensitivity analysis it seems that only parameters W2, W3, W5 and FA can

be identified. In order to check this statement or determine whether more parameters can be identified an identifiability analysis is executed.

Identifiability and uniqueness analysis

In this section, the identifiability and uniqueness of the parameters is determined based on the methods and equations described in Section 2-3. Following this approach, both the singular values and eigenvectors of the system and the correlation between the parameters are determined.

The singular values and eigenvectors are calculated with use of Eq. (2-11) and illustrated in Figure 4-6. The eigenvectors are listed from left to right, depending on the corresponding singular values. The eigenvectors 1, 2, 5, 6 and 10 more or less dominated by the parameters W2, W3, W4, W7 and W8, respectively. This means that these parameters are well identifiable according to their uniqueness. Nevertheless, the (very) low singular values for eigenvectors 5, 6 and 10 could imply that the influence on the objective function is so low that these parameters are not identifiable. In other words, the model is fairly insensitive to perturbations of parameter W4, W7 and W8. This has to be investigated with great care during the calibration phase.

The eigenvectors 3 and 4 show an influence on the model by the combination of parameter W5 and FA, while eigenvectors 7, 8 and 9 represent a combination of parameter W1, W6 and W9. These combinations mean that the parameters W5 and FA, and the parameters W1, W6 and W9 cannot be identified separately.

In Figure 4-7, the correlation matrix is illustrated. From this figure, it can be observed that parameter W1 is negatively correlated with W4. Nevertheless, these parameters have a very small influence on the model, so this correlation is not of particular interest. Furthermore, a negative correlation between the parameters FA and W2 with W3 and W5 is observed. This can be explained by the sensitivity analysis of Section 2-3, which states that these parameters are the most influential ones. Lastly, a negative correlation between W6 and W7 is noticed. The model response is, however, rather insensitive to changes in these parameters, so again this is not of great interest.

Overall, it can be concluded, from the sensitivity analysis (see Figure 4-5 and the figures in Appendix C), that the cost function is most sensitive to changes in the friction parameter at most locations. From the singular value decomposition (see Figure 4-6) and correlation matrix (see Figure 4-7), weir parameter W2 is the only weir parameter that has a significant influence the cost function. In other words, the other weir parameters are not very identifiable and are, therefore, difficult to calibrate by the OPE tool. The most important reason for the fact that the objective function is most sensitive to weir parameter W2, is that a measurement station is located at the corresponding weir ZL1-3014. This results in the a strong response of the upstream water level of the weir, when the crest level of this weir is adjusted. Therefore, the objective function is very sensitive to changes in the crest level of weir ZL1-3014. The cost function is, however, not very sensitive to changes in the other crest levels, since no observation locations are nearby these other weirs. This could, eventually, lead to long computation times, which is far from desirable when calibrating in an on-line setting. In order to overcome this issue, the weir parameters are clustered into one parameter, assuming that the weir parameters (i.e. the weirs' crest levels) follow the same seasonal pattern. This assumption is valid when

taking into account that the study area mainly consists of agricultural land. In this type of land, it is common that the weirs' crest levels follow a seasonal pattern, i.e. high crest levels in summer and low crest levels in winter.

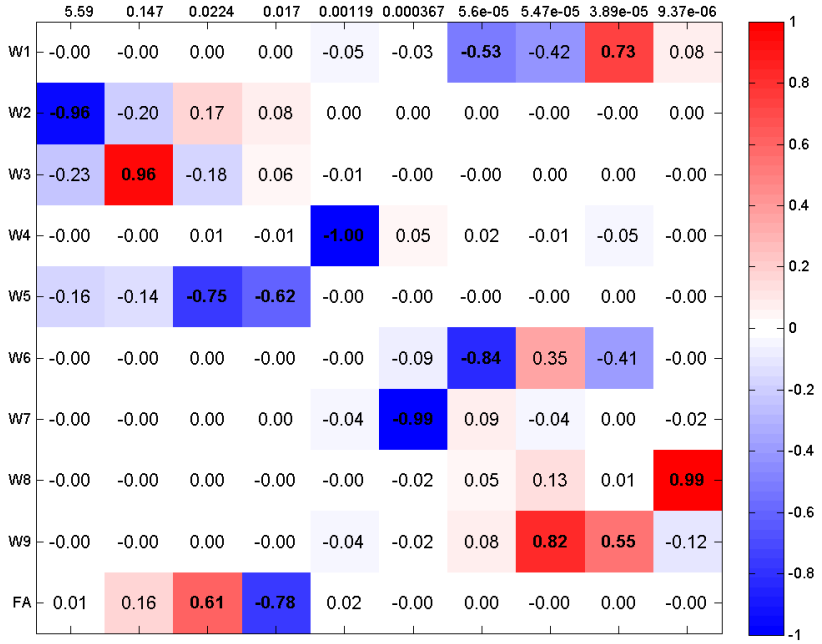

Figure 4-6: The singular value decomposition of the initial parameter analysis.

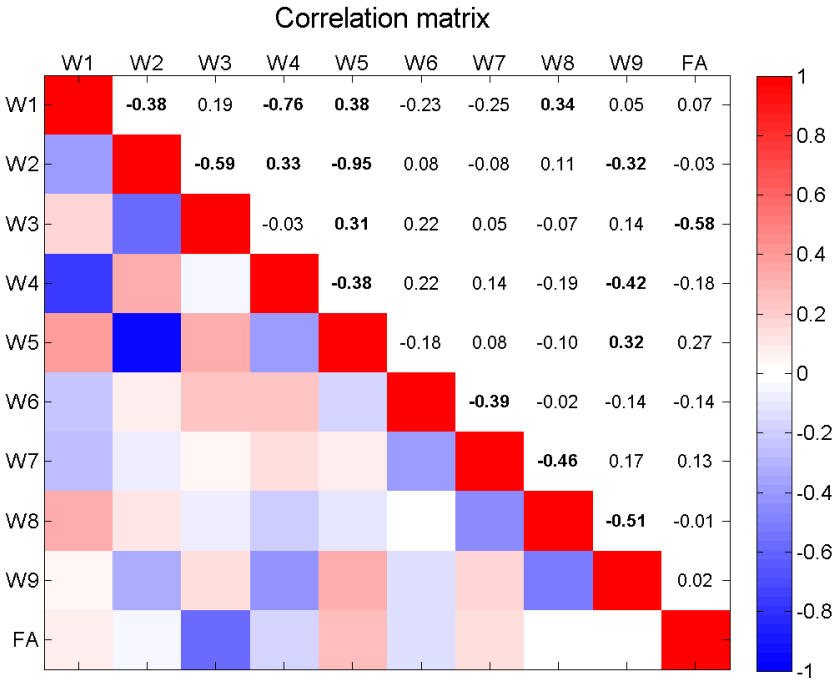

Figure 4-7: The correlation matrix of the initial parameter analysis.

4-5-2 Scenario F1W0: friction of one section, no crest levels

4-5-2-1 Model performance

In Figure 4-8, the convergence of the friction parameter as function of the iteration number for different scenarios within the base case F1W0 is illustrated. For each scenario, a fast convergence is observed. Within five iterations the actual friction value is correctly estimated by the OPE tool. No significant difference is observed between the scenarios for both difference starting points and *actual parameters values* (indicated with dashed lines).

In Figure 4-9, the cost per scenario as function of the iteration number is presented. The cost drops rapidly for each scenario, as expected from the results in Figure 4-8. No significant difference between the high (i.e. H1 and H2) and the middle (i.e. M1 and M2) scenarios is noticed. The lower scenarios L1 and L2 convergence a bit more slowly. Apparently, is it more difficult for the DuD algorithm to estimate low Strickler roughness values, which correspond with a high bed friction. Probably, the non-linear effect of introducing high bed friction are stronger compared those induced by low bed friction. This causes the DuD algorithm, which uses a linearisation approach, to converge more slowly. The performance of the OPE tool in terms of effectiveness is illustrated in Figure 4-10, where the green line demonstrates a very close approach of the observations (blue dots).

Table 4-5: The optimisation results for base scenarios F1W0 and F0W1. The twin parameter values represent the actual parameter values. The perturbed parameter values represent the initial predictions, while the calibrated parameters represent the final optimised predictions.

Base scenario	Scenario ID	Twin parameters		Perturbed parameters		Calibrated parameters	
		$k_{s,0}$ [$m^{1/3}.s^{-1}$]	$z_{s,0}$ [m]	$k_{s,0}$ [$m^{1/3}.s^{-1}$]	$z_{s,0}$ [m]	$k_{s,0}$ [$m^{1/3}.s^{-1}$]	$z_{s,0}$ [m]
F1W0	H1	20	-	14	-	19.9997	-
	H2	20	-	18	-	19.9959	-
	M1	16	-	14	-	15.9985	-
	M2	16	-	18	-	16.0002	-
	L1	12	-	14	-	12.0004	-
	L2	12	-	18	-	12.0002	-
F0W1	H1	-	10.75	-	10.00	-	10.7500
	H2	-	10.75	-	10.90	-	10.7500
	M1	-	10.45	-	10.00	-	10.4500
	M2	-	10.45	-	10.90	-	10.4500
	L1	-	10.15	-	10.00	-	10.1500
	L2	-	10.15	-	10.90	-	10.1499

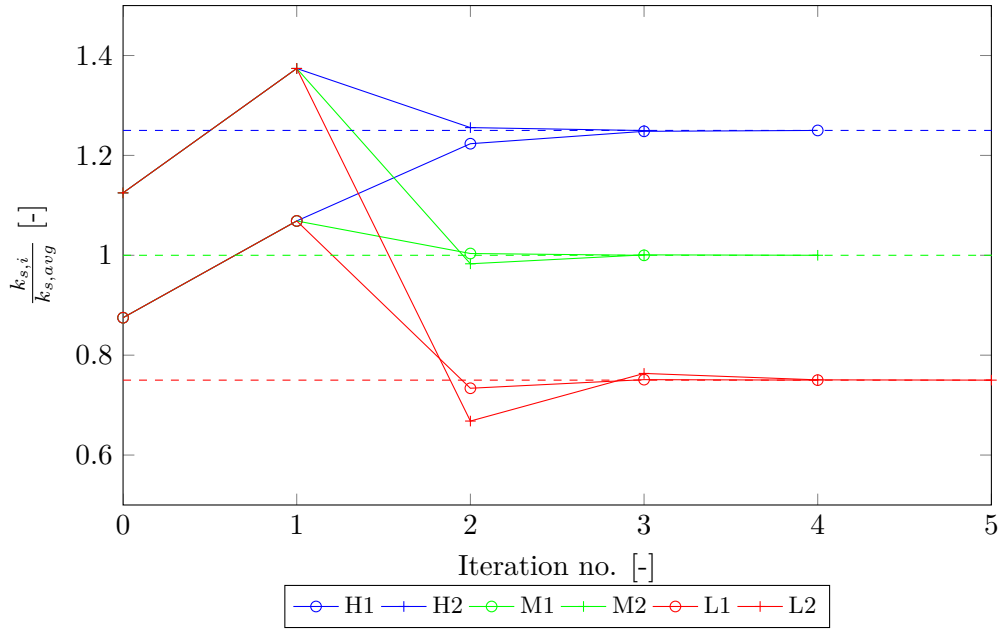

Figure 4-8: Convergence of the perturbed friction parameter from different starting points to the actual friction values for three different scenarios (indicated with the dashed lines) as function of the iterations: F1W0. The scenarios with different starting points are indicated with crosses and circles for a high and low starting point, respectively. The high, medium and low scenarios are indicated with the red, green and blue, respectively.

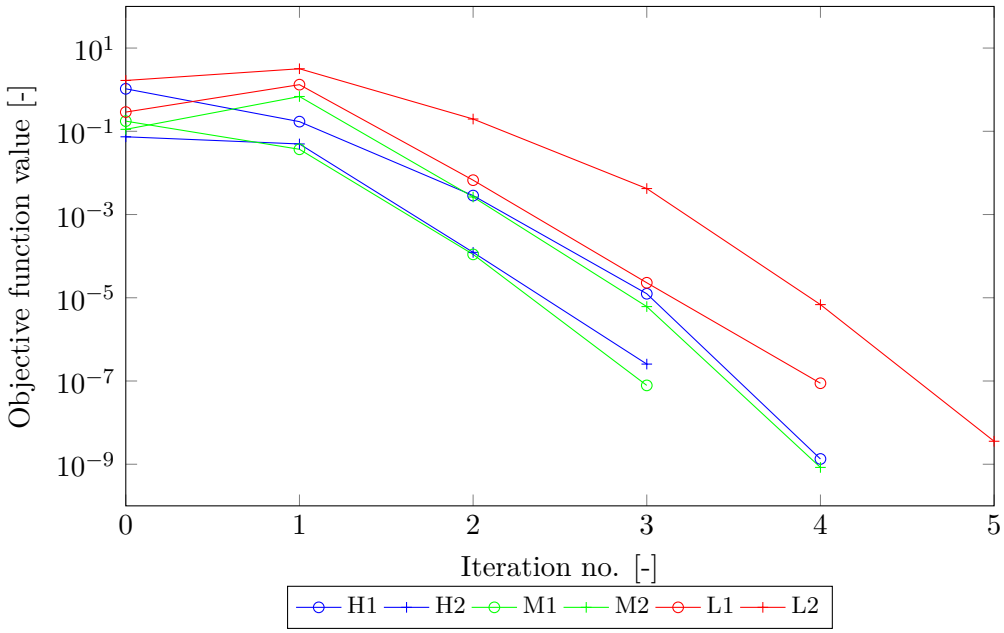

Figure 4-9: The cost function for the perturbed friction parameter for the F1W0 scenarios with different starting points and three actual friction values. The scenarios with different starting points are indicated with crosses and circles for a high and low starting point, respectively. The high, medium and low scenarios are indicated with the red, green and blue, respectively.

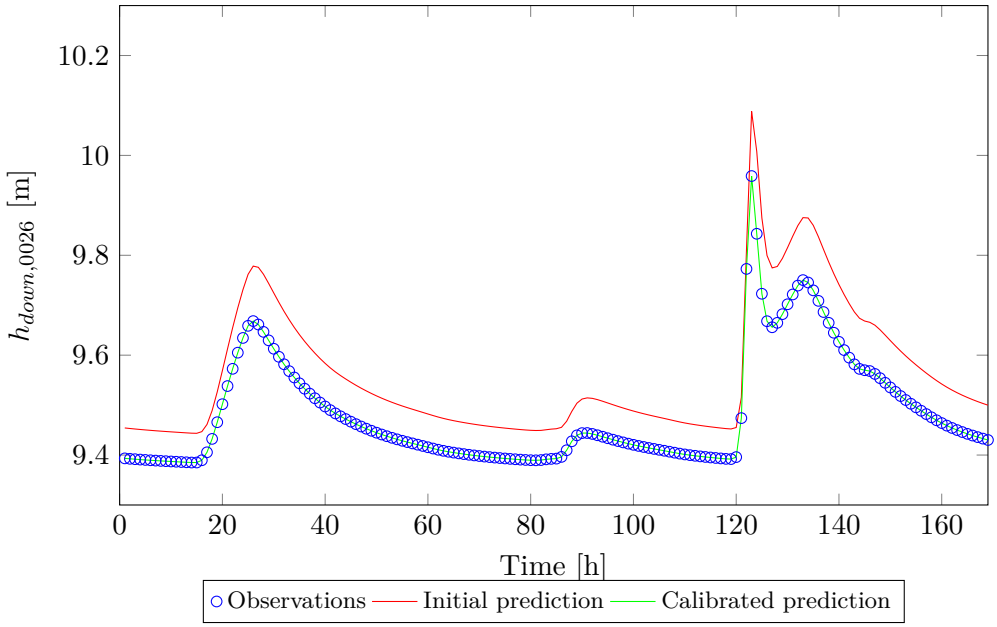

Figure 4-10: The downstream water level at location 0028 for scenario F1W0H1 as function of time in the calibration window. The blue dots represent the observational data, the red line the initial prediction and the green line the calibrated prediction.

4-5-2-2 Residual analysis

It is often very useful to analyse the residuals, when optimising the model performance by parameter calibration. A well-known tool for residual analysis is the analysis of the residuals' bias with Eq. (2-14). The differences in the bias for the scenarios does not show a clear pattern. Neither for scenarios with different starting points nor for scenarios with different *actual parameter values*, such a pattern in differences between the bias and the scenarios is observed. The differences in the bias could only be explained by the cost values of the scenarios' last iteration (see Figure 4-9), as the order in these cost values correspond with the order in the bias for the scenarios. This explanation is likely to be valid, since both the cost function (Eq. (2-3)) and the bias function (Eq. (2-14)) are based on the squared error.

There is, however, a pattern noticed in the bias as function of time, when comparing this pattern with the calibrated water levels in time (see Figure 4-10). It seems that the bias is correlated with the discharge rate. The observations are, however, obtained by use of the same hydrodynamic model, so no systematic modelling error can be the cause of this pattern. Moreover, the level of bias is still reasonably low and is within acceptable ranges. Therefore, the bias can be assumed to be insignificant (see Table 4-6). The bias appeared to be a numerical error that is induced by the OPE tool. Nonetheless, the model should be tested for different rates of precipitation intensities, as these are assumed to cause stronger water level variations.

Furthermore, it was observed that scenario L1 shows a deviating bias pattern in time compared to the other scenarios. The cause of this is not known, but it is likely that again a numerical error induced by the OPE tool is the cause.

Table 4-6: The residual statistics of base scenarios F1W0 and F0W1. The total amount of iterations, the final cost, the final root-mean-square error (RMSE), the final bias and standard deviation of the errors (STD) are presented with their weighted dimensionless values.

Base scenario	Scenario ID	Iterations [-]	Cost [-]	RMSE [-]	BIAS [-]	STD [-]
F1W0	H1	4	1.34E-009	2.93E-006	2.78E-006	9.21E-007
	H2	3	2.55E-007	4.04E-005	-3.87E-005	1.18E-005
	M1	3	7.84E-008	2.24E-005	-2.16E-005	6.13E-006
	M2	4	8.39E-010	2.32E-006	2.22E-006	6.79E-007
	L1	4	8.84E-008	2.38E-005	6.86E-006	2.29E-005
	L2	5	3.57E-009	4.78E-006	4.61E-006	1.27E-006
F0W1	H1	2	3.79E-008	2.19E-005	-2.19E-005	1.59E-007
	H2	2	8.83E-009	-8.83E-005	-9.09E-008	5.53E-007
	M1	2	4.93E-008	2.49E-005	-2.49E-005	2.61E-007
	M2	2	3.57E-008	2.12E-005	2.12E-005	2.22E-007
	L1	2	4.24E-009	7.31E-006	-7.31E-006	6.08E-008
	L2	2	2.88E-007	6.02E-005	6.02E-005	5.00E-007

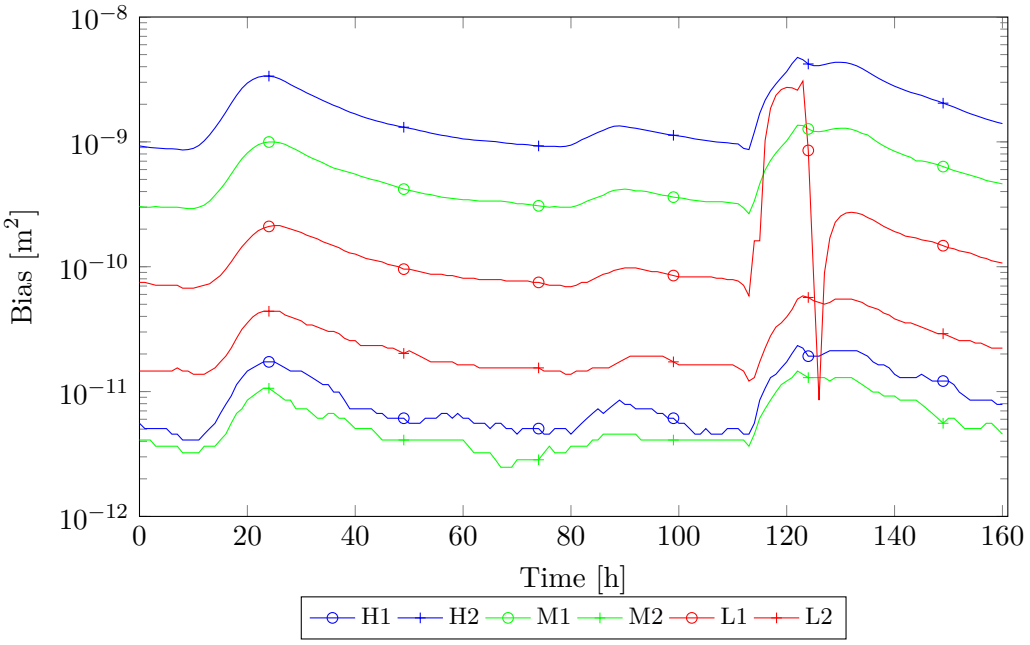

Figure 4-11: The bias for the downstream water level at location 0028 for the F1W0 scenarios with different starting points and three actual friction values as function of time in the calibration windows (with a time window $T = 2$h). The scenarios with different starting points are indicated with crosses and circles for a high and low starting point, respectively. The high, medium and low scenarios are indicated with the red, green and blue, respectively.

4-5-3 Scenario F0W1: no friction, one crest level

4-5-3-1 Model performance

In Figure 4-12, the convergence of the crest level as a calibration parameter is illustrated. The crest level is correctly predicted by the OPE tool within two iterations, which is faster than the computation time for prediction of the friction parameter. The most logical reason for this is the stronger model sensitivity to changes in the weir parameter, compared to the sensitivity to changes in the friction parameter. This is effect is illustrated in Figure 4-6. The result of effective parameter optimisation in this base case is illustrated in Figure 4-14, where the calibrated water level (the green line) approaches the observed data rather closely. The accuracy of the F0W1 result by the OPE tool are listed in Table 4-5.

The final cost each scenario is comparable with the costs for calibration of the friction parameter (see Figure 4-13). Apparently, the stopping criteria are satisfied at an equal point in the optimisation process.

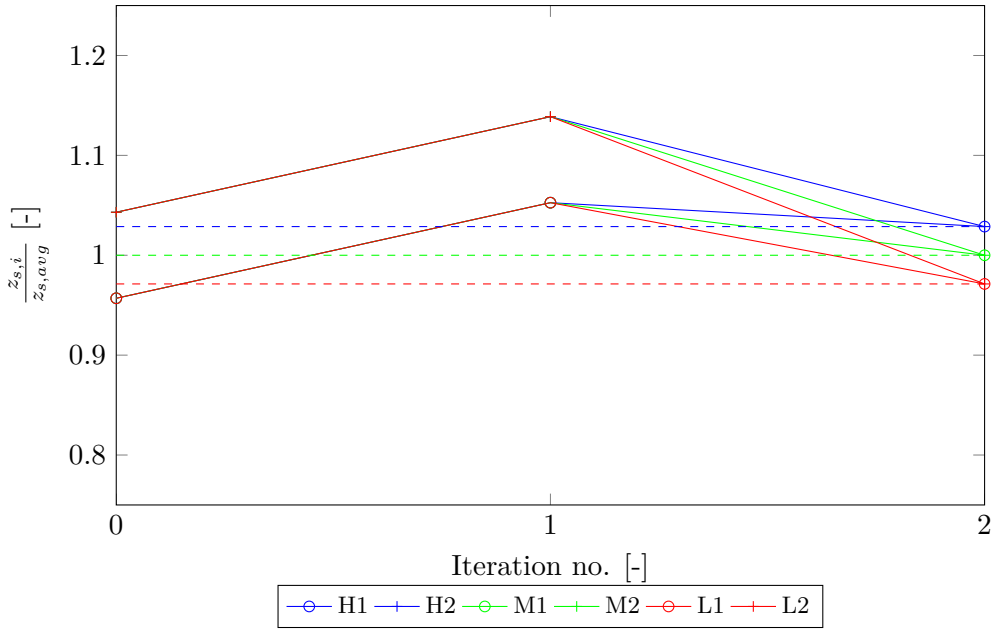

Figure 4-12: Convergence of the perturbed crest level parameter from different starting points to the actual crest level values for three different scenarios (indicated with the dashed lines) as function of the iterations: F0W1. The scenarios with different starting points are indicated with crosses and circles for a high and low starting point, respectively. The high, medium and low scenarios are indicated with the red, green and blue, respectively.

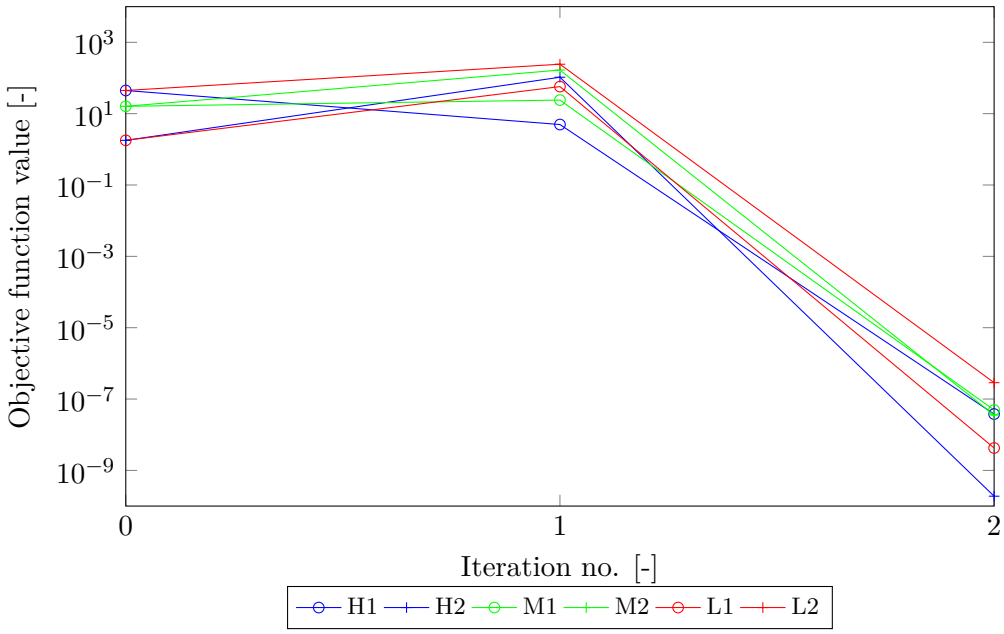

Figure 4-13: The cost function for the perturbed crest level parameter for the F0W1 scenarios with different starting points and three actual crest level values. The scenarios with different starting points are indicated with crosses and circles for a high and low starting point, respectively. The high, medium and low scenarios are indicated with the red, green and blue, respectively.

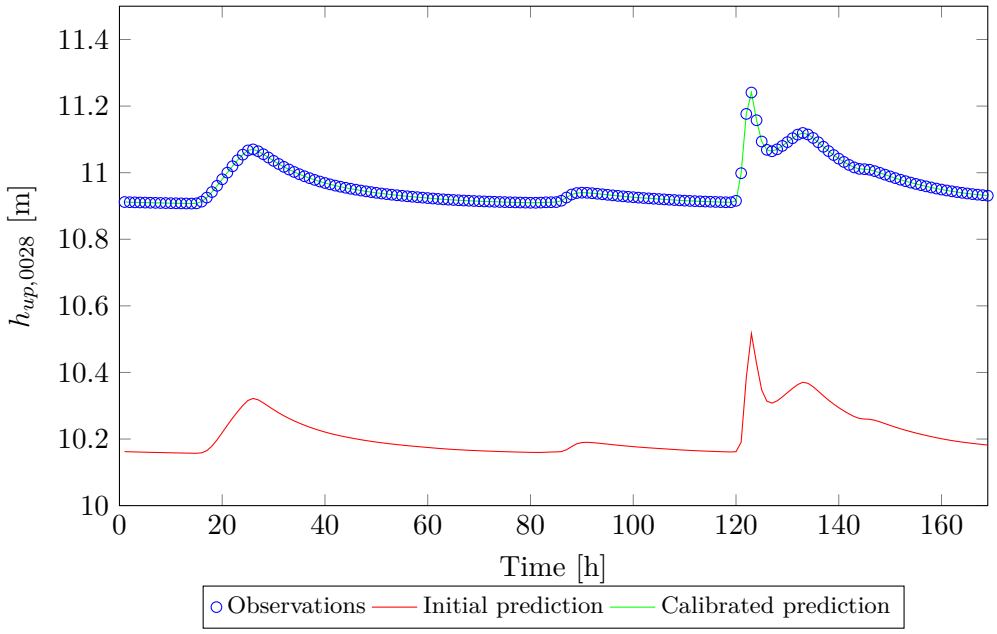

Figure 4-14: The upstream water level at location 0028 for scenario F0W1H1 as function of time in the calibration window. The blue dots represent the observational data, the red line the initial prediction and the green line the calibrated prediction.

4-5-3-2 Residual analysis

In Figure 4-15, the bias for the different scenarios as function of time is presented. The difference between the scenarios are the result of the different cost values of the scenarios' last iteration (see Figure 4-13). Furthermore, the bias for this base scenario comparable with base scenario F1W0. The main reason for this is the more or less same level of cost values that were obtained for both base scenarios. The fluctuations of the bias in this base scenario are, however, smaller or hardly not observable at all. Apparently, the bias is not linked to the discharge rate, as stated in the previous section. Nevertheless, research to the influence of extreme precipitation on the model performance should exclude this statement. Besides, according to the data presented in Table 4-6, the bias is within acceptable ranges and could therefore be recognised as insignificant.

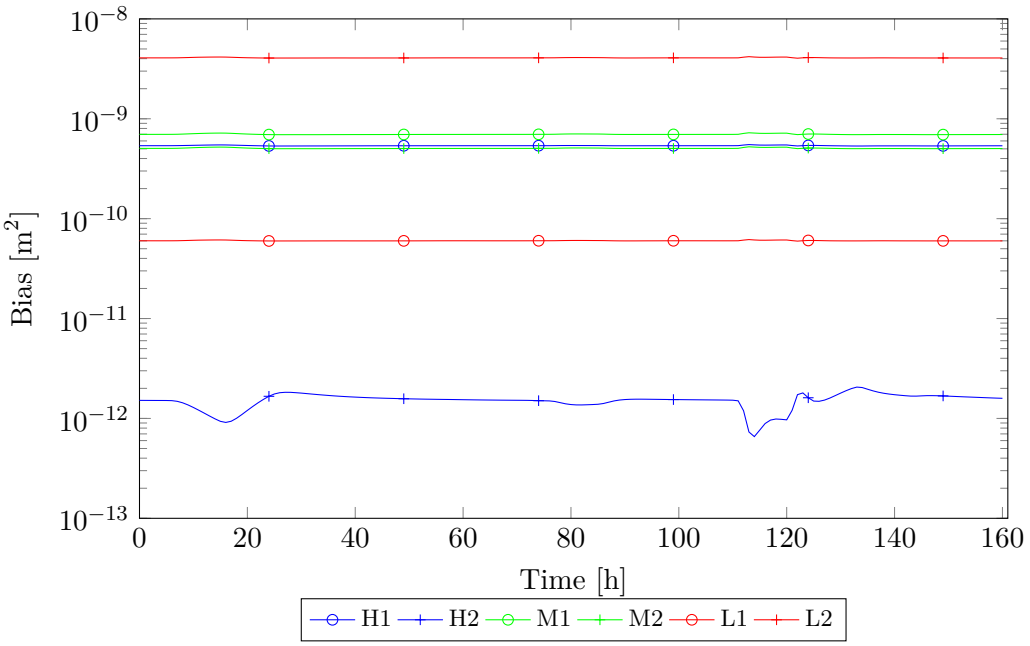

Figure 4-15: The bias for the downstream water level at location 0028 for the F0W1 scenarios with different starting points and three actual crest level values as function of time in the calibration windows (with a time window $T = 2$h). The scenarios with different starting points are indicated with crosses and circles for a high and low starting point, respectively. The high, medium and low scenarios are indicated with the red, green and blue, respectively.

4-5-4 Scenario FaWc: global friction, clustered crest levels

4-5-4-1 Model performance

In order to present the all the result without creating disordered figures, the base scenario FaWc is split up in three group (G1, G2 and G3) according to Table 4-7. In Figure 4-17, Figure 4-20 and Figure 4-20[2], the convergence of friction parameter is illustrated for G1, G2 and G3, respectively. Figure 4-18, Figure 4-21 and Figure 4-24[2] present the convergence of the clustered crest level parameter. These parameter convergence figures show that for all scenarios (in each group) within ten iterations the *actual parameter value* is predicted accurately. So, the efficiency compared to the base scenarios F1W0 and F0W1 is lower, since these base scenarios only require at most five iteration. The main for this is that these base scenarios only consider one parameter during the optimisation, while the base scenario FaWc attempts to optimise two parameters. Nevertheless, between the scenarios in the base scenario FaWc no significant differences in terms of efficiency are noticed. In other words, the efficiency of the OPE tool in this base scenario is not dependent on the initial parameter prediction or on the actual parameter values.

Figure 4-16, Figure 4-19 and Figure 4-22[2] show the cost as function of the iteration number for the FaWc scenario groups G1, G2 and G3, respectively. No large differences between the scenarios are noticed. Only scenario M2L1 deviates from the overall convergence pattern that is observed in the FaWc scenarios. Nonetheless, the final cost is similar to those of the other scenarios, indicating that also the robustness of the OPE tool is not dependent on the initial parameter guess or on the actual parameter values.

In Appendix D, the model performance is expressed in calibrated model states (i.e. water levels and discharges) compared with the observed data and the initial predicted states for different measurement locations.

[2]In the figures, the scenarios with different starting points are indicated with crosses, circles, squares and asterisks. The crosses and circles represent high and low starting points, respectively, for the weir parameter and a low starting point for the friction parameter. The squares and asterisks represent high and low starting points, respectively, for the weir parameter and a high starting point for the friction parameter. The high, medium and low scenarios for the weir parameter are indicated with the red, green and blue, respectively.

Table 4-7: The optimisation results for base scenario FaWc. The twin parameter values represent the actual parameter values. The perturbed parameter values represent the initial predictions, while the calibrated parameters represent the final optimised predictions.

Base scenario	Group	Scenario ID	Twin parameter value		Perturbed parameters		Parameter value	
			$k_{s,0}$ [$m^{1/3}.s^{-1}$]	$z_{s,c,0}$ [m]	$k_{s,0}$ [$m^{1/3}.s^{-1}$]	$z_{s,c,0}$ [m]	$k_{s,0}$ [$m^{1/3}.s^{-1}$]	$z_{s,c,0}$ [m]
FaWc	G1	H1H1	20	0.8	14	0.1	19.9990	0.80000
		H1H2	20	0.8	14	0.9	20.0002	0.80000
		H2H1	20	0.8	18	0.1	19.9992	0.80001
		H2H2	20	0.8	18	0.9	19.9995	0.80000
		H1M1	20	0.6	14	0.1	20.0016	0.59998
		H1M2	20	0.6	14	0.9	19.9989	0.60000
		H2M1	20	0.6	18	0.1	19.9951	0.60000
		H2M2	20	0.6	18	0.9	19.9972	0.60000
		H1L1	20	0.4	14	0.1	20.0007	0.39999
		H1L2	20	0.4	14	0.9	20.0090	0.40009
		H2L1	20	0.4	18	0.1	19.9976	0.40000
		H2L2	20	0.4	18	0.9	20.0006	0.40000
	G2	M1H1	16	0.8	14	0.1	15.9999	0.80000
		M1H2	16	0.8	14	0.9	15.9994	0.80000
		M2H1	16	0.8	18	0.1	16.0000	0.80000
		M2H2	16	0.8	18	0.9	15.9995	0.80000
		M1M1	16	0.6	14	0.1	15.9999	0.60001
		M1M2	16	0.6	14	0.9	15.9997	0.60000
		M2M1	16	0.6	18	0.1	15.9999	0.59999
		M2M2	16	0.6	18	0.9	15.9990	0.60004
		M1L1	16	0.4	14	0.1	15.9982	0.39999
		M1L2	16	0.4	14	0.9	16.0015	0.39998
		M2L1	16	0.4	18	0.1	16.0016	0.40001
		M2L2	16	0.4	18	0.9	15.9953	0.39994
	G3	L1H1	12	0.8	14	0.1	11.9999	0.80000
		L1H2	12	0.8	14	0.9	11.9998	0.80000
		L2H1	12	0.8	18	0.1	12.0000	0.80000
		L2H2	12	0.8	18	0.9	12.0000	0.80000
		L1M1	12	0.6	14	0.1	11.9996	0.59996
		L1M2	12	0.6	14	0.9	11.9998	0.60000
		L2M1	12	0.6	18	0.1	12.0001	0.60000
		L2M2	12	0.6	18	0.9	12.0002	0.60000
		L1L1	12	0.4	14	0.1	12.0000	0.40001
		L1L2	12	0.4	14	0.9	11.9999	0.40000
		L2L1	12	0.4	18	0.1	12.0021	0.40008
		L2L2	12	0.4	18	0.9	12.0064	0.39993

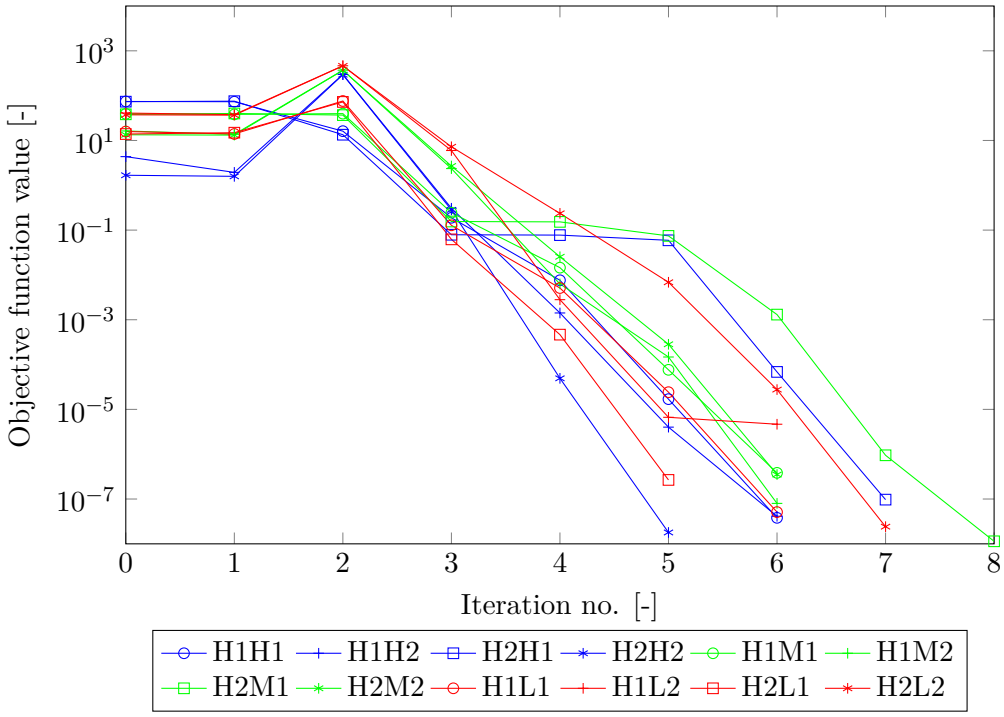

Figure 4-16: The cost function for the perturbed parameters for the FaWc group 1 (G1) scenarios with different starting points, three actual crest level values and one actual friction value.

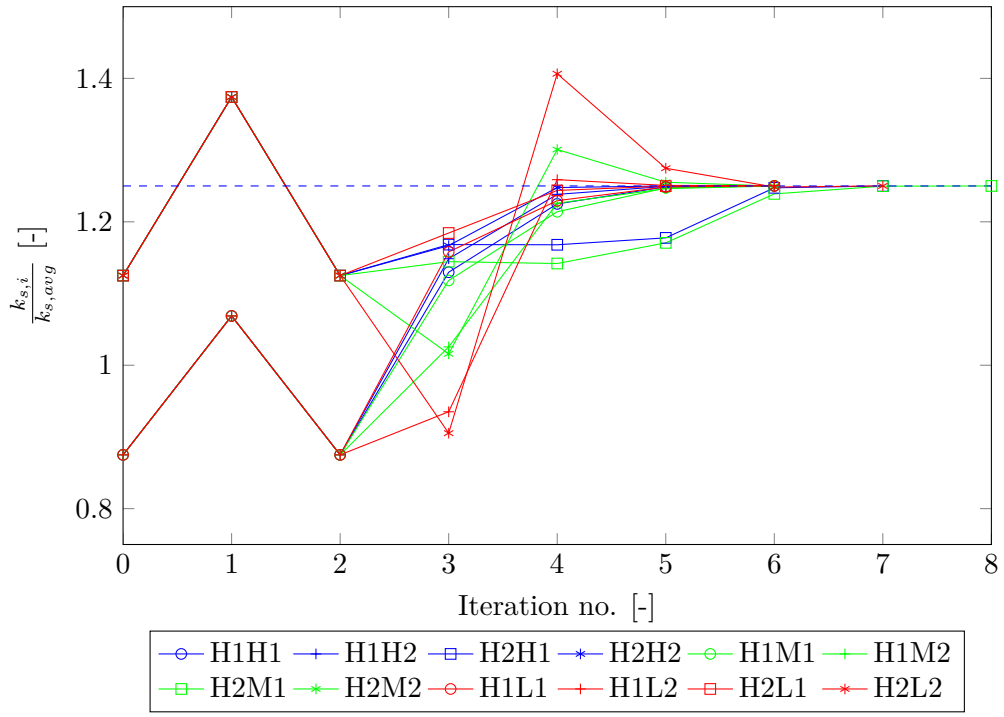

Figure 4-17: Convergence of the perturbed parameters from different starting points, three actual crest level values and one actual friction value (indicated with the dashed line) for the FaWc G1 scenarios.

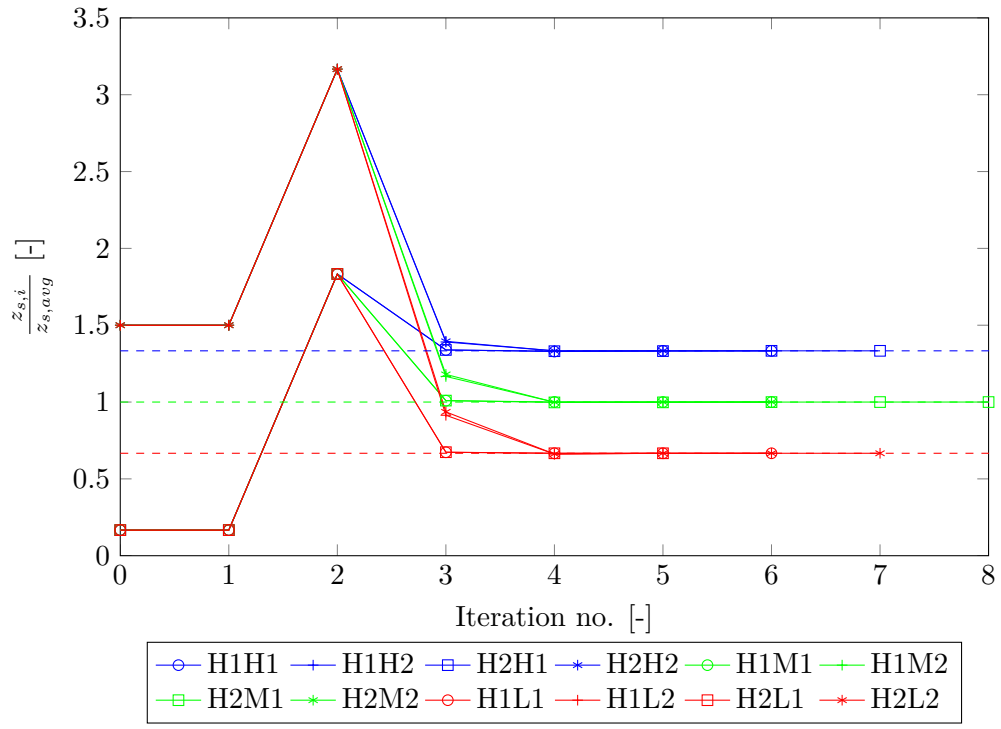

Figure 4-18: Convergence of the perturbed parameters from different starting points, three actual crest level values (indicated with the dashed lines) and one actual friction value for the FaWc G1 scenarios.

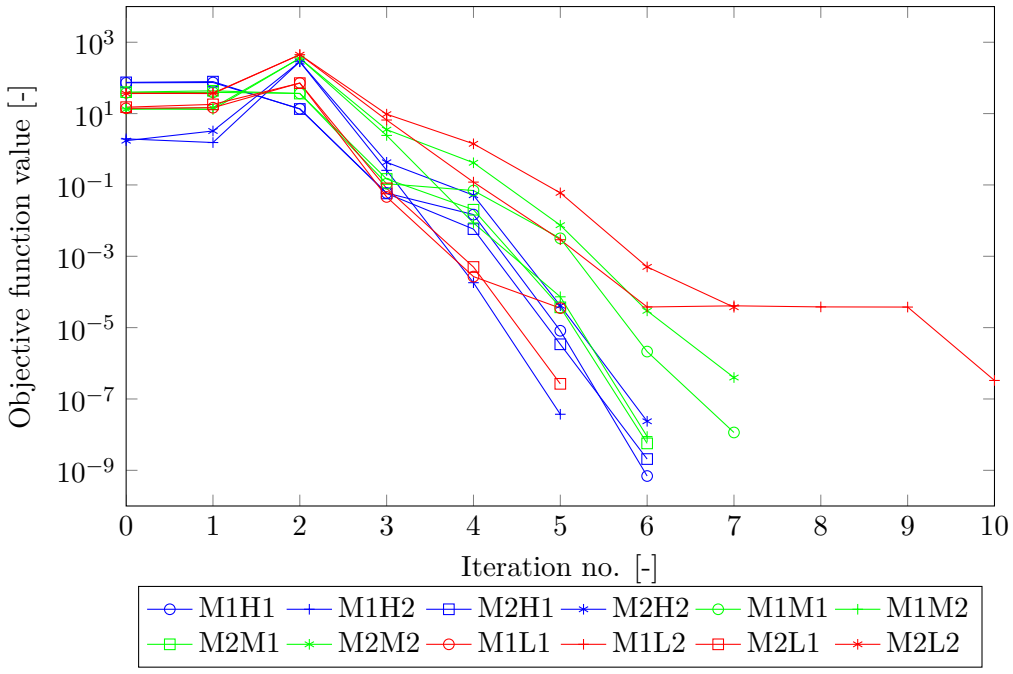

Figure 4-19: The cost function for the perturbed parameters for the FaWc group 2 (G2) scenarios with different starting points, three actual crest level values and one actual friction value.

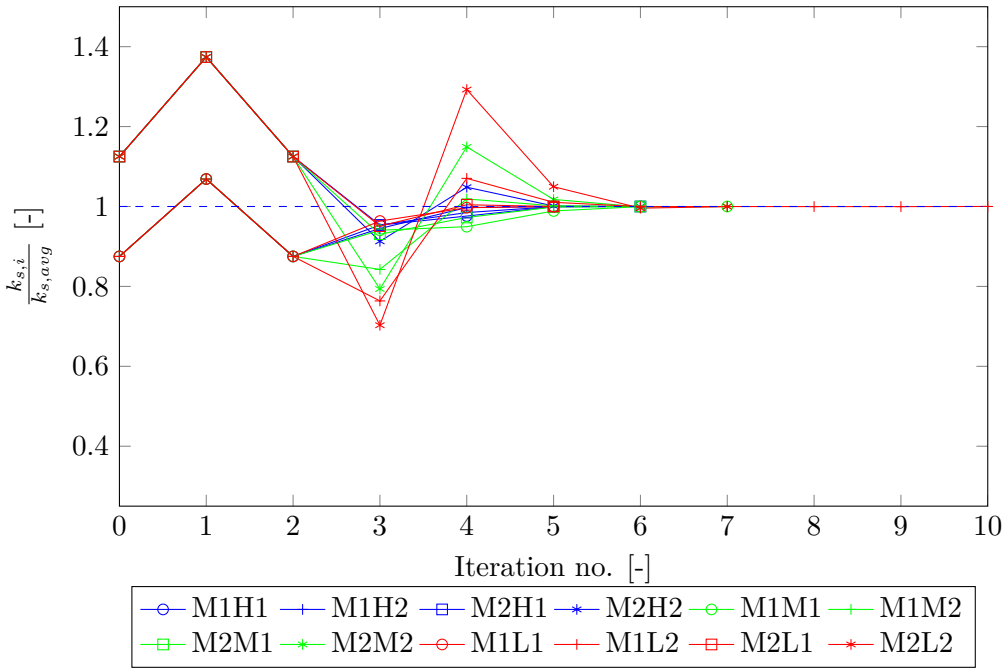

Figure 4-20: Convergence of the perturbed parameters from different starting points, three actual crest level values and one actual friction value (indicated with the dashed line) for the FaWc G2 scenarios.

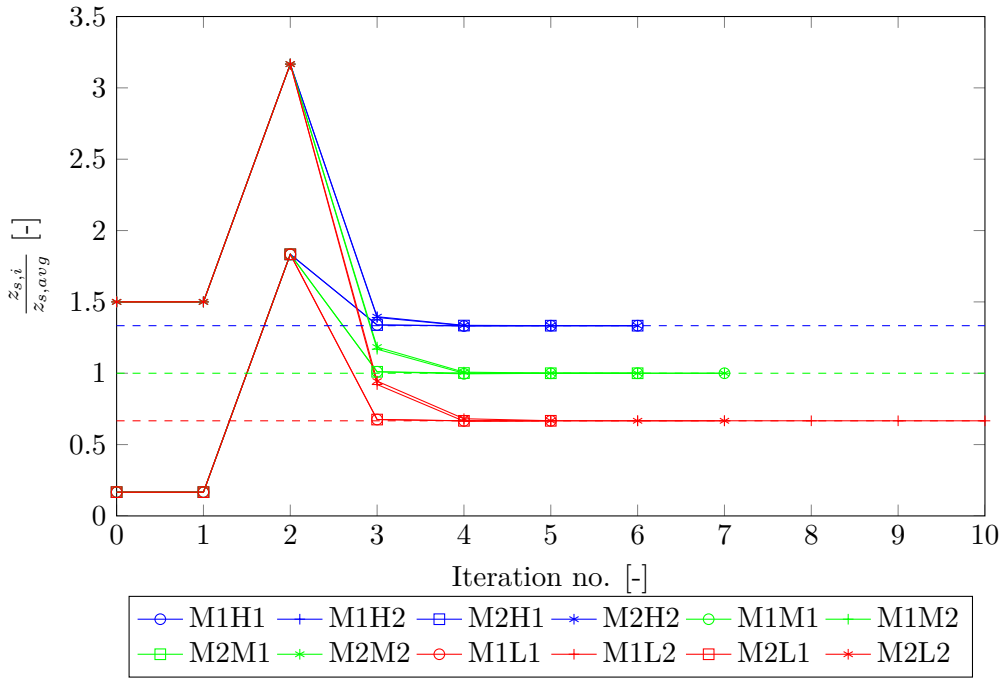

Figure 4-21: Convergence of the perturbed parameters from different starting points, three actual crest level values (indicated with the dashed lines) and one actual friction value for the FaWc G2 scenarios.

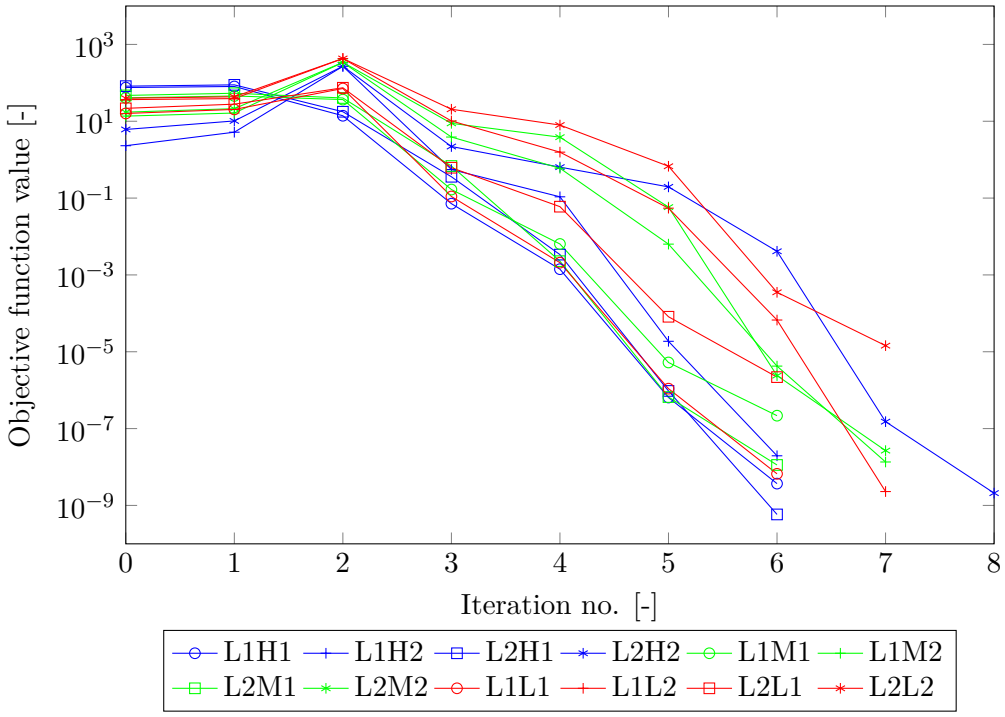

Figure 4-22: The cost function for the perturbed parameters for the FaWc group 3 (G3) scenarios with different starting points, three actual crest level values and one actual friction value.

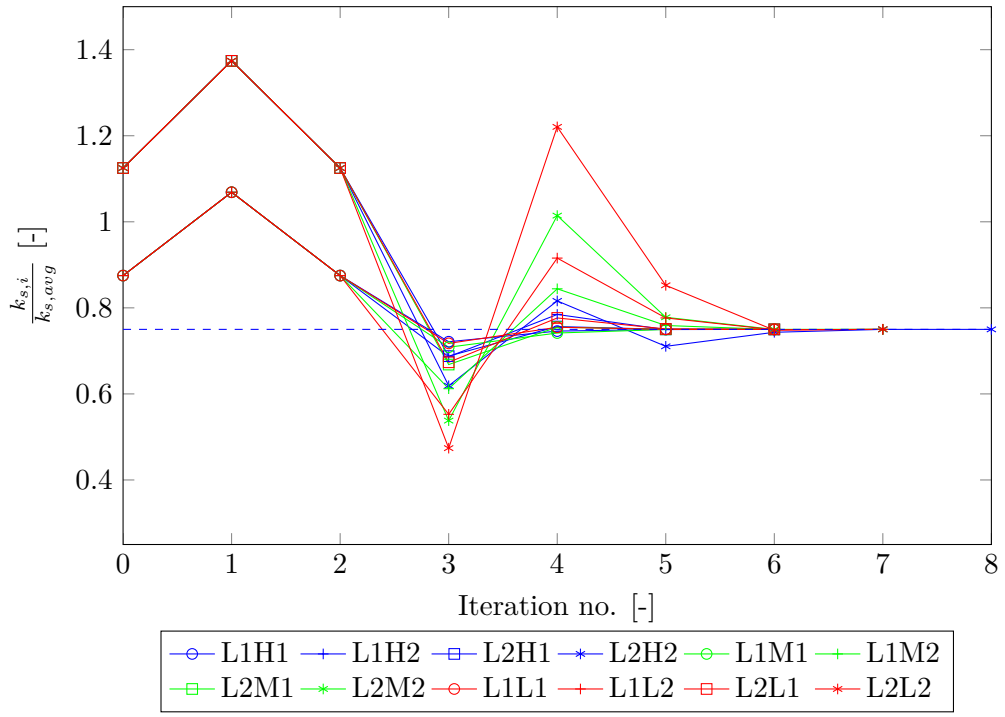

Figure 4-23: Convergence of the perturbed parameters from different starting points, three actual crest level values and one actual friction value (indicated with the dashed line) for the FaWc G3 scenarios.

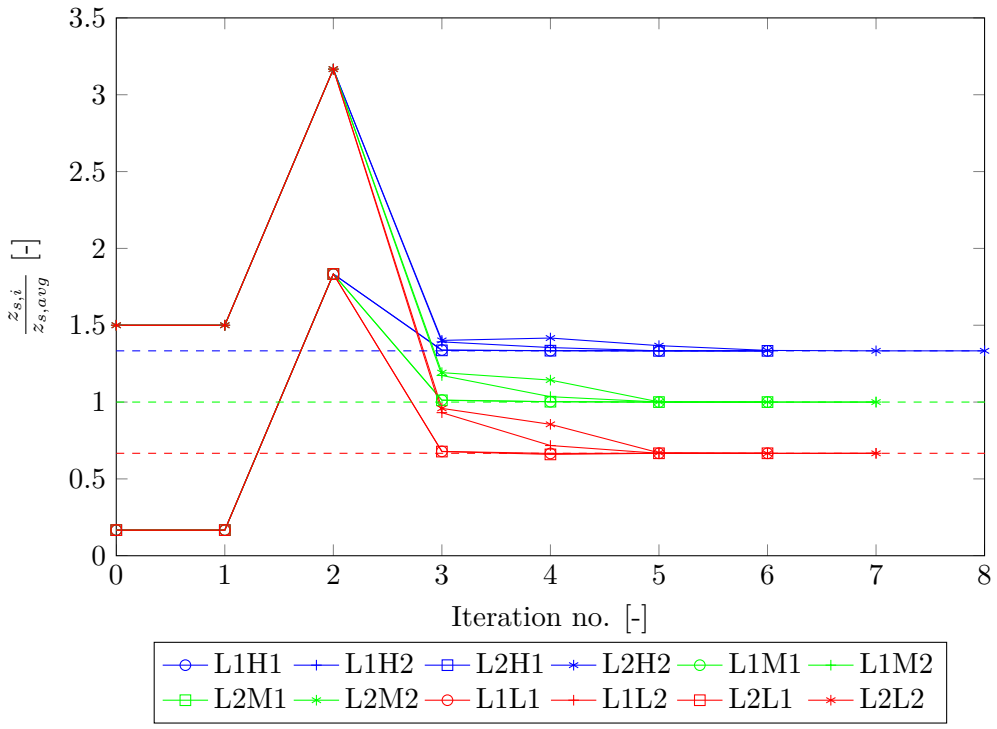

Figure 4-24: Convergence of the perturbed parameters from different starting points, three actual crest level values (indicated with the dashed lines) and one actual friction value for the FaWc G3 scenarios.

4-5-4-2 Residual analysis

In Figure 4-25, an example of a typical bias pattern for the FaWc scenarios as function of time is presented. The figures for the bias for all (other) FaWc scenarios at different measurement locations are presented in Appendix D No overall trend in the different scenarios was discovered, when comparing the bias with the model states (also presented in Appendix D) in both temporal and spatial scale. In other words, different initials parameter predictions or different actual parameter values do not contribute in a possible systematic error.

For the observed differences between the scenarios, no logical reason was found. Some scenarios show a similar pattern as the modelled states, indicating at a possible systematic modelling error, while other scenarios did not illustrate a significant temporal pattern. Nonetheless, according to the data presented in Table 4-8, the bias is for all scenarios within acceptable ranges and could therefore be recognised as insignificant.

Table 4-8: The residual statistics of base scenario FaWc. The total amount of iterations, the final cost, the final root-mean-square error (RMSE), the final bias and standard deviation of the errors (STD) are presented with their weighted dimensionless values. The values provide information of the complete study area, i.e. all measurement locations are incorporated.

Base scenario	Group	Scenario ID	Iterations	Cost [-]	RMSE [-]	BIAS [-]	STD [-]
FaWc	G1	H1H1	6	3.81E-008	7.84E-005	-2.16E-005	5.16E-005
		H1H2	6	4.13E-008	9.30E-005	-3.19E-005	8.36E-005
		H2H1	7	9.69E-008	1.44E-004	-8.56E-005	9.68E-005
		H2H2	5	1.79E-008	6.26E-005	1.75E-006	5.26E-005
		H1M1	6	3.83E-007	2.75E-004	1.56E-004	1.72E-004
		H1M2	6	7.99E-008	1.37E-004	-7.71E-007	1.14E-004
		H2M1	8	1.14E-008	5.74E-005	-1.45E-005	4.56E-005
		H2M2	6	3.52E-007	2.24E-004	-1.11E-004	1.40E-004
		H1L1	6	5.11E-008	9.52E-005	7.77E-005	3.43E-005
		H1L2	6	4.66E-006	8.18E-004	2.38E-004	4.12E-004
		H2L1	5	2.67E-007	1.69E-004	-1.06E-004	8.08E-005
		H2L2	7	2.42E-008	5.72E-005	4.54E-005	2.70E-005
	G2	M1H1	6	6.92E-010	7.89E-006	-6.41E-006	3.65E-006
		M1H2	5	3.73E-008	5.69E-005	-3.34E-005	2.44E-005
		M2H1	6	2.07E-009	1.33E-005	1.18E-005	2.85E-006
		M2H2	6	2.37E-008	4.62E-005	-3.74E-005	1.90E-005
		M1M1	7	1.15E-008	3.27E-005	-3.01E-005	5.68E-006
		M1M2	6	8.83E-009	2.99E-005	-2.46E-005	1.17E-005
		M2M1	6	5.69E-009	2.52E-005	7.04E-006	7.67E-006
		M2M2	7	3.99E-007	2.26E-004	-1.93E-004	5.14E-005
		M1L1	5	3.52E-005	9.27E-004	-3.63E-005	8.38E-004
		M1L2	10	3.31E-007	2.08E-004	1.78E-004	6.16E-005
		M2L1	5	2.66E-007	1.64E-004	9.61E-005	7.26E-005
		M2L2	7	3.73E-005	1.22E-003	-1.04E-004	9.51E-004
	G3	L1H1	6	3.70E-009	1.98E-005	2.30E-006	6.68E-006
		L1H2	6	1.96E-008	4.39E-005	-3.23E-005	2.29E-005
		L2H1	6	5.82E-010	6.15E-006	-5.04E-006	1.81E-006
		L2H2	8	2.09E-009	1.51E-005	7.86E-007	5.45E-006
		L1M1	6	2.17E-007	1.51E-004	5.17E-005	4.79E-005
		L1M2	8	1.35E-008	4.09E-005	-3.30E-005	1.49E-005
		L2M1	6	1.13E-008	4.27E-005	2.13E-005	3.16E-005
		L2M2	7	2.67E-008	6.76E-005	4.60E-005	3.87E-005
		L1L1	6	6.64E-009	2.34E-005	-2.06E-005	3.59E-006
		L1L2	7	2.30E-009	1.80E-005	-1.53E-005	5.65E-006
		L2L1	6	2.19E-006	5.64E-004	-3.71E-006	2.34E-004
		L2L2	7	1.44E-005	1.33E-003	1.04E-003	5.19E-004

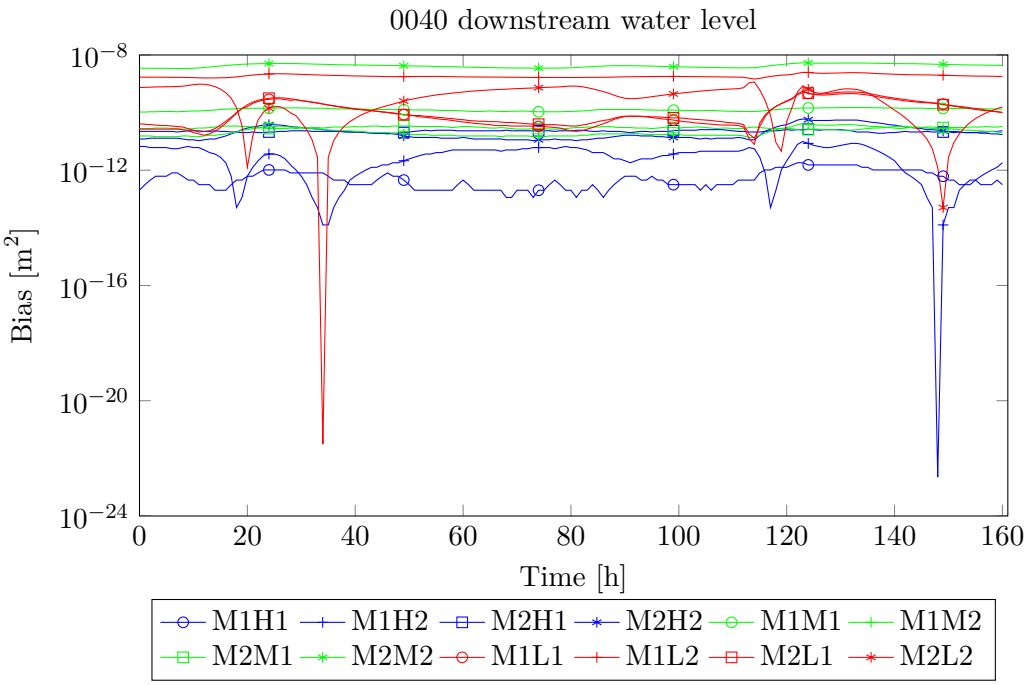

Figure 4-25: The bias for the downstream water level at location 0040 for the FaWc (G2) scenarios with different starting points, three actual crest level values and one actual friction value as function of time in the calibration windows (with a time window $T = 2$h).

4-5-5 Scenario FaWcP: global friction, clustered crest levels, extreme precipitation

4-5-5-1 Model performance

In Figure 4-27 and Figure 4-28[3], the converge of the friction and clustered crest level parameter, respectively, is illustrated for the scenarios of base scenario FaWcP (see Table 4-9). Only one scenario (L2H2) tends to need more iterations for correctly predicting the actual parameter values, although the other scenarios give comparable results when using low-intensity precipitation, e.g. in base scenario FaWc. Apparently, it is difficult for the DuD algorithm to predict the weir parameter for scenario L2H2 (see Figure 4-28). The reason for this is unknown, since for the previous base scenarios the L2H2 scenario did show a decrease in the convergence rate. No significant differences in convergence rate is noticed between the other scenarios that use different starting points and different actual parameter values. In other words, the effectiveness of the OPE tool is not dependent on the initial parameter prediction and on the actual parameter values.

[3]In the figures, the scenarios with different starting points are indicated with crosses, circles, squares and asterisks. The crosses and circles represent high and low starting points, respectively, for the weir parameter and a low starting point for the friction parameter. The squares and asterisks represent high and low starting points, respectively, for the weir parameter and a high starting point for the friction parameter. The blue lines represent the high scenarios for both the friction and weir parameter. The green lines represent the high scenarios for the friction parameter and the low scenarios for the weir parameter. The red lines represent the opposite of the green lines: low friction value scenarios and high weir parameter value scenarios. The scenarios for both low friction values and low weir parameter values are represented by the yellow lines.

In Figure 4-26[3], the decrease in cost as function of the iteration number is illustrated for each scenario. No significant differences with the base scenario FaWc with low-intensity precipitation is observed. Again, the low convergence rate of scenario L2H2 is observed. The final cost, however, of scenario L2H2 is comparable with the other scenarios. This indicates the robustness of the OPE tool is high, as it is not dependent on the initial parameter estimation or on the actual parameter values.

In Appendix E, the model performance for base scenario FaWcP, expressed in calibrated model states (i.e. water levels and discharges) compared with the observed data and the initial predicted states for different measurement locations is presented.

Table 4-9: The optimisation results for base scenario FaWcP. The twin parameter values represent the actual parameter values. The perturbed parameter values represent the initial predictions, while the calibrated parameters represent the final optimised predictions.

Base scenario	Scenario ID	Twin parameter value		Perturbed parameters		Parameter value	
		$k_{s,0}$ [$m^{1/3}.s^{-1}$]	$z_{s,c,0}$ [m]	$k_{s,0}$ [$m^{1/3}.s^{-1}$]	$z_{s,c,0}$ [m]	$k_{s,0}$ [$m^{1/3}.s^{-1}$]	$z_{s,c,0}$ [m]
FaWcP	H1H1	20	0.8	14	0.1	20.0000	0.8000
	H1H2	20	0.8	14	0.9	19.9859	0.7999
	H2H1	20	0.8	18	0.1	19.9994	0.8000
	H2H2	20	0.8	18	0.9	20.0025	0.8000
	H1L1	20	0.4	14	0.1	19.9999	0.4000
	H1L2	20	0.4	14	0.9	19.9997	0.4000
	H2L1	20	0.4	18	0.1	20.0000	0.4000
	H2L2	20	0.4	18	0.9	19.9997	0.4000
	L1H1	12	0.8	14	0.1	11.9999	0.8000
	L1H2	12	0.8	14	0.9	11.9998	0.8000
	L2H1	12	0.8	18	0.1	12.0011	0.7997
	L2H2	12	0.8	18	0.9	12.0011	0.8000
	L1L1	12	0.4	14	0.1	12.0000	0.4000
	L1L2	12	0.4	14	0.9	11.9997	0.4000
	L2L1	12	0.4	18	0.1	12.0000	0.4000
	L2L2	12	0.4	18	0.9	11.9999	0.4000

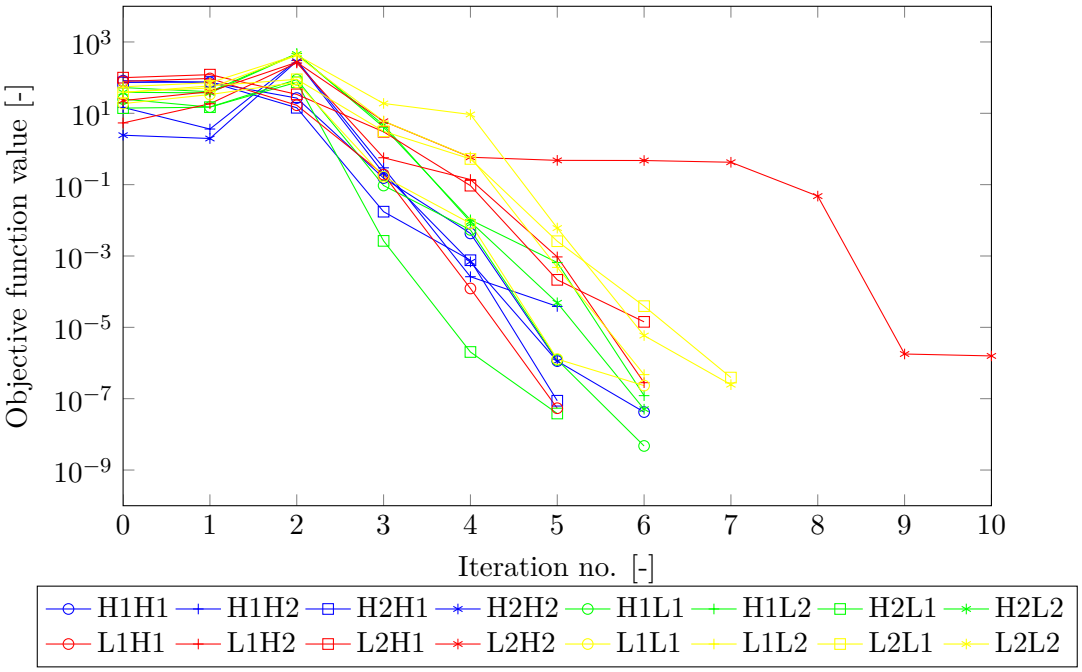

Figure 4-26: The cost function for the perturbed parameters for the FaWcP scenarios with different starting points, two actual crest level values and two actual friction values.

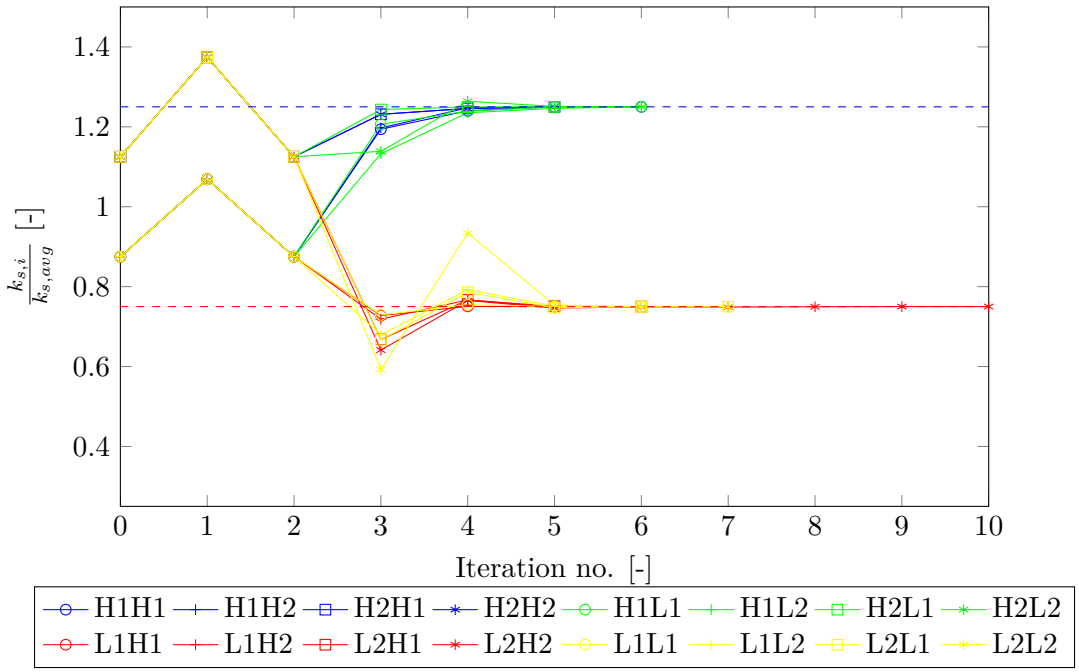

Figure 4-27: Convergence of the perturbed parameters from different starting points, two actual crest level values and two actual friction values (indicated with the dashed lines) for the FaWcP scenarios.

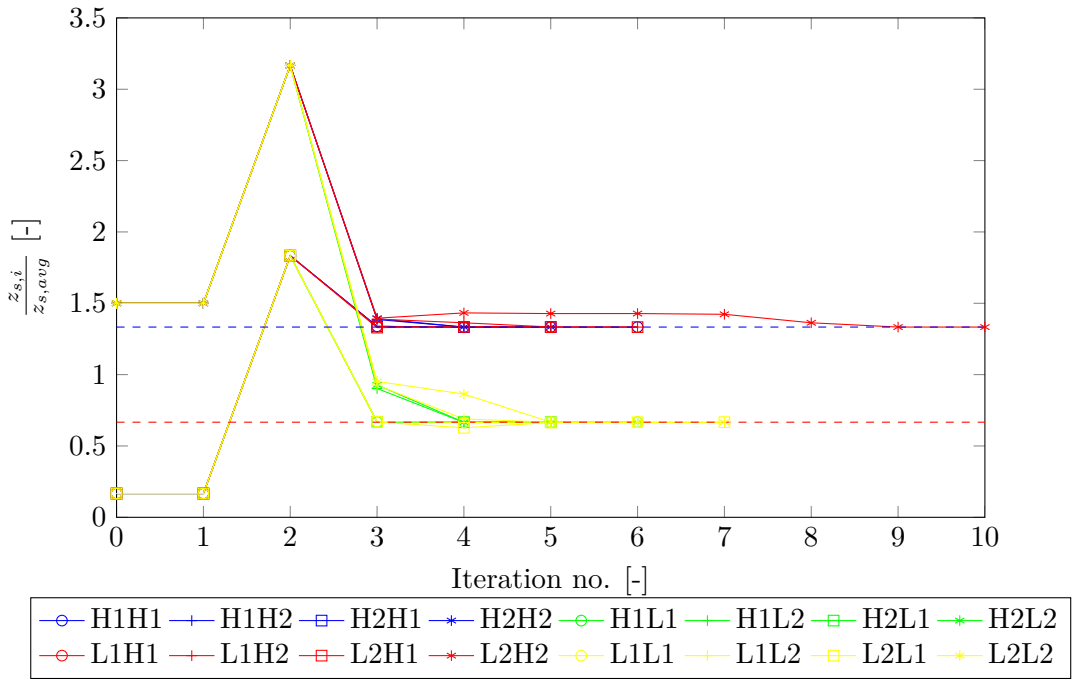

Figure 4-28: Convergence of the perturbed parameters from different starting points, two actual crest level values (indicated with the dashed lines) and two actual friction values for the FaWcP scenarios.

4-5-5-2 Residual analysis

An example of a typical bias pattern for the FaWcP scenarios as function of time is presented in Figure 4-29[3]. The bias for all other FaWcP scenarios at different measurement stations is illustrated in figures provided in Appendix E. As for the scenarios using low-intensity precipitation, the bias does not show an overall pattern for the FaWcP scenarios in both temporal and spatial scale. There is, however, a deviating pattern observed in the scenarios H2L1 and L1L1. Nevertheless, these two scenarios do not show a similar pattern as the observed states (see Figure E-19). The large shifts of the bias in time for these two scenarios have probably a numerical cause, since the values of the bias itself are rather low. Moreover, the observations are artificially created by using the model, so no systematic modelling error could be present in this data. The statistical data presented in Table 4-10 demonstrates that the bias for all scenarios is within acceptable ranges and could thus be recognised as insignificant.

Table 4-10: The residual statistics of base scenario FaWcP. The total amount of iterations, the final cost, the final root-mean-square error (RMSE), the final bias and standard deviation of the errors (STD) are presented with their weighted dimensionless values. The values provide information of the complete study area, i.e. all measurement locations are incorporated.

Base scenario	Scenario ID	Iterations	Cost [-]	RMSE [-]	BIAS [-]	STD [-]
FaWcP	H1H1	6	4.21E-008	9.48E-005	-3.81E-005	8.58E-005
	H1H2	5	3.86E-005	1.90E-003	-8.62E-004	1.03E-003
	H2H1	5	8.76E-008	1.23E-004	-5.12E-005	9.09E-005
	H2H2	5	1.12E-006	3.28E-004	2.16E-004	1.90E-004
	H1L1	6	4.73E-009	3.72E-005	-2.38E-007	2.64E-005
	H1L2	6	1.22E-007	1.85E-004	-6.32E-005	1.60E-004
	H2L1	5	3.84E-008	9.06E-005	-3.75E-005	8.21E-005
	H2L2	6	5.08E-008	1.32E-004	-9.02E-006	1.22E-004
	L1H1	5	5.40E-008	1.18E-004	-2.12E-005	1.04E-004
	L1H2	6	2.81E-007	2.43E-004	-5.25E-005	2.29E-004
	L2H1	6	1.43E-005	1.30E-003	1.05E-003	4.54E-004
	L2H2	10	1.58E-006	3.80E-004	2.54E-004	2.10E-004
	L1L1	6	2.32E-007	2.24E-004	4.47E-005	2.20E-004
	L1L2	6	4.73E-007	3.18E-004	-1.36E-005	2.99E-004
	L2L1	7	3.91E-007	2.95E-004	2.84E-005	2.92E-004
	L2L2	7	2.47E-007	2.39E-004	-1.11E-005	2.31E-004

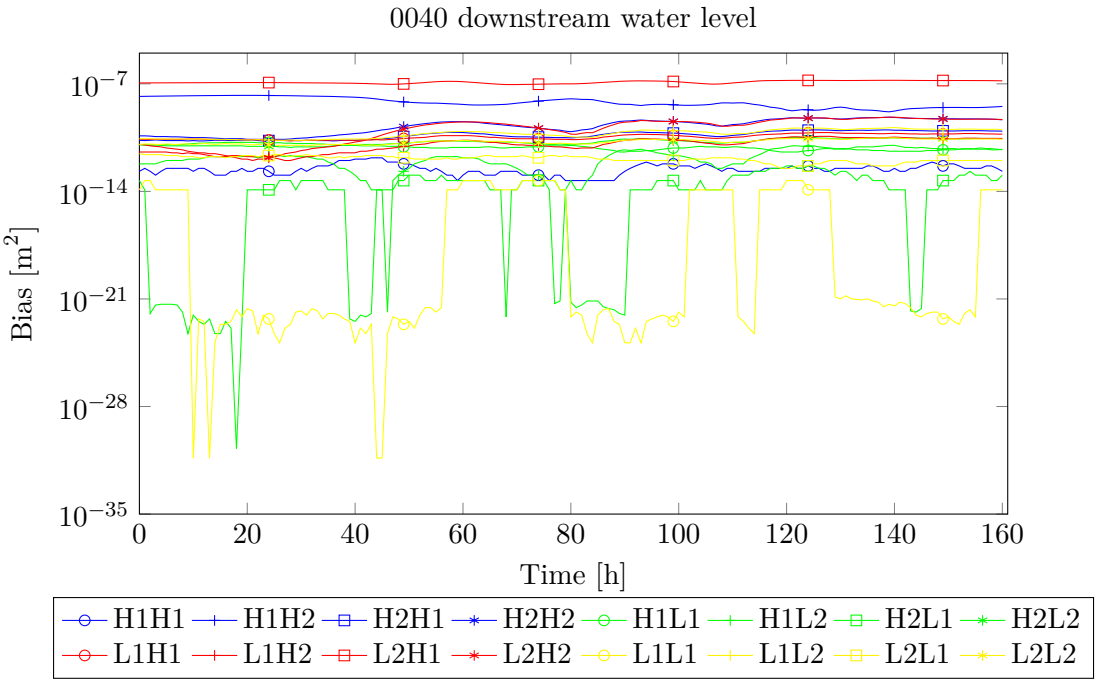

Figure 4-29: The bias for the downstream water level at location 0040 for the FaWcP scenarios with different starting points, two actual crest level values and two actual friction values as function of time in the calibration windows (with a time window $T = 2$h).

4-5-6 Scenario FaWcN: global friction, clustered crest levels, additive noise

4-5-6-1 Model performance

The convergence rates of the friction and clustered crest level parameter for the scenarios of base scenario FaWcN (see Table 4-9) are illustrated in Figure 4-31 and Figure 4-32[3], respectively. These figures clearly demonstrate the additive noise causes the OPE tool to execute more iterations for correct prediction of the actual parameters. As for the base scenario FaWcP with extreme precipitation, the scenario L2H2 requires significantly more iterations to estimate the actual parameter values. In fact, correct parameter estimations are already produced after ten iterations, but the DuD algorithm continues with the search to better predictions. Apparently, the stopping criteria are not yet satisfied up to that point and the DuD algorithm continues with converging of the predicted parameter values to the actual parameter values. Nonetheless, all scenarios converged still rather rapidly till accurate parameter predictions (see Table 4-9). This indicates that the effectiveness of the OPE tool is high regardless of the different scenarios.

The cost values of the FaWcN scenarios as function of the iteration number are illustrated in Figure 4-30[3]. Again, the larger number of required iterations for the base scenario FaWcN, compared with the noise-free FaWc scenarios, is demonstrated. Furthermore, the difficulty for the DuD algorithm to satisfy one of the stopping criteria for scenario L2H2 is observed. Nevertheless, all scenarios converge till an equal (low) value for the objective function. This demonstrates the robustness of the OPE tool is high and independent of the starting point and the actual parameter value, even when using data with additive noise. It should, however, be noted that there may be a reconsideration of the stopping criteria, when applying the OPE tool in the real world. The main reason for this is that the utilised stopping criteria in this thesis may be too strict to apply at data with a lot of noise, which is common for real world observations.

Appendix F provides the model performance for base scenario FaWcN by calibrated model states compared with the observed data and the initial predicted states for different measurement locations.

Table 4-11: The optimisation results for base scenario FaWcN. The twin parameter values represent the actual parameter values. The perturbed parameter values represent the initial predictions, while the calibrated parameters represent the final optimised predictions.

Base scenario	Scenario ID	Twin parameter value		Perturbed parameters		Parameter value	
		$k_{s,0}$ [$m^{1/3}.s^{-1}$]	$z_{s,c,0}$ [m]	$k_{s,0}$ [$m^{1/3}.s^{-1}$]	$z_{s,c,0}$ [m]	$k_{s,0}$ [$m^{1/3}.s^{-1}$]	$z_{s,c,0}$ [m]
FaWcN	H1H1	20	0.8	14	0.1	20.0331	0.7997
	H1H2	20	0.8	14	0.9	20.0728	0.8002
	H2H1	20	0.8	18	0.1	20.0048	0.8001
	H2H2	20	0.8	18	0.9	20.0768	0.7990
	H1L1	20	0.4	14	0.1	19.9611	0.4007
	H1L2	20	0.4	14	0.9	20.0400	0.4012
	H2L1	20	0.4	18	0.1	20.0653	0.4001
	H2L2	20	0.4	18	0.9	19.9633	0.3997
	L1H1	12	0.8	14	0.1	11.9851	0.8019
	L1H2	12	0.8	14	0.9	11.9860	0.8000
	L2H1	12	0.8	18	0.1	11.9957	0.7994
	L2H2	12	0.8	18	0.9	12.0100	0.7996
	L1L1	12	0.4	14	0.1	11.9780	0.3995
	L1L2	12	0.4	14	0.9	11.9832	0.4003
	L2L1	12	0.4	18	0.1	11.9836	0.4005
	L2L2	12	0.4	18	0.9	11.9793	0.4000

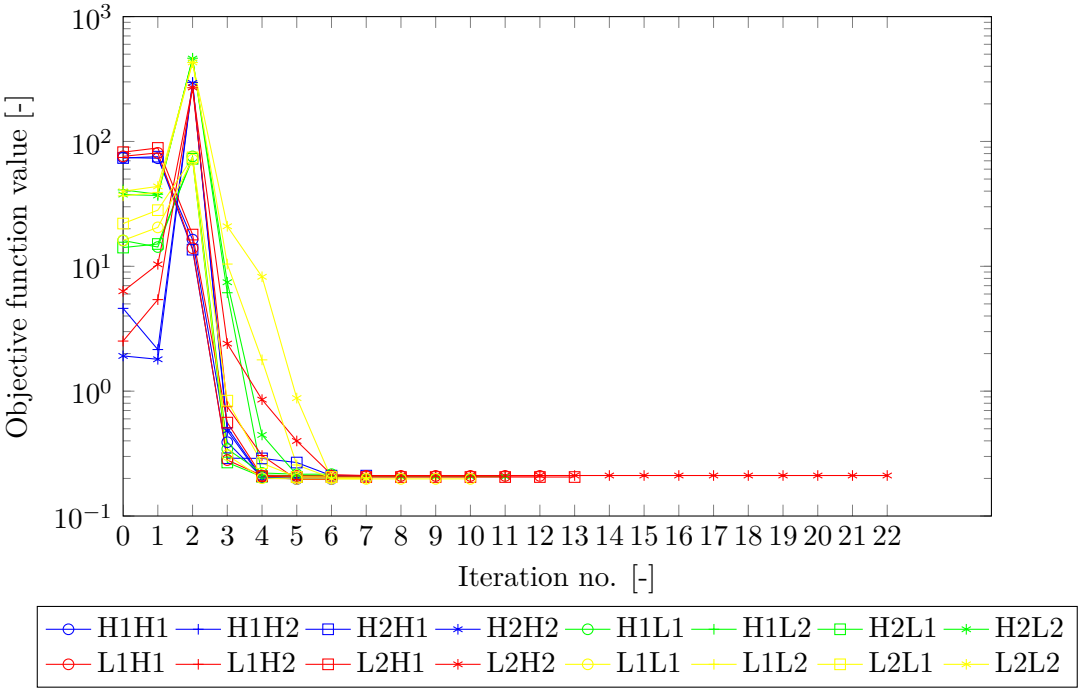

Figure 4-30: The cost function for the perturbed parameters for the FaWcN scenarios with different starting points, two actual crest level values and two actual friction values.

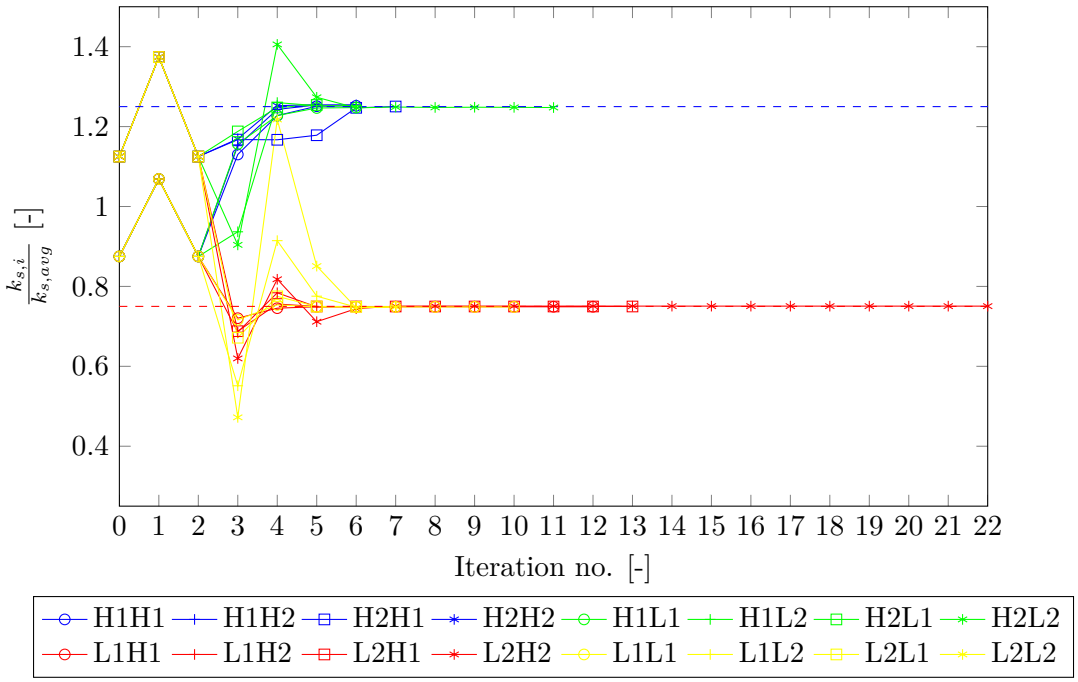

Figure 4-31: Convergence of the perturbed parameters from different starting points, two actual crest level values and two actual friction values (indicated with the dashed lines) for the FaWcN scenarios.

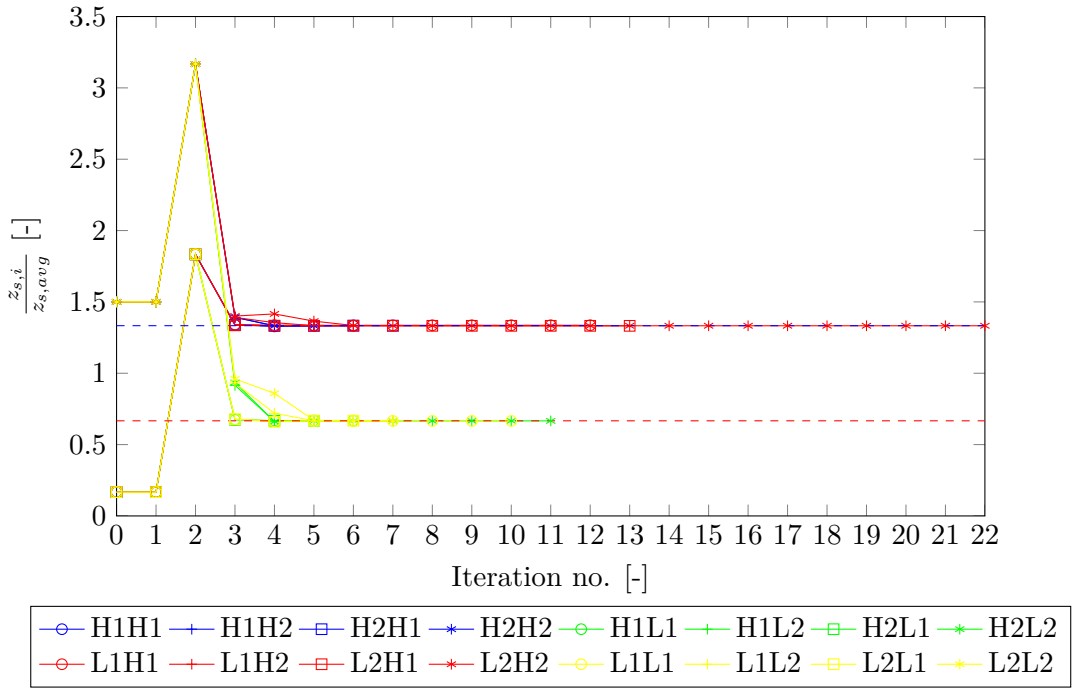

Figure 4-32: Convergence of the perturbed parameters from different starting points, two actual crest level values (indicated with the dashed lines) and two actual friction values for the FaWcN scenarios.

4-5-6-2 Residual analysis

In Figure 4-33[3], an example of a typical bias pattern for the FaWcN scenarios as function of time is illustrated. The bias for all other FaWcN scenarios, combined with the modelled states in comparison to the observed data, is presented in Appendix F. The bias is completely random for each scenario and is not comparable with the noise-free scenarios. Also, the values for the bias are significantly larger, as presented in Table 4-12. These effects demonstrate that the contribution of the measurement error in form of noise is much larger than the possible systematic modelling error.

Table 4-12: The residual statistics of base scenario FaWcN. The total amount of iterations, the final cost, the final root-mean-square error (RMSE), the final bias and standard deviation of the errors (STD) are presented with their dimensionless values. The values provide information of the complete study area, i.e. all measurement locations are incorporated.

Base scenario	Scenario ID	Iterations	Cost [-]	RMSE [-]	BIAS [-]	STD [-]
FaWcN	H1H1	6	1.98E-001	1.57E-001	2.83E-003	1.57E-001
	H1H2	6	2.01E-001	1.59E-001	-2.04E-003	1.59E-001
	H2H1	7	2.11E-001	1.59E-001	5.28E-004	1.59E-001
	H2H2	5	2.00E-001	1.57E-001	5.69E-003	1.57E-001
	H1L1	6	2.16E-001	1.62E-001	-1.95E-003	1.62E-001
	H1L2	6	2.10E-001	1.61E-001	1.59E-003	1.61E-001
	H2L1	5	2.06E-001	1.59E-001	-3.86E-004	1.59E-001
	H2L2	11	2.07E-001	1.60E-001	-4.89E-003	1.60E-001
	L1H1	12	2.10E-001	1.62E-001	7.51E-004	1.62E-001
	L1H2	6	1.96E-001	1.57E-001	-3.11E-003	1.57E-001
	L2H1	13	2.05E-001	1.60E-001	-1.80E-003	1.60E-001
	L2H2	22	2.11E-001	1.61E-001	3.44E-003	1.61E-001
	L1L1	10	1.98E-001	1.57E-001	9.20E-004	1.57E-001
	L1L2	7	2.02E-001	1.56E-001	-3.96E-003	1.56E-001
	L2L1	6	2.05E-001	1.58E-001	-3.35E-003	1.58E-001
	L2L2	7	1.99E-001	1.59E-001	3.28E-003	1.59E-001

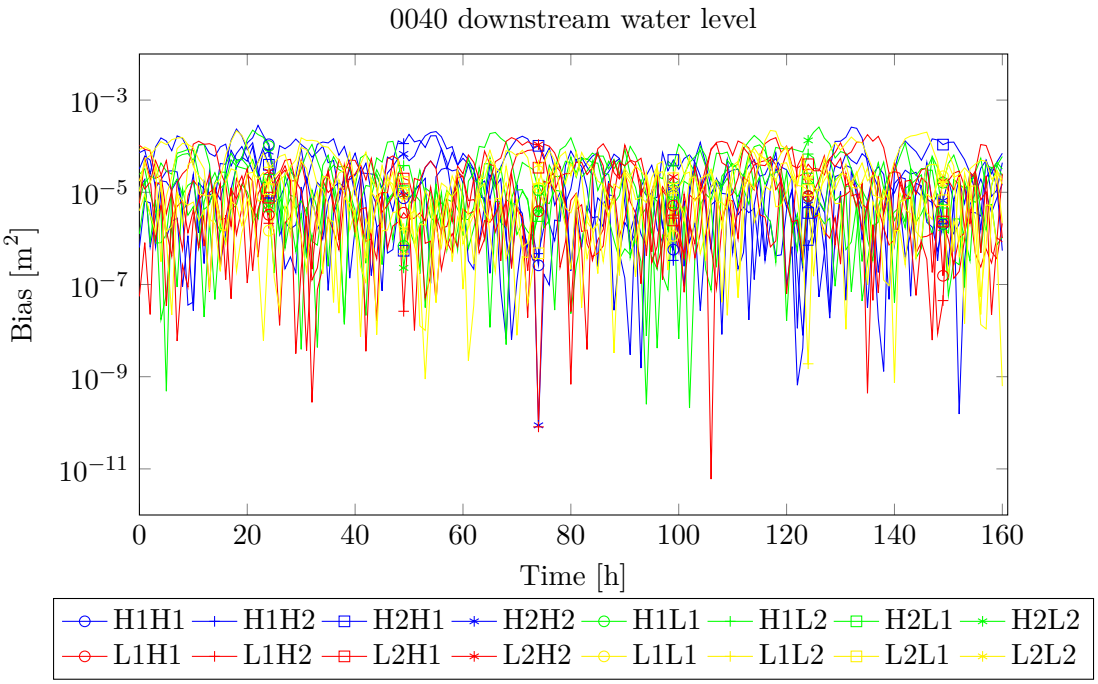

Figure 4-33: The bias for the downstream water level at location 0040 for the FaWcN scenarios with different starting points, two actual crest level values and two actual friction values as function of time in the calibration windows (with a time window $T = 2$h).

Chapter 5

Implementation of on-line parameter updating in water resources management

5-1 Introduction

The previous chapter demonstrated that On-line Parameter Estimation (OPE) tool can be applied to improve the performance of Decision Support System (DSS). The practical implications of implementing the OPE tool in DSS are, however, not yet highlighted. In this chapter, these implications are discussed with respect to both *global* and *local* transitions in parameter values. In the global transitions, the parameters values of the global friction parameter or the crest levels of all weirs are changed. The local transitions only alter the friction parameter of a single section or the crest level of a single weir.

As mentioned in Chapter 2, the friction parameter and crest levels change due to human interaction with the water system. The change in the bed friction is mainly induced by pruning or removing vegetation. According to [13],[14], the maintenance of vegetation in the river network is primarily executed in fall of the year. At this moment of the year, also the crest levels of the weirs are lowered. Both measures are executed in order to guarantee a certain conveyance capacity that is needed to get rid of excessive precipitation. The observational data used during the experiments is similar to the data used in the previous chapter. The moment of the parameter transitions is set at the 1st of November 2010.

First of all, it is investigated whether the OPE tool can capture the parameter values prior and posterior to global and local transitions. Also, the differences with the observations and original DSS is analysed. The scenarios that are applied for the analyses are described in Section 5-2, whereas the analyses of the results are provided in Section 5-3.

5-2 Scenarios

5-2-1 Global parameter transitions

In this section, the practical implications of using the OPE tool during a *global* transition in parameter values are determined. For this thesis, this means that the consequences for the model performance of changing either the global friction parameter or the crest levels of all weirs are determined. This analysis is executed for the period between two weeks prior to and two weeks posterior to the transition itself (e.g. see Figure 5-4). These results are compared with the results of the original DSS. The global friction parameter was already utilised by the DSS developed by Witteveen+Bos (W+B). Before the start of this thesis, the global friction parameter was fixed at $k_s = 16\ \mathrm{m^{1/3}\,s^{-1}}$. However, when implementing the advices for vegetation pruning of water board De Dommel, [13],[14], it is very well possible that the friction parameter increases to $k_s = 25\ \mathrm{m^{1/3}\,s^{-1}}$, [58]. This statement is based on the assumption that excessive vegetation is removed in the fall of the year, [13],[14] . This global transition is applied at the practical implication scenario PI-Fg.

Next to the global friction parameter, the clustered weir parameter is introduced in during this thesis. The original model, however, contains crest levels that do not correspond with an overall clustered value. Therefore, the practical implications caused by using the clustered weir parameter are determined differently. This implies that the observational data is determined by the configuration of the weirs that is also applied to the original DSS (see see Table 5-1). The global transition is introduced by reducing the weirs' crest levels with 15 cm (see Table 5-3). The practical implications of this global transition are determined by assigning this transition to scenario PI-Wg.

For both the changed global friction parameter and the clustered weir parameter, the practical implications are visualised by two plots. The first plot illustrates the predicted water levels in time during the transition phase (two weeks prior and posterior to the transitions) by the original DSS and the OPE tool. The water levels of some locations are visualised that are affected highly by the parameter changes. The up- and downstream water levels at weir ZL1-5930 are used for visualisation of the changes in water levels induced by the global transitions. The second plot visualises the average error in time for the complete study area that is caused by using the original DSS and the OPE tool.

5-2-2 Local parameter transitions

In the previous section, the methods for determining the practical implication of using the OPE tool during global transitions in parameter values are described. This section focuses on the methodology of determining the practical implications during *local* transitions in parameter values. This means that either the friction of one section or the crest level of one weir is changed, which causes local changes in the observational data. The OPE tool, on the other hand, persists with using the global friction and clustered weir parameter. The original DSS continues with using the fixed global friction $k_s = 16\ \mathrm{m^{1/3}\,s^{-1}}$ and fixed crest levels according Table 5-4.

The first scenario for local transition in parameter values concerns changing the friction of canal section Nriv_ZL_1_9820, which is illustrated in Figure 5-1. In this scenario, called PI-

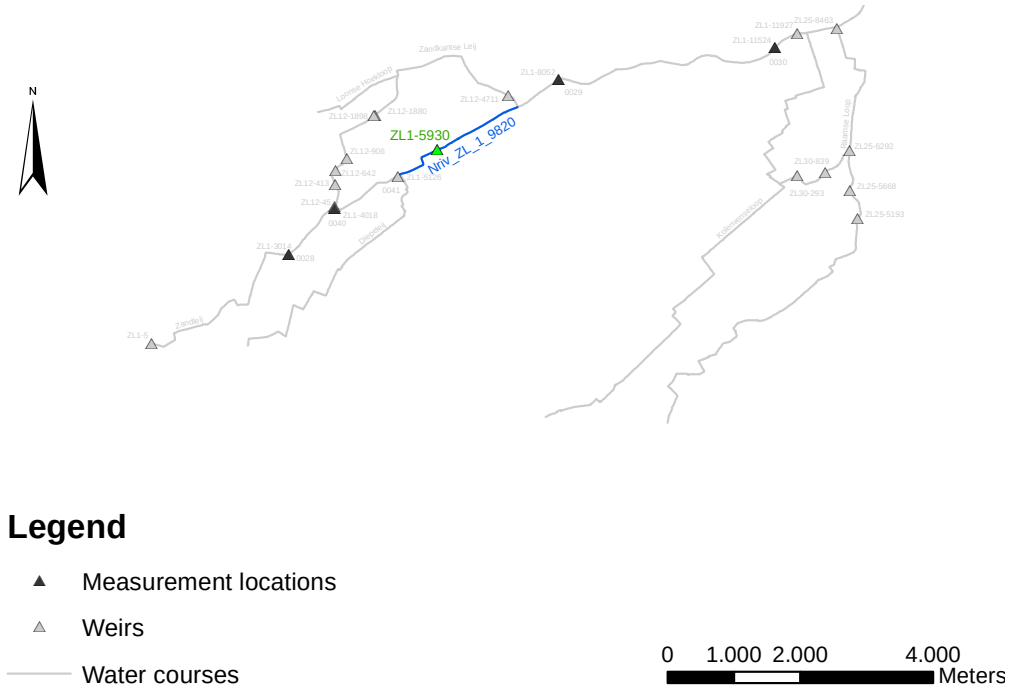

Figure 5-1: A graphical interpretation of locations where the local transition were assigned to. The green triangle (weir ZL1-5930) represents the location where the transition of a single weir is introduced for scenario PI-WI. The blue line (section Nriv_ZL_1_9820) represents the section where the transition of a single section is introduced for scenario PI-FI.

Fl, the friction parameter is changed to $k_{s,Nriv\_ZL\_1\_9820} = 25\ \mathrm{m}^{1/3}\,\mathrm{s}^{-1}$. The second scenario, called PI-Wl, implements the local transition of one weir's crest level. The crest level of weir ZL1-5930 (see Figure 5-1) is decreased 15 cm from its original level (see Table 5-5). The results are compared with the results of the original DSS and the observations: one figure illustrates the predicted water in time during the local transition by the original DSS and the OPE tool, whereas the second figure illustrates the average error induced by using the original DSS and the OPE tool.

5-3 Results and discussion

5-3-1 Scenario PI-0: situation prior to transitions

In Figure 5-2 and Figure 5-3, the average error in the predicted water levels, $\Delta\hat{y}_{avg}$ [m], with the observational data per calculation point is given for the original DSS and the OPE tool, respectively. The average error of the DSS is 0 m, since the settings of the model are completely similar to those used to obtain the artificial data (see Table 5-1). This is why there are no colours observed in Figure 5-2. The OPE tool, however, estimated the crest levels and friction at different values (see Table 5-1). The friction is predicted rather accurate, but the crest levels are not all near to the actual crest levels. These deviations in crest levels are caused by the fact that the OPE tool uses the clustered weir parameter instead of decoupled crest levels, which are applied to obtain the artificial data. Therefore, the error is largest

near the weirs with the adjustable crest levels. The negative errors are obtained when the crest level determined by the OPE tool is lower compared to the actual crest level. Positive errors are caused by higher predicted crest levels by the OPE tool compared to the actual crest levels.

In Figure 5-4, an example of the water level predictions by the original DSS and the OPE tool prior to the transition is illustrated by the left blue line. Also here the similar predictions by the original DSS compared with the measurement data is observed. As described above, the OPE tool provided accurate predictions as well.

Table 5-1: The crest levels and (global) bed friction of the DSS and the OPE tool prior to the transitions compared to those used to obtain the observational data (True).

Parameter	ID	True I [m]	DSS [m]	OPE I [m]
W1	ZL1-5	10.82	10.82	10.83
W2	ZL1-3014	10.45	10.45	10.46
W3	ZL1-5126	8.40	8.40	8.10
W4	ZL1-5930	7.14	7.14	7.15
W5	ZL12-45	9.15	9.15	9.24
W6	ZL12-1880	7.20	7.20	7.37
W7	ZL12-4711	6.75	6.75	6.59
W8	ZL25-6292	5.78	5.78	5.85
W9	ZL25-8463	4.60	4.60	4.77
FA	Global friction	16.00	16.00	16.16
F1	Nriv_ZL_1_9820	-	-	-

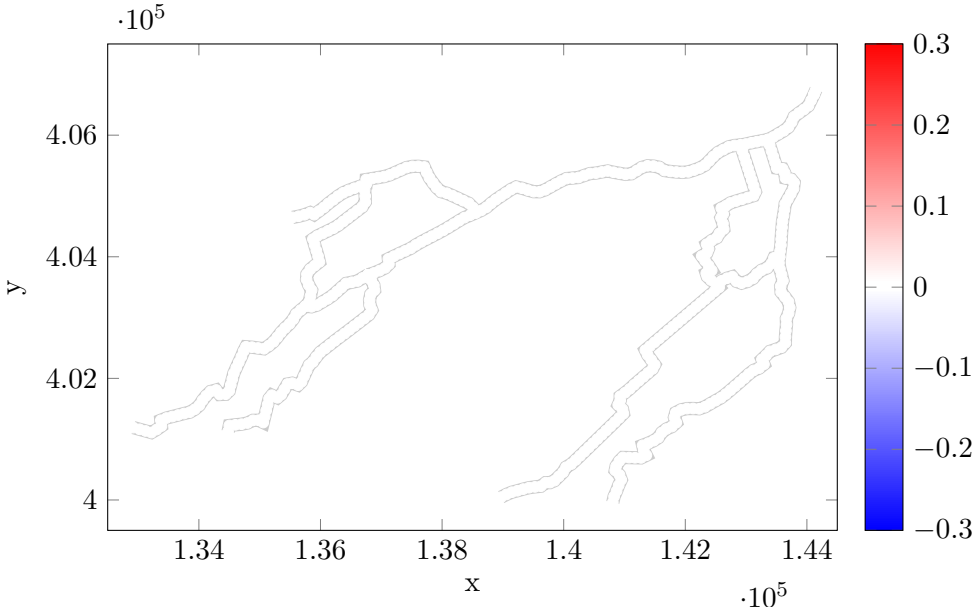

Figure 5-2: The average error in water level $\Delta\hat{y}_{avg}$ [m] with the observational data per calculation point for the original DSS prior to the transitions. The predictions were obtained after 8 iterations.

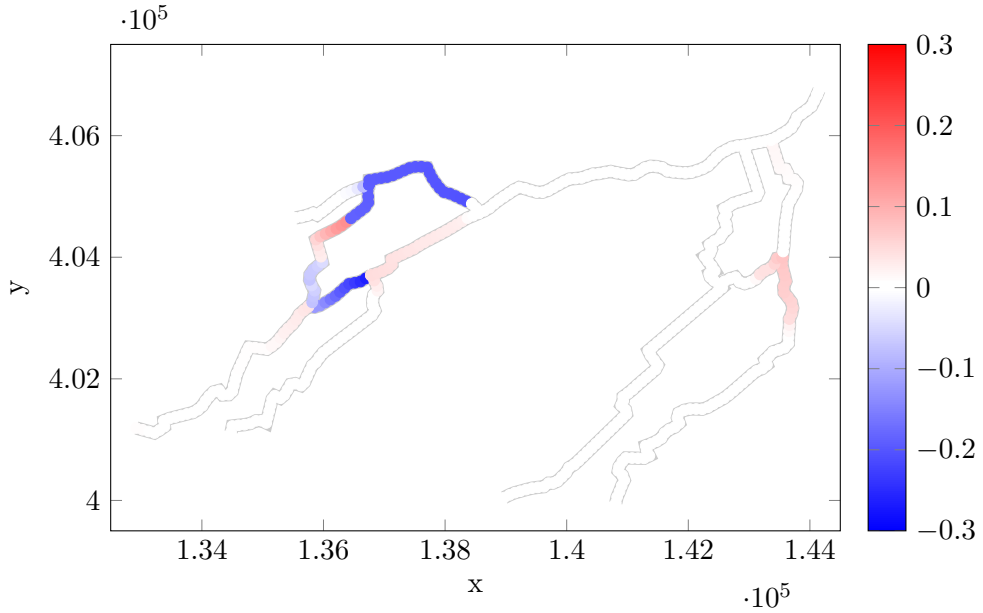

Figure 5-3: The average error in water level $\Delta\hat{y}_{avg}$ [m] with the observational data per calculation point for the OPE tool prior to the transitions. The predictions were obtained after 8 iterations.

5-3-2 Scenario PI-Fg: transition in global friction

In Table 5-2, the predicted crest levels and bed friction by the OPE tool after a transition in global friction are presented. The bed friction is estimated rather accurate. The crest levels, however, vary significantly from the actual crest levels. The reason for this is the use of clustered crest levels by the OPE tool. The parameter W2 is estimated the most accurate, since the clustered weir parameter is most sensitive to the observations obtained nearby this parameter. This results overall in small average errors with the observations, while nearby the adjustable weirs the largest average errors are observed (see Figure 5-6). The water level predictions at weir ZL1-5930 are very accurate (see Figure 5-4[4]), but this is due to its location rather than the overall performance of the OPE tool.

The original DSS showed an overestimation of the water levels for almost the complete river network. This overestimation is induced by the lower Strickler roughness value, which represents a higher bed frictions, and is illustrated in Figure 5-4[4] and Figure 5-5.

[4]The transition in global friction is initiated at the 1st of November 2010 and is indicated with the dashed black line.

Table 5-2: The crest levels and (global) bed friction of the DSS and the OPE tool posterior to the transition of global friction compared to those used to obtain the observational data (True).

Parameter	ID	True II (PI-Fg) [m]	DSS [m]	OPE II (PI-Fg) [m]
W1	ZL1-5	10.82	10.82	10.83
W2	ZL1-3014	10.45	10.45	10.46
W3	ZL1-5126	8.40	8.40	8.10
W4	ZL1-5930	7.14	7.14	7.15
W5	ZL12-45	9.15	9.15	9.24
W6	ZL12-1880	7.20	7.20	7.37
W7	ZL12-4711	6.75	6.75	6.59
W8	ZL25-6292	5.78	5.78	5.85
W9	ZL25-8463	4.60	4.60	4.77
FA	Global friction	25.00	16.00	25.24
F1	Nriv_ZL_1_9820	-	-	-

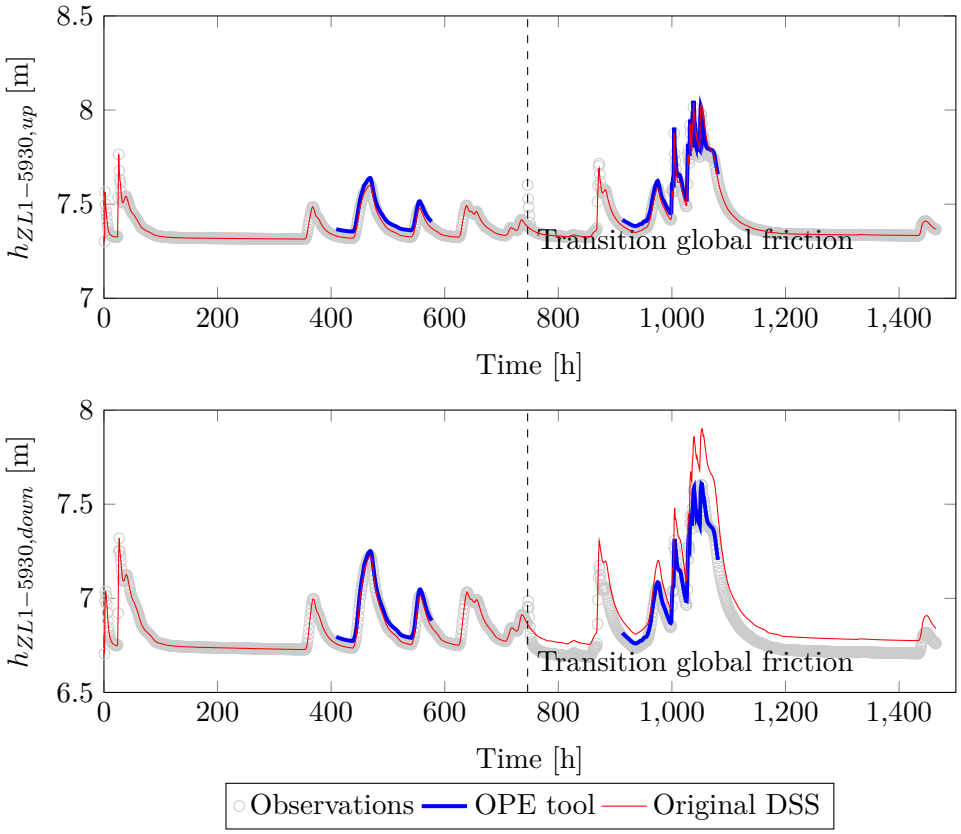

Figure 5-4: The up- and downstream water level predictions [m] at weir ZL1-5930 for the original DSS (red line) and the OPE tool (blue line) compared with the observational data (grey circles).

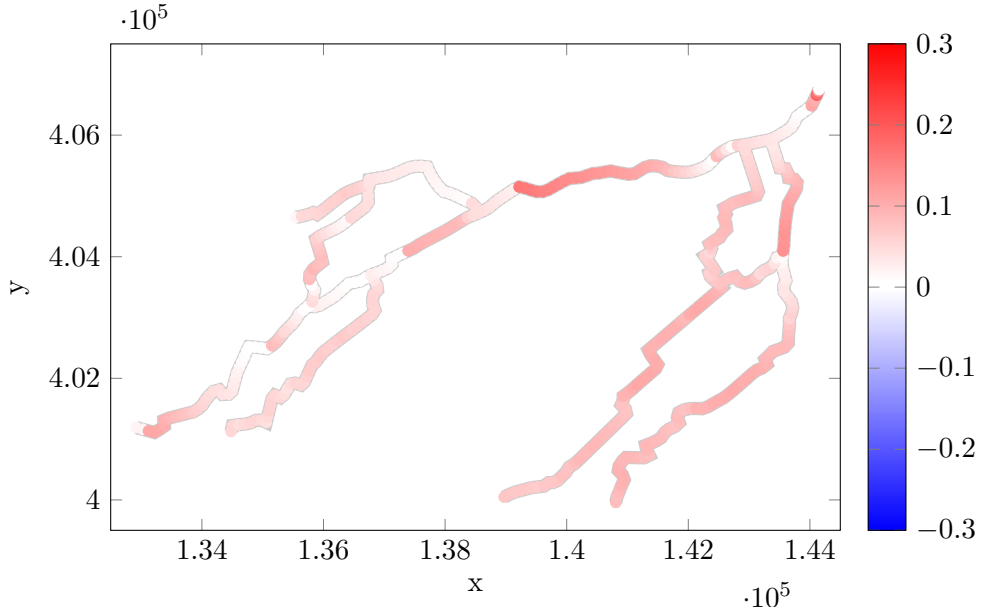

Figure 5-5: The average error in water level $\Delta\hat{y}_{avg}$ [m] with the observational data per calculation point for the original DSS posterior to the transition of global friction. The predictions were obtained after 8 iterations.

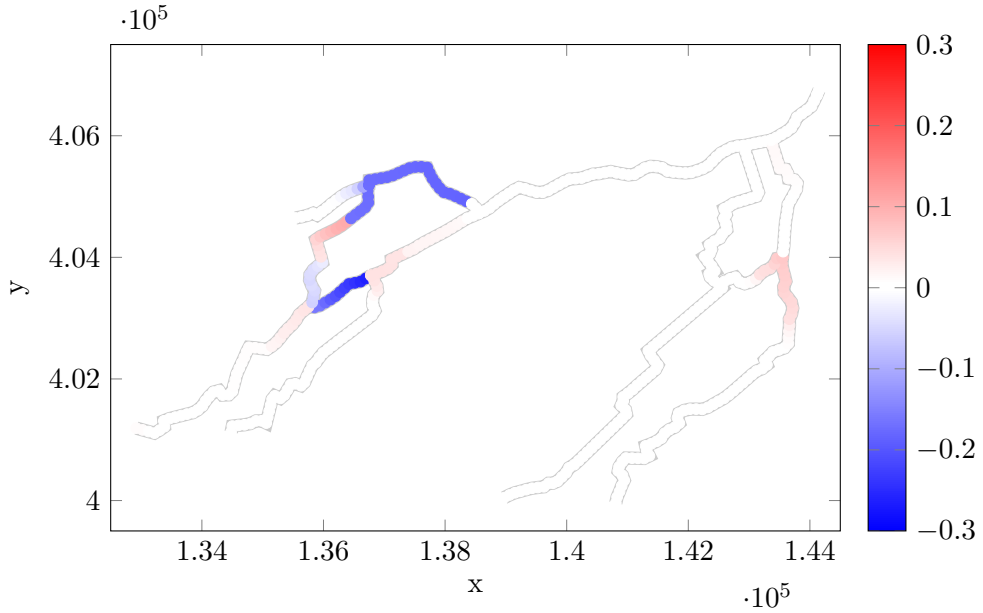

Figure 5-6: The average error in water level $\Delta\hat{y}_{avg}$ [m] with the observational data per calculation point for the OPE tool posterior to the transition of global friction. The predictions were obtained after 8 iterations.

5-3-3 Scenario PI-Wg: transition in crest levels of all weirs

The predicted crest levels and global bed friction parameter by the OPE tool posterior to the transition in all crest levels are presented in Table 5-3. Again, the bed friction is estimated accurately. Furthermore, the clustered weir parameter is optimised such that the weir parameter W2 equals the actual parameter value of that weir (ZL1-3014). The main reason for this is provided in Section 4-5-1, where it was demonstrated that the clustered weir parameter is mainly affected by the observations nearby located by weir parameter W2. As result of this, the other weir parameters deviated from the actual values. In other words, accurate water level predictions by the OPE tool are observed for the complete system (see Figure 5-7[4]), but nearby the adjustable weirs discrepancies with the observational data are observed. These discrepancies, in the form of average water level errors, are illustrated in Figure 5-9.

The prediction of the original DSS are somewhat worse than the OPE tool, demonstrated in Figure 5-7[4]. For the original DSS, none of the crest levels follow the decrease in the actual crest levels, while for the OPE tool at least some crest levels do. The effect of these fixed crest levels for the original DSS is illustrated in Figure 5-8, where nearby every adjustable weir large discrepancies with the observations are noticed.

Table 5-3: The crest levels and (global) bed friction of the DSS and the OPE tool posterior to the transition of all crest levels compared to those used to obtain the observational data (True).

Parameter	ID	True II (PI-Wg) [m]	DSS [m]	OPE II (PI-Wg) [m]
W1	ZL1-5	10.67	10.82	10.60
W2	ZL1-3014	10.30	10.45	10.30
W3	ZL1-5126	8.25	8.40	7.93
W4	ZL1-5930	6.99	7.14	7.07
W5	ZL12-45	9.00	9.15	9.10
W6	ZL12-1880	7.05	7.20	7.22
W7	ZL12-4711	6.60	6.75	6.42
W8	ZL25-6292	5.63	5.78	5.68
W9	ZL25-8463	4.45	4.60	4.62
FA	Global friction	16.00	16.00	16.09
F1	Nriv_ZL_1_9820	-	-	-

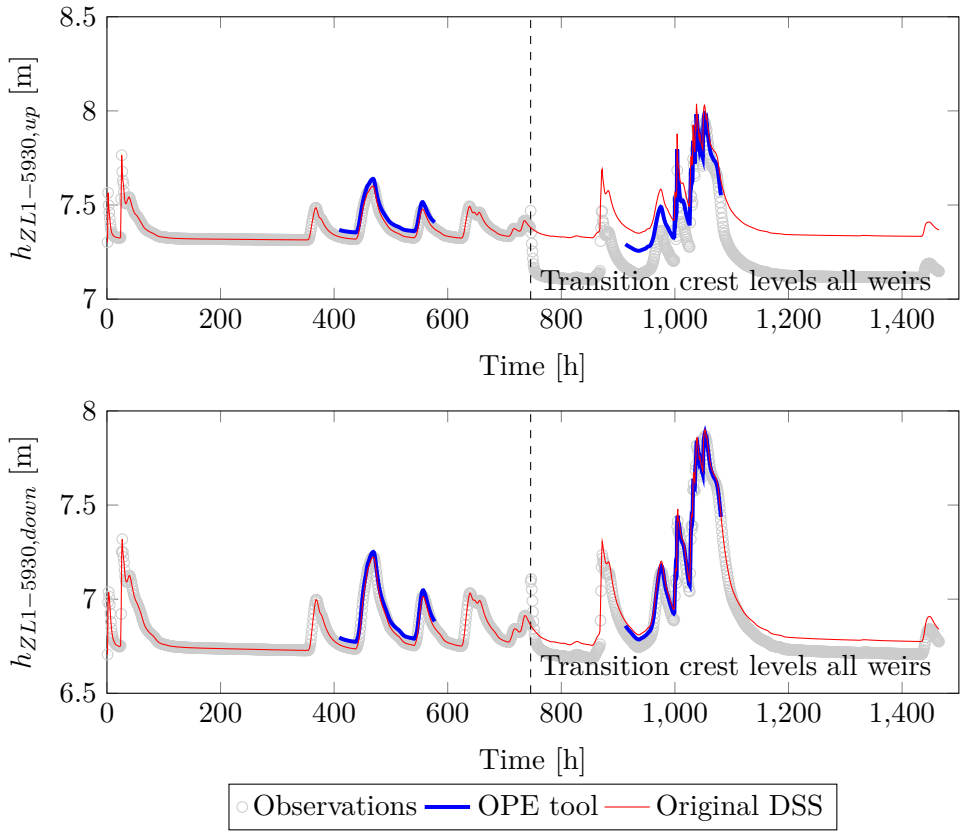

Figure 5-7: The up- and downstream water level predictions [m] at weir ZL1-5930 for the original DSS (red line) and the OPE tool (blue line) compared with the observational data (grey circles).

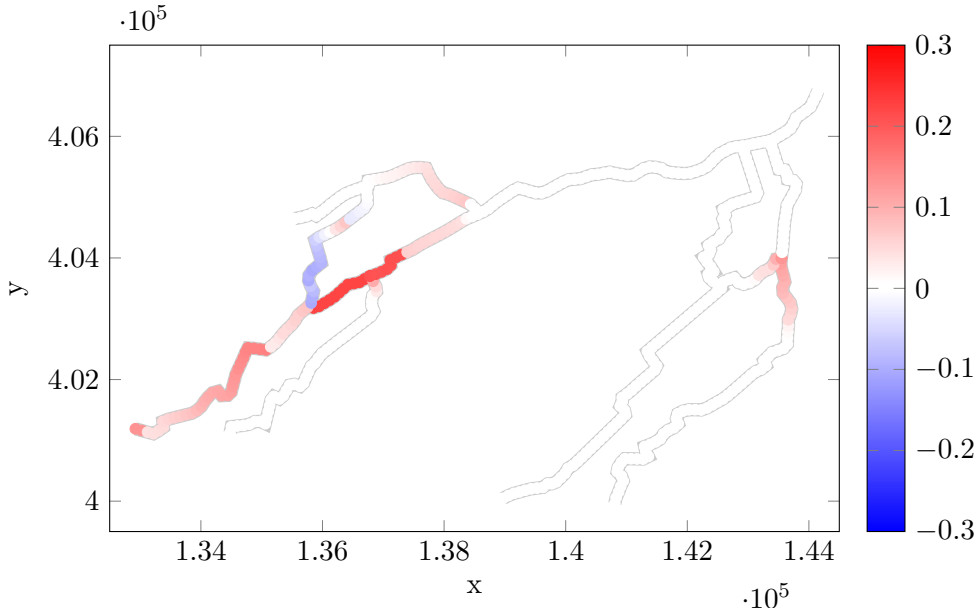

Figure 5-8: The average error in water level $\Delta\hat{y}_{avg}$ [m] with the observational data per calculation point for the original DSS posterior to the transition of all crest levels. The predictions were obtained after 8 iterations.

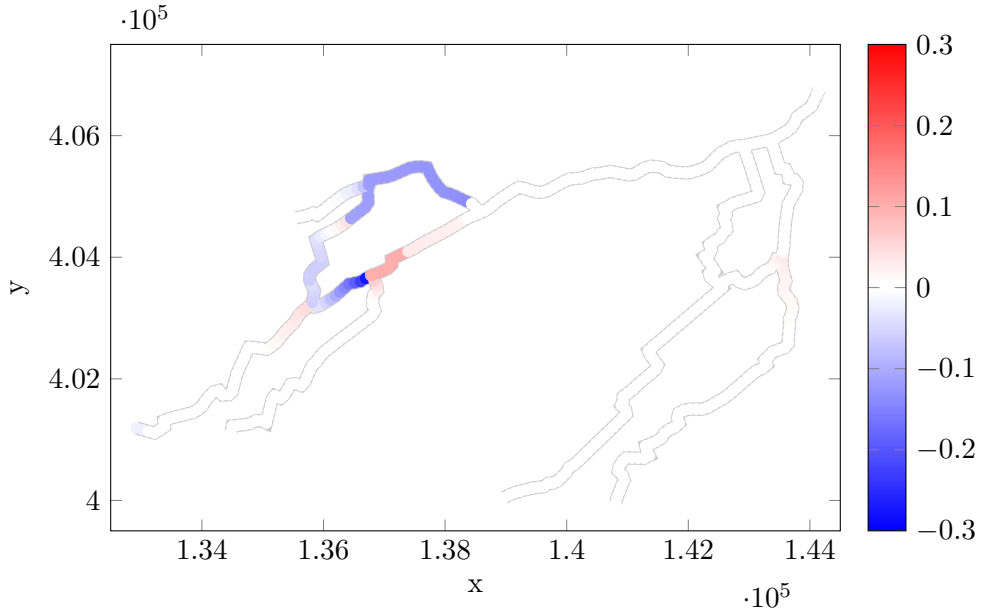

Figure 5-9: The average error in water level $\Delta\hat{y}_{avg}$ [m] with the observational data per calculation point for the OPE tool posterior to the transition of all crest levels. The predictions were obtained after 8 iterations.

5-3-4 Scenario PI-FI: transition in local friction

In Table 5-4, the predicted crest levels and bed friction by the OPE tool as result of a transition in the friction of one section are listed. The values are almost equal to those estimated prior to the transition (see Table 5-1). Apparently, the local friction transition has (almost) no effect on the predicted global friction. The main reason behind this is that there are no observation stations located near the section where the friction was changed. In other words, the OPE tool did not notice the induced changes by the local friction transition and could, therefore, not respond accordingly. Consequently, a similar pattern in the average error in the predicted water levels compared to the situation before the transition (see Figure 5-3) is observed. The errors, presented in Figure 5-12, are mainly caused by utilisation of the clustered weir parameter by the OPE tool. The fact that the bed friction parameter is not corrected for the local friction transition, created the errors that were observed in that particular section (Nriv_ZL_1_9820). Nonetheless, the results for the predicted water levels nearby weir ZL1-5930 are reasonably accurate (see Figure 5-10[4]), although this weir is located in section Nriv_ZL_1_9820.

In this scenario, the original DSS performs a lot better. The only section where errors were observed, is in the section Nriv_ZL_1_9820 (see Figure 5-11). Only in this section, the friction deviated from the friction used for obtaining the observational data, all the other parameters remained equal. Therefore, the best predictions in *this* scenario were obtained by the original DSS. This, however, does not imply that this statement holds for all local friction transitions. In this scenario, the settings of the original DSS are exactly the same as those used for obtaining the observations "by accident", but this is not always true.

Table 5-4: The crest levels and (global) bed friction of the DSS and the OPE tool posterior to the transition of the friction of section Nriv_ZL_1_9820 compared to those used to obtain the observational data (True).

Parameter	ID	True II (PI-Fl) [m]	DSS [m]	OPE II (PI-Fl) [m]
W1	ZL1-5	10.82	10.82	10.83
W2	ZL1-3014	10.45	10.45	10.45
W3	ZL1-5126	8.40	8.40	8.10
W4	ZL1-5930	7.14	7.14	7.15
W5	ZL12-45	9.15	9.15	9.23
W6	ZL12-1880	7.20	7.20	7.37
W7	ZL12-4711	6.75	6.75	6.59
W8	ZL25-6292	5.78	5.78	5.85
W9	ZL25-8463	4.60	4.60	4.77
FA	Global friction	16.00	16.00	16.06
F1	Nriv_ZL_1_9820	25.00	-	-

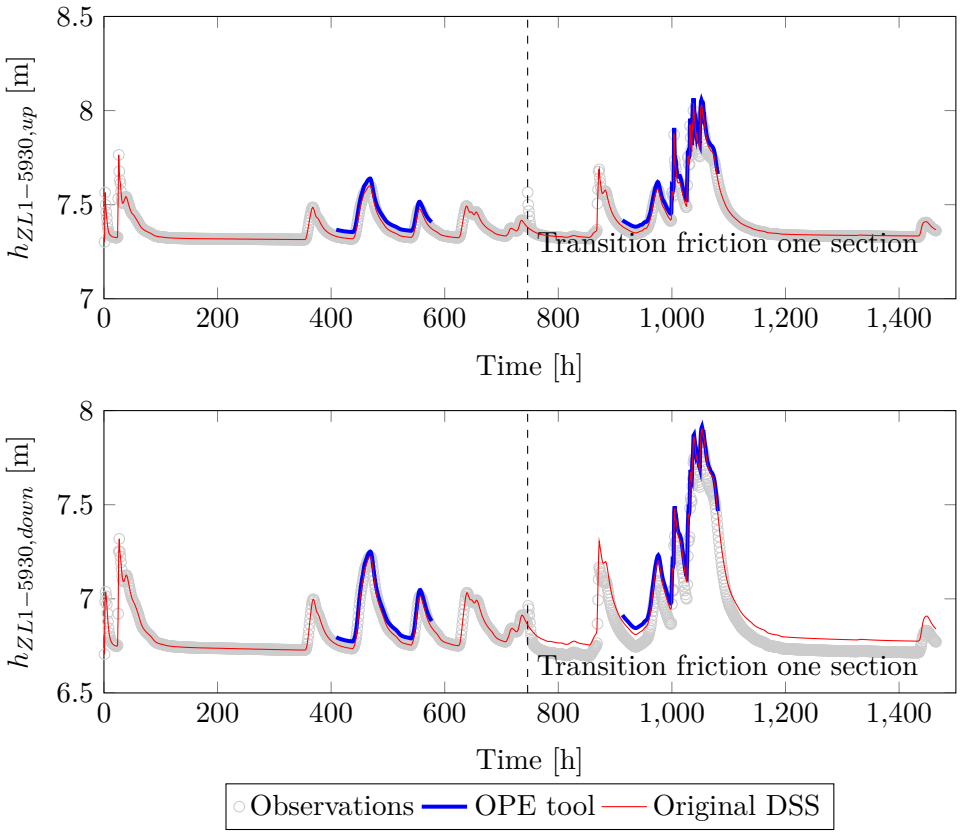

Figure 5-10: The up- and downstream water level predictions [m] at weir ZL1-5930 for the original DSS (red line) and the OPE tool (blue line) compared with the observational data (grey circles).

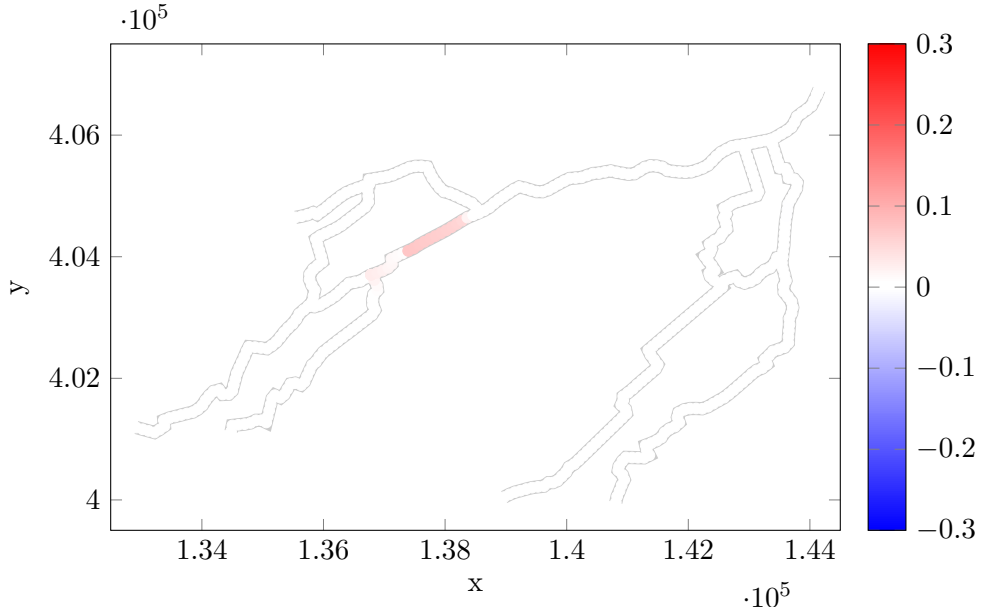

Figure 5-11: The average error in water level $\Delta\hat{y}_{avg}$ [m] with the observational data per calculation point for the original DSS posterior to the transition of the friction of section Nriv_ZL_1_9820. The predictions were obtained after 8 iterations.

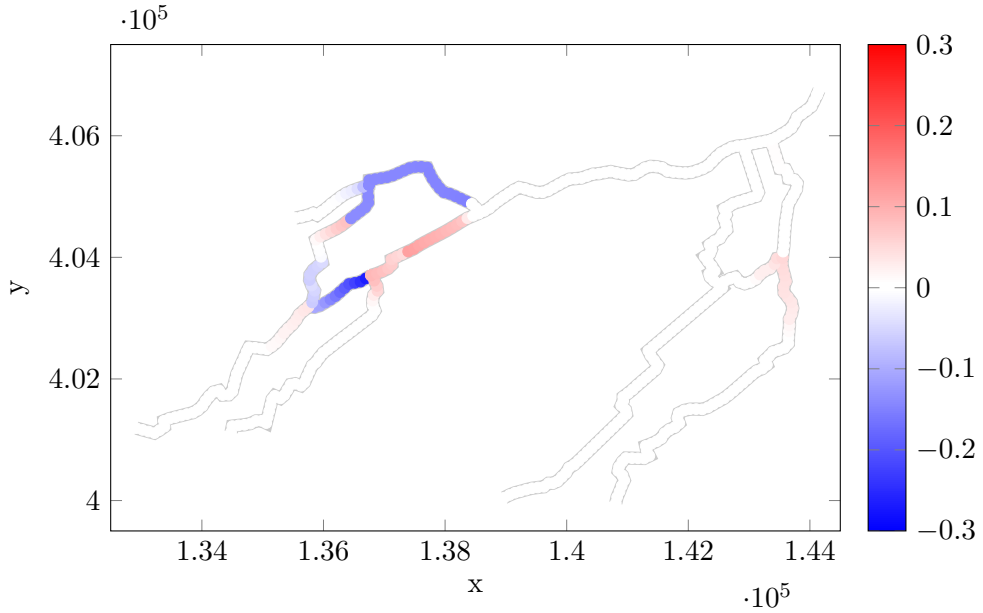

Figure 5-12: The average error in water level $\Delta\hat{y}_{avg}$ [m] with the observational data per calculation point for the OPE tool posterior to the transition of the friction of section Nriv_ZL_1_9820. The predictions were obtained after 8 iterations.

5-3-5 Scenario PI-Wl: transition in crest level of one weir

The results of the OPE tool for the transition of a crest of the weir ZL1-5930 are similar to those as result of local friction transition (see Table 5-5). The reason for this is that also this transition in one crest level is not noticed by the OPE tool, as no measurement stations are located near this weir. Therefore, the clustered weir parameter is adjusted similar to before the transition and the average errors are the largest near the adjustable weirs, illustrated in Figure 5-15. The bed friction parameter, however, is estimated accurately, which results in accurate water level predictions in the other sections (see Figure 5-14).

The original DSS provided more accurate water level predictions than the OPE tool, although the local weir transition caused discrepancies in the water level predictions nearby weir ZL1-5930 (see Figure 5-13[4]). In short, the OPE tool does not provide better predictions than the original DSS for *this* situation of a local weir transition. However, also here the assumption that the original DSS parameter settings correspond exactly with reality does not hold for all cases.

Table 5-5: The crest levels and (global) bed friction of the DSS and the OPE tool posterior to the transition of the crest level of weir ZL1-5930 compared to those used to obtain the observational data (True).

Parameter	ID	True II (PI-Wl) [m]	DSS [m]	OPE II (PI-Wl) [m]
W1	ZL1-5	10.82	10.82	10.83
W2	ZL1-3014	10.45	10.45	10.45
W3	ZL1-5126	8.40	8.40	8.10
W4	ZL1-5930	6.99	7.14	7.15
W5	ZL12-45	9.15	9.15	9.23
W6	ZL12-1880	7.20	7.20	7.37
W7	ZL12-4711	6.75	6.75	6.59
W8	ZL25-6292	5.78	5.78	5.85
W9	ZL25-8463	4.60	4.60	4.77
FA	Global friction	16.00	16.00	16.06
F1	Nriv_ZL_1_9820	-	-	-

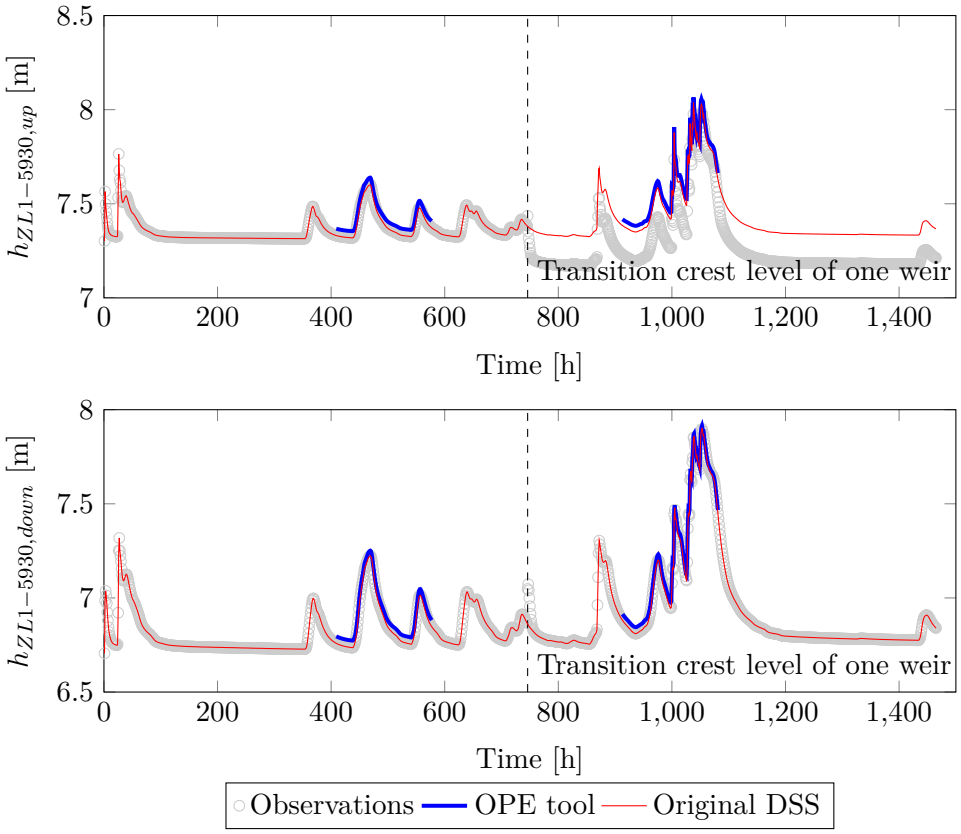

Figure 5-13: The up- and downstream water level predictions [m] at weir ZL1-5930 for the original DSS (red line) and the OPE tool (blue line) compared with the observational data (grey circles).

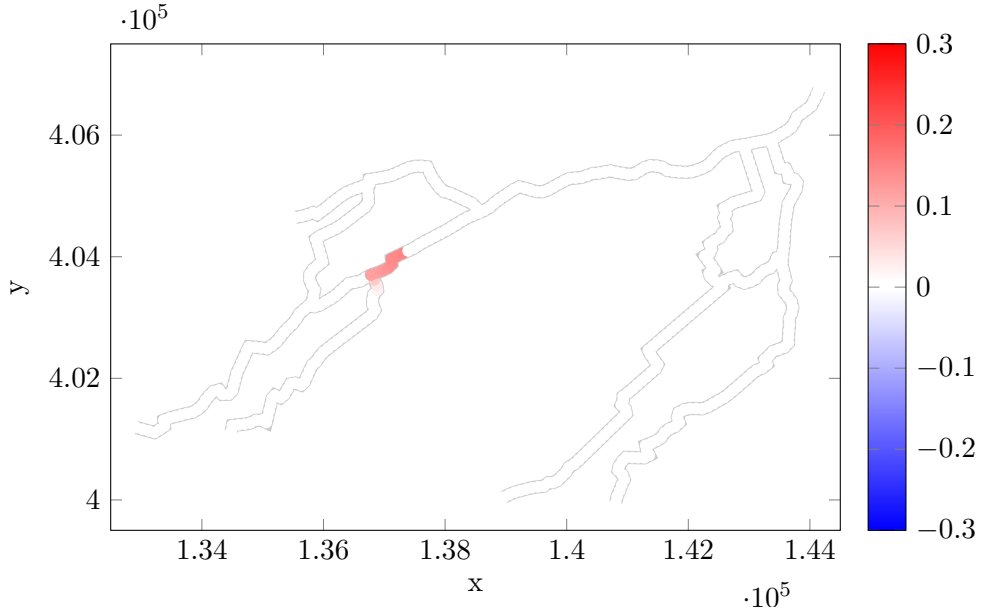

Figure 5-14: The average error in water level $\Delta\hat{y}_{avg}$ [m] with the observational data per calculation point for the original DSS posterior to the transition of the crest level of weir ZL1-5930. The predictions were obtained after 8 iterations.

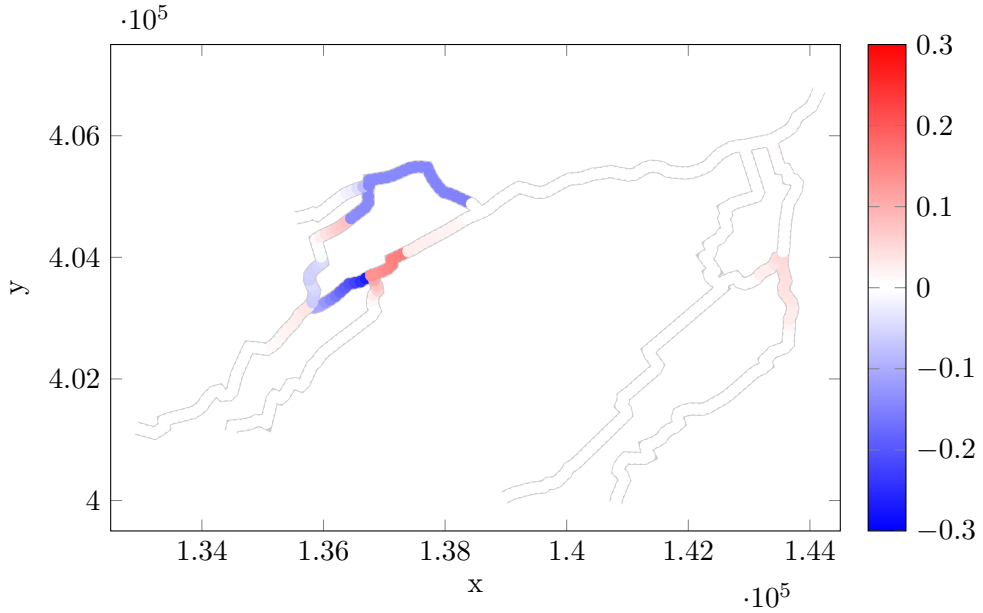

Figure 5-15: The average error in water level $\Delta\hat{y}_{avg}$ [m] with the observational data per calculation point for the OPE tool posterior to the transition of the crest level of weir ZL1-5930. The predictions were obtained after 8 iterations.

Chapter 6

Conclusions and recommendations

In this thesis, a research is performed with the general objective to improve the performance of DSS by making an assessment of the applicability of data assimilation regarding on-line updating of model parameters, based on effectiveness, efficiency, robustness and practical implications for water resources management. For that, a hydrodynamic model that is applied in the case of the 'Brabantse Waterschappen' (project BOS 2.0, a product of Witteveen+Bos (W+B) and Deltares) and observational data of the study area De Dommel are utilised. The results, discussions, conclusions and recommendations are described extensively in the previous chapters. In this chapter, an overview of the conclusions drawn in this thesis is provided. Furthermore, recommendations for implementation of an On-line Parameter Estimation (OPE) tool and for future research are provided.

6-1 Conclusions

Research questions

- **What is the state-of-the-art knowledge on optimisation of DSS regarding MPC of large-scale river networks, data assimilation, parameter updating and optimisation techniques?**
  Human interactions with the river network in terms of changing parameters with sharp transitions in time, need to be included in Decision Support System (DSS). The main reason for this is that these parameter are not changed in the DSS, which can lead to large discrepancies between the observed and modelled states. Two parameters are identified as such parameters: the bed friction and the weirs' crest levels. This implicates that the hydrodynamic model has to be updated after every parameter transition. Former studies confirmed on-line parameter updating can be applied to decrease the model discrepancies. A calibration window of one week is identified as an appropriate time window to capture the parameter transitions, while still being efficient.
  Most studies on on-line parameter estimation in environment studies consider gradual changes in parameter values. The innovation of this study is that it considers sharp

transitions in parameter values as result of sudden human interference with the river system.

- **With use of what algorithms and what software can parameter updating be implemented and coupled to existing hydrodynamic models?**
  The generic, open source framework OpenDA proved to be an effective toolbox for coupling optimisation techniques to the hydrodynamic model. Initially, two algorithms were selected for the on-line parameter estimation: the Doesn't Use Derivatives (DuD) algorithm and the Shuffled Complex Evolution (SCE) method. The DuD algorithm demonstrated to be a robust and efficient tool for data assimilation and parameter updating in the field of Model Predictive Control (MPC) of large-scale river networks and urban drainage, [3],[4]. SCE algorithm, [2], demonstrated to be robust and accurate tool for global optimisation in the field of hydrology, [2],[6], and water distribution networks, [7]. So, from past studies, it was concluded that the DuD is more efficient in finding a parameter prediction, but the SCE method is more robust in finding the global minimum. Different scenarios were tested with varying initial parameter predictions and actual parameter values. The results from these scenarios were assessed on their influence on the model performance in terms of robustness, effectiveness, efficiency and model bias (see the Glossary for a detailed definition).
  From these analyses, it was observed that the DuD algorithm was very robust, i.e. it was able to find the global minimum regardless of the initial parameter prediction and the actual parameter value. Therefore, it can be concluded that the DuD algorithm applied by the OpenDA framework is suitable for providing an accurate parameter prediction for similar river networks.

- **Is automatic parameter updating possible with reasonable results in a twin experiment set-up, with respect to model sensitivity, parameter identifiability, model bias and model performance? And what is the model response to different normative scenarios?**
  In order to test this research question, first an initial model analysis was performed. In this analysis, the model's sensitivity and parameter correlation was determined by introducing perturbed parameter values for the global bed friction and for the crest levels of the adjustable weirs. From this analysis, it was concluded that besides the global bed friction only one crest level was really identifiable uniquely. Therefore, the weirs' crest levels were clustered into one clustered weir parameter in order to get a more efficient optimisation process. In other words, together with the global friction parameter, only two parameters are optimised. This resulted in a process that costs less computation time, since the amount of required iterations grow exponentially with the amount of parameters to optimise. Moreover, the optimisation is much smoother, as for less parameters the optimal solution becomes more distinct.
  The OPE tool was first assigned to the DSS for parameter estimation of one parameter, i.e. the bed friction of one cross-section or the crest level of one weir. From here, the OPE tool was constructively up-scaled by assigning global friction and the clustered weir parameter simultaneously, by assigning extreme precipitation and by assigning observational data with additive noise. For all these model configurations, several scenarios with different initial parameter predictions and different actual parameter values were optimised. For all configurations, the OPE tool proved to be an effective tool for

parameter estimation, i.e. the OPE tool demonstrated to provide very accurate predictions for the optimisation parameters. Furthermore, the OPE tool proved to be a robust tool, i.e. the OPE tool provided the global solution regardless of the applied scenarios. Besides, the OPE tool showed that the parameter can be estimated within a short computation period, which makes this OPE tool also efficient. Some results indicated that the bias is dependent on the level of discharge rate. However, the base scenario assigned with extreme precipitation demonstrated that this bias pattern is not consistent for each scenario. The origin of the bias following the discharge rate seemed to be a numerical issue rather than a systematic modelling error. Moreover, the level of bias is was very small, i.e. smaller than $1.05 \cdot 10^{-3}$ m^2. Therefore, it was concluded that the level of bias caused by the OPE tool can be neglected.

- **Is automatic parameter updating possible with reasonable results when using real measurement data?**
  In order to test the performance of the OPE tool when using real measurement data, the artificial data was assigned with additive noise. The results demonstrated that assigning noise to the observational data affects the effectiveness and efficiency of the OPE tool. However, the accuracy of the parameter predictions is still rather high (and within the acceptations bounds), while the required computation time is only increased with a factor two. The OPE tool estimated the parameters correctly for each scenario, indicating that additive noise does not influence the robustness of the OPE tool. The results for the bias showed that additive noise increases the level of the bias compared to the situation when using noise-free data. Nonetheless, the bias levels were within the acceptance level. Consequently, it can be concluded that additive noise only influences the performance of the OPE tool in term of efficiency. In other words, application of the OPE tool in real DSS increases the performance significantly, when assuming that the hydrodynamic model environment is representative for the real river network and that the parameters are changed globally (i.e. the friction is changed globally and the crest levels are changed according one clustered weir parameter).
  Furthermore, the bias seemed to be completely random, following the randomness of the assigned white noise, and was not linked with the discharge rate. Therefore, it was concluded that the additive noise has a larger contribution to the bias than discharge rate and, thus, no significant error was induced by the OPE tool.

- **How much does the performance improve when implementing some form of parameter updating?**
  The practical implications of utilisation of the OPE tool in an existing DSS were determined by assigning practical real scenarios. These scenarios consisted of global and local transitions. The global transitions were divided into two scenarios: one altered the global friction, the other changed the crest levels of all weirs. The local transitions were split up in two scenarios as well: one changed the friction of one single section, while the other modified the crest level of a single weir. From the scenarios with global transitions, it was observed that the OPE tool outperformed the original DSS. When using the OPE tool, the global friction was estimated correctly, while also some crest levels were predicted reasonably accurate. The utilisation of the clustered weir parameter, however, forced an offset for some other crest levels, when comparing the optimised predictions with the observations.

From the scenarios with the local transitions, it was observed that the OPE tool is not capable to capture the local changes. This was mainly due to the fact that the local transitions were introduced in an area where no observations were obtained. The OPE tool was thus not able to notice the local transitions. On the other hand, the OPE tool was, therefore, able to capture the overall parameter value. Also here, the clustered weir parameters forced some crest levels to deviate from their real value. The deviations of these crest levels, and thus the predicted water levels nearby these weirs, are rather consistent. This is caused by the fact that the clustered weir parameter is most sensitive to water level observations around weir W2 (ZL1-3014). Consequently, the weir parameter W2 is the most accurate, which means that the other crest levels have a more or less constant deviation with the observations. In general, the OPE tool is able to improve the performance of the original DSS when global transitions in the global friction or the crests levels of all weirs occur. The OPE tool is, however, not able to capture all local transitions. This mainly depends on the location of the local transition compared with the locations of the measurement stations. The original DSS, on the other hand, caused large discrepancies in the modelled states compared with observed states. The fact that the original DSS performed better than the OPE tool for local transitions, was more coincidental than due to the capabilities of the original DSS. The reason for this is that it was assumed that the parameter values in the original DSS exactly correspond with the actual parameters values, which is of course not the case when applying DSS in an on-line environment. Therefore, it can be concluded that the OPE tool improves the performance of original DSS and that, even in the current configuration, it is *essential* for water managers to implement some form of OPE in on-line systems. Nonetheless, more research should be executed on influence on the model performance by the adding extra measurement locations, applying different noise models, including of water control operations, discretising the transition phase and up-scaling to more calibration parameters.

6-2 Recommendations for implementation

- **Use a generic optimisation toolbox**
  First of all, it is recommended to use a generic optimisation toolbox that can be applied at different models and different platforms. In this way, the knowledge about the optimisation tool can be transferred easily to improve the performance of other models. The optimisation tool used in this thesis, called OpenDA, is such a generic toolbox, which can be implemented rather easily.

- **Use DuD algorithm**
  The second recommendation is to use the DuD algorithm or a similar optimisation algorithm. The main reason is that this algorithm does not require prior information on the mathematical system. Furthermore, this thesis proved that the DuD algorithm provides a high level of robustness and effectiveness in the optimisation of parameters. Moreover, the DuD algorithm demonstrated that it optimises the parameter efficiently, which is a useful characteristic when implementing the tool in an on-line environment.

- **Use a (hydrodynamic) model with optional control operations**
  In this thesis, operational control actions were not taken into account, because this

simplified the assessment whether the OPE tool does what is should do (i.e. improve the performance of DSS by optimisation of the calibration parameters). Nonetheless, the DSS that are currently used by water managers comprise these control actions. Therefore, it is recommended to use a software package that contains the option to implement the control actions. Furthermore, it should be able to save the status of the control actions, since it was demonstrated by [4] that not transferring this status from one calibration window to the next one could lead to large discrepancies in the modelled states compared with observations. A package that comprises these control actions and saving of its status is SOBEK 3, which is a product of Deltares. Another advantage of using SOBEK 3 is that it makes easy configuration changes possible by its built-in Python scripting module.

- **Select a proper calibration window**
  A calibration window with a length of one week was recommended. For the research project of this thesis, this window was able to capture the complete transition in modelled states induced by the sharp transition in parameter values. Furthermore, with observations every hour for a window of one week, this results in a sufficient amount of data that can be used for optimisation of multiple parameters, [9]. Moreover, utilisation of a calibration window of one week is still efficient, whereas a longer window can increase the optimisation time significantly while it not necessarily improves the effectiveness of the OPE tool.

6-3 Recommendations for further research

- **More measurement locations**
  At two point during this thesis, it was noticed that the potential of the OPE tool was restricted to the amount of available observational data. The first moment was when the clustered weir parameter was introduced, since some crest level were simply not identifiable for the OPE as result of the "lack of data". The second moment emerged when the OPE tool was implemented in water management scenarios and systematic errors were caused by the utilisation of the clustered weir parameter (see Chapter 5). A possible improvement for this could be installing more measurement locations. [52] proposed a method that can be used to determine the most optimal locations for additional measurement stations and which also makes sure that only practical locations (e.g. locations that can be reached easily) are taken into account.

- **Other additive noise assigned to observations**
  In this thesis, so-called white noise was assigned to the observational data in order to simulate 'real' data. However, before making the step to true measurement data, the model should be tested to other forms of noise. An example of perhaps more realistic noise could be so-called pink noise, which is inversely proportional to the frequency of occurrence of the data. This implies that the observed states that occur less often are assumed to contain more noise, compared to states that occur more frequently.

- **Include control actions**
  As described above, the currently used DSS also comprise operational control actions. The effect of these actions on the performance of the OPE tool are, however, not yet

studied. Therefore, the effect of including operations from e.g. pump stations or controlled weirs on the model performance should be investigated. [4] demonstrated that also the status of these operations should be transferred from one calibration window to the next one. When this is not done properly, large modelling discrepancies can be caused.

- **Discretisation of transition phase**
  In this thesis, the parameters and states prior to and posterior to parameter changes are predicted. The transition itself, however, is not determined, since sharp transitions cannot be predicted accurately as result of using the calibration window with the assumptions of this study. For this calibration windows, only one value per calibration parameter is determined, which means that during the transition it is very well possible that the OPE tool will predict an average value for the parameter. Of course, this average value does not correspond with the parameter value before the transition, neither it does for the parameter value after the transition. Therefore, the OPE tool should be extended with a function that identifies the transition and the corresponding parameter values prior to and posterior to this transition. One way to obtain this, is by discretisation of the parameter value in three other parameters: a value for the parameter before the transition, a value for the parameter after the transition and a value for the transition in the parameter value itself.
  It should, however, be noted that the discretisation of the transition phase introduces more optimisation parameters, which in turn increases the computation time exponentially and makes the optimisation problem less distinct (see the Glossary for a detailed definition). Moreover, before implementing discretisation of the transition phase, it first should be tested extensively.

- **More parameters**
  Finally, it is recommended to investigate the influence of optimising more model parameters on the model performance. More parameters can be obtained by decoupling of the clustered weir parameter or by introducing sectional friction instead of global friction. More parameters can also be obtained, however, by up-scaling the model to a larger study area and river network. Then, the "global friction" and clustered weir parameters are determined for each sub-area. The focus should of course be on the efficiency of the OPE tool, as more calibration parameters causes the computation time to increase exponentially. The focus should, however, also be on the effectiveness and robustness of the OPE tool, since more calibration parameters cause the optimisation problem to be less distinct.

Appendix A

Shuffled Complex Evolution (SCE) algorithm

Shuffled Complex Evolution (SCE) is simple, but powerful optimisation algorithm developed by Duan et al., [2], which is capable of finding a global minimum of a function with several parameters, [5],[7]. The SCE method is based on four concepts, which have been proven successful [2]:

- Combination of deterministic and probabilistic approaches (controlled random search), [59].
- Systematic evolution of a complex of points spanning parameter space in the direction of global improvement, [60].
- Competitive evolution, [61].
- Complex shuffling, [2].

SCE finds the global minimum of minimisation problem by executing the following steps, [2]. The algorithm starts with a randomly selected set of points from user-defined parameter distributions. Each point is generated by a set of values of the calibration parameters. The corresponding costs for each point are determined. Next, the points are sorted and partitioned into complexes based on their cost. Each complex is evolved by use of an iterative procedure. This method applies the Competitive Complex Evolution (CCE) algorithm for local search, based on the downhill simplex method developed by Nelder and Mead, [60]. In the first step of the iterative procedure, the complexes are divided into simplexes. The simplex method lets the simplexes propagate, to search for new solutions with smaller costs by applying reflection and inside contraction. When the iterative procedure is ended, the complexes are pooled together. All solutions are reshuffled and reassigned to new complexes. This process is repeated till the point the solutions converge to the global minimum and one of the following stopping criteria is fulfilled:

Steps applied in the SCE method:

1. Initialise problem and algorithm parameter set: Eq. (2-3).
2. Generate samples.
3. Rank solution points.
4. Partition into complexes.
5. Evolve complexes by use of CCE algorithm.
6. Complex shuffling.
7. Check convergence by use of stopping criteria.

Figure A-1: Step-by-step description of the SCE algorithm.

- When the maximum number of outer and inner iterations is reached.
- When the maximum absolute difference between the costs of two best parameter estimates approaches T_4: $|Q(\theta_{new}) - Q(\theta_0)| \leq T_4$.
- When the maximum relative difference between the costs of two best parameter estimates approaches T_5: $\frac{|Q(\theta_{new}) - Q(\theta_0)|}{Q(\theta_0)} \leq T_5$.
- When the maximum number of complexes is reached.

The global optimisation process described above is described step-by-step in Figure A-1 and visualised in a flowchart (see Figure A-3). The procedure steps and flowchart of the local search method CCE are presented in Figure A-2. A mathematical description is provided in e.g. [2],[7].

Steps used in the CCE algorithm:

(a) Subcomplexes construction

(b) Worst solution of subcomplex is identified and centroid of subcomplex without worst point is determined.

(c) Try reflection of worst solution through centroid. If this newly constructed point is within the feasible space then go to (d), else create randomly new solution within feasible space and continue with (f).

(d) If newly constructed solution is better than worst solution, then replace worst solution by new solution and go to (g). If not, continue with (e).

(e) Attempt of contraction of calculation of point between centroid and worst solution. If better than worst solution, then replace the latter by the contraction point and continue with (g). Else, go to (f).

(f) Generate randomly a solution within feasible space and replace the worst solution by this newly generated point.

(g) Repeat steps (b)-(f) α times and steps (a)-(g) β times.

Figure A-2: Procedure of the CCE algorithm.

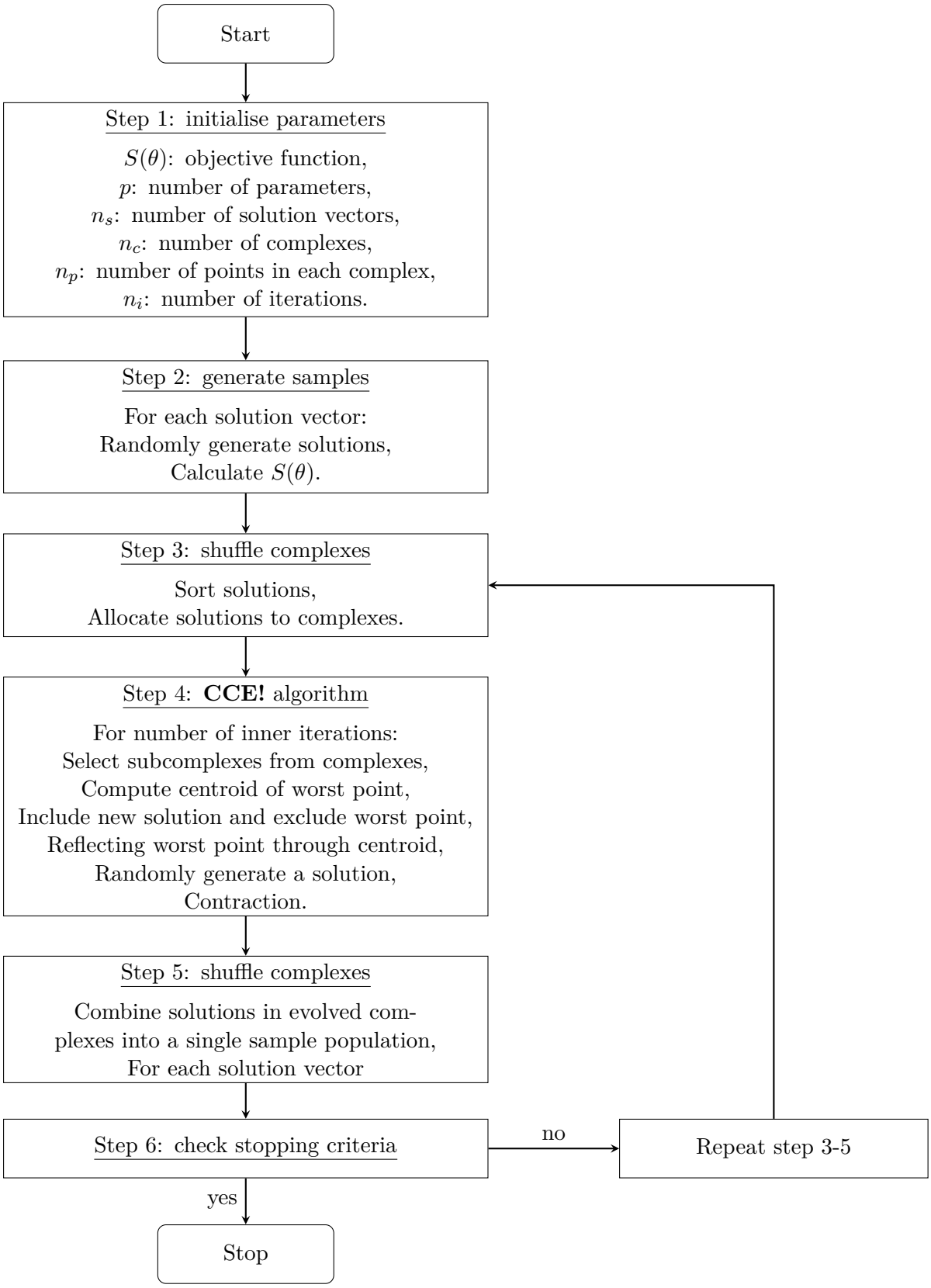

Figure A-3: Flowchart of the SCE method, modified from [7].

Appendix B

OpenDA-SOBEK structure

Table B-1: Modification that are made on the already existing OpenDA-SOBEK structure, developed by Deltares.

Component (number)	Modification
Algorithm config	Use two different algorithms: DuD, SCE Evaluation/stop criteria Constraints? Cost function additional term?
Model config	aliasValues timeInfo exchangeItems
Wrapper config	aliasDefinitions ioObjects
StochModel config	parameters predictor
StochObserver config	timeSeries noosObserver
API	Add new and improve functionality of (already defined) functions
Input and Output Python	Access and adjust default roughness Access and adjust crest level of weirs Export output results at structures

Table B-2: An overview of the components and elements that are used to couple OpenDA with SOBEK.

Component	Elements	Input type: subelements (E) or attributes (A)	Input name
Algorithm config	costFunction	A	weakParameterConstraint, class
	outerLoop	A	maxIterations, absTolerance, relTolerance, relToleranceLinearCost
stochObserverConfig	timeSeries	A	standardDeviation, status
stochModelConfig	modelConfig	E	file
	file	A	skb3BosThModel.xml
	vectorSpecification	E	parameters
	parameters	E	regularisationConstant
	regularisationConstant	E	stdDev, vector
	stdDev	A	value, transformation
	vector	A	id
	predictor	E	vector
	vector	A	id, sourceVectorId
modelConfig	wrapperConfig	E	file
	file	A	skb3BosThWrapper.xml
	aliasValues	E	alias
	alias	A	key, value
	timeInfo	A	start, end
	exchangeItems	E	vector
	vector	A	id, ioObjectId
	doCleanUp	A	false
wrapperConfig	aliasDefinitions	A	defaultKeyPrefix, defaultKeySuffix
		E	alias
	alias	A	key, value
	run	E	initializeActionsUsingDirClone, computeActions, finalizeActions
	initializeActionsUsingDirClone	A	instanceDir, templateDir
	computeActions	E	action
	action	A	workingDirectory, windowsExe
	inputOutput	E	
	ioObject	A	className
		E	file, id, arg
	file	A	%frictionTemplateFile%
	id	A	friction
	arg	A	%frictionFile%

Appendix C

Results initial model analysis

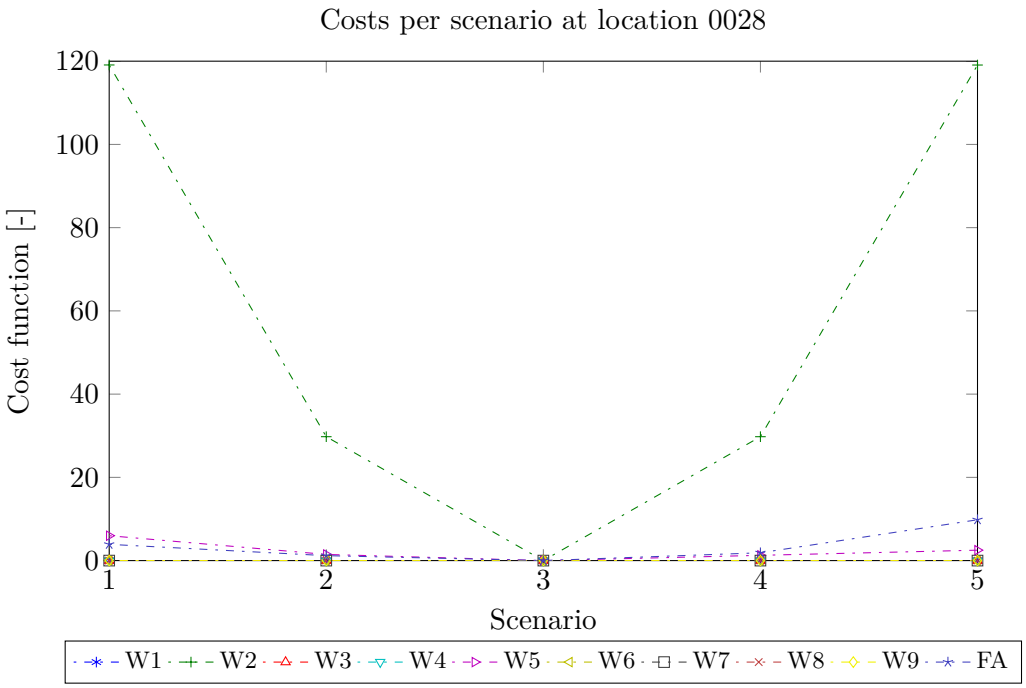

Figure C-1: The cost caused by perturbations in parameter values at location 0028.

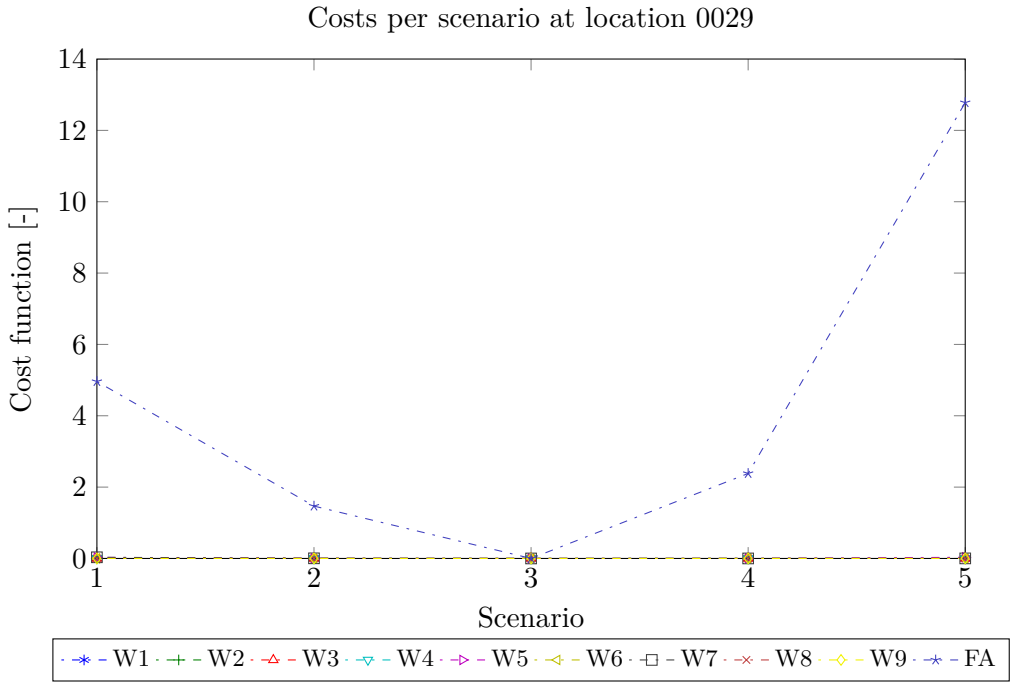

Figure C-2: The cost caused by perturbations in parameter values at location 0029.

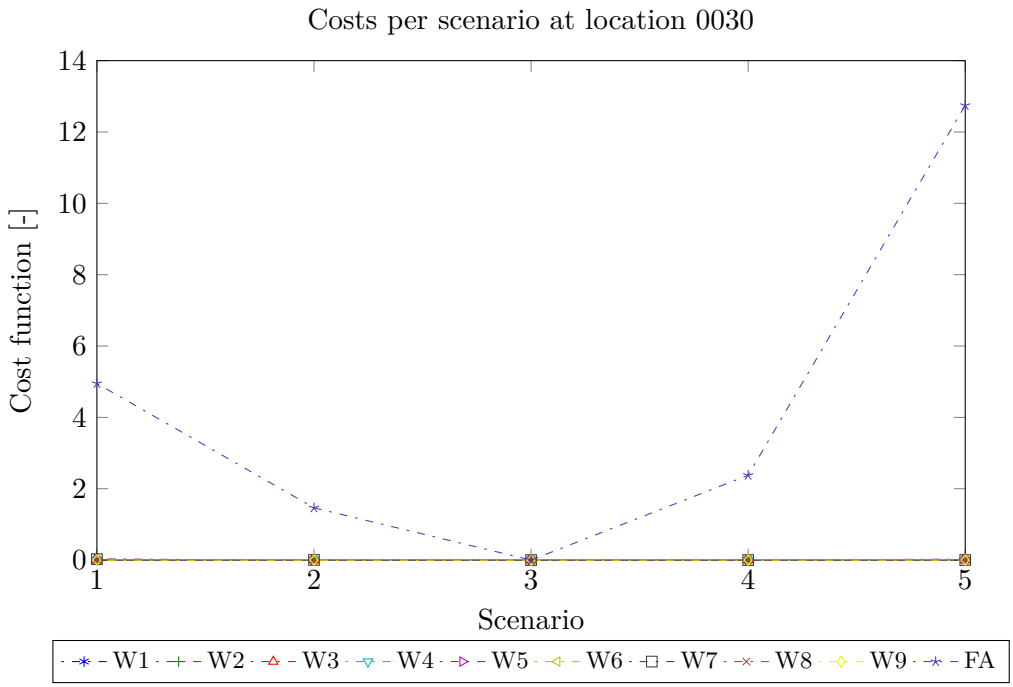

Figure C-3: The cost caused by perturbations in parameter values at location 0030.

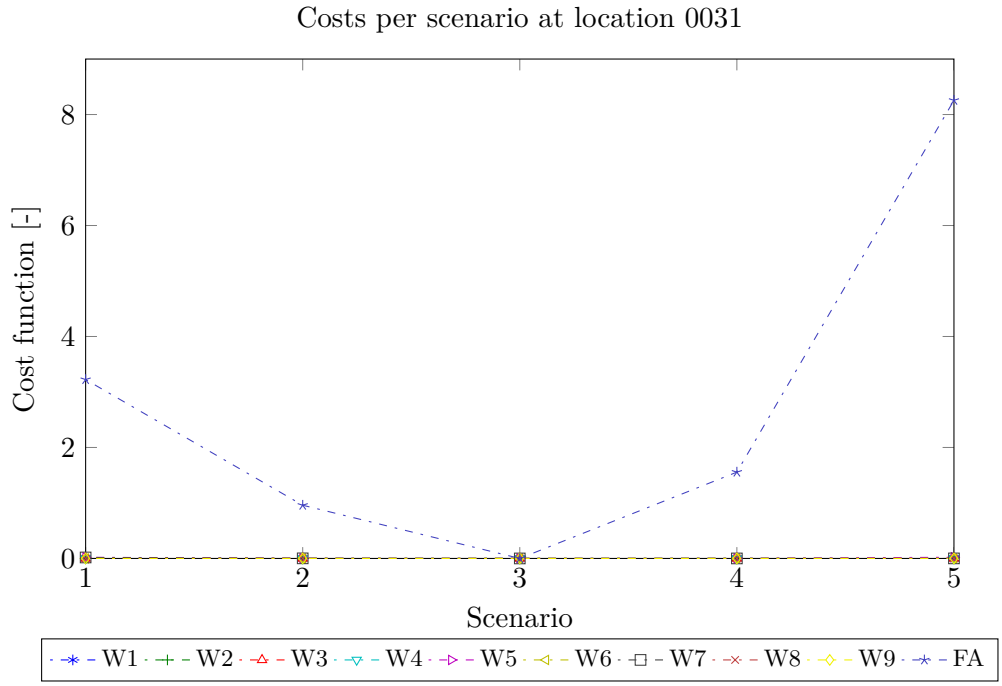

Figure C-4: The cost caused by perturbations in parameter values at location 0031.

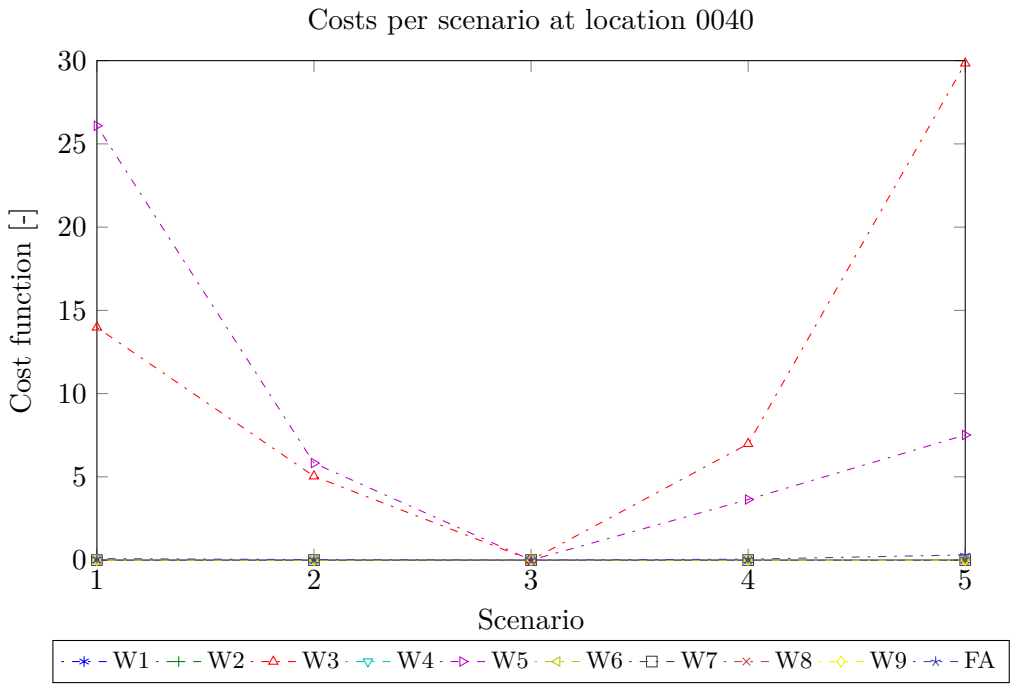

Figure C-5: The cost caused by perturbations in parameter values at location 0040.

Appendix D

Results optimisation scenarios FaWc

In the bias figures, the scenarios with different starting points are indicated with crosses, circles, squares and asterisks. The crosses and circles represent high and low starting points, respectively, for the weir parameter and a low starting point for the friction parameter. The squares and asterisks represent high and low starting points, respectively, for the weir parameter and a high starting point for the friction parameter. The high, medium and low scenarios for the weir parameter are indicated with the red, green and blue, respectively.

D-1 Results group 1 (G1)

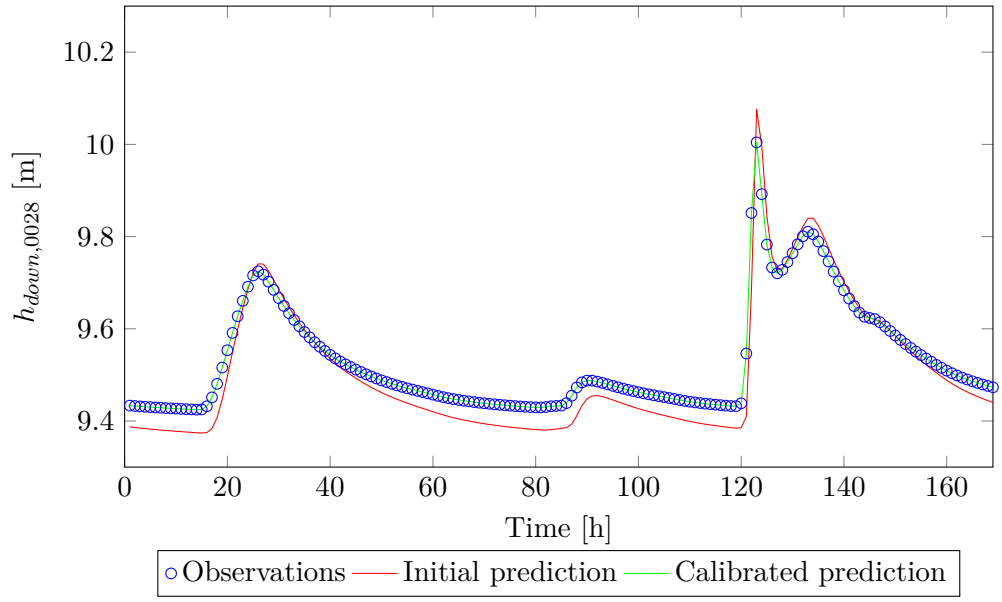

Figure D-1: The downstream water level at location 0028 for scenario FaWcH1H1 (G1) as function of time in the calibration window. The blue dots represent the observational data, the red line the initial prediction and the green line the calibrated prediction.

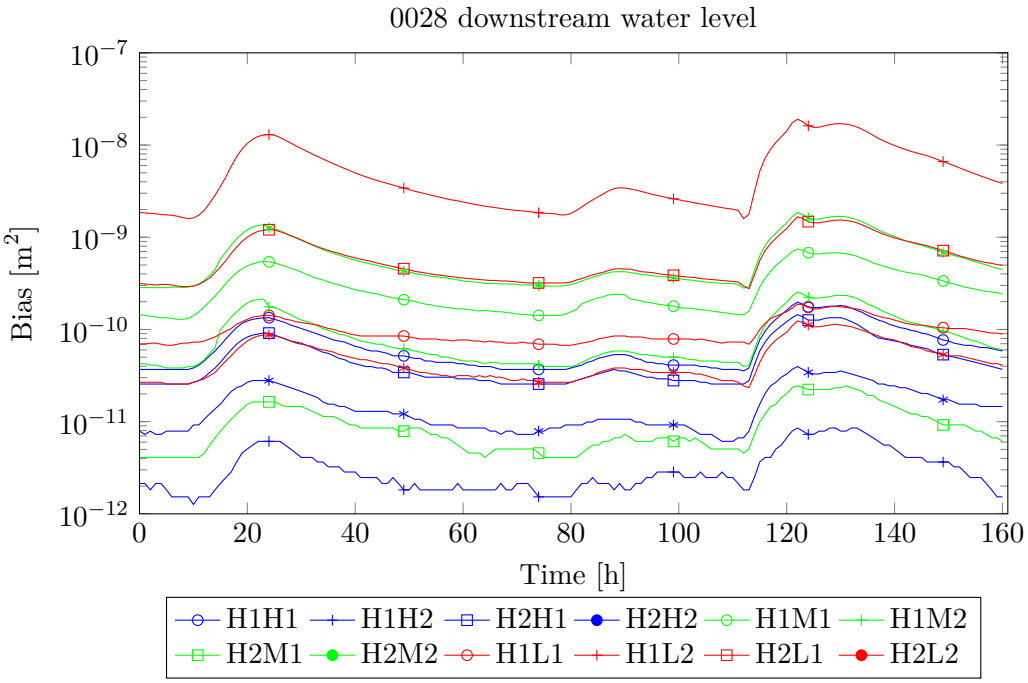

Figure D-2: The bias for the downstream water level at location 0028 for the FaWc (G1) scenarios with different starting points, three actual crest level values and one actual friction value as function of time in the calibration windows (with a time window $T = 2$h).

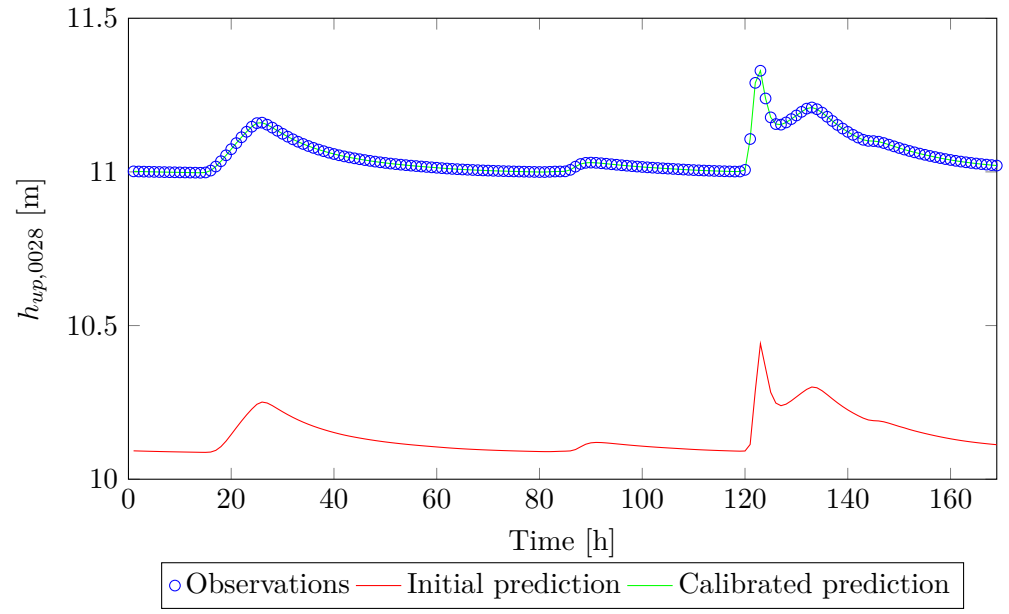

Figure D-3: The upstream water level at location 0028 for scenario FaWcH1H1 (G1) as function of time in the calibration window. The blue dots represent the observational data, the red line the initial prediction and the green line the calibrated prediction.

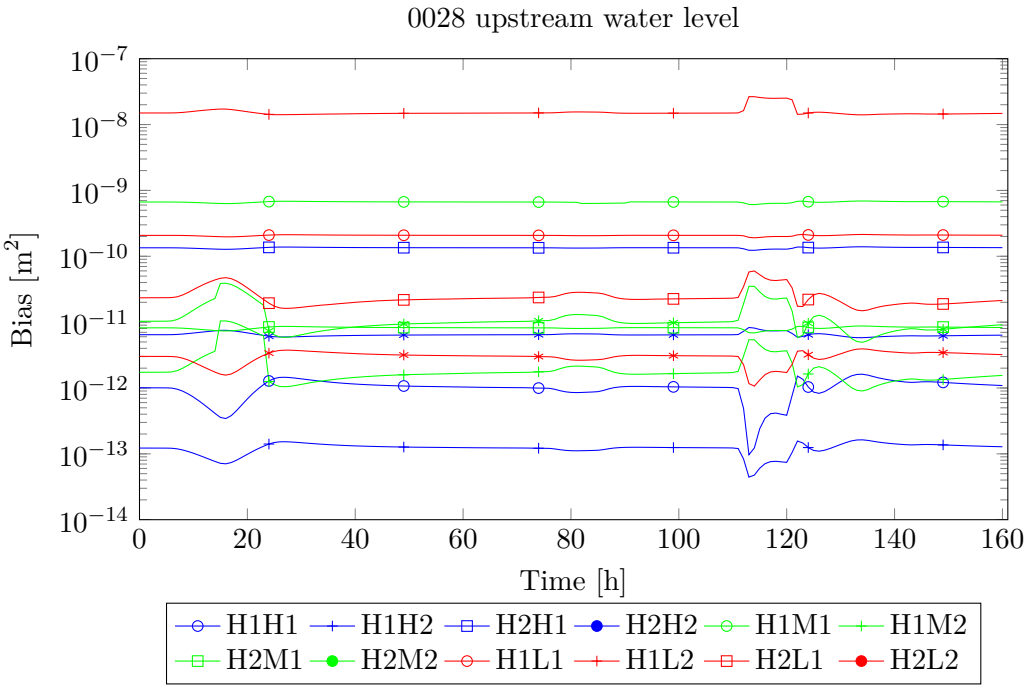

Figure D-4: The bias for the upstream water level at location 0028 for the FaWc (G1) scenarios with different starting points, three actual crest level values and one actual friction value as function of time in the calibration windows (with a time window $T = 2$h).

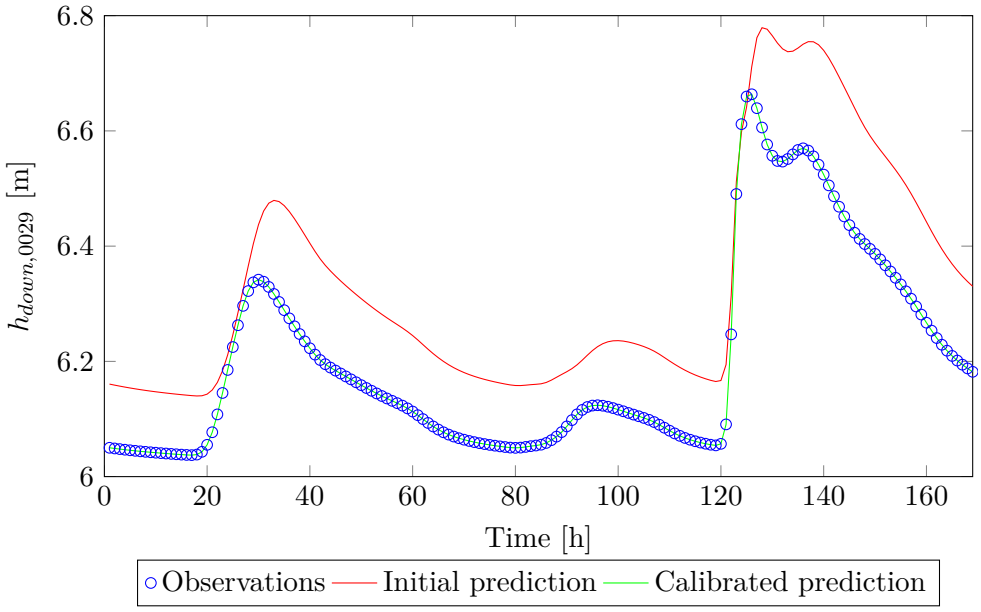

Figure D-5: The downstream water level at location 0029 for scenario FaWcH1H1 (G1) as function of time in the calibration window. The blue dots represent the observational data, the red line the initial prediction and the green line the calibrated prediction.

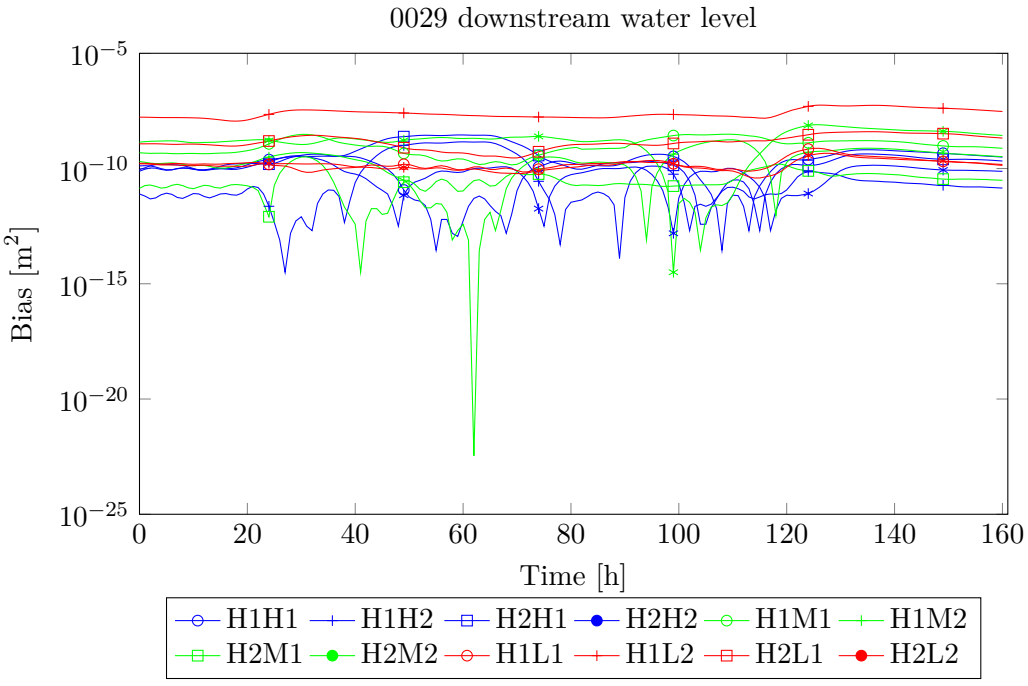

Figure D-6: The bias for the downstream water level at location 0029 for the FaWc (G1) scenarios with different starting points, three actual crest level values and one actual friction value as function of time in the calibration windows (with a time window $T = 2$h).

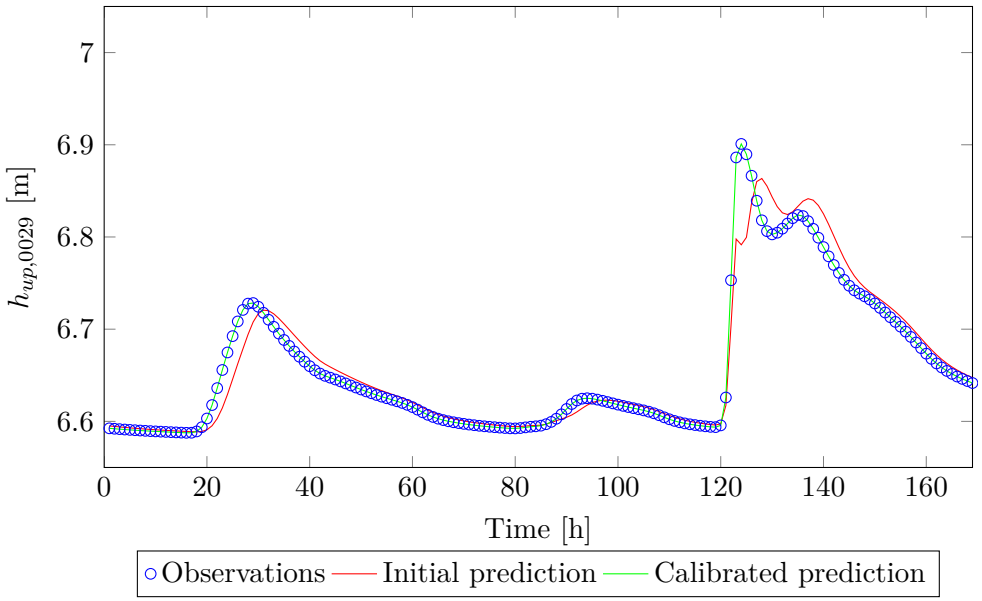

Figure D-7: The upstream water level at location 0029 for scenario FaWcH1H1 (G1) as function of time in the calibration window. The blue dots represent the observational data, the red line the initial prediction and the green line the calibrated prediction.

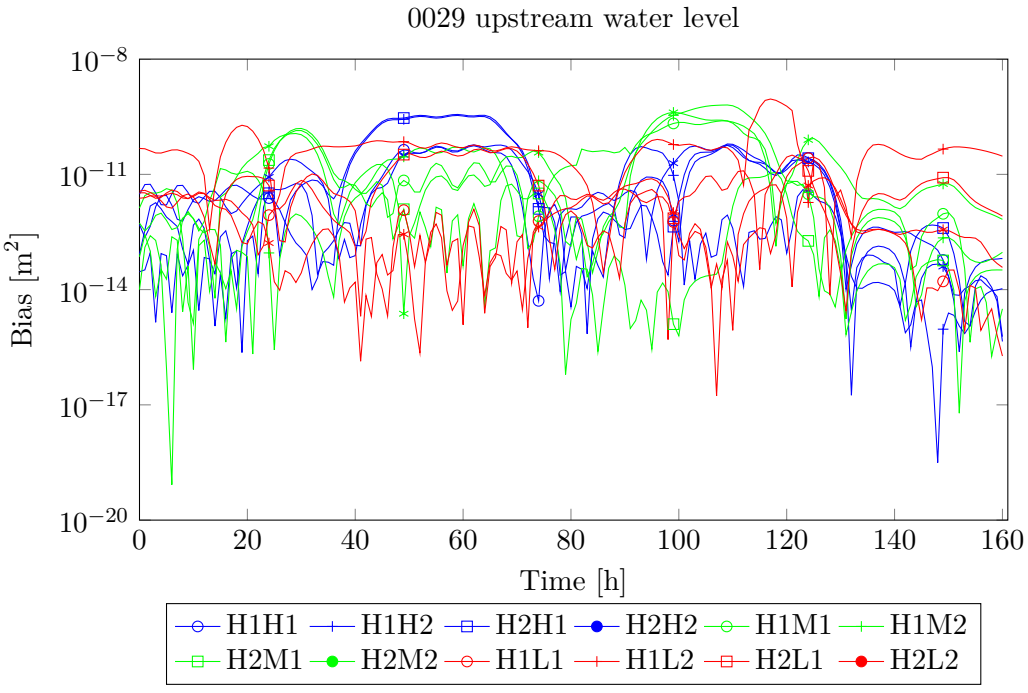

Figure D-8: The bias for the upstream water level at location 0029 for the FaWc (G1) scenarios with different starting points, three actual crest level values and one actual friction value as function of time in the calibration windows (with a time window $T = 2$h).

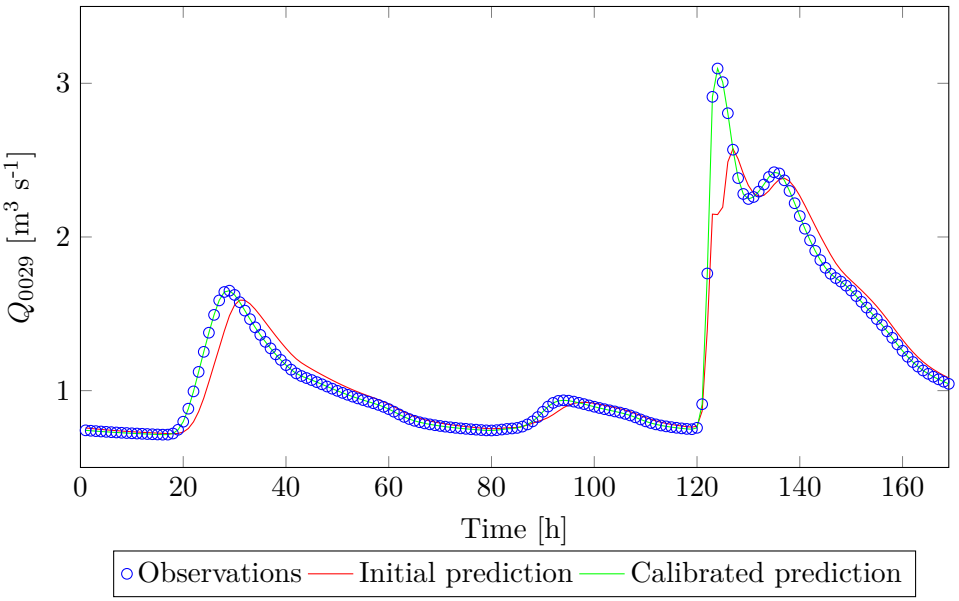

Figure D-9: The discharge at location 0029 for scenario FaWcH1H1 (G1) as function of time in the calibration window. The blue dots represent the observational data, the red line the initial prediction and the green line the calibrated prediction.

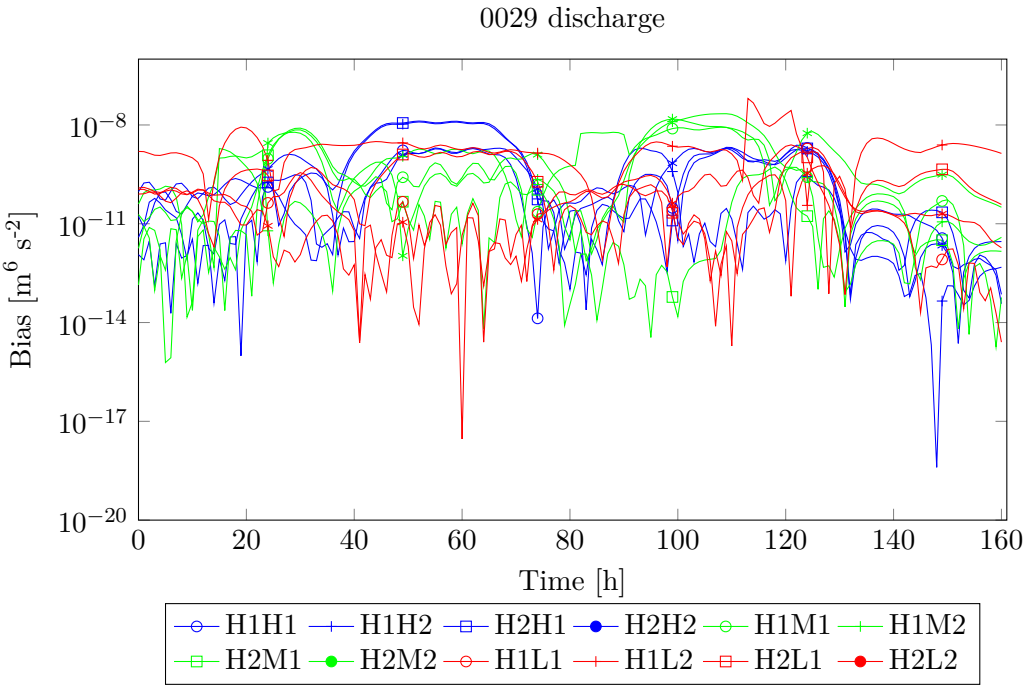

Figure D-10: The bias for the discharge at location 0029 for the FaWc (G1) scenarios with different starting points, three actual crest level values and one actual friction value as function of time in the calibration windows (with a time window $T = 2$h).

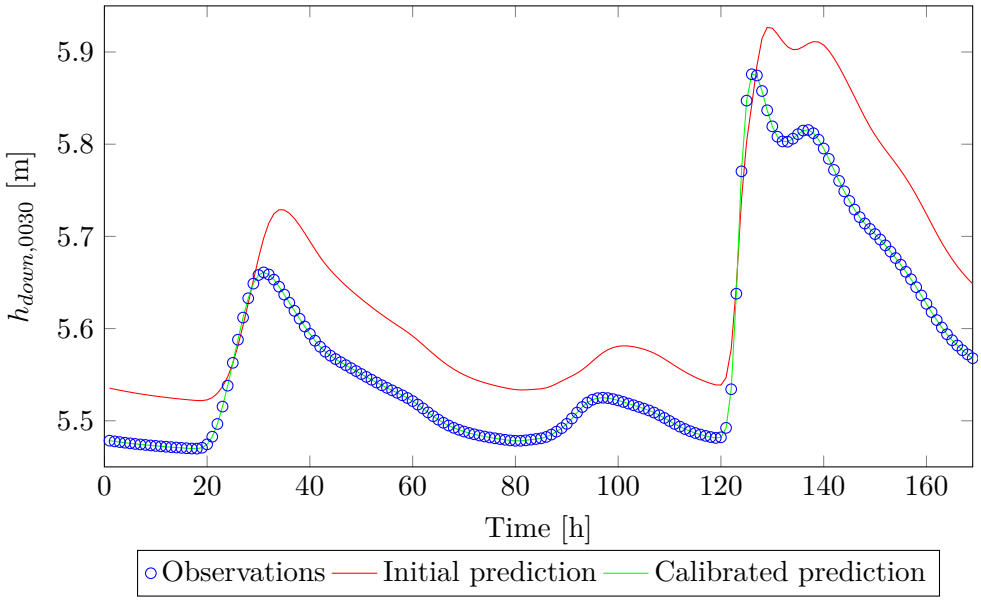

Figure D-11: The downstream water level at location 0030 for scenario FaWcH1H1 (G1) as function of time in the calibration window. The blue dots represent the observational data, the red line the initial prediction and the green line the calibrated prediction.

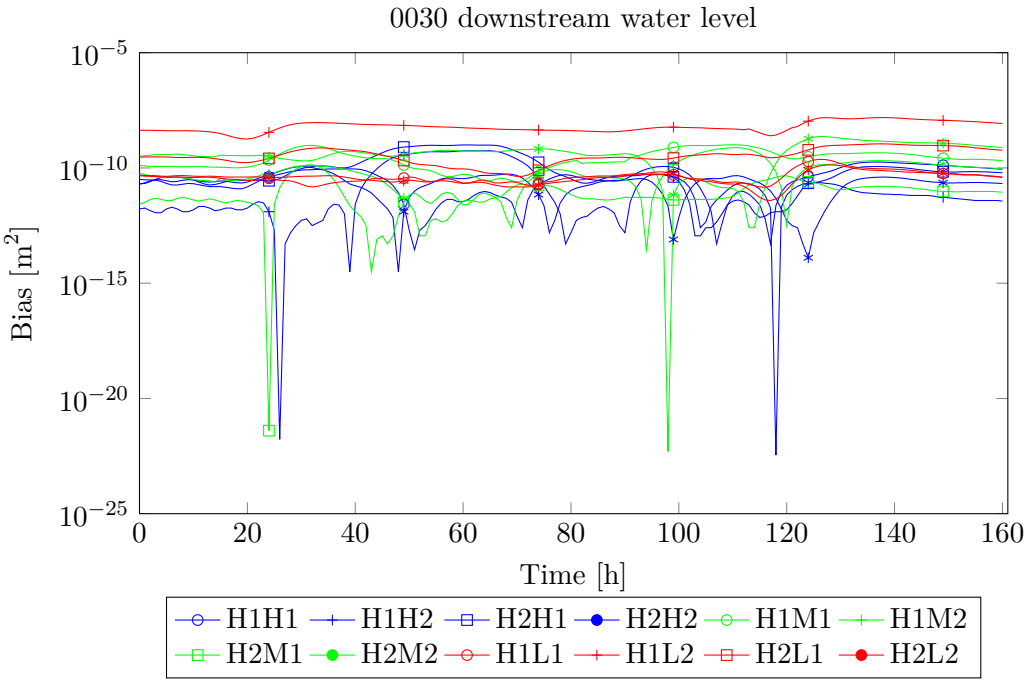

Figure D-12: The bias for the downstream water level at location 0030 for the FaWc (G1) scenarios with different starting points, three actual crest level values and one actual friction value as function of time in the calibration windows (with a time window $T = 2$h).

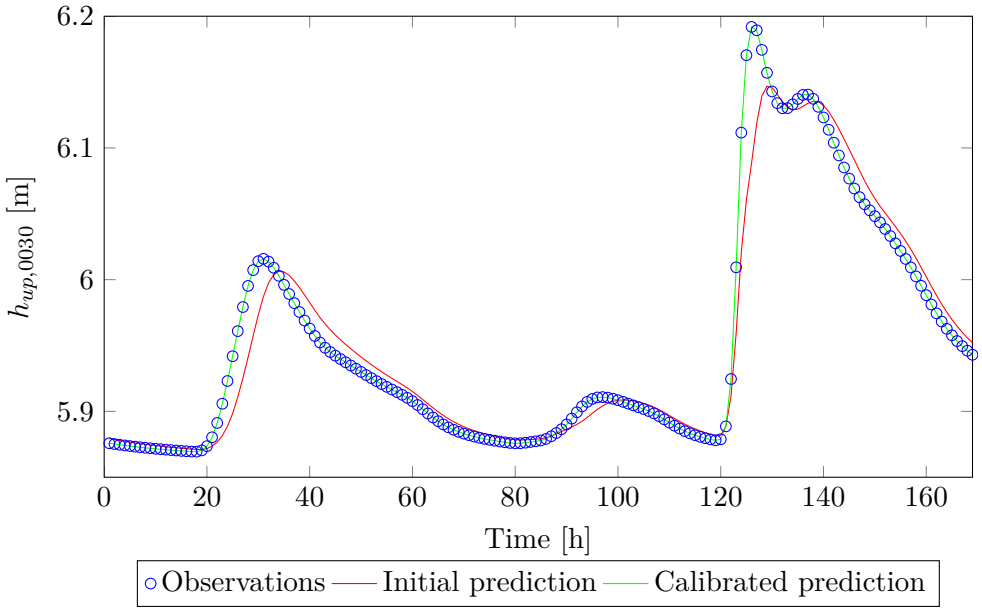

Figure D-13: The upstream water level at location 0030 for scenario FaWcH1H1 (G1) as function of time in the calibration window. The blue dots represent the observational data, the red line the initial prediction and the green line the calibrated prediction.

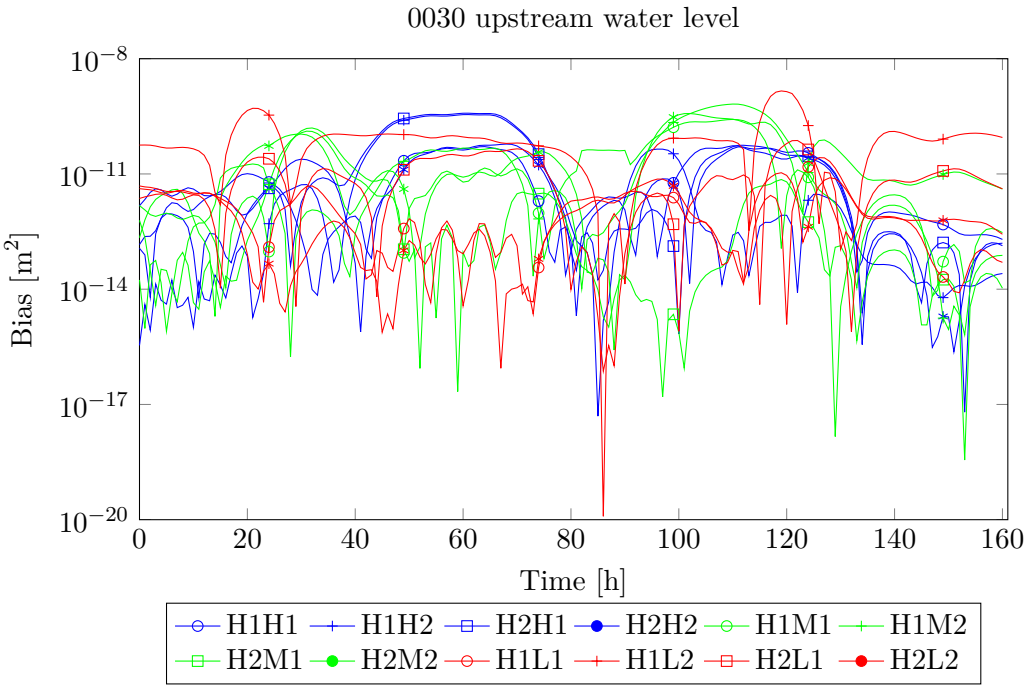

Figure D-14: The bias for the upstream water level at location 0030 for the FaWc (G1) scenarios with different starting points, three actual crest level values and one actual friction value as function of time in the calibration windows (with a time window $T = 2$h).

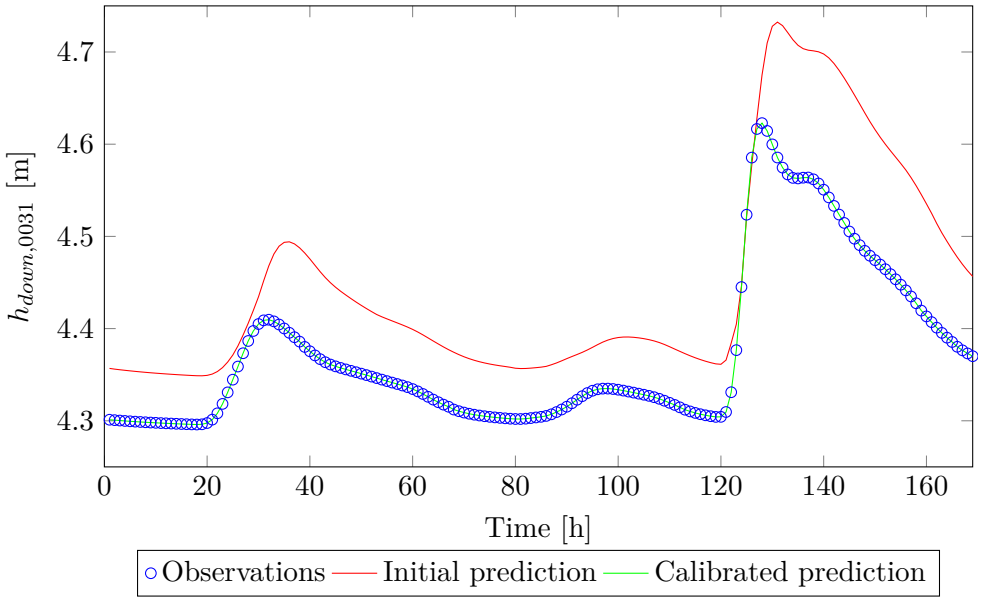

Figure D-15: The downstream water level at location 0031 for scenario FaWcH1H1 (G1) as function of time in the calibration window. The blue dots represent the observational data, the red line the initial prediction and the green line the calibrated prediction.

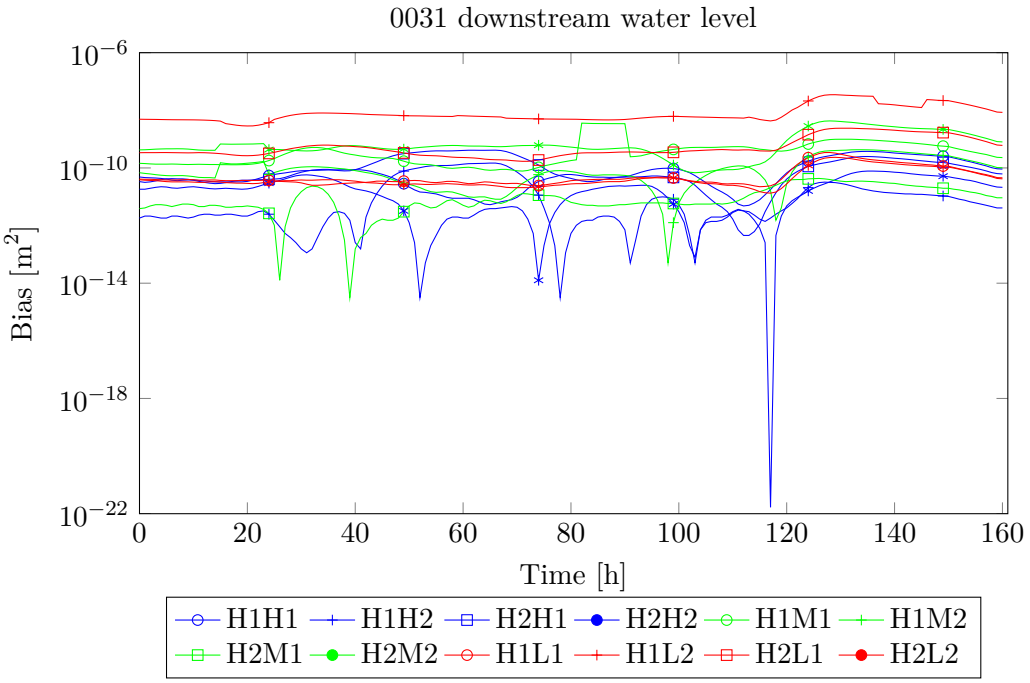

Figure D-16: The bias for the downstream water level at location 0031 for the FaWc (G1) scenarios with different starting points, three actual crest level values and one actual friction value as function of time in the calibration windows (with a time window $T = 2$h).

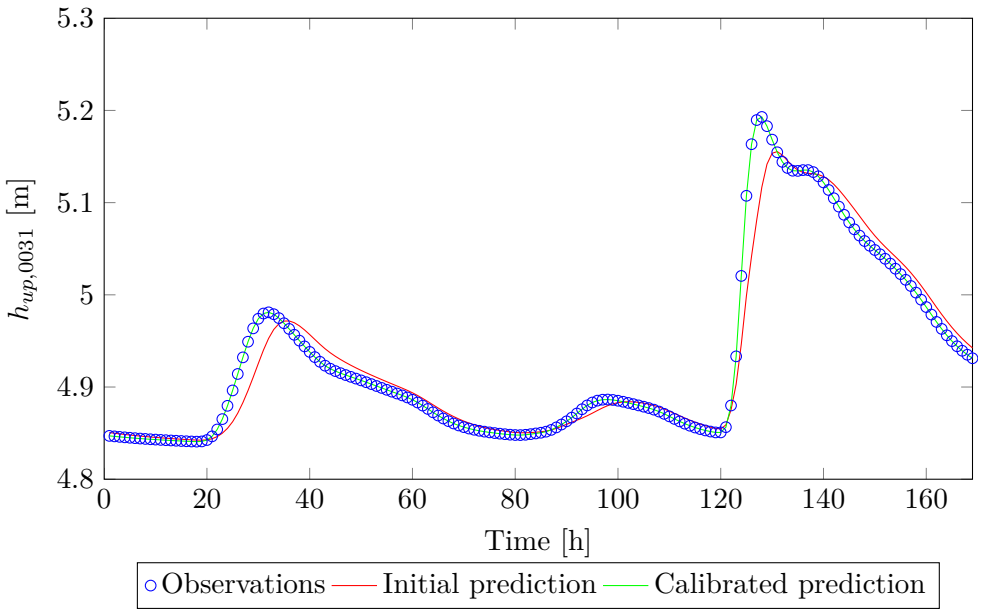

Figure D-17: The upstream water level at location 0031 for scenario FaWcH1H1 (G1) as function of time in the calibration window. The blue dots represent the observational data, the red line the initial prediction and the green line the calibrated prediction.

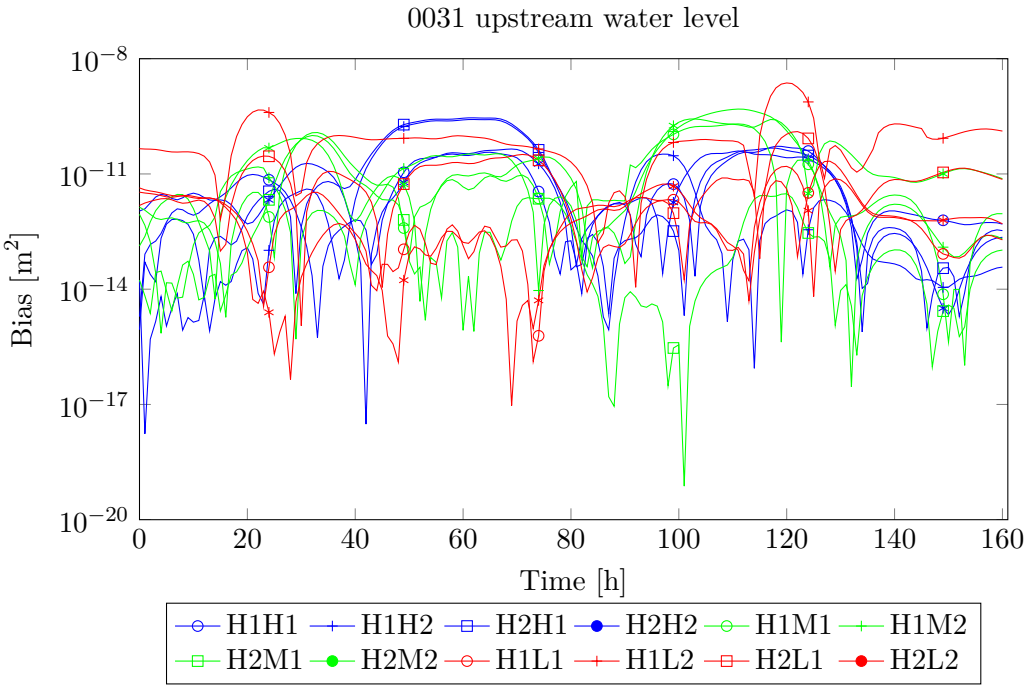

Figure D-18: The bias for the upstream water level at location 0031 for the FaWc (G1) scenarios with different starting points, three actual crest level values and one actual friction value as function of time in the calibration windows (with a time window $T = 2$h).

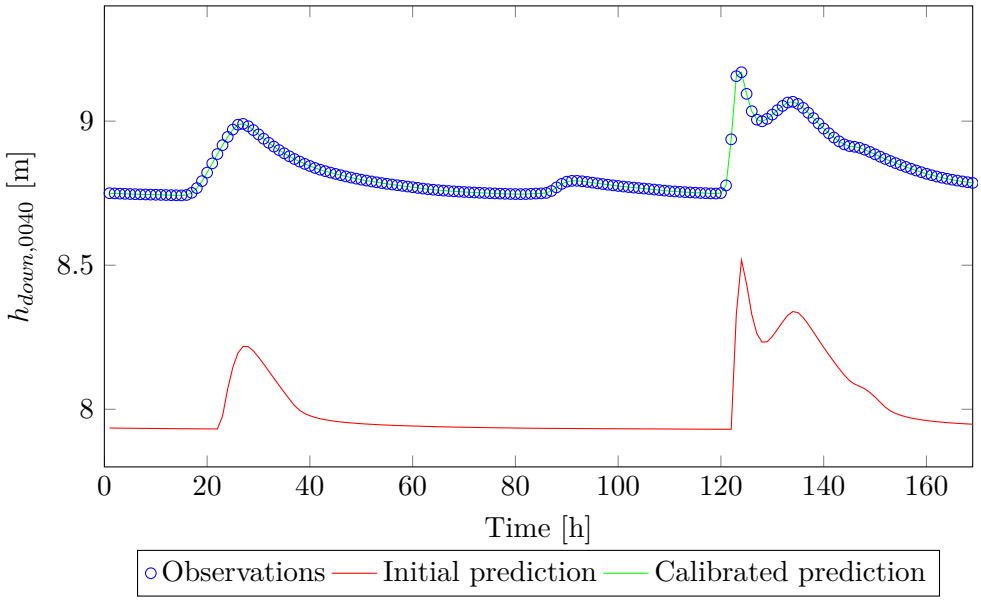

Figure D-19: The downstream water level at location 0040 for scenario FaWcH1H1 (G1) as function of time in the calibration window. The blue dots represent the observational data, the red line the initial prediction and the green line the calibrated prediction.

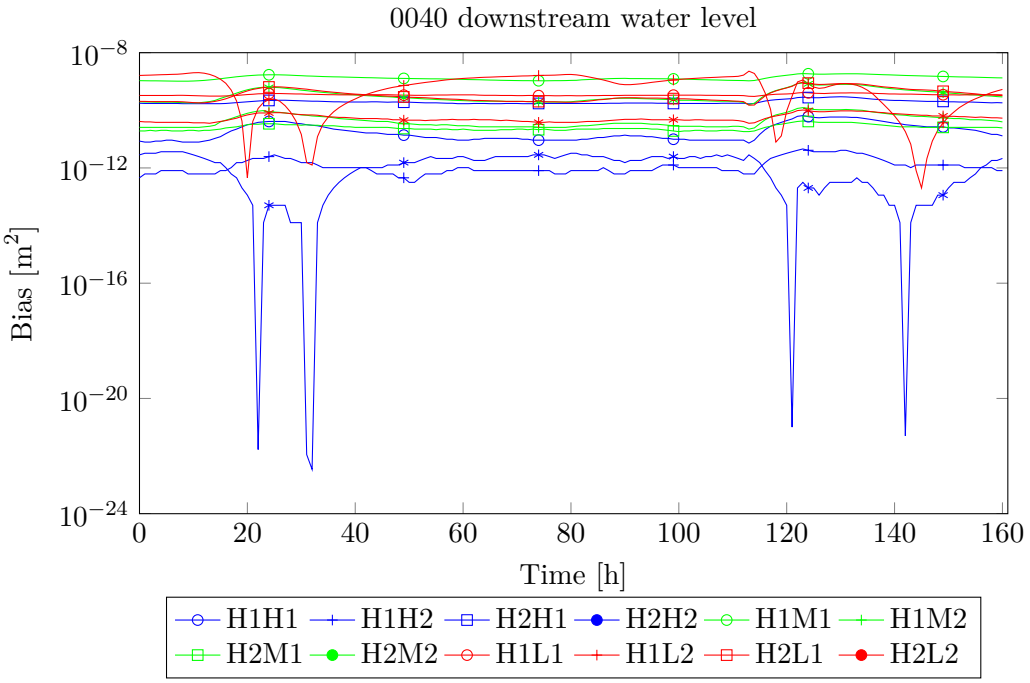

Figure D-20: The bias for the downstream water level at location 0040 for the FaWc (G1) scenarios with different starting points, three actual crest level values and one actual friction value as function of time in the calibration windows (with a time window $T = 2$h).

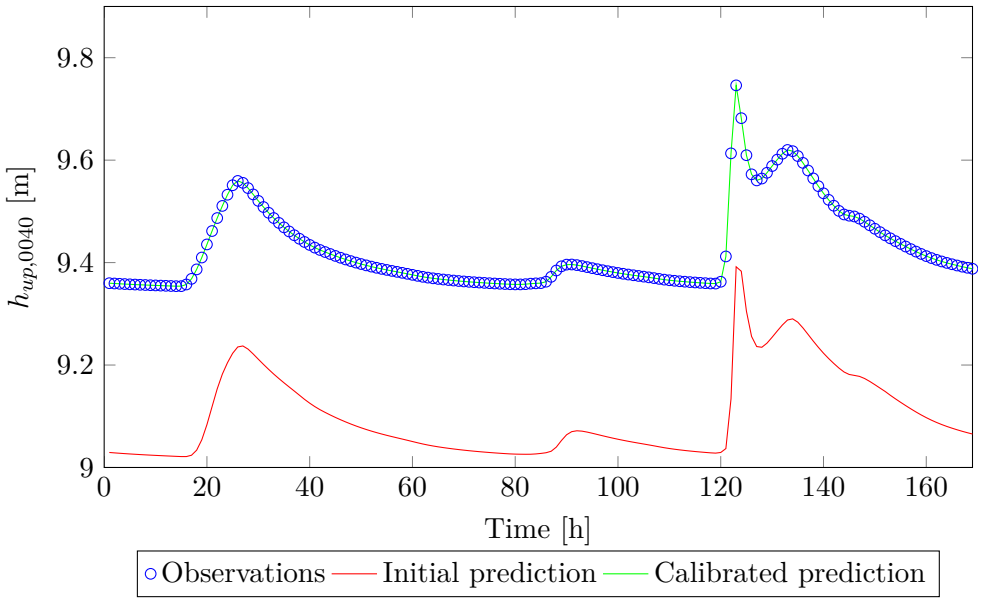

Figure D-21: The upstream water level at location 0040 for scenario FaWcH1H1 (G1) as function of time in the calibration window. The blue dots represent the observational data, the red line the initial prediction and the green line the calibrated prediction.

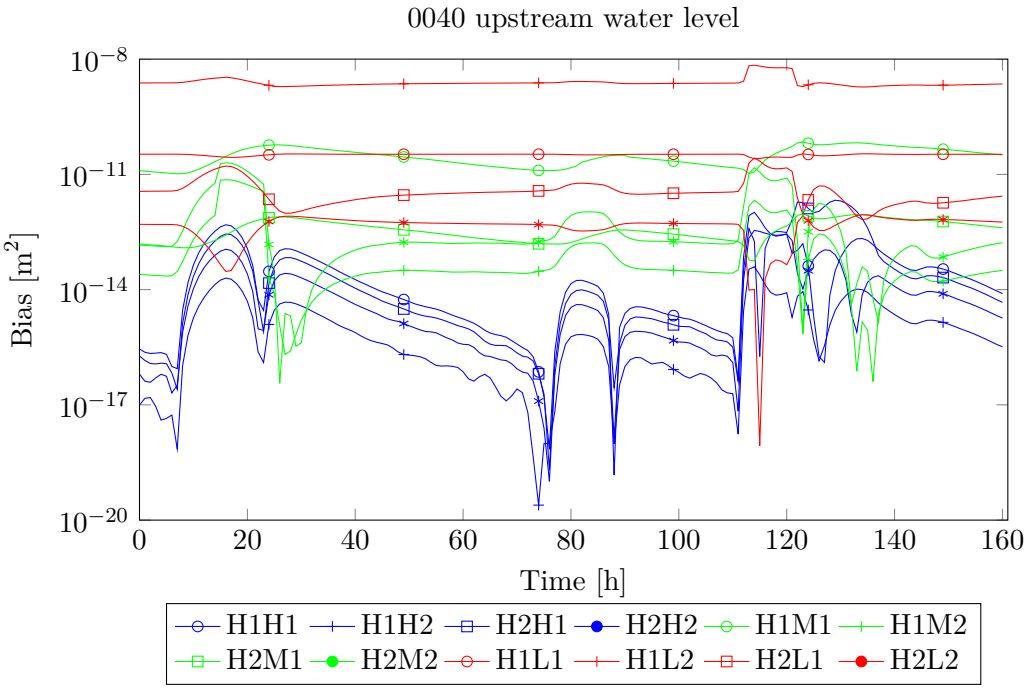

Figure D-22: The bias for the upstream water level at location 0040 for the FaWc (G1) scenarios with different starting points, three actual crest level values and one actual friction value as function of time in the calibration windows (with a time window $T = 2$h).

D-2 Results group 2 (G2)

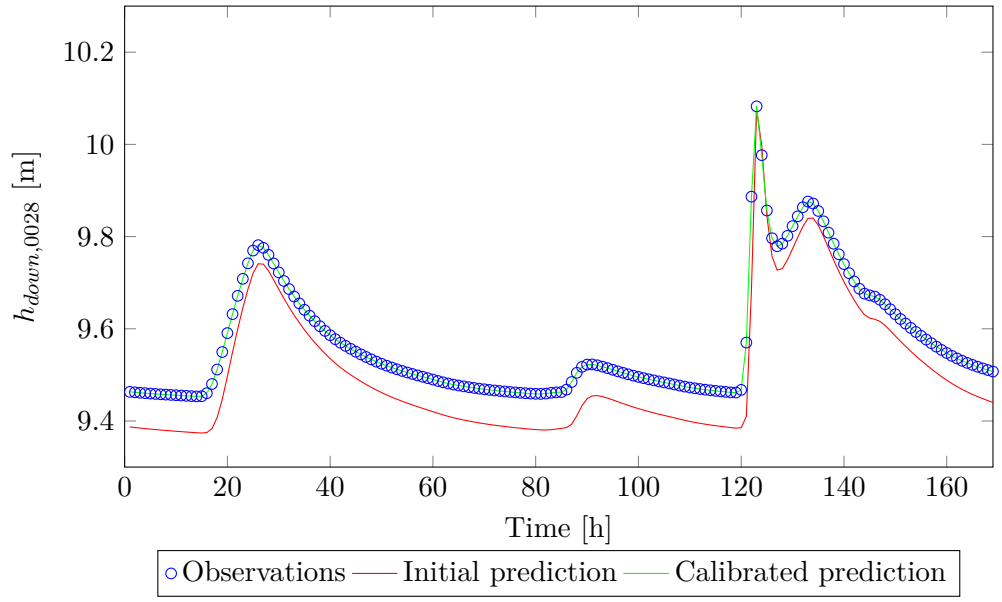

Figure D-23: The downstream water level at location 0028 for scenario FaWcM1H1 (G2) as function of time in the calibration window. The blue dots represent the observational data, the red line the initial prediction and the green line the calibrated prediction.

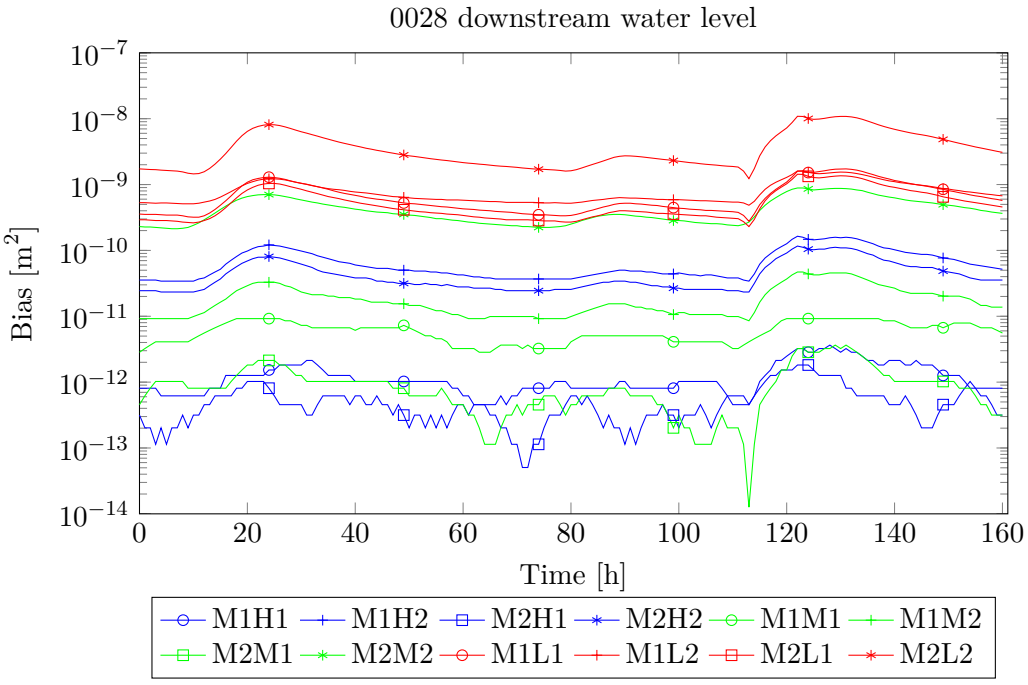

Figure D-24: The bias for the downstream water level at location 0028 for the FaWc (G2) scenarios with different starting points, three actual crest level values and one actual friction value as function of time in the calibration windows (with a time window $T = 2$h).

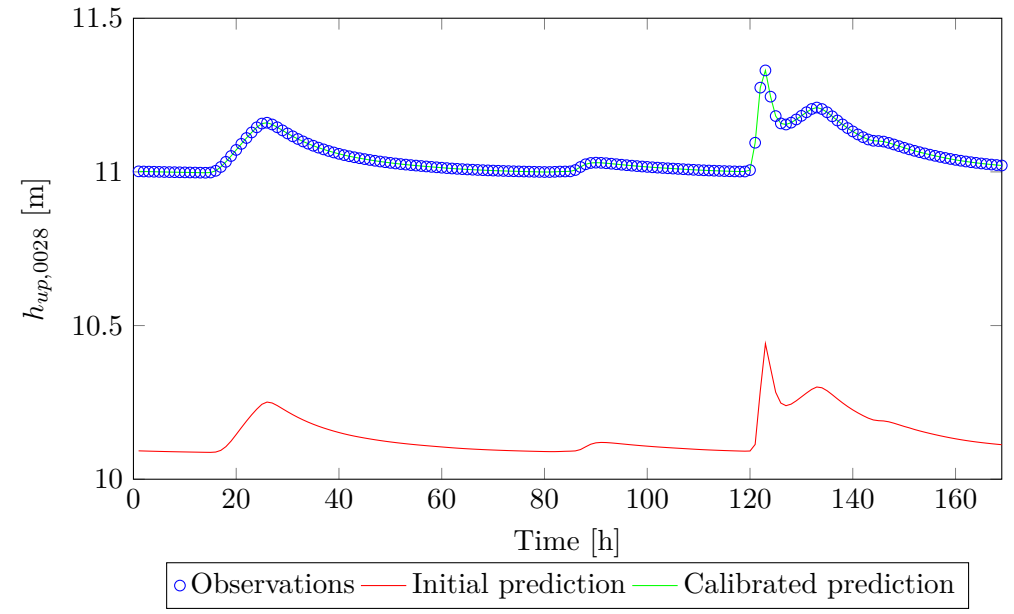

Figure D-25: The upstream water level at location 0028 for scenario FaWcM1H1 (G2) as function of time in the calibration window. The blue dots represent the observational data, the red line the initial prediction and the green line the calibrated prediction.

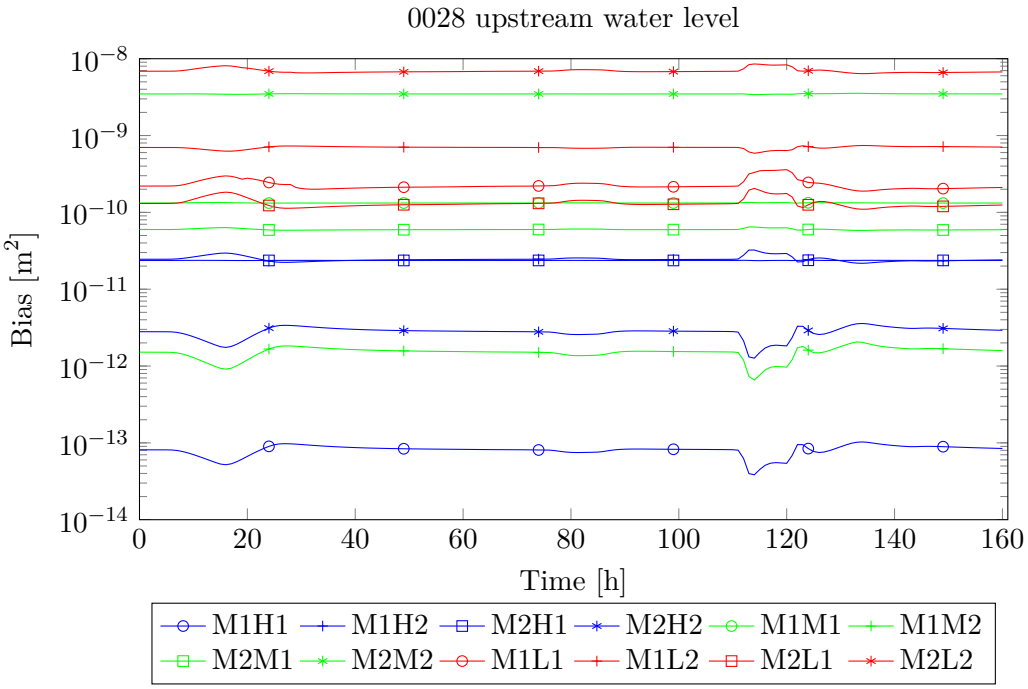

Figure D-26: The bias for the upstream water level at location 0028 for the FaWc (G2) scenarios with different starting points, three actual crest level values and one actual friction value as function of time in the calibration windows (with a time window $T = 2$h).

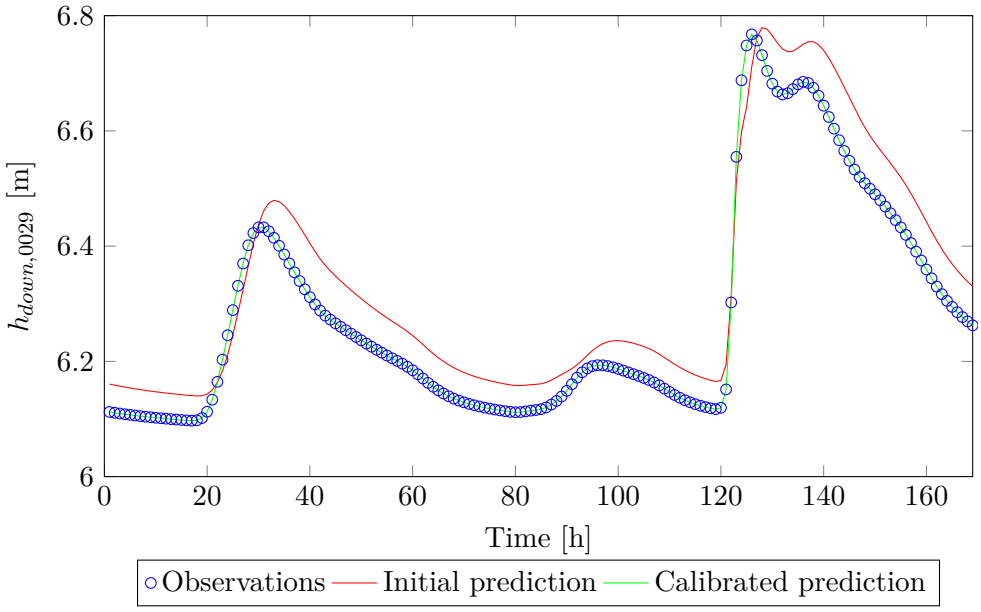

Figure D-27: The downstream water level at location 0029 for scenario FaWcM1H1 (G2) as function of time in the calibration window. The blue dots represent the observational data, the red line the initial prediction and the green line the calibrated prediction.

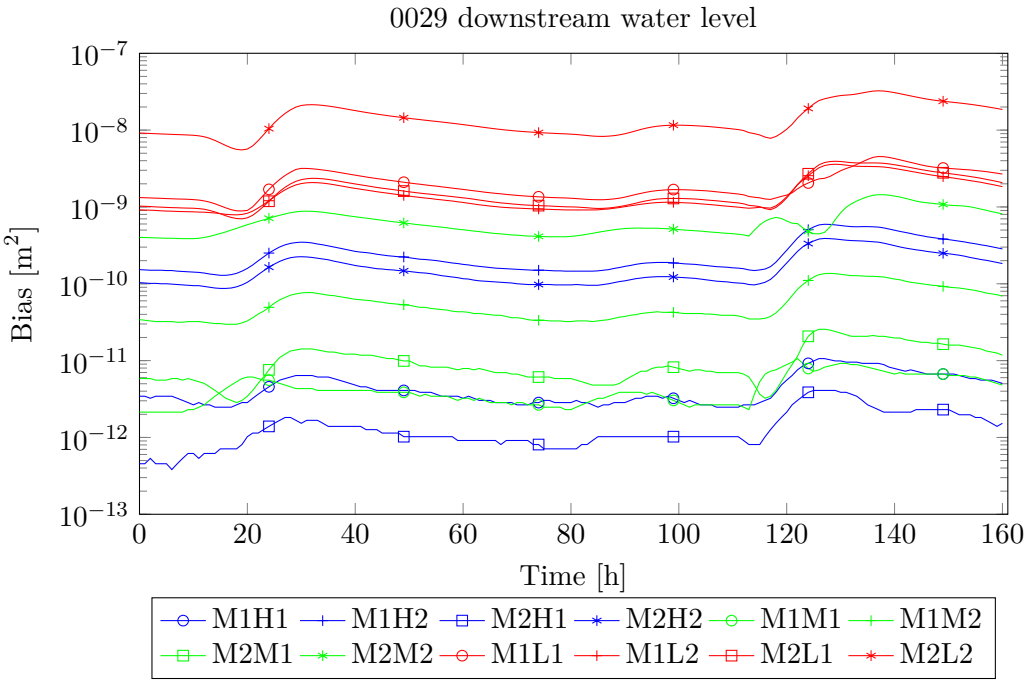

Figure D-28: The bias for the downstream water level at location 0029 for the FaWc (G2) scenarios with different starting points, three actual crest level values and one actual friction value as function of time in the calibration windows (with a time window $T = 2$h).

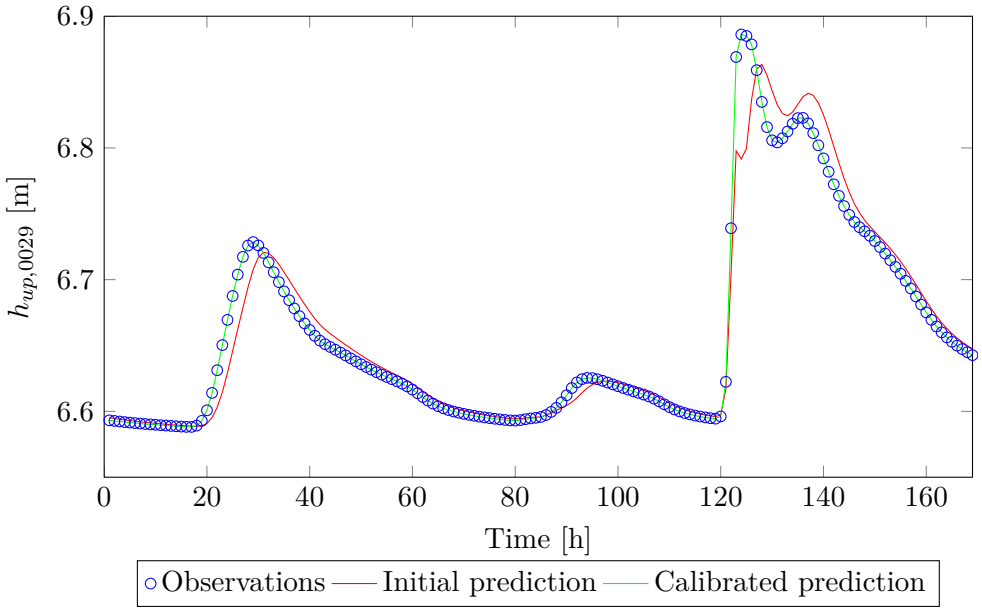

Figure D-29: The upstream water level at location 0029 for scenario FaWcM1H1 (G2) as function of time in the calibration window. The blue dots represent the observational data, the red line the initial prediction and the green line the calibrated prediction.

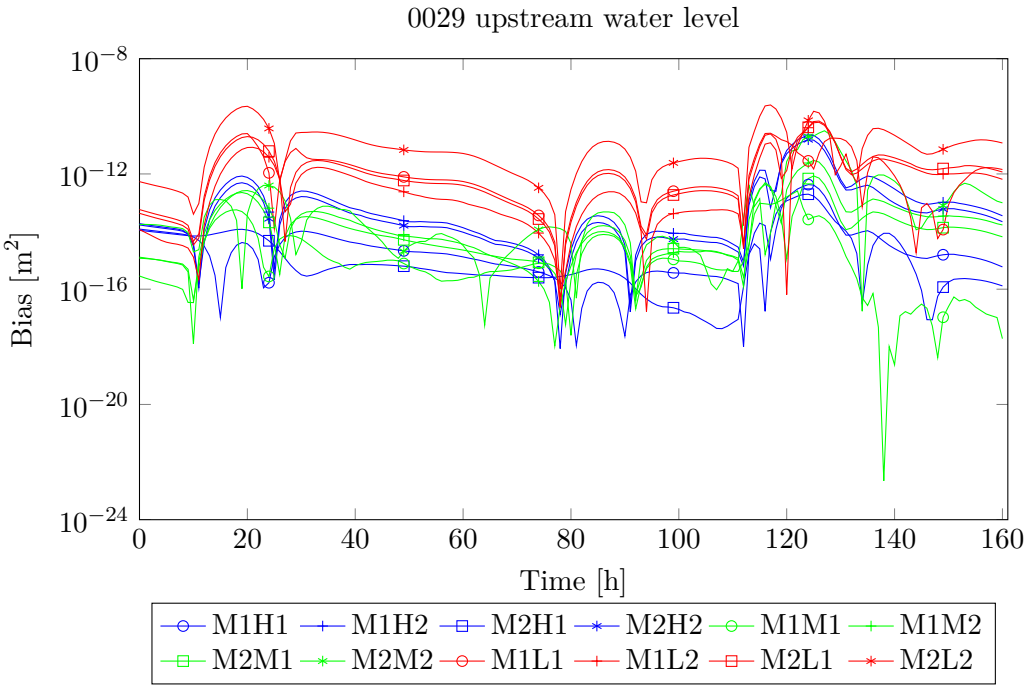

Figure D-30: The bias for the upstream water level at location 0029 for the FaWc (G2) scenarios with different starting points, three actual crest level values and one actual friction value as function of time in the calibration windows (with a time window $T = 2$h).

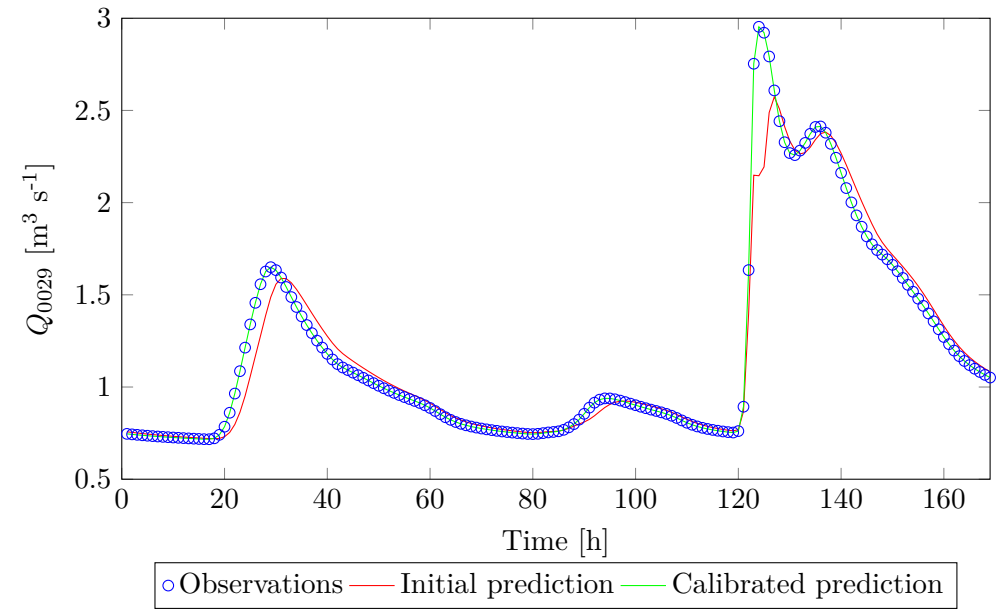

Figure D-31: The discharge at location 0029 for scenario FaWcM1H1 (G2) as function of time in the calibration window. The blue dots represent the observational data, the red line the initial prediction and the green line the calibrated prediction.

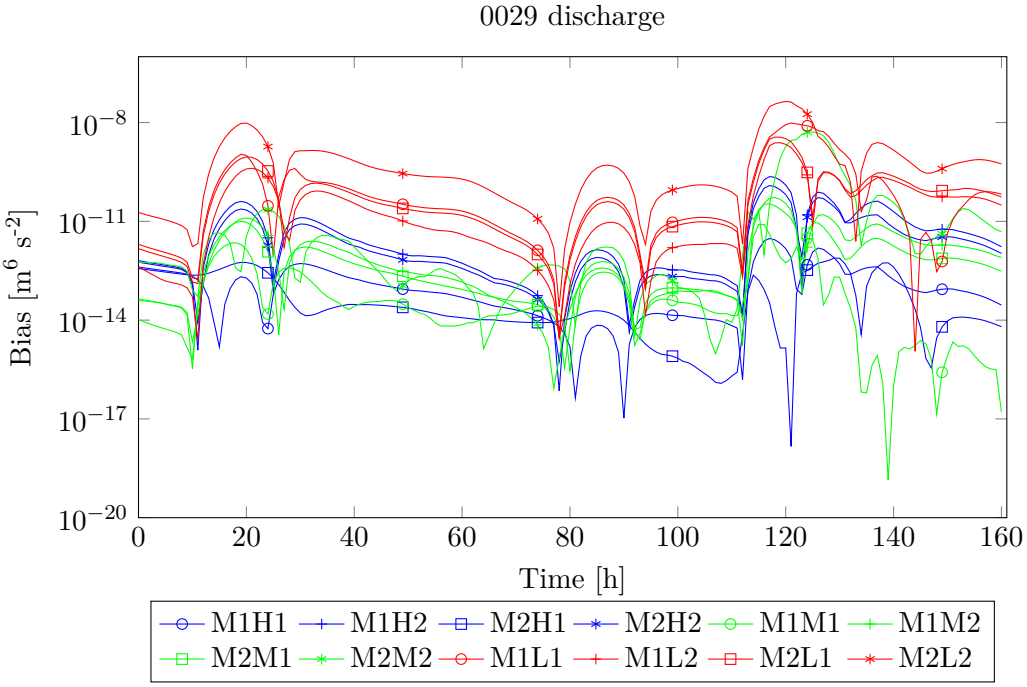

Figure D-32: The bias for the discharge at location 0029 for the FaWc (G2) scenarios with different starting points, three actual crest level values and one actual friction value as function of time in the calibration windows (with a time window $T = 2$h).

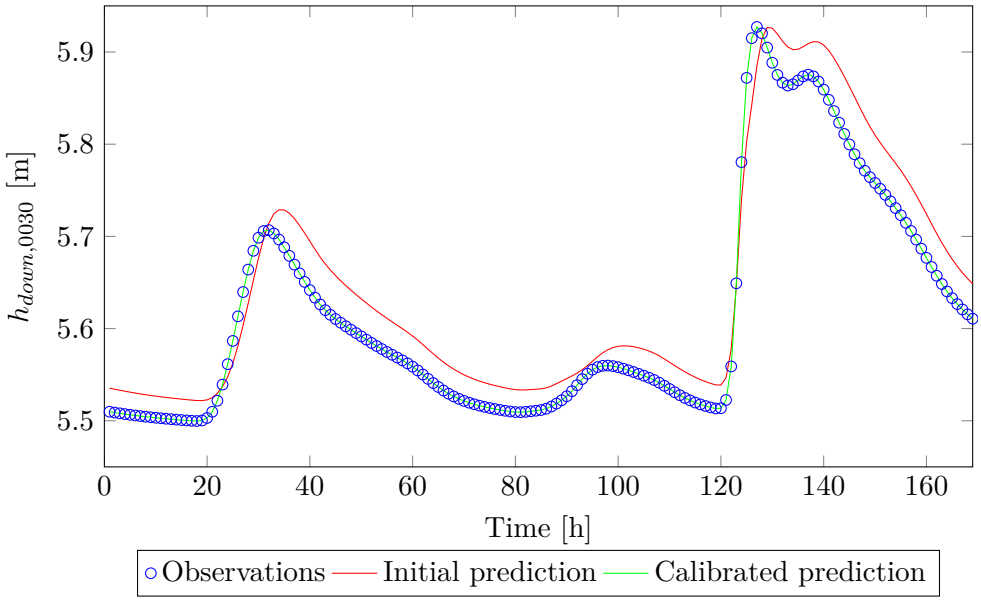

Figure D-33: The downstream water level at location 0030 for scenario FaWcM1H1 (G2) as function of time in the calibration window. The blue dots represent the observational data, the red line the initial prediction and the green line the calibrated prediction.

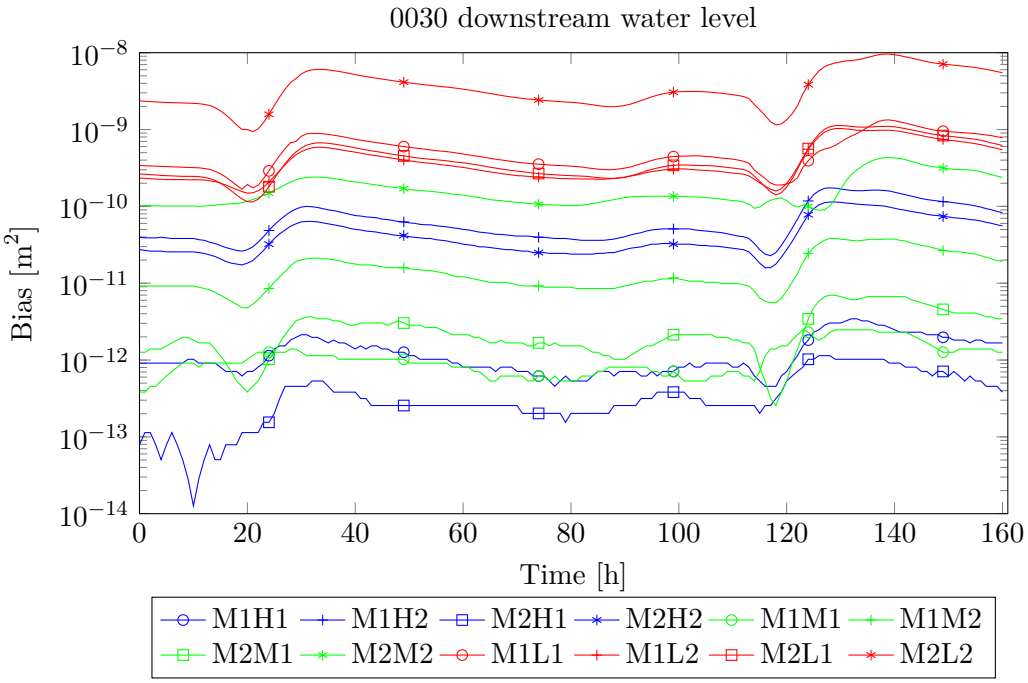

Figure D-34: The bias for the downstream water level at location 0030 for the FaWc (G2) scenarios with different starting points, three actual crest level values and one actual friction value as function of time in the calibration windows (with a time window $T = 2$h).

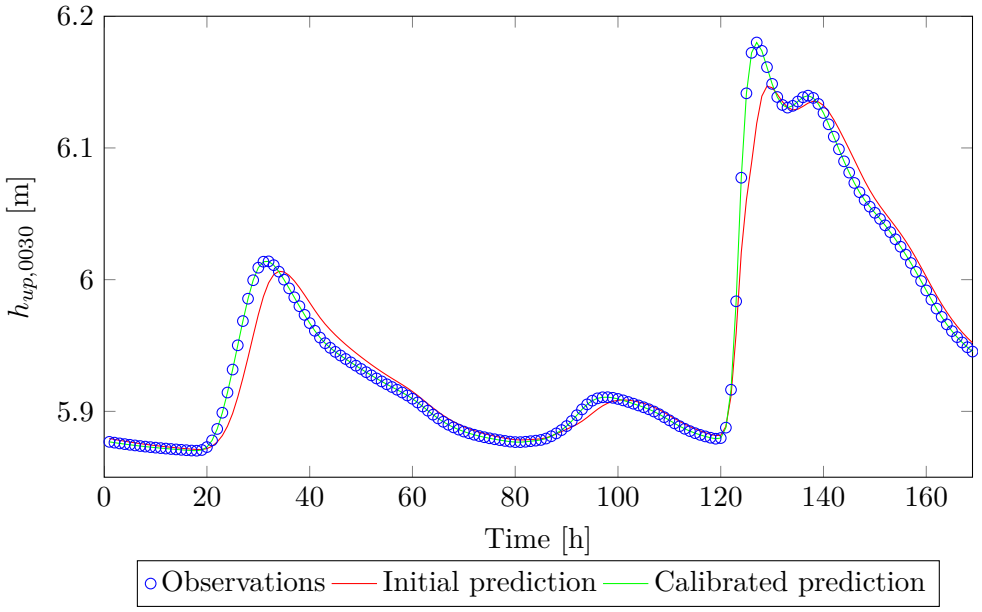

Figure D-35: The upstream water level at location 0030 for scenario FaWcM1H1 (G2) as function of time in the calibration window. The blue dots represent the observational data, the red line the initial prediction and the green line the calibrated prediction.

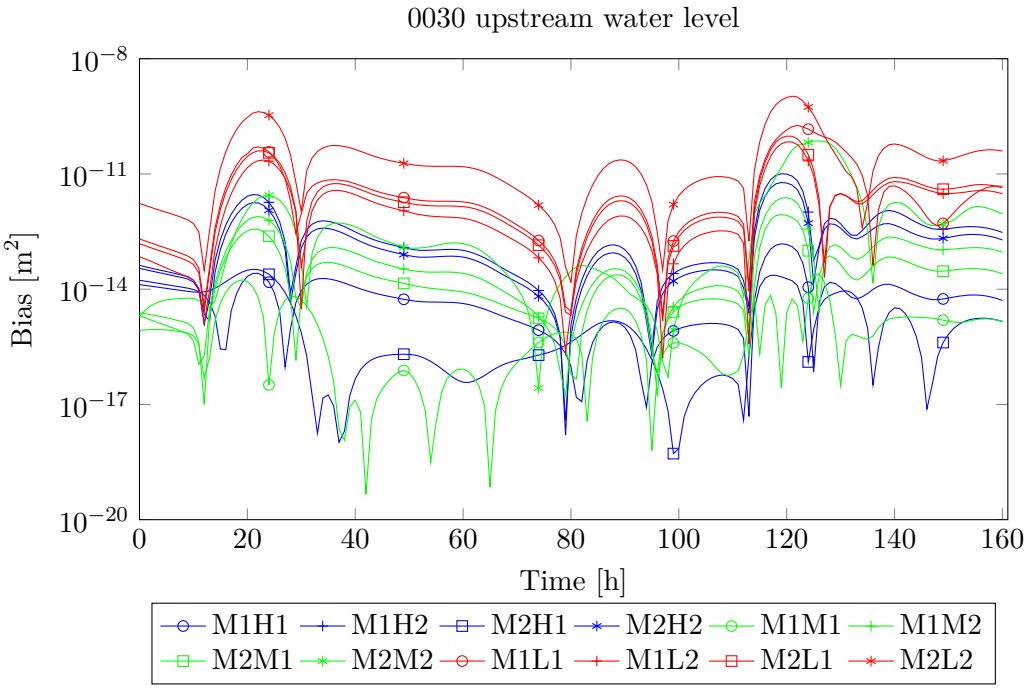

Figure D-36: The bias for the upstream water level at location 0030 for the FaWc (G2) scenarios with different starting points, three actual crest level values and one actual friction value as function of time in the calibration windows (with a time window $T = 2$h).

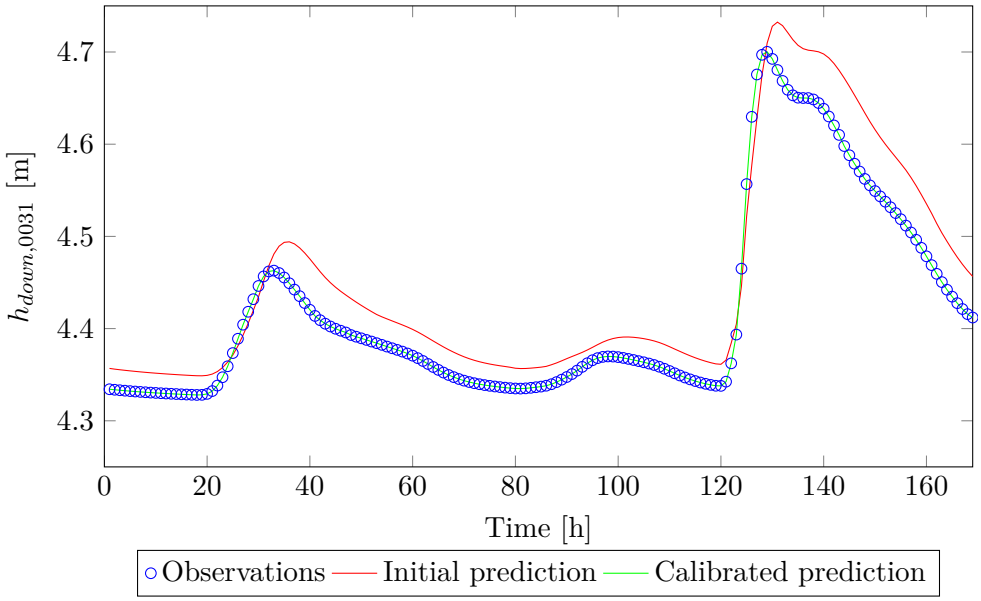

Figure D-37: The downstream water level at location 0031 for scenario FaWcM1H1 (G2) as function of time in the calibration window. The blue dots represent the observational data, the red line the initial prediction and the green line the calibrated prediction.

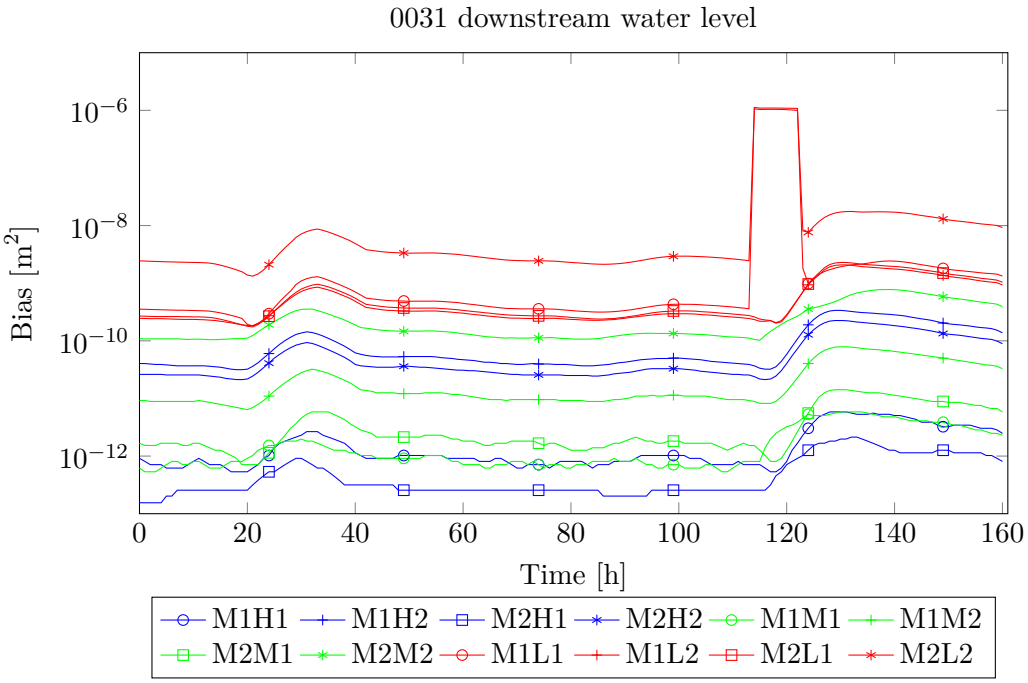

Figure D-38: The bias for the downstream water level at location 0031 for the FaWc (G2) scenarios with different starting points, three actual crest level values and one actual friction value as function of time in the calibration windows (with a time window $T = 2$h).

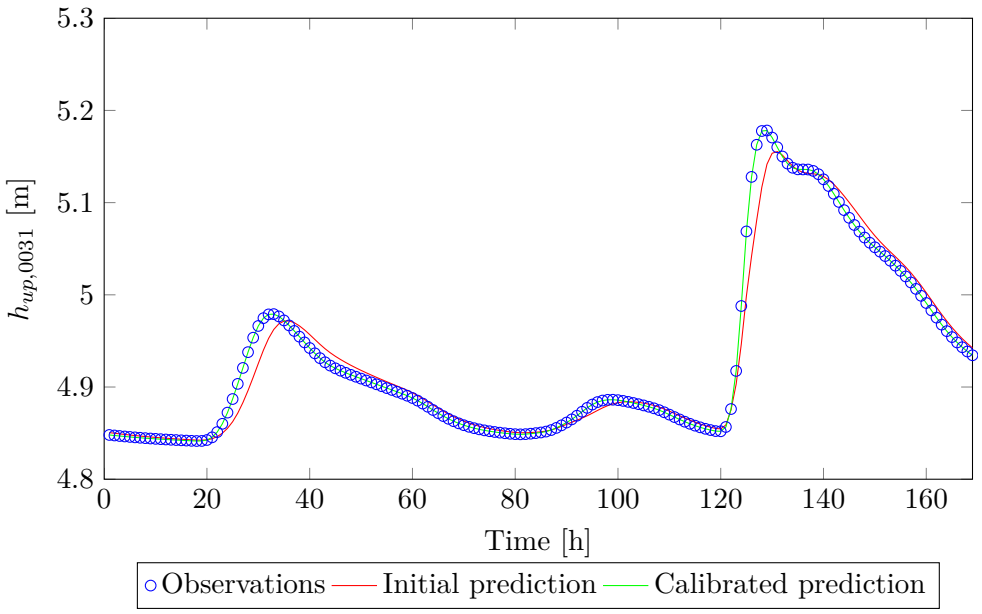

Figure D-39: The upstream water level at location 0031 for scenario FaWcM1H1 (G2) as function of time in the calibration window. The blue dots represent the observational data, the red line the initial prediction and the green line the calibrated prediction.

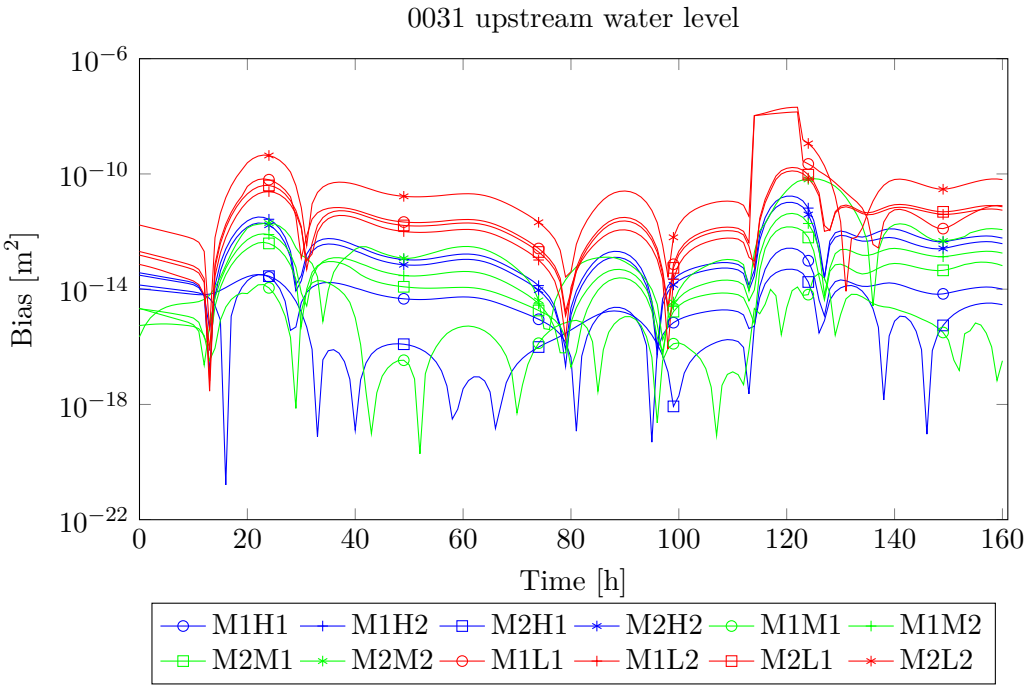

Figure D-40: The bias for the upstream water level at location 0031 for the FaWc (G2) scenarios with different starting points, three actual crest level values and one actual friction value as function of time in the calibration windows (with a time window $T = 2$h).

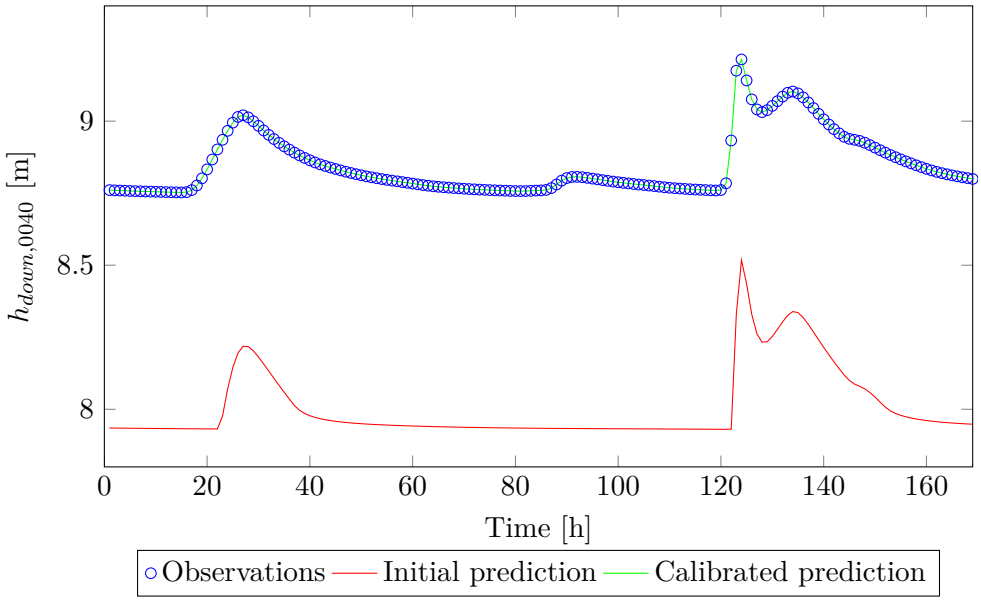

Figure D-41: The downstream water level at location 0040 for scenario FaWcM1H1 (G2) as function of time in the calibration window. The blue dots represent the observational data, the red line the initial prediction and the green line the calibrated prediction.

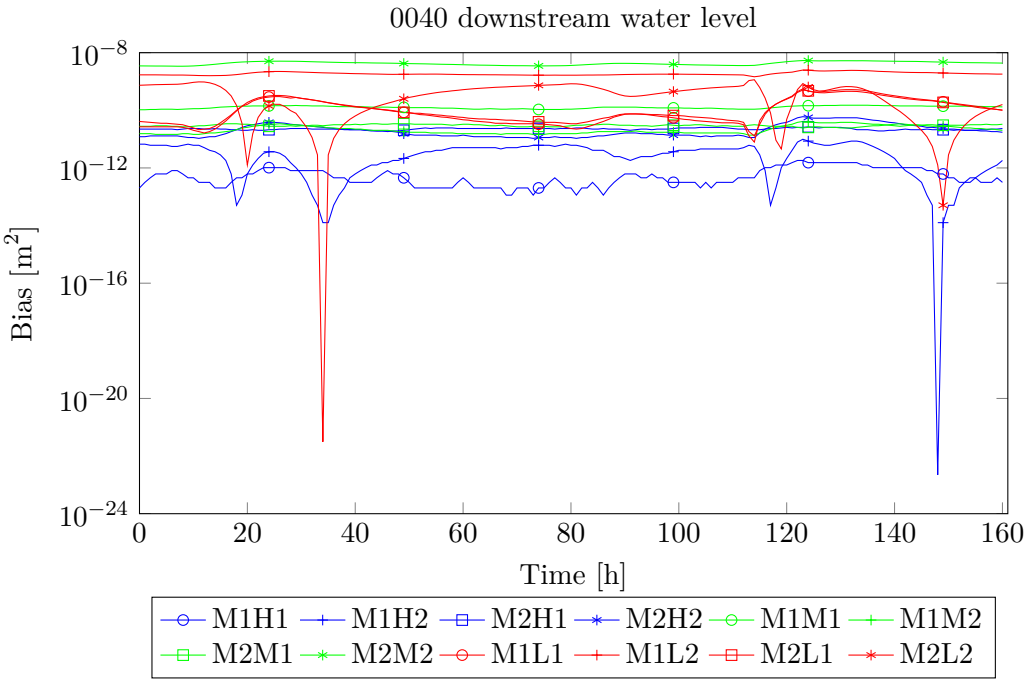

Figure D-42: The bias for the downstream water level at location 0040 for the FaWc (G2) scenarios with different starting points, three actual crest level values and one actual friction value as function of time in the calibration windows (with a time window $T = 2$h).

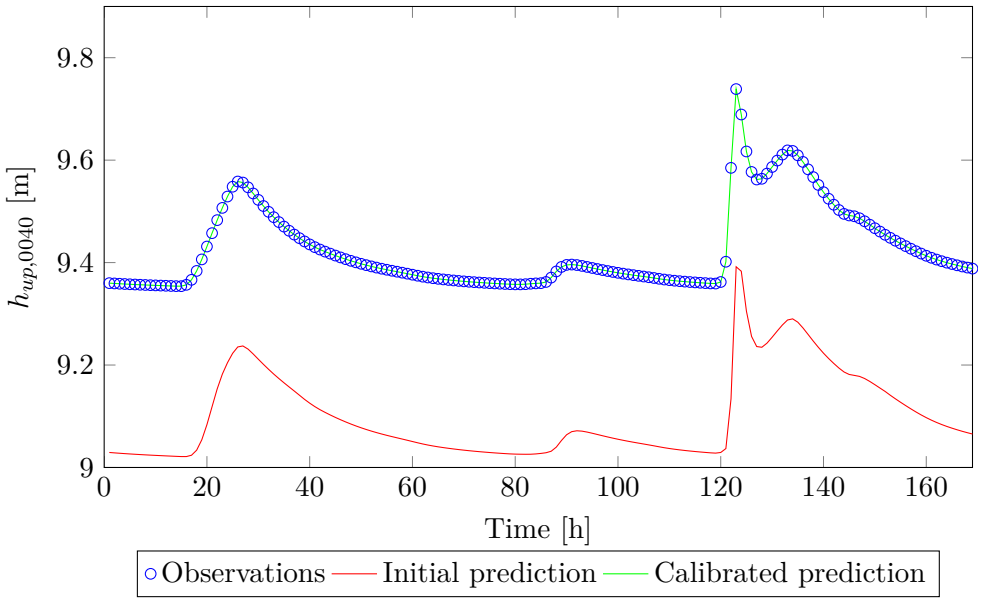

Figure D-43: The upstream water level at location 0040 for scenario FaWcM1H1 (G2) as function of time in the calibration window. The blue dots represent the observational data, the red line the initial prediction and the green line the calibrated prediction.

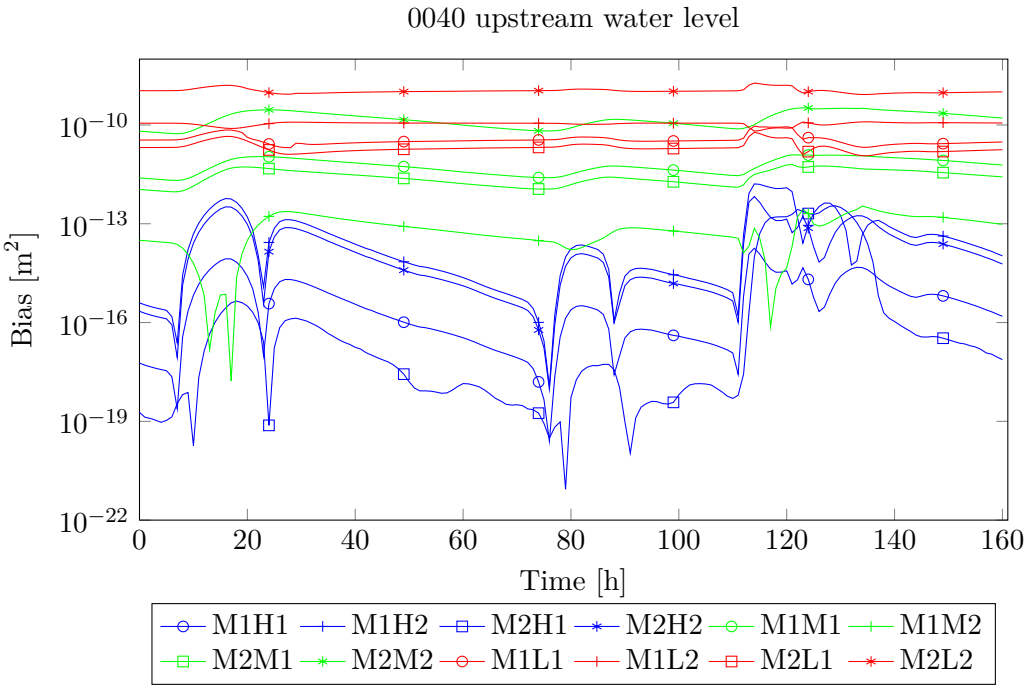

Figure D-44: The bias for the upstream water level at location 0040 for the FaWc (G2) scenarios with different starting points, three actual crest level values and one actual friction value as function of time in the calibration windows (with a time window $T = 2$h).

D-3 Results group 3 (G3)

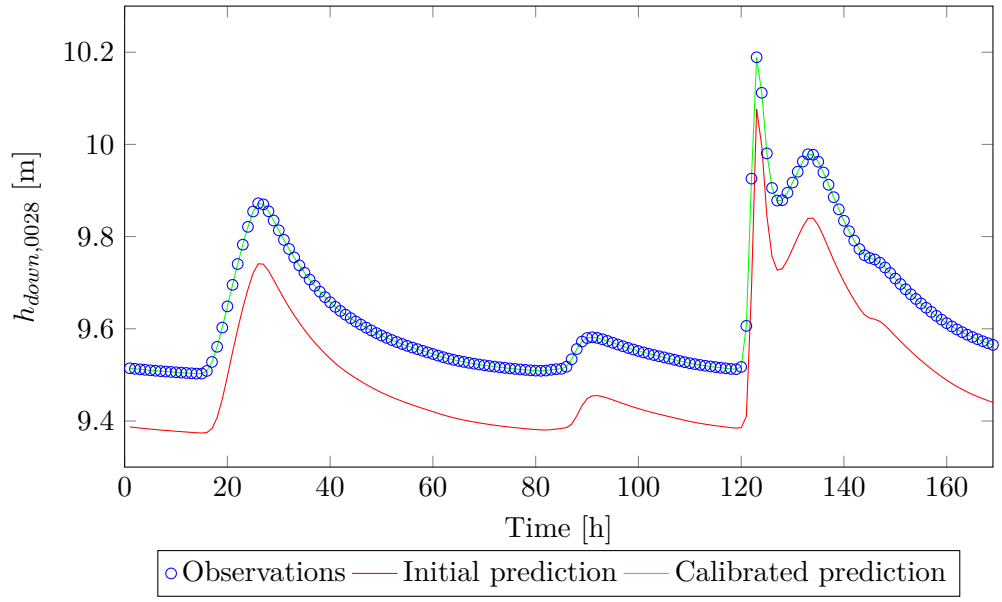

Figure D-45: The downstream water level at location 0028 for scenario FaWcL1H1 (G3) as function of time in the calibration window. The blue dots represent the observational data, the red line the initial prediction and the green line the calibrated prediction.

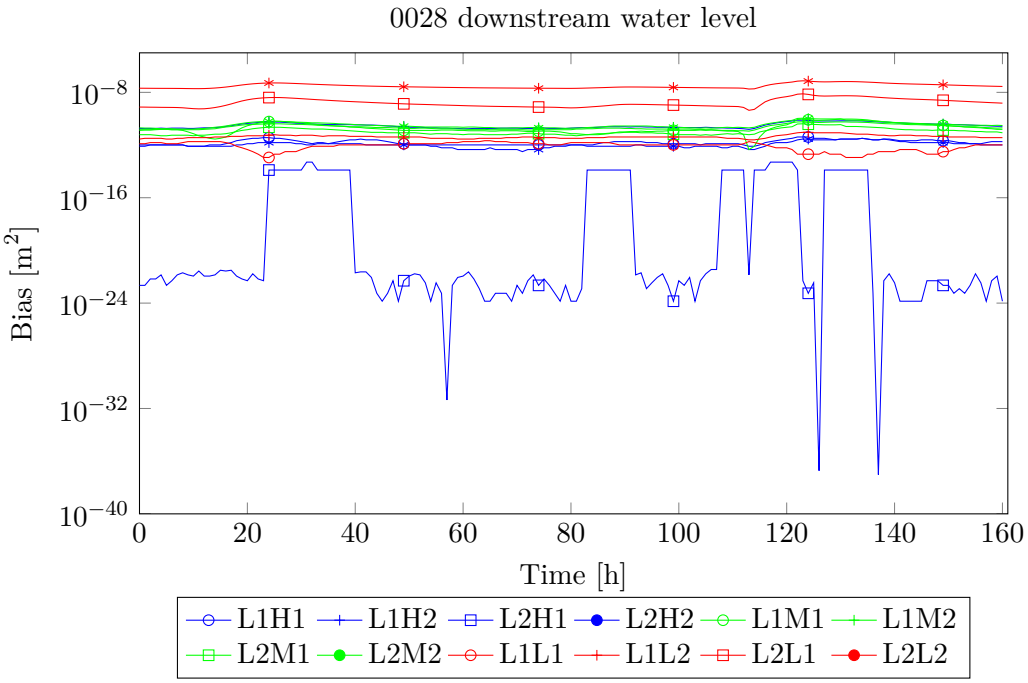

Figure D-46: The bias for the downstream water level at location 0028 for the FaWc (G3) scenarios with different starting points, three actual crest level values and one actual friction value as function of time in the calibration windows (with a time window $T = 2$h).

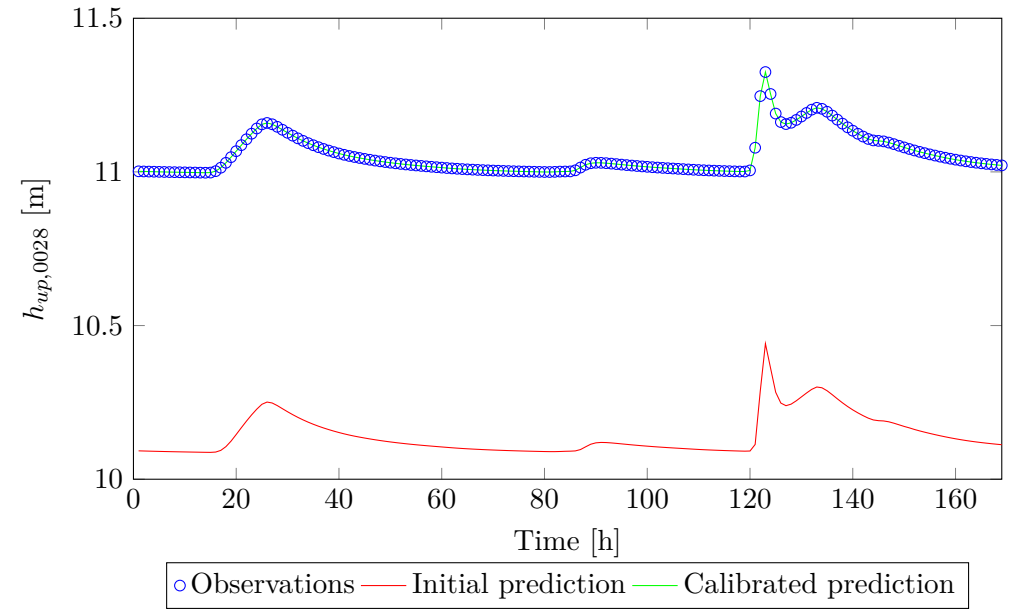

Figure D-47: The upstream water level at location 0028 for scenario FaWcL1H1 (G3) as function of time in the calibration window. The blue dots represent the observational data, the red line the initial prediction and the green line the calibrated prediction.

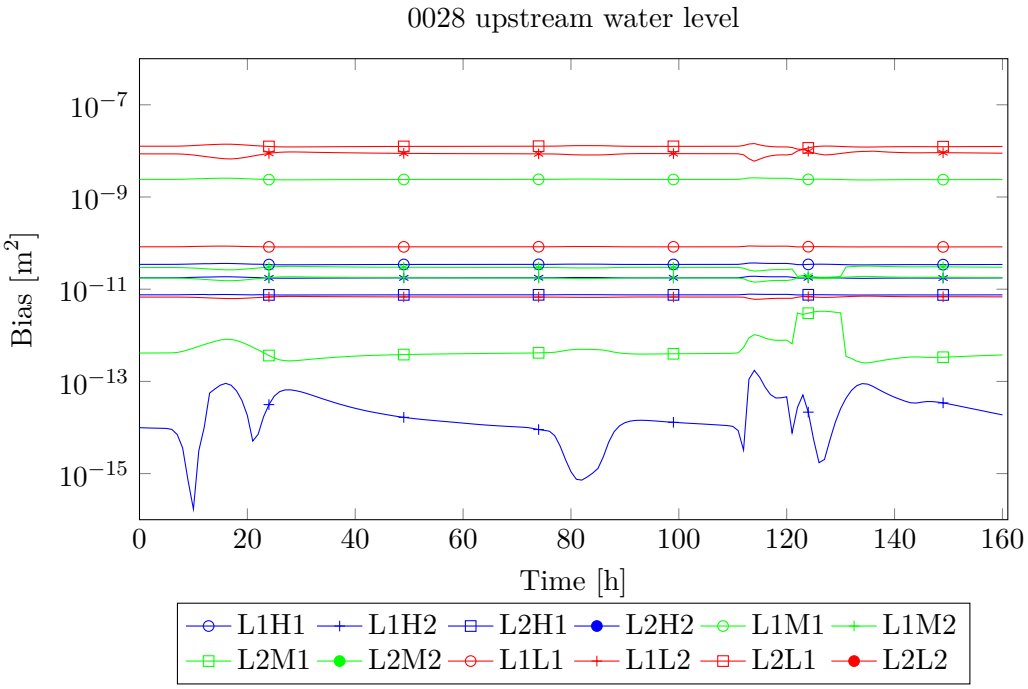

Figure D-48: The bias for the upstream water level at location 0028 for the FaWc (G3) scenarios with different starting points, three actual crest level values and one actual friction value as function of time in the calibration windows (with a time window $T = 2$h).

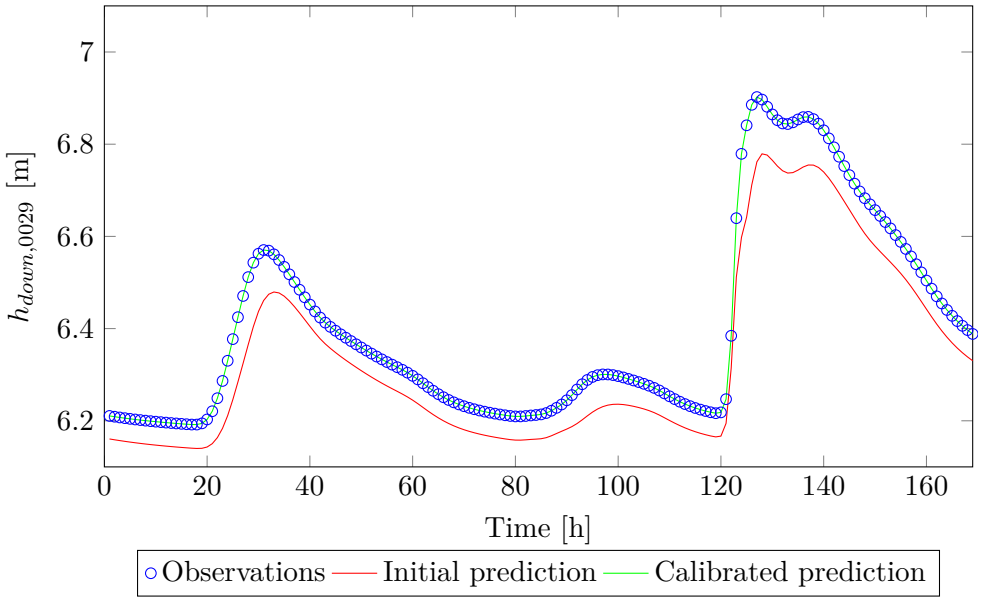

Figure D-49: The downstream water level at location 0029 for scenario FaWcL1H1 (G3) as function of time in the calibration window. The blue dots represent the observational data, the red line the initial prediction and the green line the calibrated prediction.

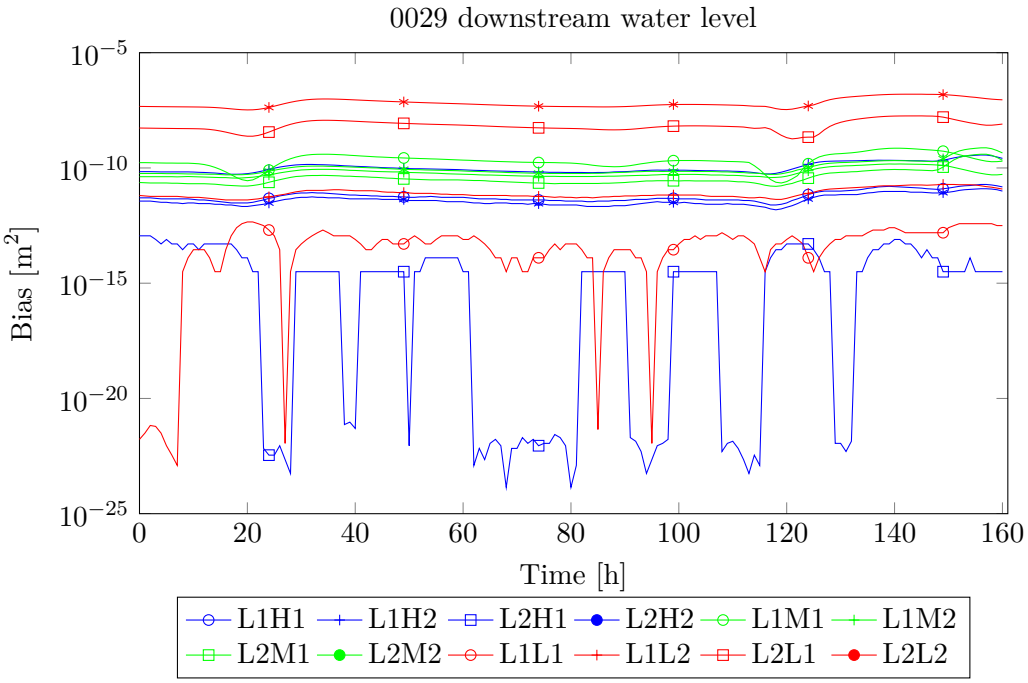

Figure D-50: The bias for the downstream water level at location 0029 for the FaWc (G3) scenarios with different starting points, three actual crest level values and one actual friction value as function of time in the calibration windows (with a time window $T = 2$h).

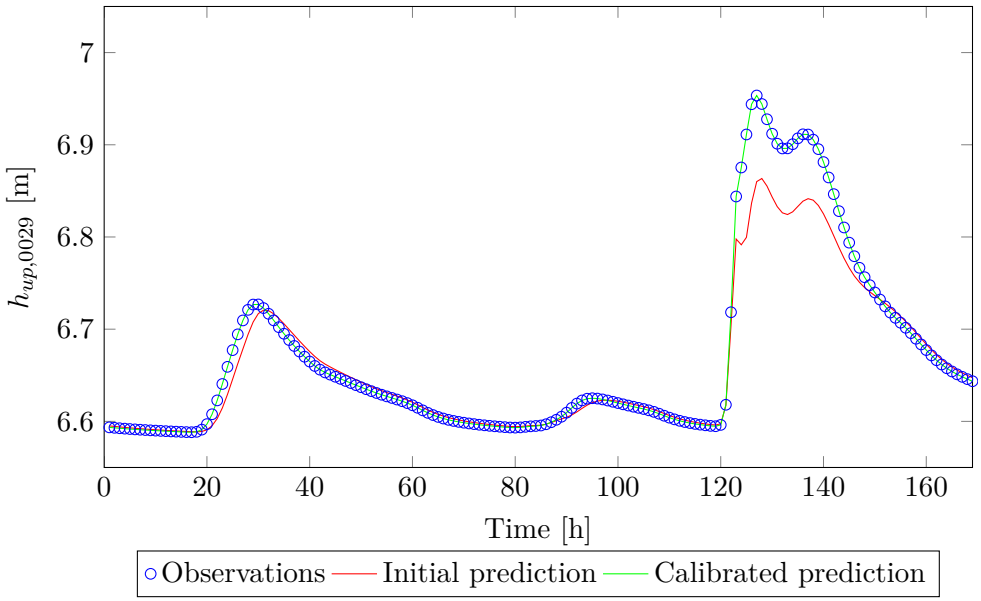

Figure D-51: The upstream water level at location 0029 for scenario FaWcL1H1 (G3) as function of time in the calibration window. The blue dots represent the observational data, the red line the initial prediction and the green line the calibrated prediction.

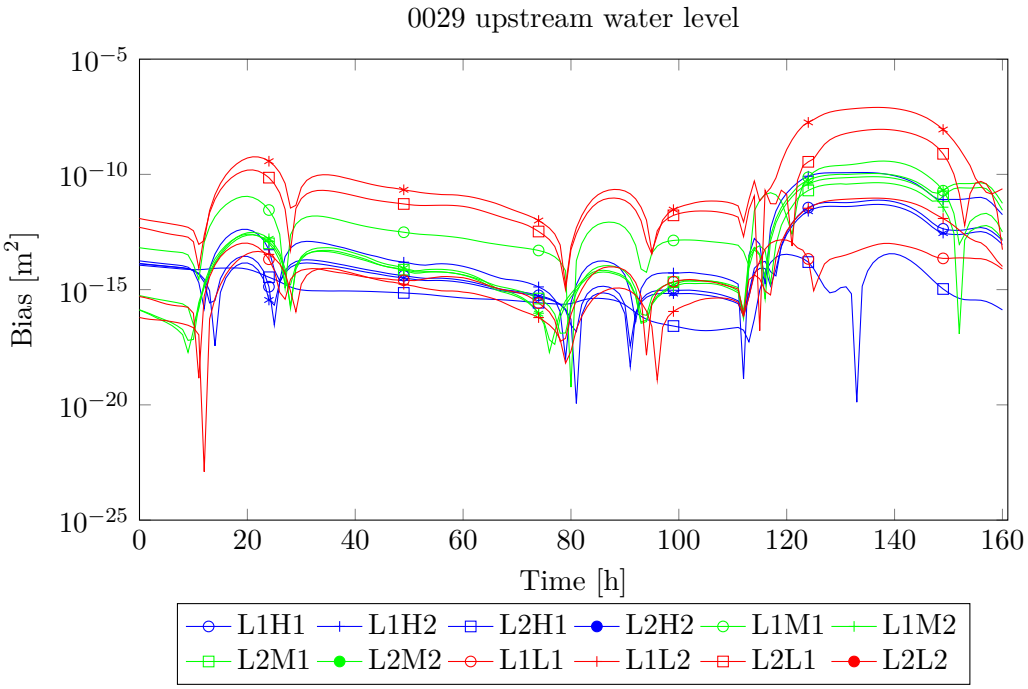

Figure D-52: The bias for the upstream water level at location 0029 for the FaWc (G3) scenarios with different starting points, three actual crest level values and one actual friction value as function of time in the calibration windows (with a time window $T = 2$h).

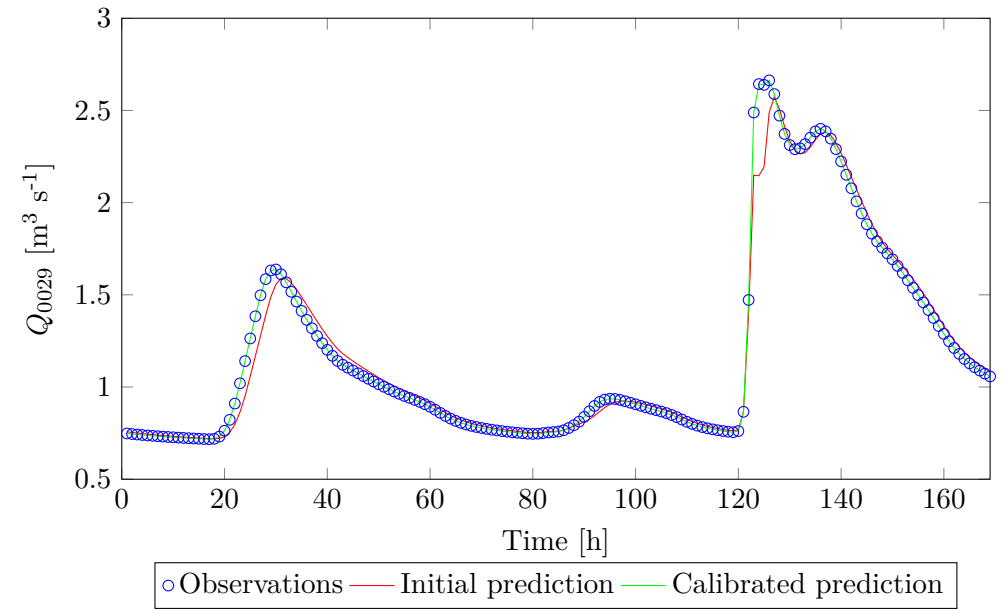

Figure D-53: The discharge at location 0029 for scenario FaWcL1H1 (G3) as function of time in the calibration window. The blue dots represent the observational data, the red line the initial prediction and the green line the calibrated prediction.

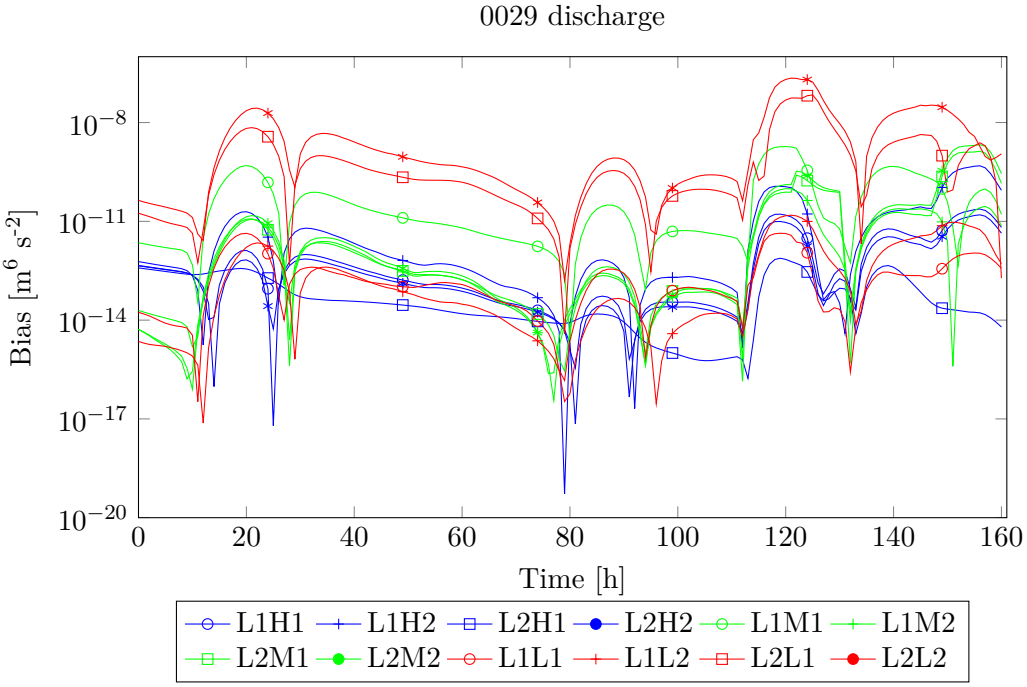

Figure D-54: The bias for the discharge at location 0029 for the FaWc (G3) scenarios with different starting points, three actual crest level values and one actual friction value as function of time in the calibration windows (with a time window $T = 2$h).

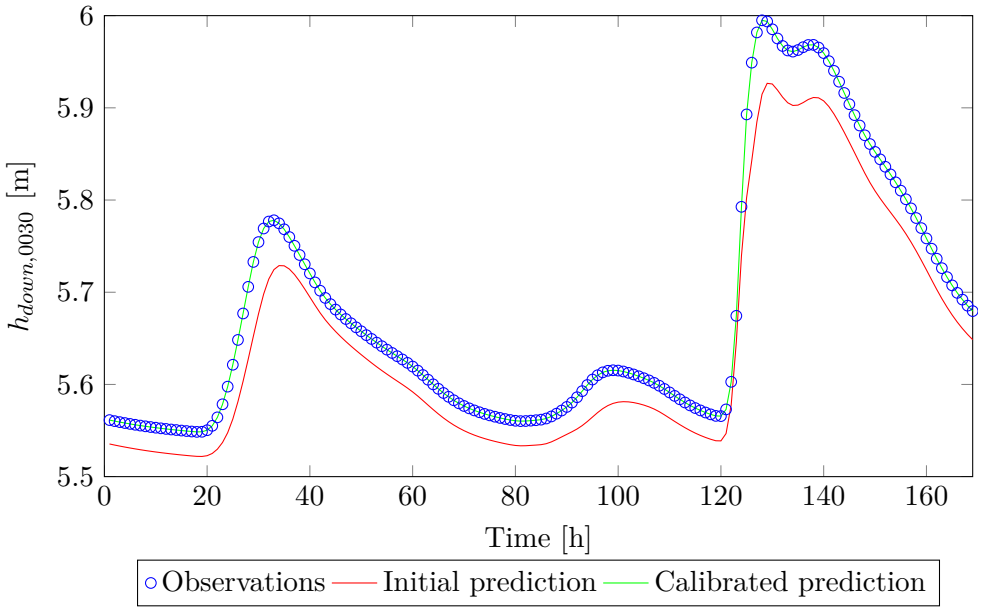

Figure D-55: The downstream water level at location 0030 for scenario FaWcL1H1 (G3) as function of time in the calibration window. The blue dots represent the observational data, the red line the initial prediction and the green line the calibrated prediction.

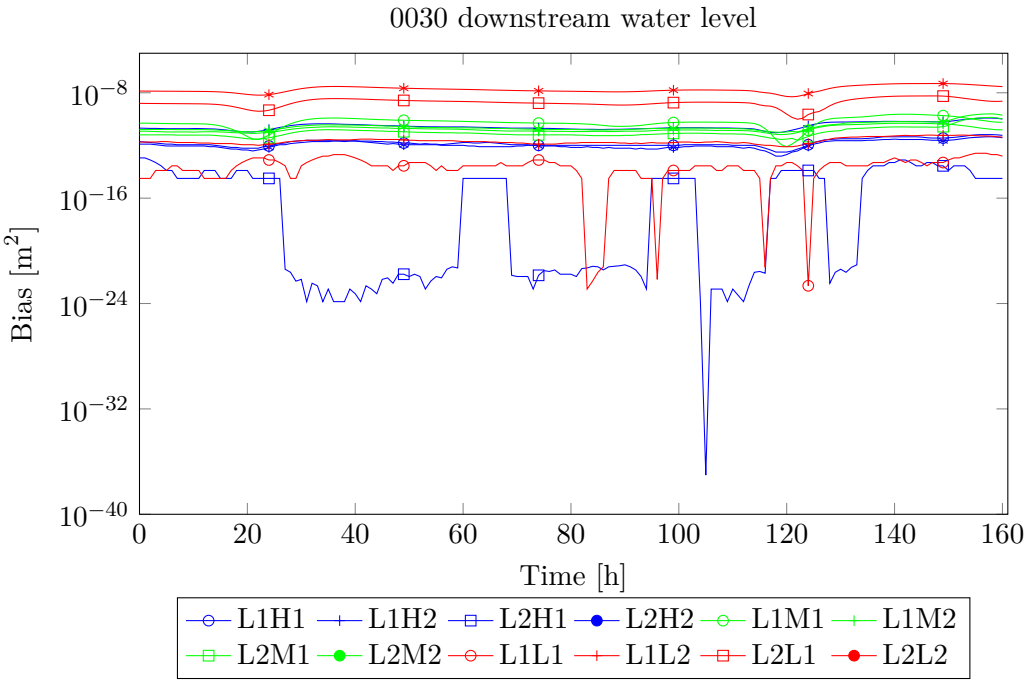

Figure D-56: The bias for the downstream water level at location 0030 for the FaWc (G3) scenarios with different starting points, three actual crest level values and one actual friction value as function of time in the calibration windows (with a time window $T = 2$h).

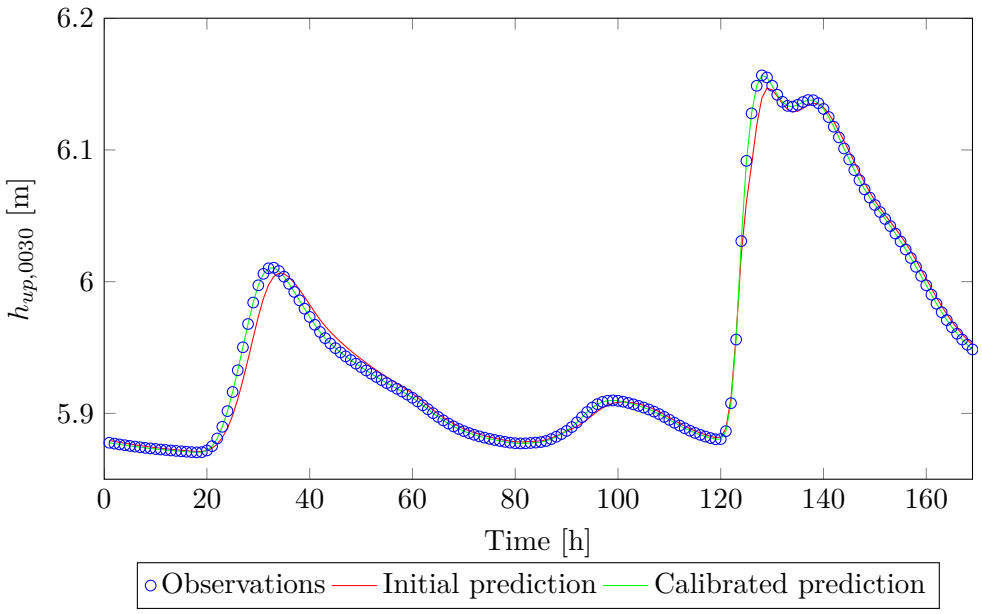

Figure D-57: The upstream water level at location 0030 for scenario FaWcL1H1 (G3) as function of time in the calibration window. The blue dots represent the observational data, the red line the initial prediction and the green line the calibrated prediction.

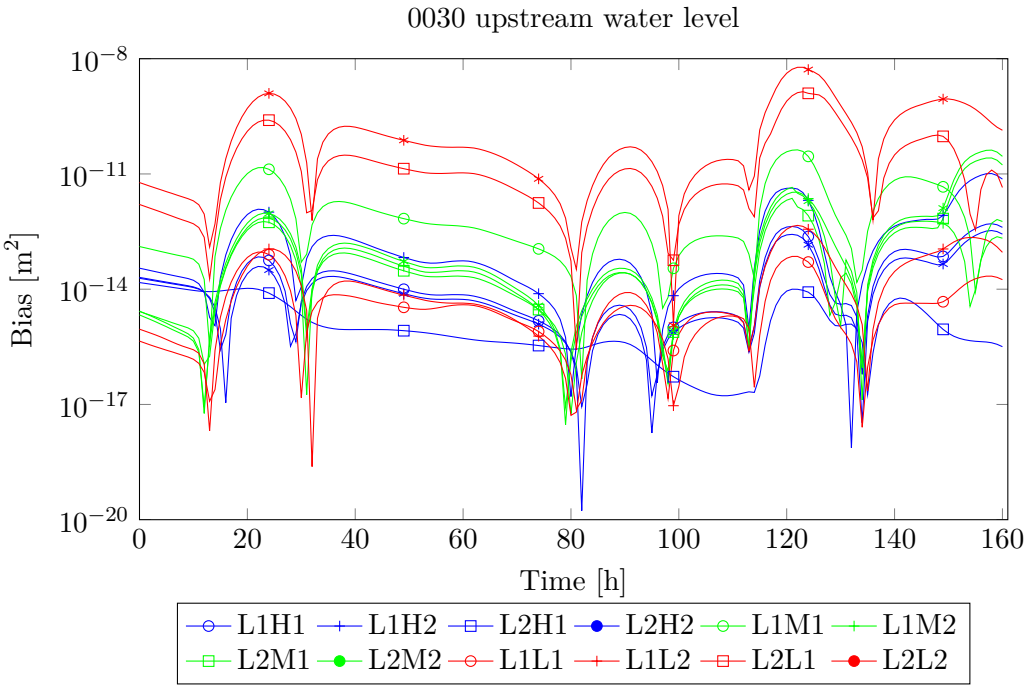

Figure D-58: The bias for the upstream water level at location 0030 for the FaWc (G3) scenarios with different starting points, three actual crest level values and one actual friction value as function of time in the calibration windows (with a time window $T = 2$h).

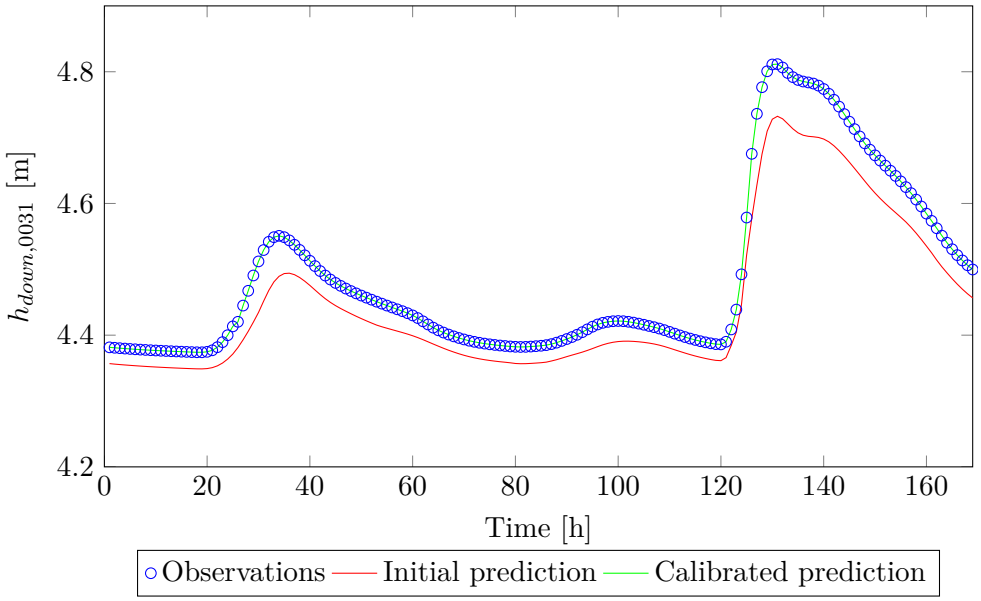

Figure D-59: The downstream water level at location 0031 for scenario FaWcL1H1 (G3) as function of time in the calibration window. The blue dots represent the observational data, the red line the initial prediction and the green line the calibrated prediction.

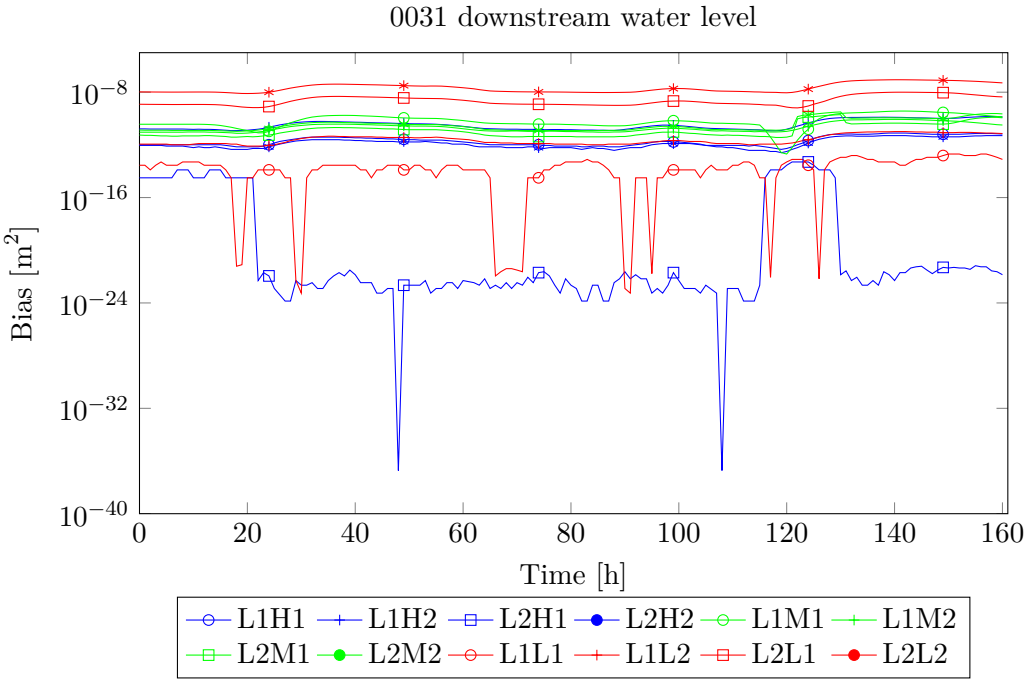

Figure D-60: The bias for the downstream water level at location 0031 for the FaWc (G3) scenarios with different starting points, three actual crest level values and one actual friction value as function of time in the calibration windows (with a time window $T = 2$h).

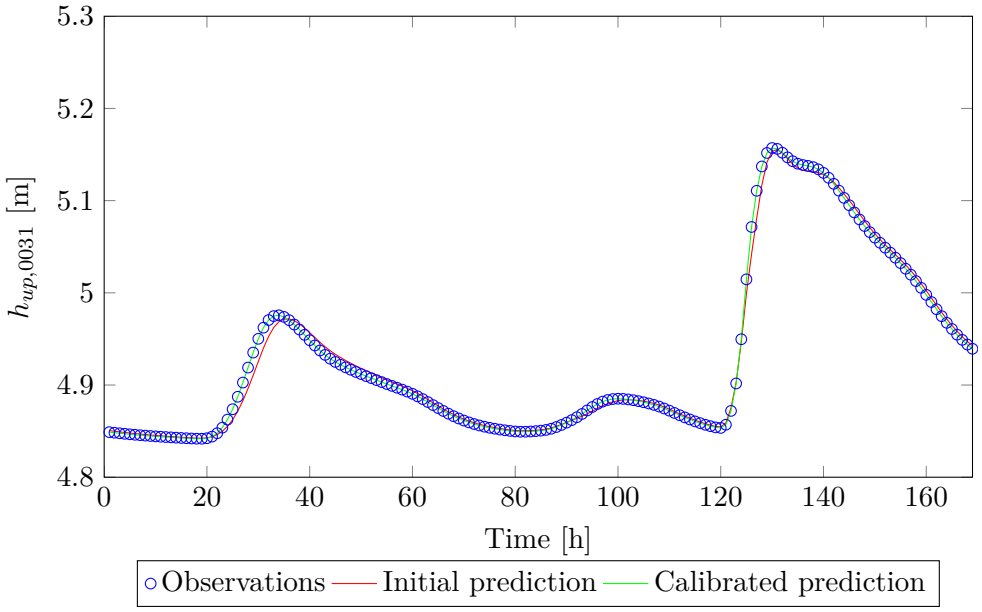

Figure D-61: The upstream water level at location 0031 for scenario FaWcL1H1 (G3) as function of time in the calibration window. The blue dots represent the observational data, the red line the initial prediction and the green line the calibrated prediction.

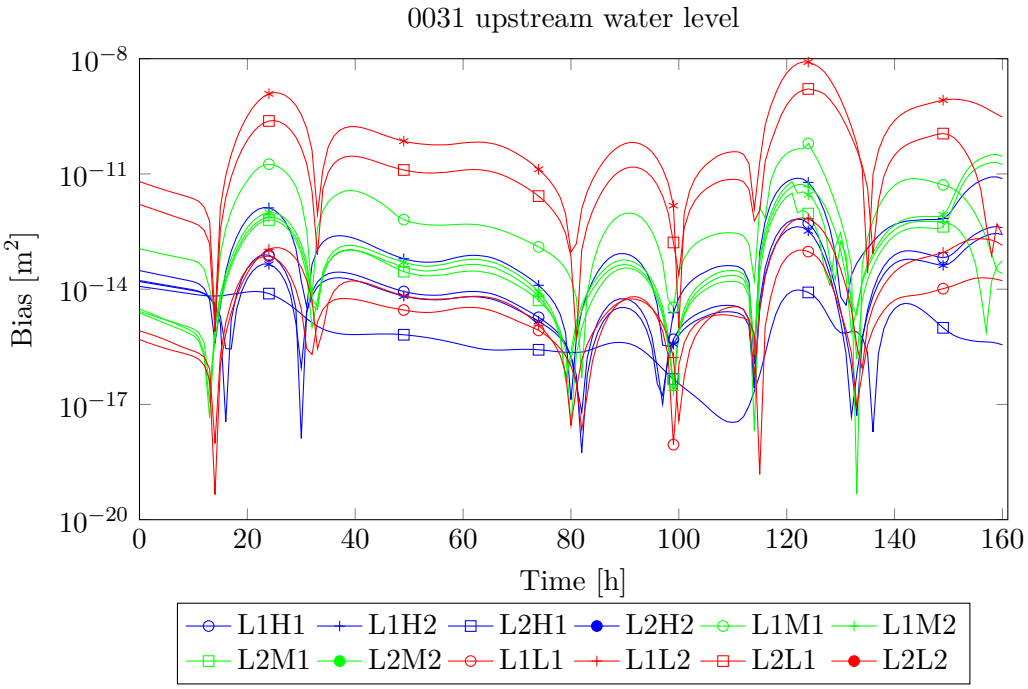

Figure D-62: The bias for the upstream water level at location 0031 for the FaWc (G3) scenarios with different starting points, three actual crest level values and one actual friction value as function of time in the calibration windows (with a time window $T = 2$h).

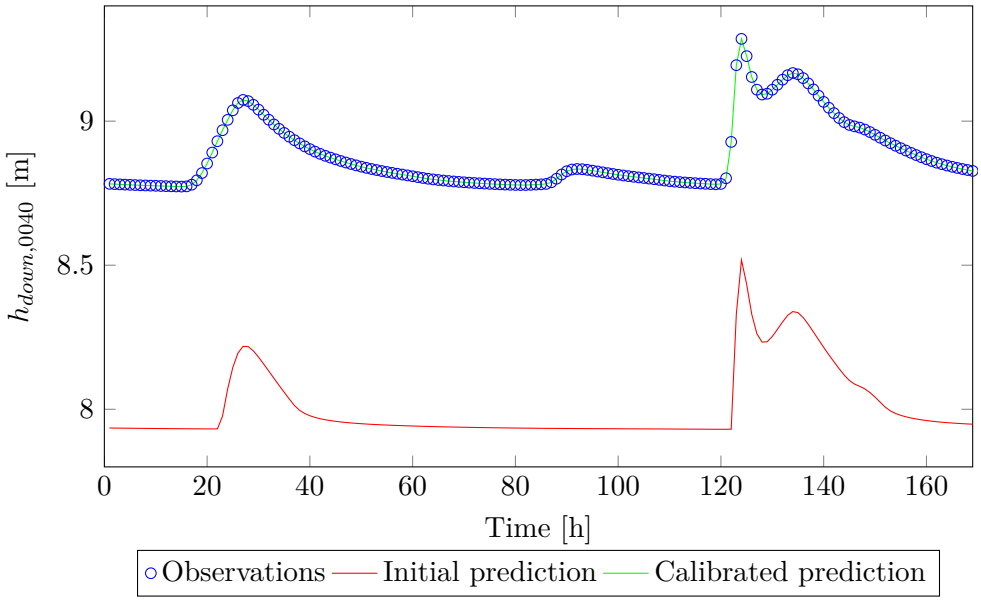

Figure D-63: The downstream water level at location 0040 for scenario FaWcL1H1 (G3) as function of time in the calibration window. The blue dots represent the observational data, the red line the initial prediction and the green line the calibrated prediction.

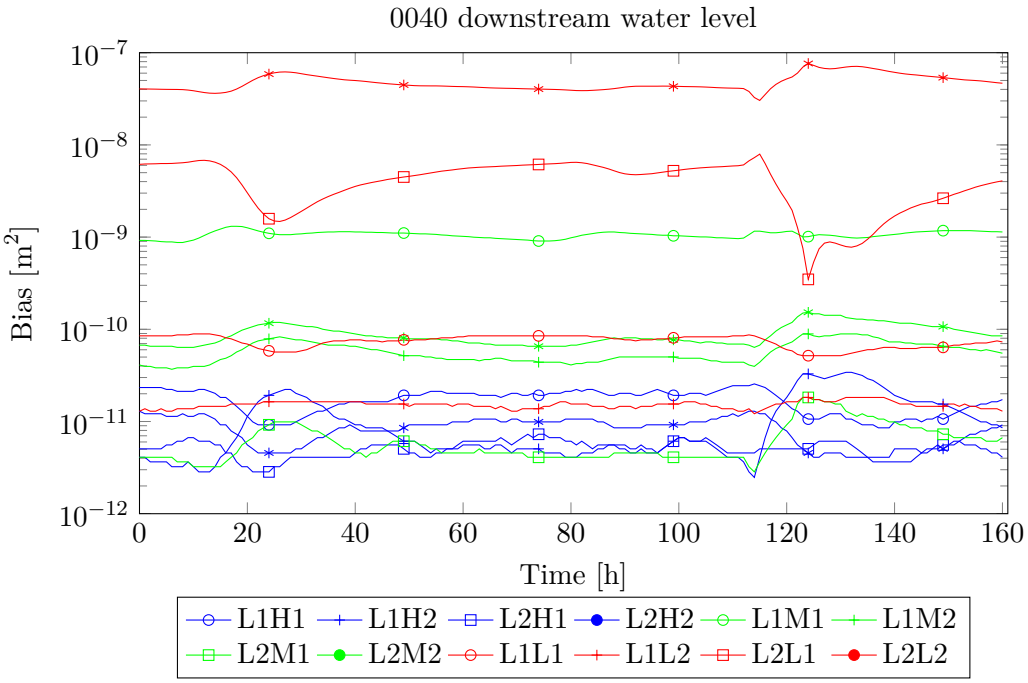

Figure D-64: The bias for the downstream water level at location 0040 for the FaWc (G3) scenarios with different starting points, three actual crest level values and one actual friction value as function of time in the calibration windows (with a time window $T = 2$h).

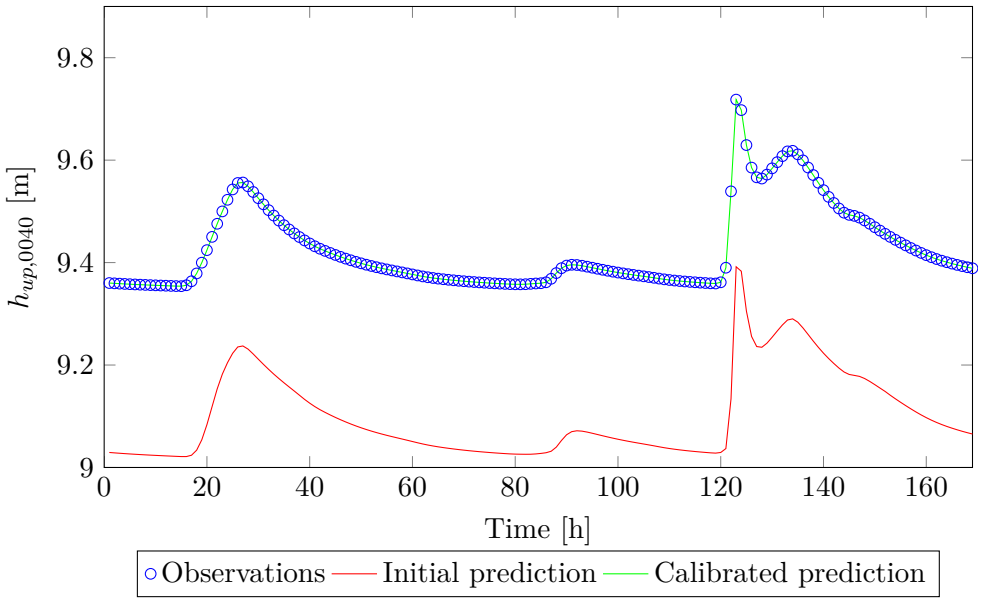

Figure D-65: The upstream water level at location 0040 for scenario FaWcL1H1 (G3) as function of time in the calibration window. The blue dots represent the observational data, the red line the initial prediction and the green line the calibrated prediction.

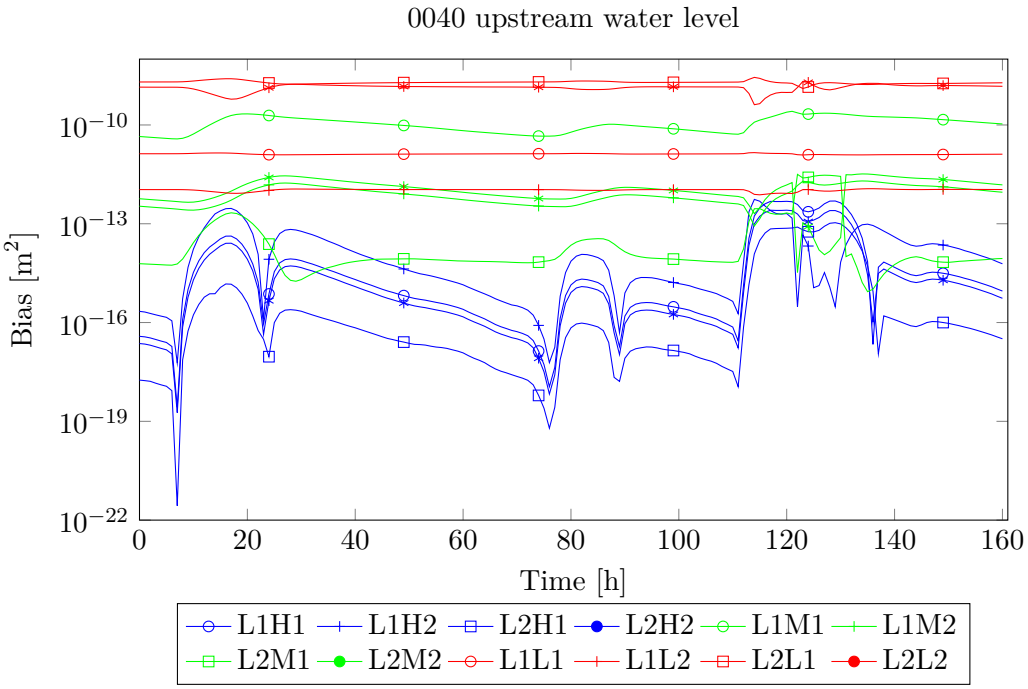

Figure D-66: The bias for the upstream water level at location 0040 for the FaWc (G3) scenarios with different starting points, three actual crest level values and one actual friction value as function of time in the calibration windows (with a time window $T = 2$h).

Appendix E

Results optimisation scenarios FaWcP

In the bias figures, the scenarios with different starting points are indicated with crosses, circles, squares and asterisks. The crosses and circles represent high and low starting points, respectively, for the weir parameter and a low starting point for the friction parameter. The squares and asterisks represent high and low starting points, respectively, for the weir parameter and a high starting point for the friction parameter. The blue lines represent the high scenarios for both the friction and weir parameter. The green lines represent the high scenarios for the friction parameter and the low scenarios for the weir parameter. The red lines represent the opposite of the green lines: low friction value scenarios and high weir parameter value scenarios. The scenarios for both low friction values and low weir parameter values are represented by the yellow lines.

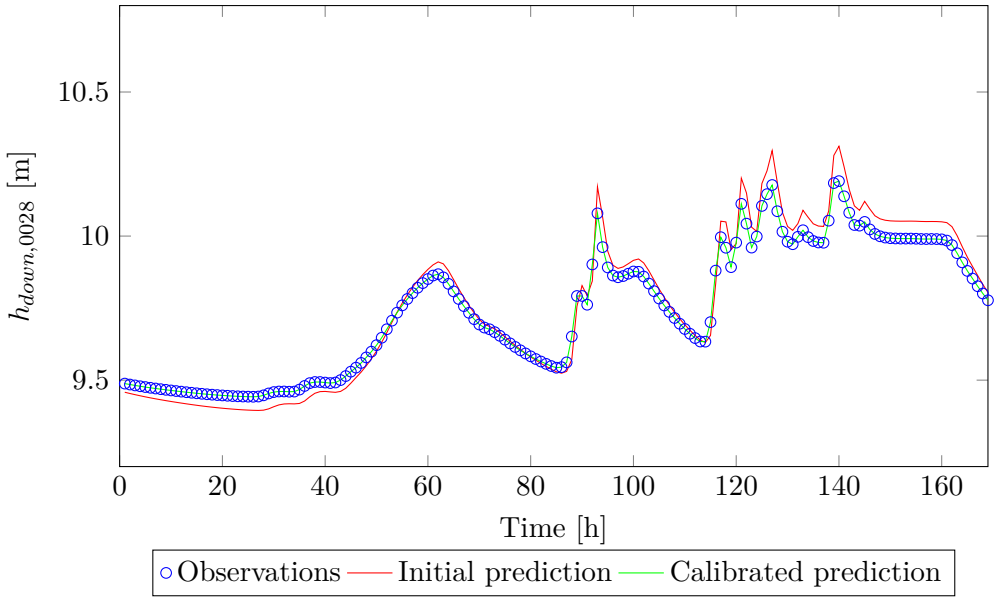

Figure E-1: The downstream water level at location 0028 for scenario FaWcPH1H1 as function of time in the calibration window. The blue dots represent the observational data, the red line the initial prediction and the green line the calibrated prediction.

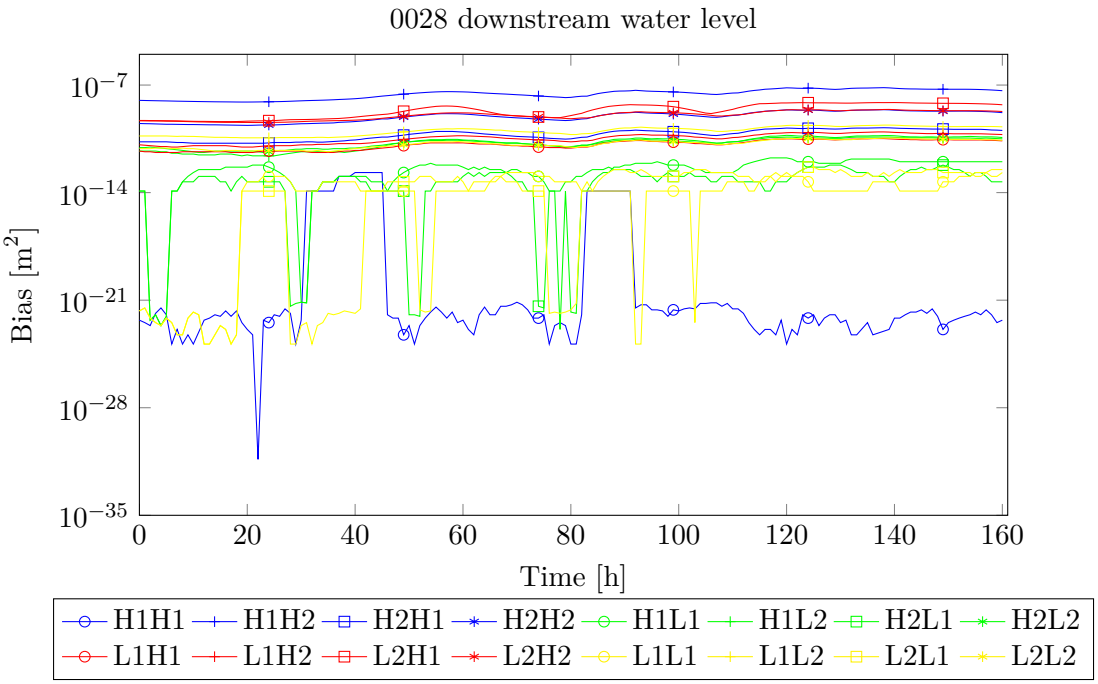

Figure E-2: The bias for the downstream water level at location 0028 for the FaWcP scenarios with different starting points, two actual crest level values and two actual friction values as function of time in the calibration windows (with a time window $T = 2$h).

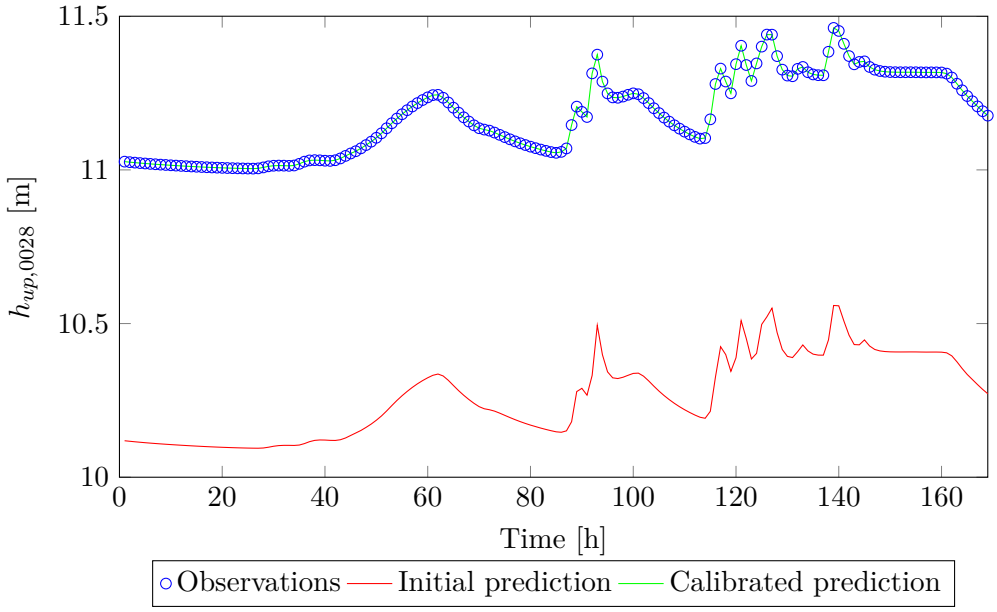

Figure E-3: The upstream water level at location 0028 for scenario FaWcPH1H1 as function of time in the calibration window. The blue dots represent the observational data, the red line the initial prediction and the green line the calibrated prediction.

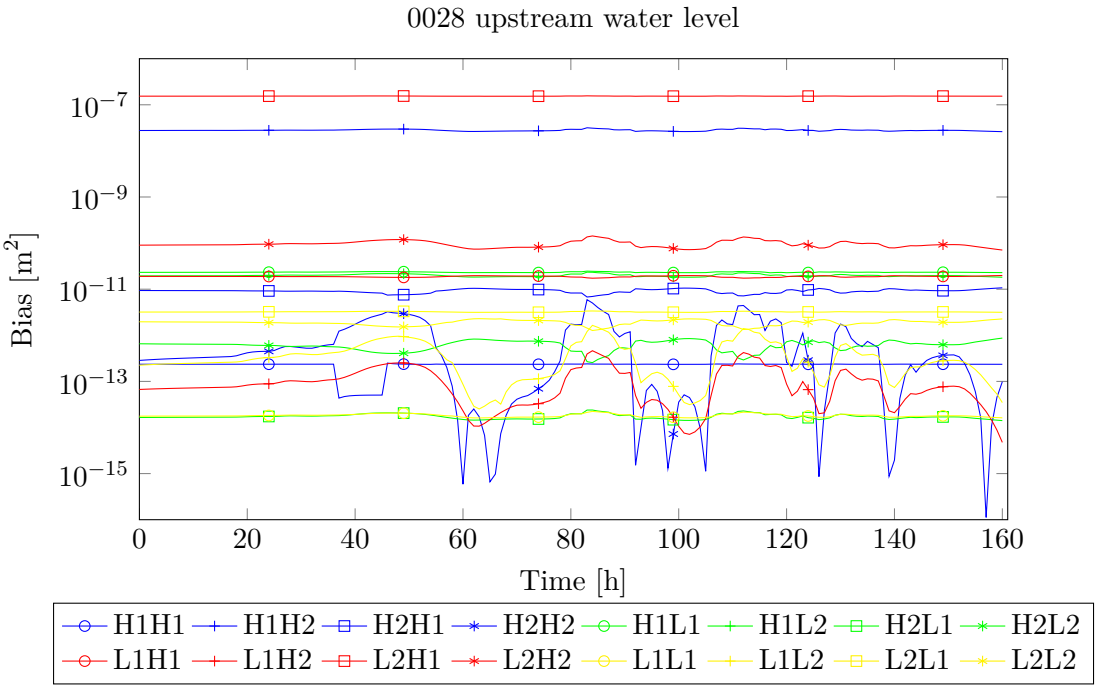

Figure E-4: The bias for the upstream water level at location 0028 for the FaWcP scenarios with different starting points, two actual crest level values and two actual friction values as function of time in the calibration windows (with a time window $T = 2$h).

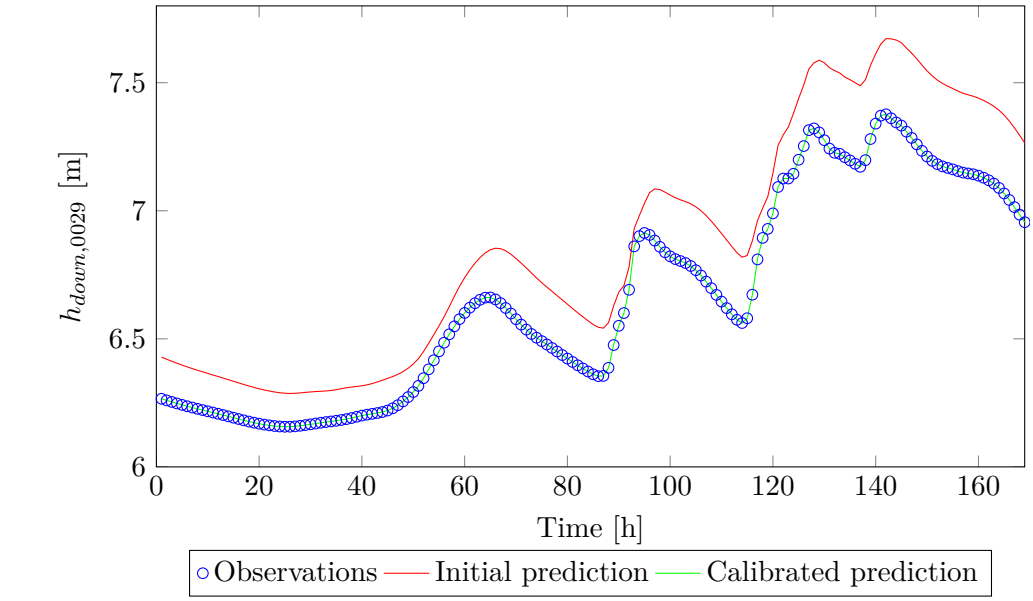

Figure E-5: The downstream water level at location 0029 for scenario FaWcPH1H1 as function of time in the calibration window. The blue dots represent the observational data, the red line the initial prediction and the green line the calibrated prediction.

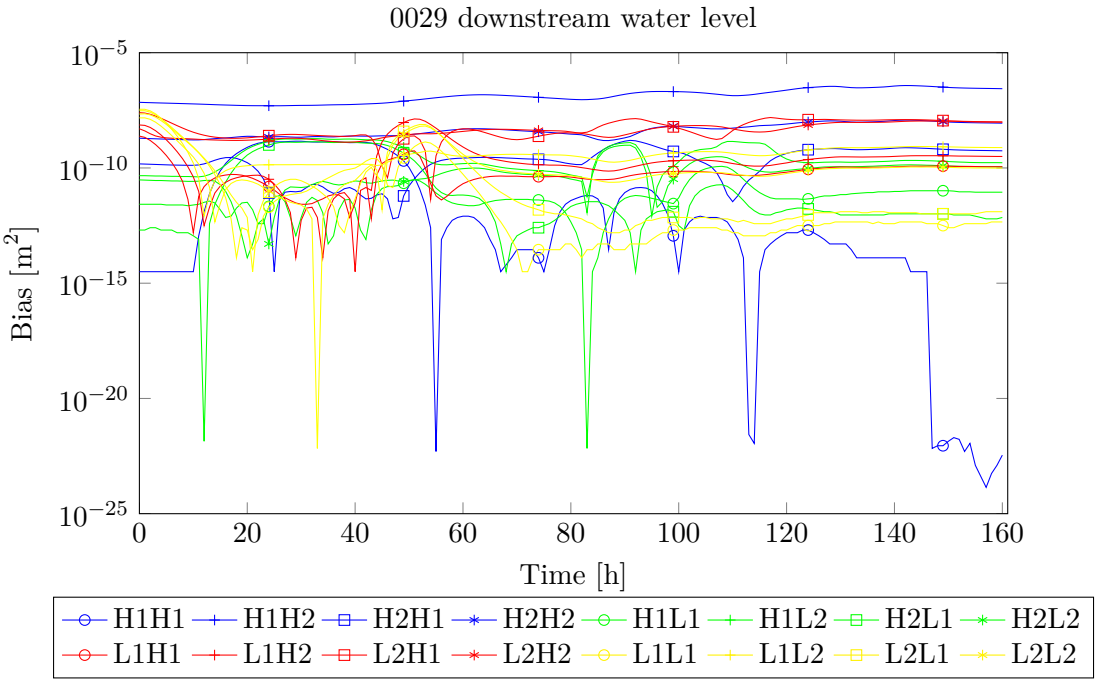

Figure E-6: The bias for the downstream water level at location 0029 for the FaWcP scenarios with different starting points, two actual crest level values and two actual friction values as function of time in the calibration windows (with a time window $T = 2$h).

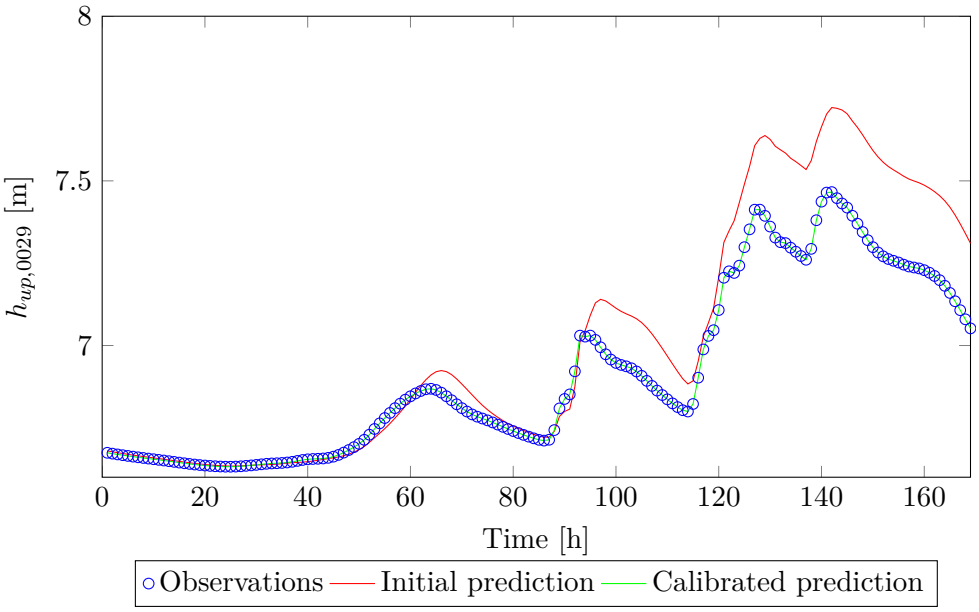

Figure E-7: The upstream water level at location 0029 for scenario FaWcPH1H1 as function of time in the calibration window. The blue dots represent the observational data, the red line the initial prediction and the green line the calibrated prediction.

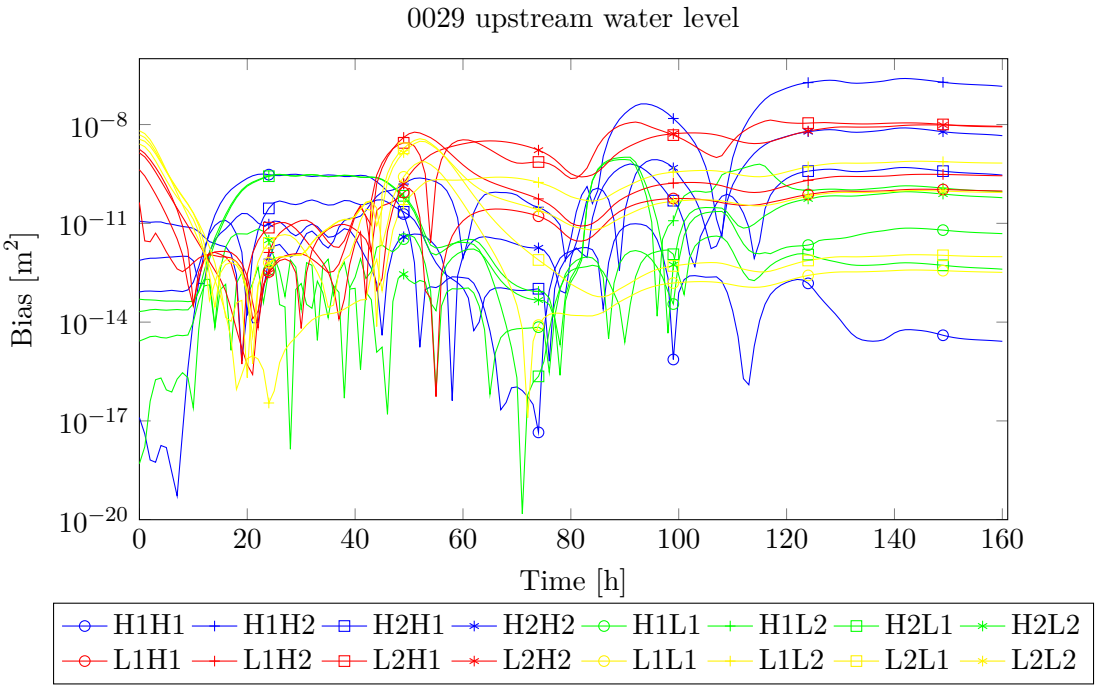

Figure E-8: The bias for the upstream water level at location 0029 for the FaWcP scenarios with different starting points, two actual crest level values and two actual friction values as function of time in the calibration windows (with a time window $T = 2$h).

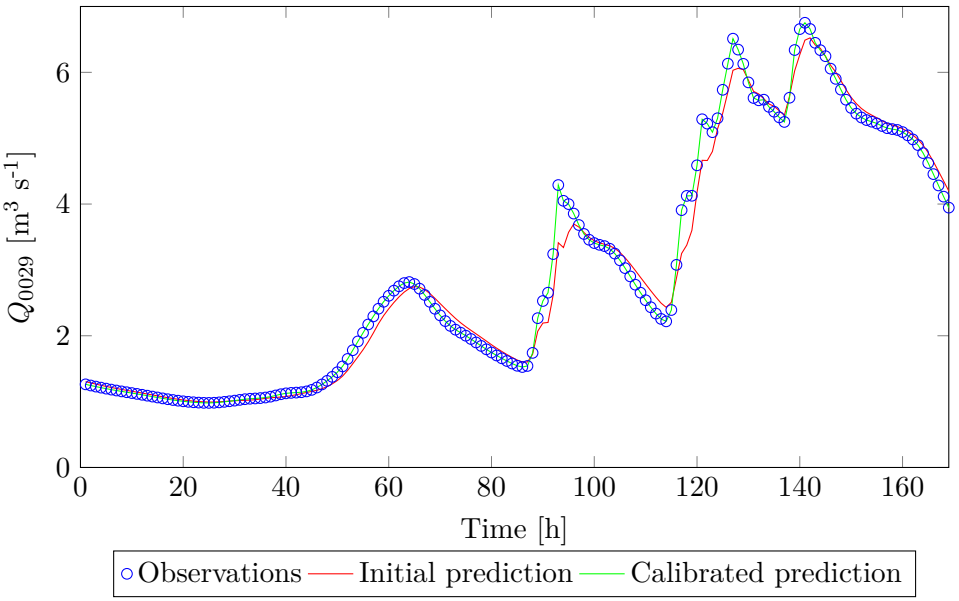

Figure E-9: The discharge at location 0029 for scenario FaWcPH1H1 as function of time in the calibration window. The blue dots represent the observational data, the red line the initial prediction and the green line the calibrated prediction.

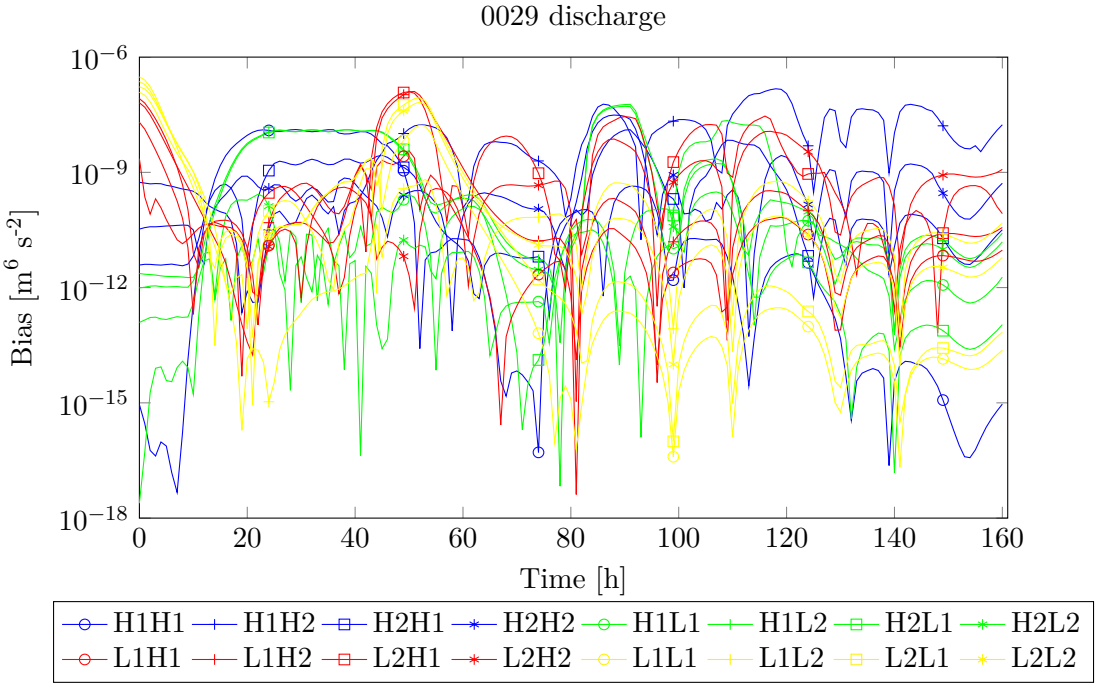

Figure E-10: The bias for the discharge at location 0029 for the FaWcP scenarios with different starting points, two actual crest level values and two actual friction values as function of time in the calibration windows (with a time window $T = 2$h).

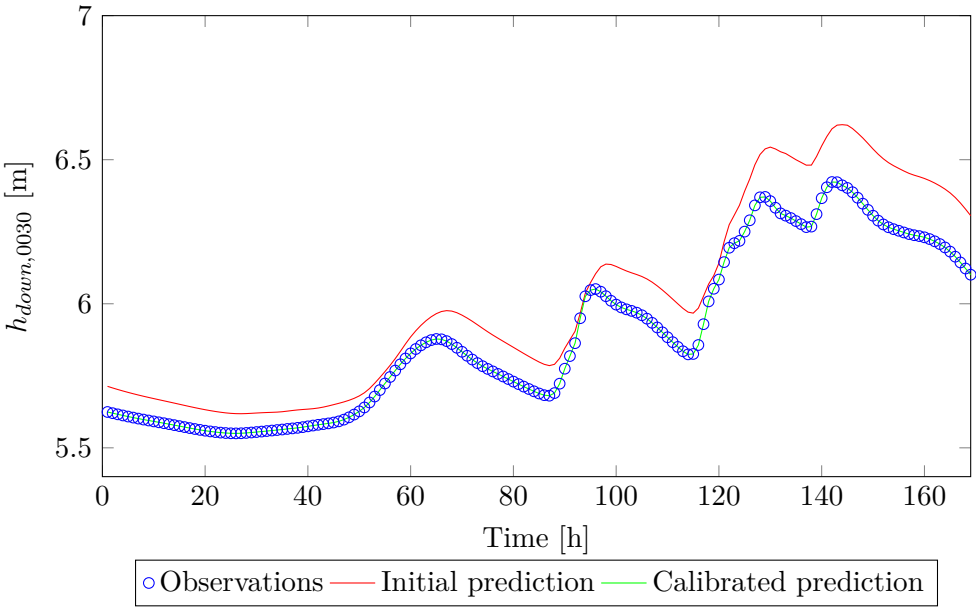

Figure E-11: The downstream water level at location 0030 for scenario FaWcPH1H1 as function of time in the calibration window. The blue dots represent the observational data, the red line the initial prediction and the green line the calibrated prediction.

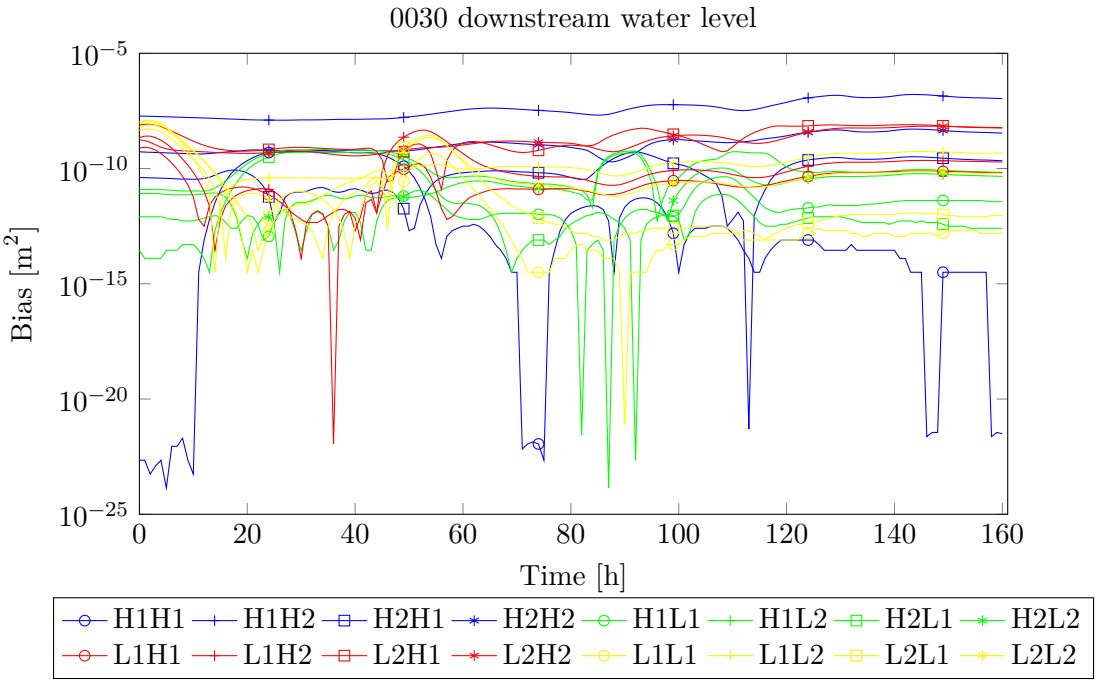

Figure E-12: The bias for the downstream water level at location 0030 for the FaWcP scenarios with different starting points, two actual crest level values and two actual friction values as function of time in the calibration windows (with a time window $T = 2$h).

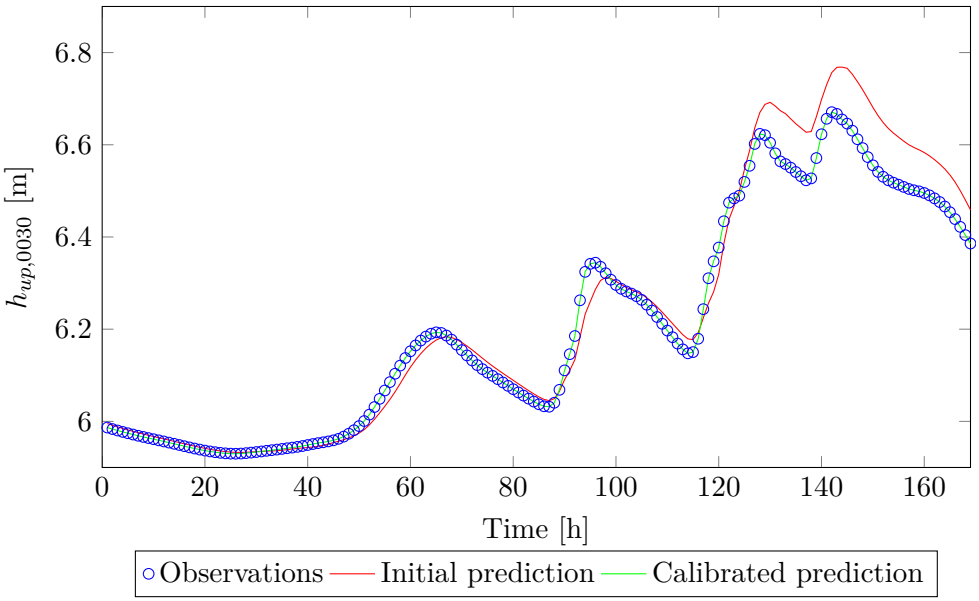

Figure E-13: The upstream water level at location 0030 for scenario FaWcPH1H1 as function of time in the calibration window. The blue dots represent the observational data, the red line the initial prediction and the green line the calibrated prediction.

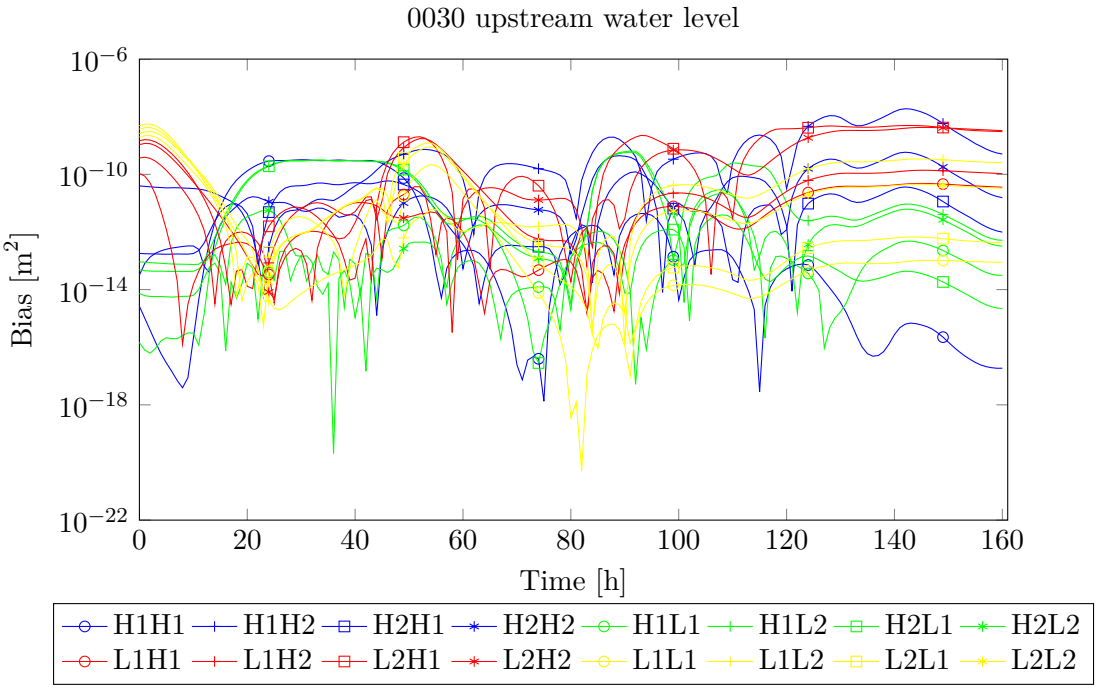

Figure E-14: The bias for the upstream water level at location 0030 for the FaWcP scenarios with different starting points, two actual crest level values and two actual friction values as function of time in the calibration windows (with a time window $T = 2$h).

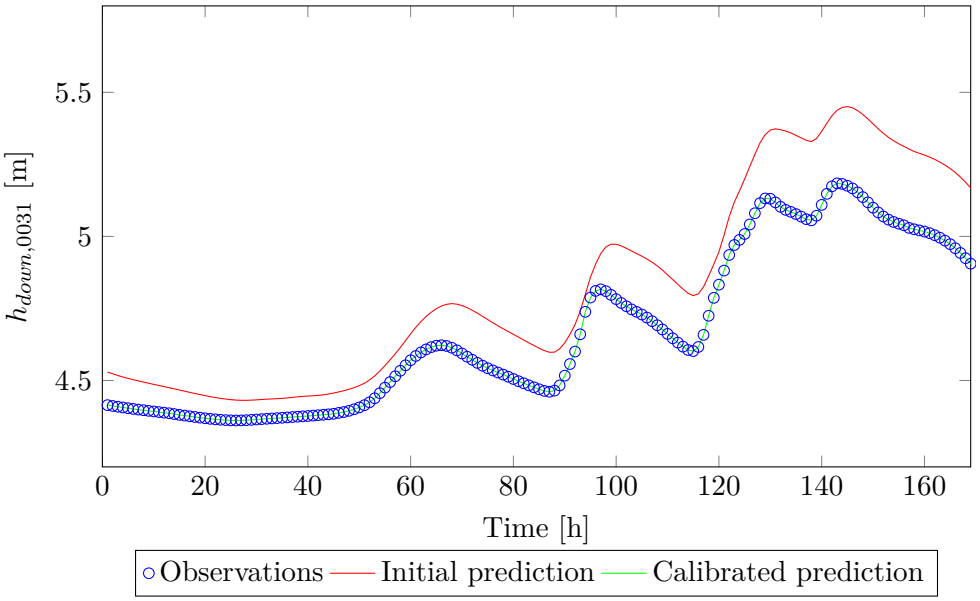

Figure E-15: The downstream water level at location 0031 for scenario FaWcPH1H1 as function of time in the calibration window. The blue dots represent the observational data, the red line the initial prediction and the green line the calibrated prediction.

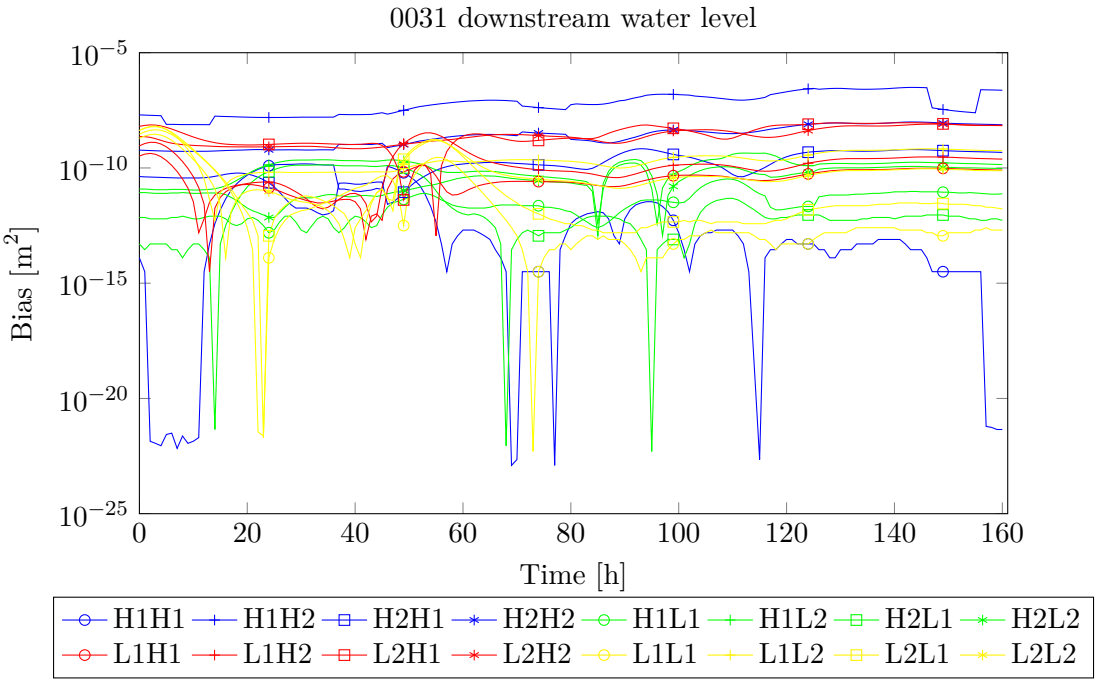

Figure E-16: The bias for the downstream water level at location 0031 for the FaWcP scenarios with different starting points, two actual crest level values and two actual friction values as function of time in the calibration windows (with a time window $T = 2$h).

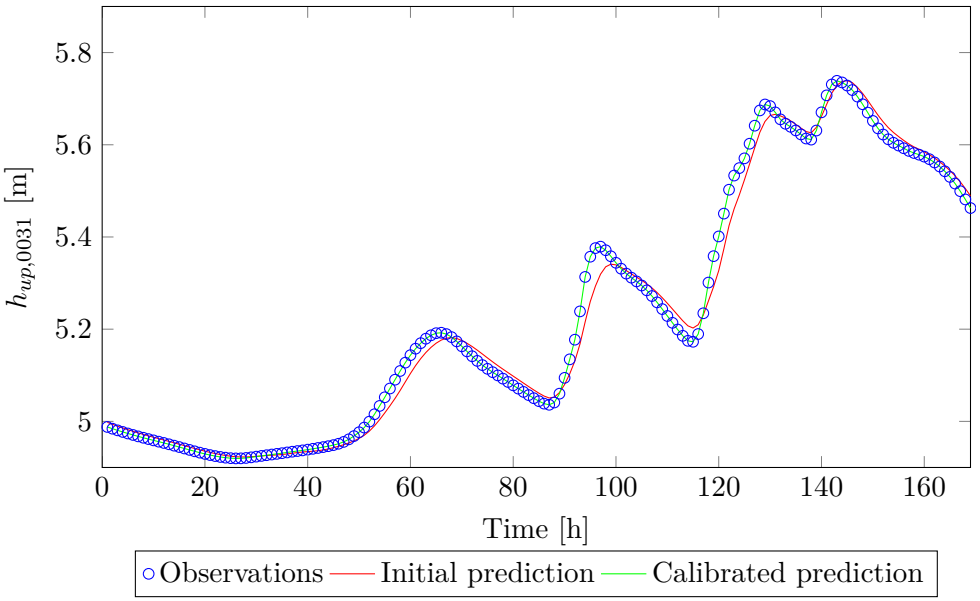

Figure E-17: The upstream water level at location 0031 for scenario FaWcPH1H1 as function of time in the calibration window. The blue dots represent the observational data, the red line the initial prediction and the green line the calibrated prediction.

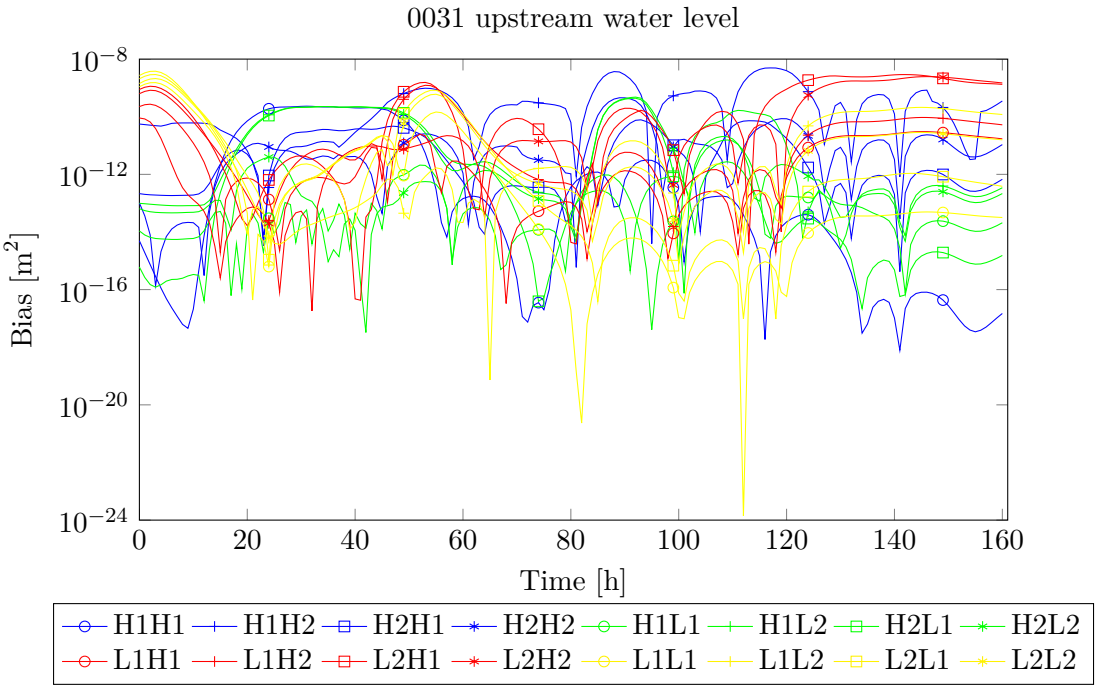

Figure E-18: The bias for the upstream water level at location 0031 for the FaWcP scenarios with different starting points, two actual crest level values and two actual friction values as function of time in the calibration windows (with a time window $T = 2$h).

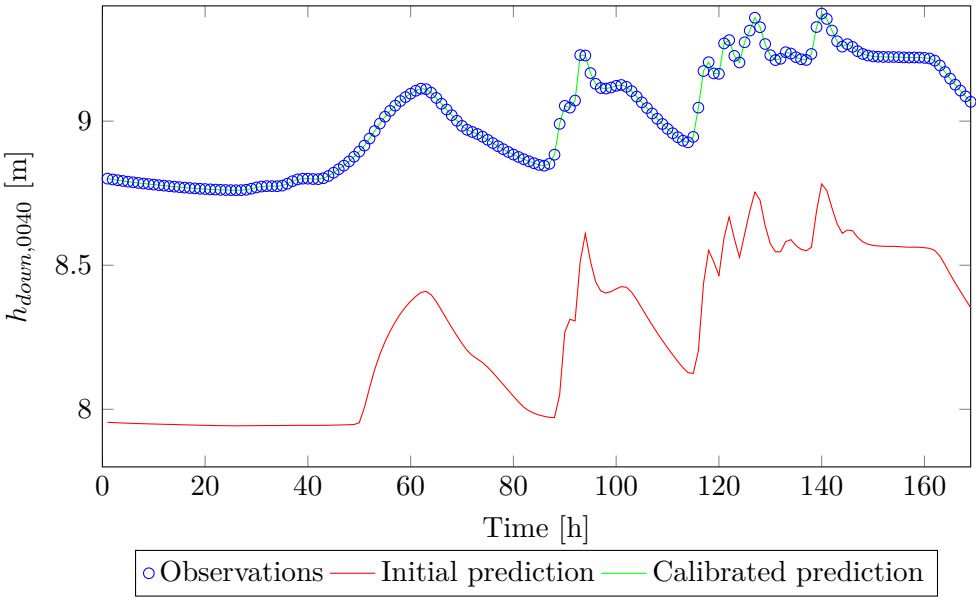

Figure E-19: The downstream water level at location 0040 for scenario FaWcPH1H1 as function of time in the calibration window. The blue dots represent the observational data, the red line the initial prediction and the green line the calibrated prediction.

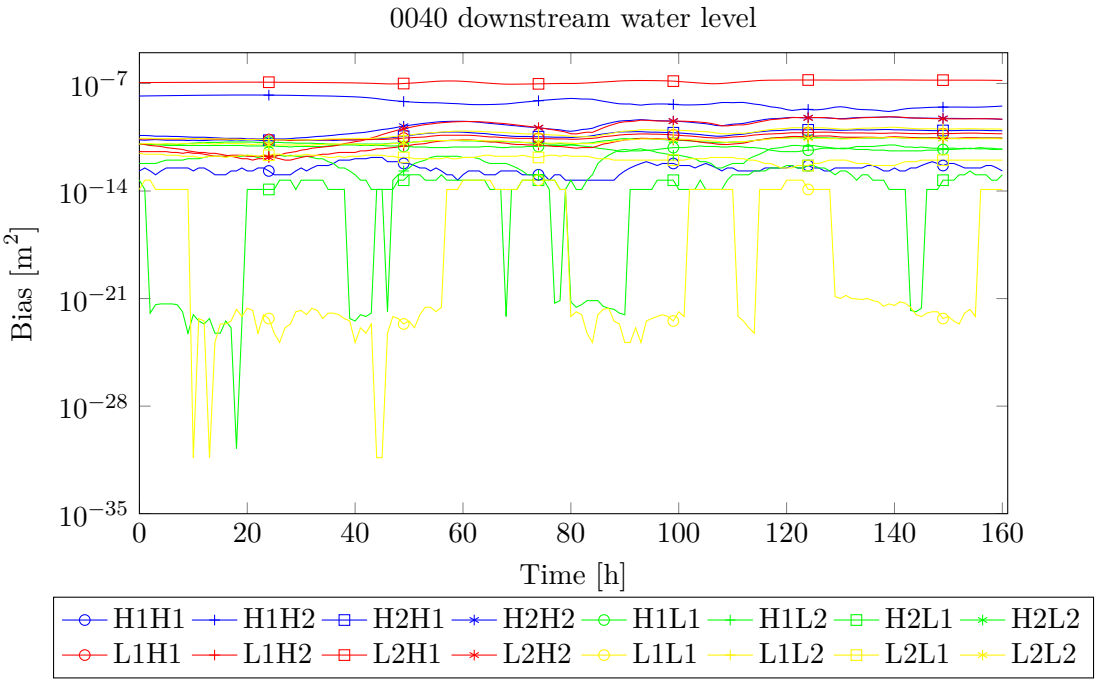

Figure E-20: The bias for the downstream water level at location 0040 for the FaWcP scenarios with different starting points, two actual crest level values and two actual friction values as function of time in the calibration windows (with a time window $T = 2$h).

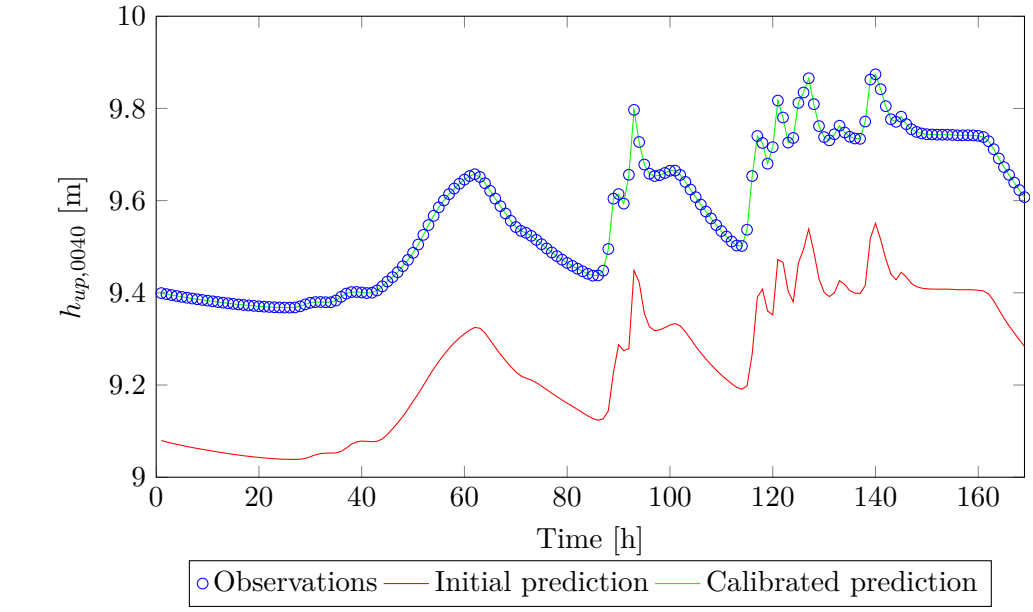

Figure E-21: The upstream water level at location 0040 for scenario FaWcPH1H1 as function of time in the calibration window. The blue dots represent the observational data, the red line the initial prediction and the green line the calibrated prediction.

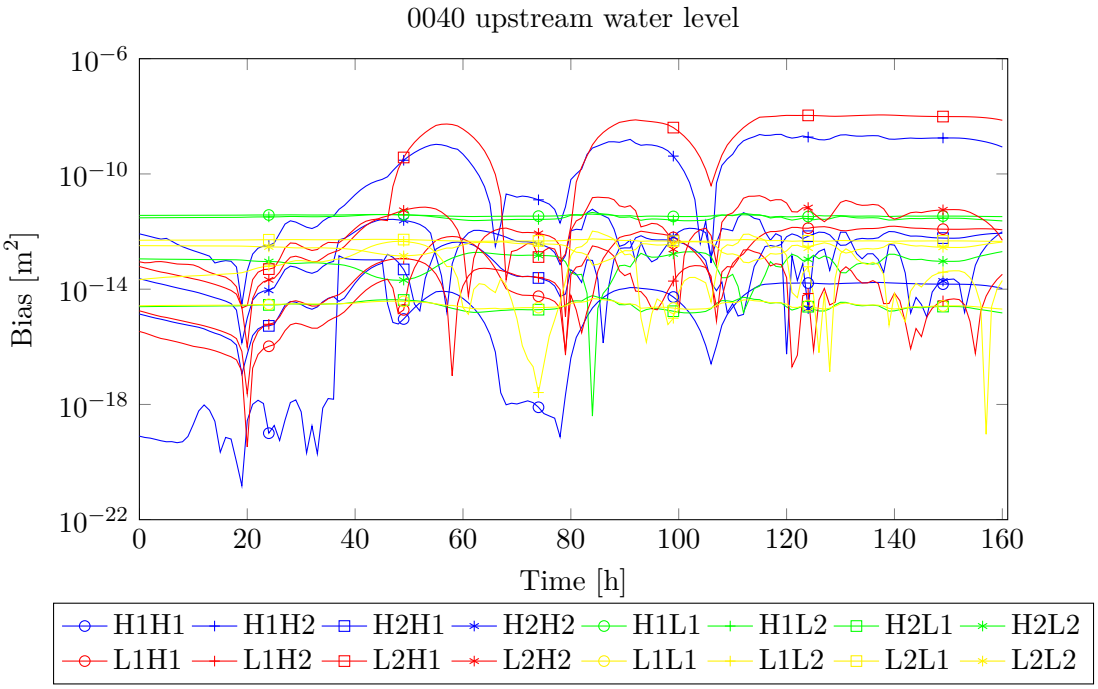

Figure E-22: The bias for the upstream water level at location 0040 for the FaWcP scenarios with different starting points, two actual crest level values and two actual friction values as function of time in the calibration windows (with a time window $T = 2$h).

Appendix F

Results optimisation scenarios FaWcN

In the bias figures, the scenarios with different starting points are indicated with crosses, circles, squares and asterisks. The crosses and circles represent high and low starting points, respectively, for the weir parameter and a low starting point for the friction parameter. The squares and asterisks represent high and low starting points, respectively, for the weir parameter and a high starting point for the friction parameter. The blue lines represent the high scenarios for both the friction and weir parameter. The green lines represent the high scenarios for the friction parameter and the low scenarios for the weir parameter. The red lines represent the opposite of the green lines: low friction value scenarios and high weir parameter value scenarios. The scenarios for both low friction values and low weir parameter values are represented by the yellow lines.

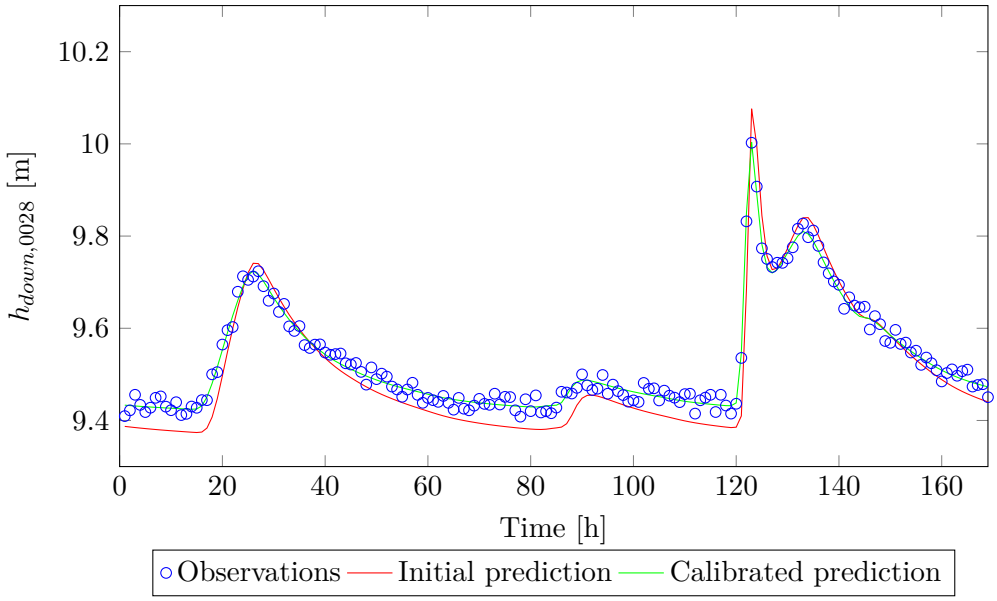

Figure F-1: The downstream water level at location 0028 for scenario FaWcNH1H1 as function of time in the calibration window. The blue dots represent the observational data, the red line the initial prediction and the green line the calibrated prediction.

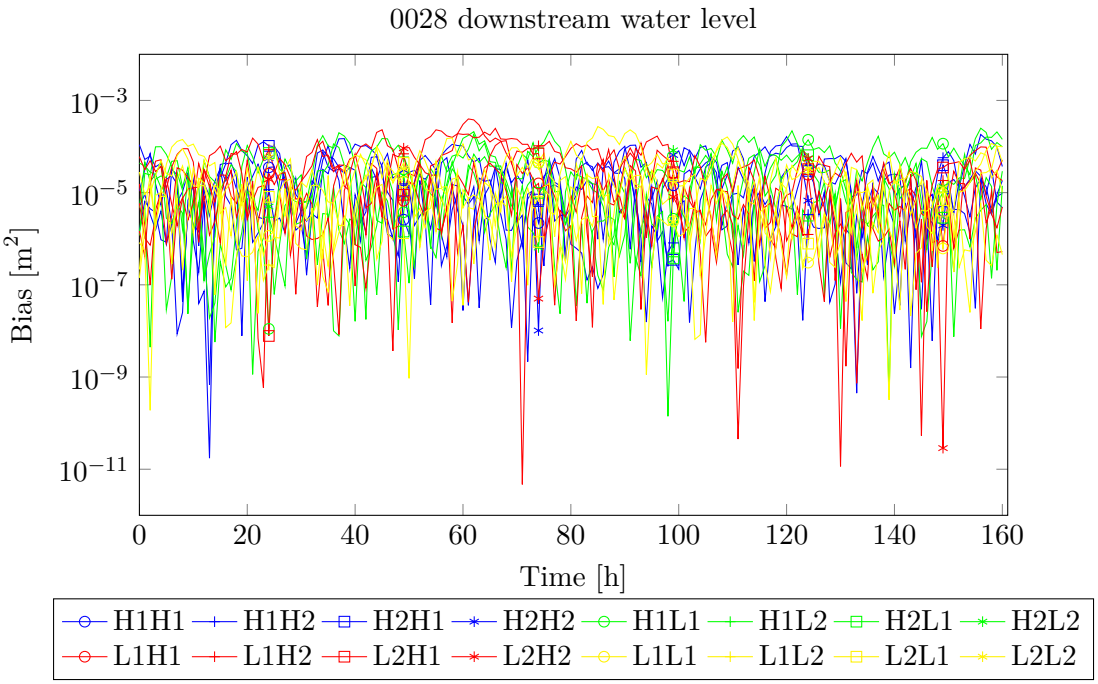

Figure F-2: The bias for the downstream water level at location 0028 for the FaWcN scenarios with different starting points, two actual crest level values and two actual friction values as function of time in the calibration windows (with a time window $T = 2$h).

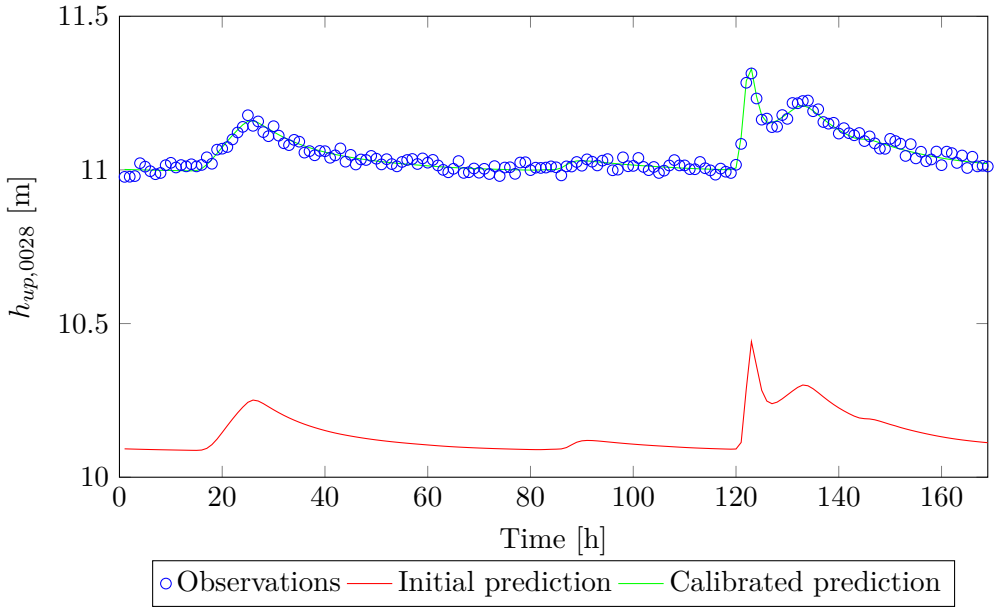

Figure F-3: The upstream water level at location 0028 for scenario FaWcNH1H1 as function of time in the calibration window. The blue dots represent the observational data, the red line the initial prediction and the green line the calibrated prediction.

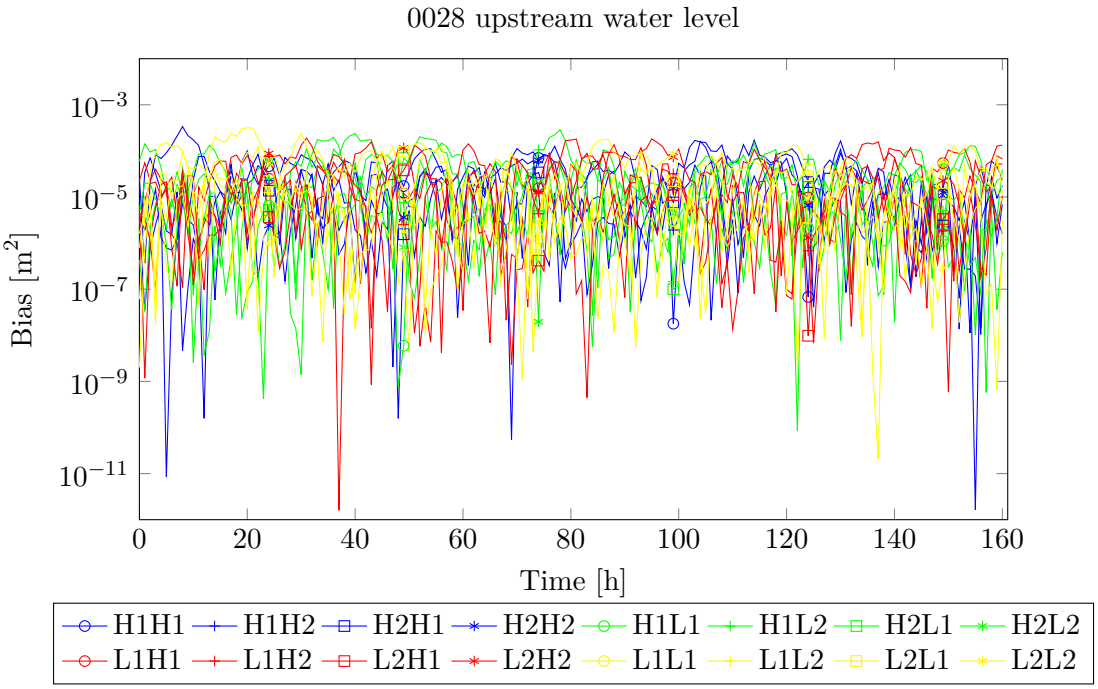

Figure F-4: The bias for the upstream water level at location 0028 for the FaWcN scenarios with different starting points, two actual crest level values and two actual friction values as function of time in the calibration windows (with a time window $T = 2$h).

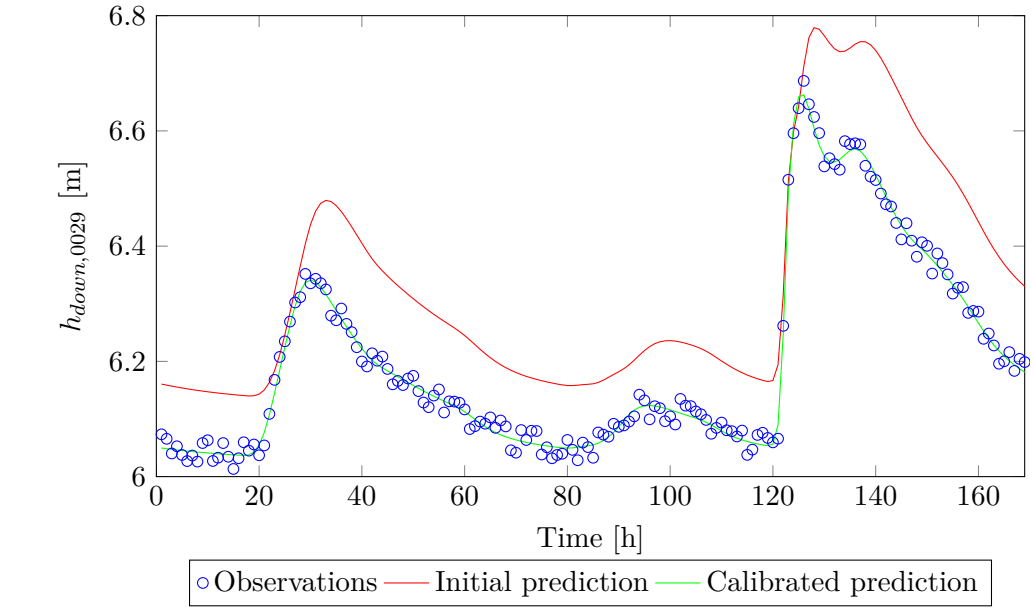

Figure F-5: The downstream water level at location 0029 for scenario FaWcNH1H1 as function of time in the calibration window. The blue dots represent the observational data, the red line the initial prediction and the green line the calibrated prediction.

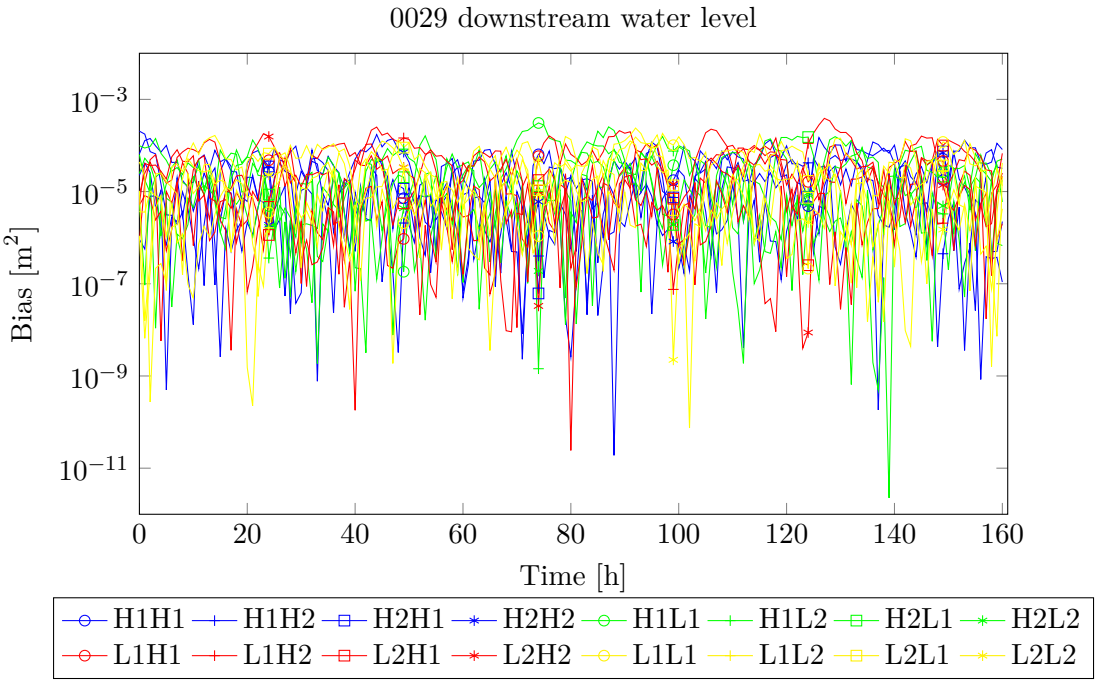

Figure F-6: The bias for the downstream water level at location 0029 for the FaWcN scenarios with different starting points, two actual crest level values and two actual friction values as function of time in the calibration windows (with a time window $T = 2$h).

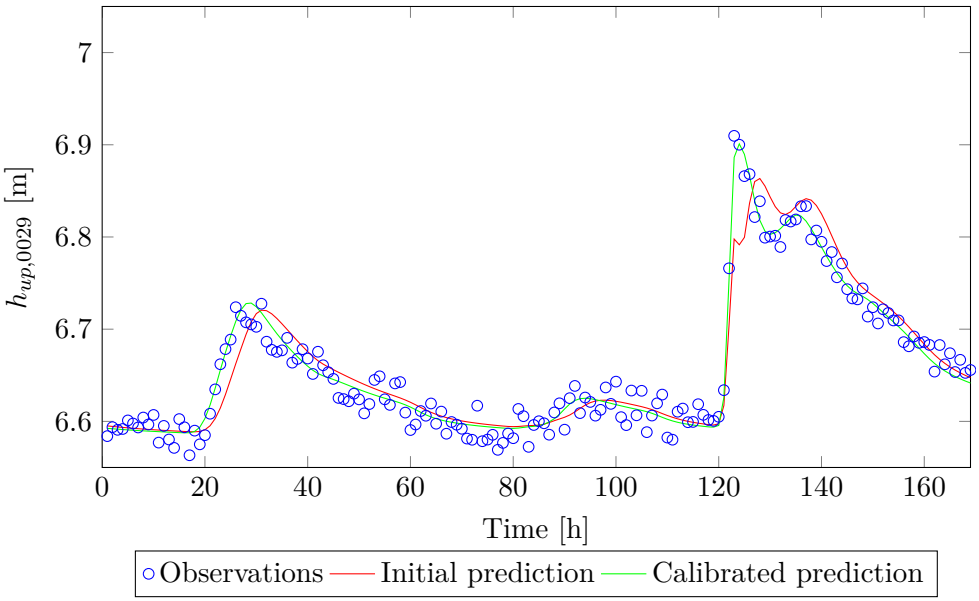

Figure F-7: The upstream water level at location 0029 for scenario FaWcNH1H1 as function of time in the calibration window. The blue dots represent the observational data, the red line the initial prediction and the green line the calibrated prediction.

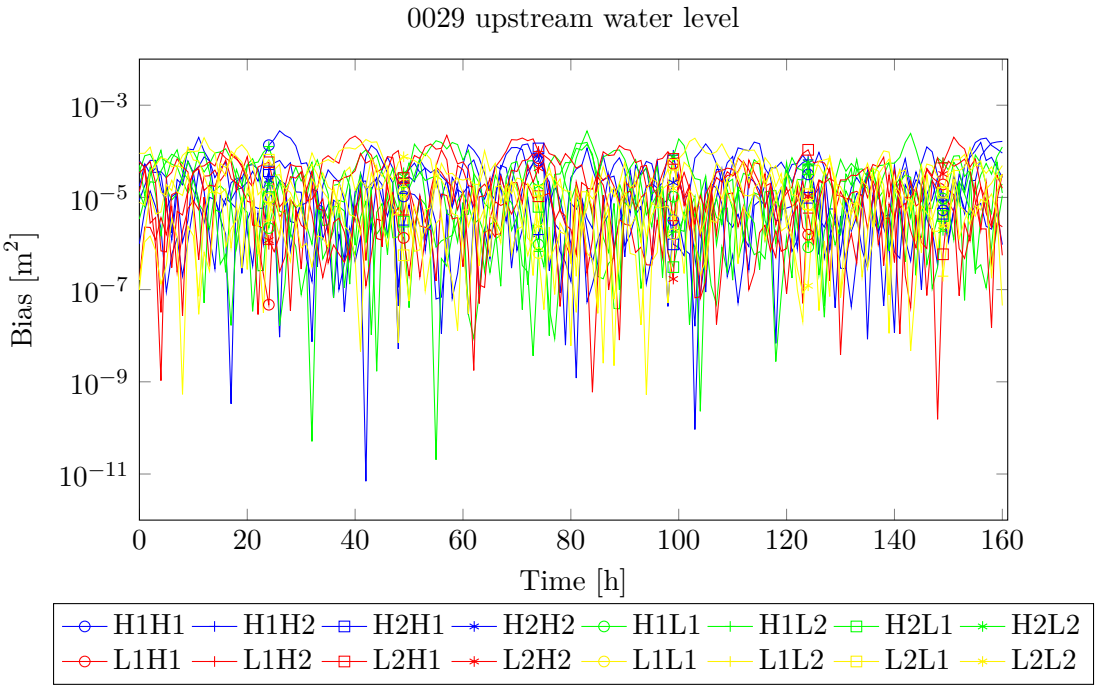

Figure F-8: The bias for the upstream water level at location 0029 for the FaWcN scenarios with different starting points, two actual crest level values and two actual friction values as function of time in the calibration windows (with a time window $T = 2$h).

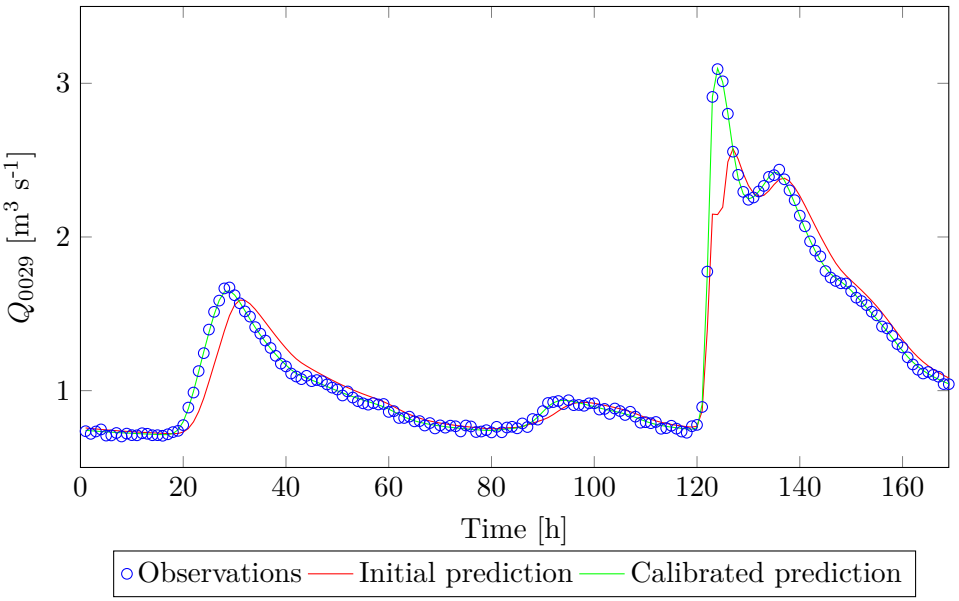

Figure F-9: The discharge at location 0029 for scenario FaWcNH1H1 as function of time in the calibration window. The blue dots represent the observational data, the red line the initial prediction and the green line the calibrated prediction.

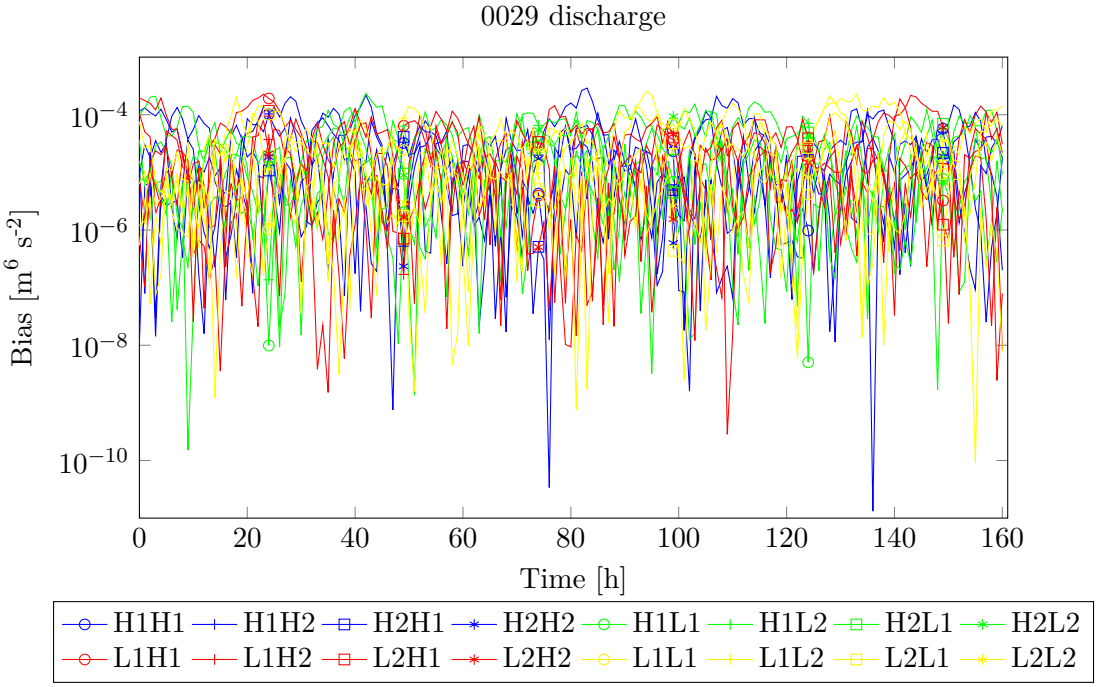

Figure F-10: The bias for the discharge at location 0029 for the FaWcN scenarios with different starting points, two actual crest level values and two actual friction values as function of time in the calibration windows (with a time window $T = 2$h).

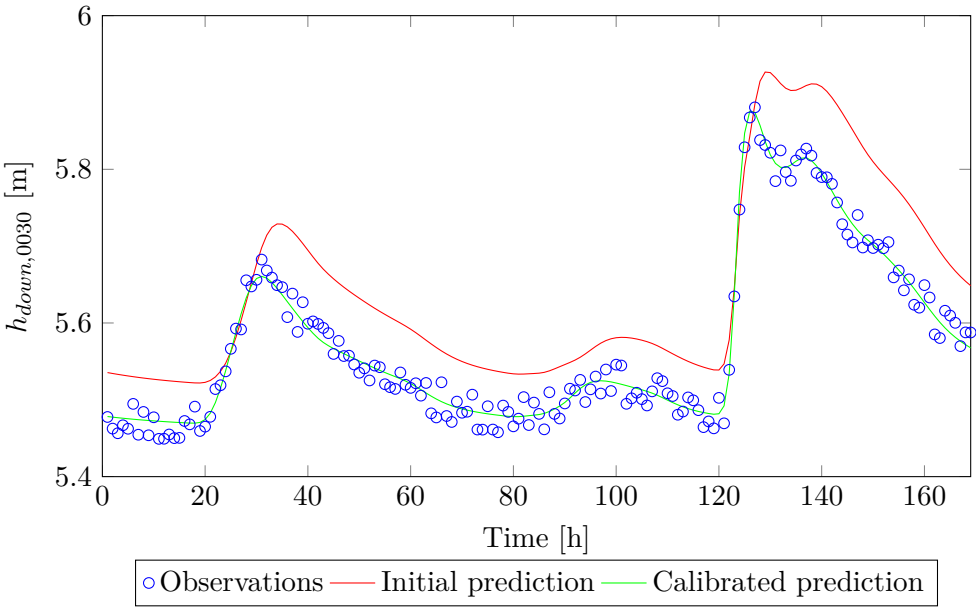

Figure F-11: The downstream water level at location 0030 for scenario FaWcNH1H1 as function of time in the calibration window. The blue dots represent the observational data, the red line the initial prediction and the green line the calibrated prediction.

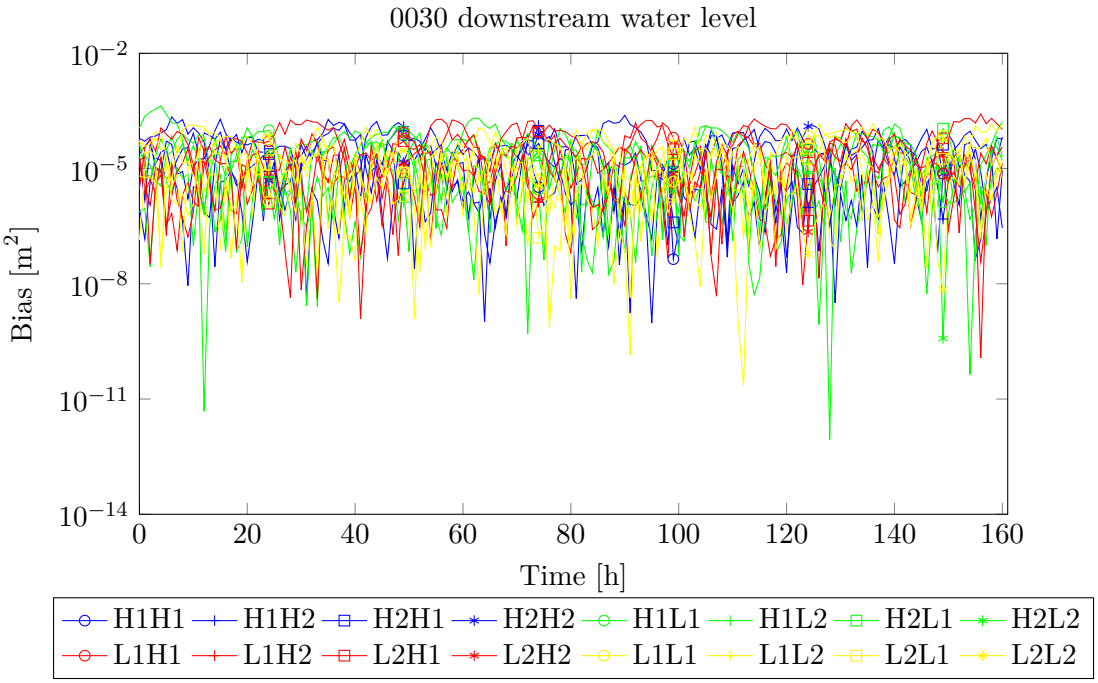

Figure F-12: The bias for the downstream water level at location 0030 for the FaWcN scenarios with different starting points, two actual crest level values and two actual friction values as function of time in the calibration windows (with a time window $T = 2$h).

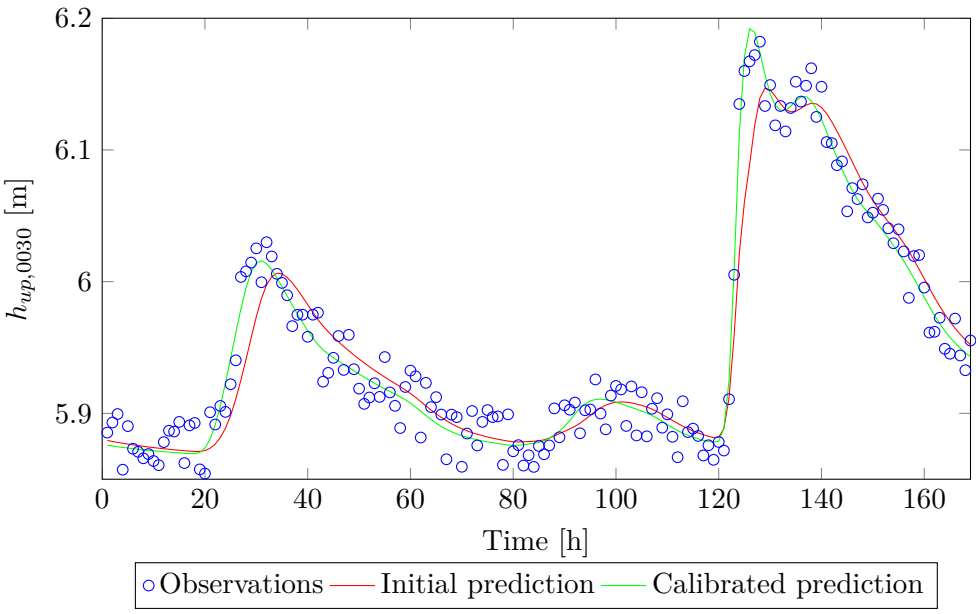

Figure F-13: The upstream water level at location 0030 for scenario FaWcNH1H1 as function of time in the calibration window. The blue dots represent the observational data, the red line the initial prediction and the green line the calibrated prediction.

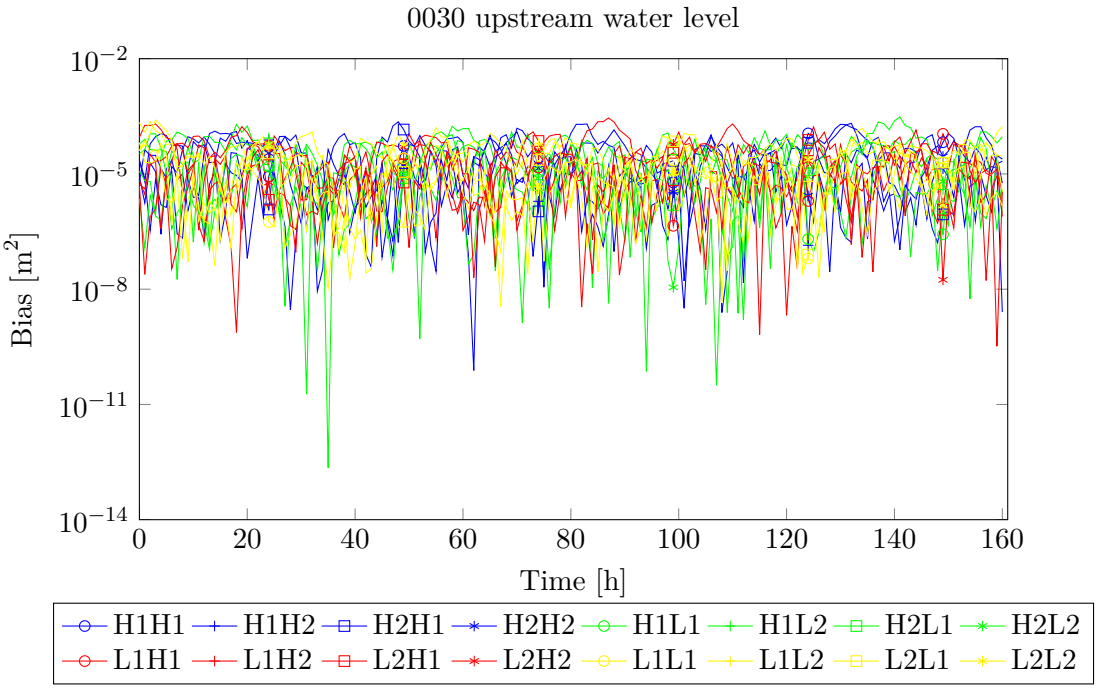

Figure F-14: The bias for the upstream water level at location 0030 for the FaWcN scenarios with different starting points, two actual crest level values and two actual friction values as function of time in the calibration windows (with a time window $T = 2$h).

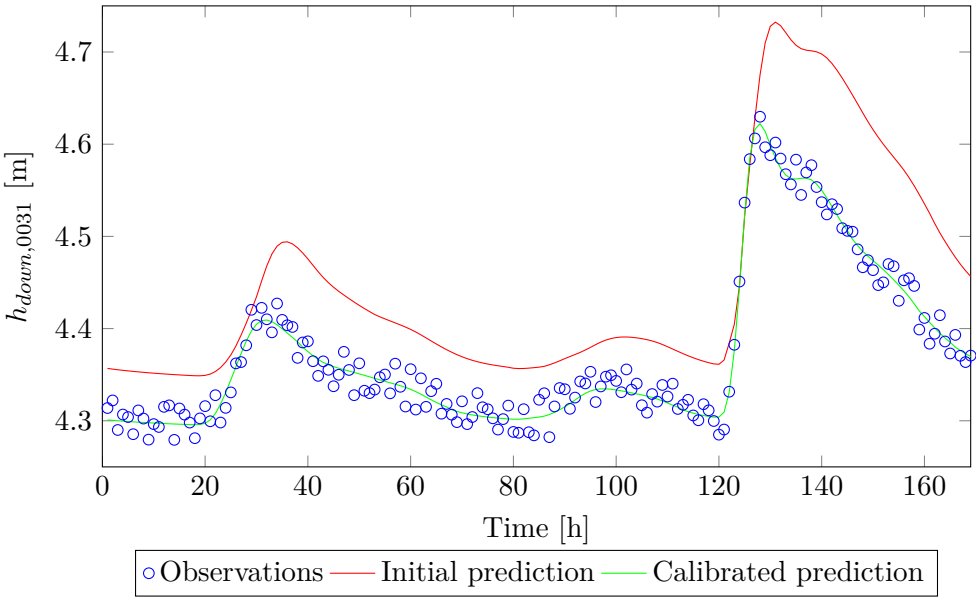

Figure F-15: The downstream water level at location 0031 for scenario FaWcNH1H1 as function of time in the calibration window. The blue dots represent the observational data, the red line the initial prediction and the green line the calibrated prediction.

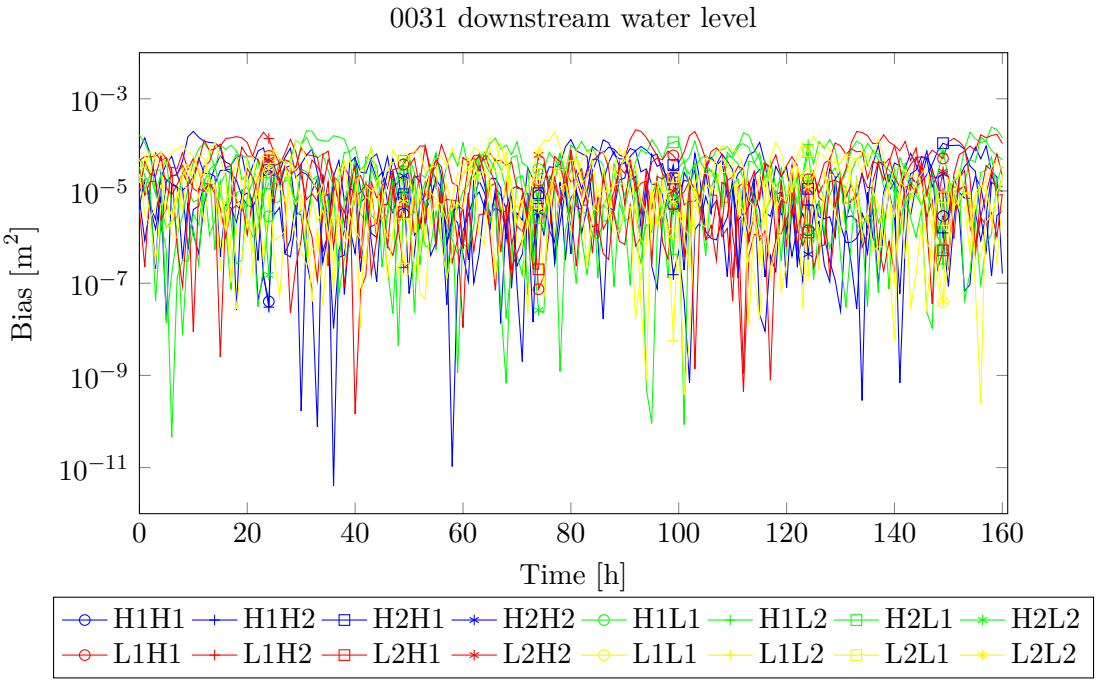

Figure F-16: The bias for the downstream water level at location 0031 for the FaWcN scenarios with different starting points, two actual crest level values and two actual friction values as function of time in the calibration windows (with a time window $T = 2$h).

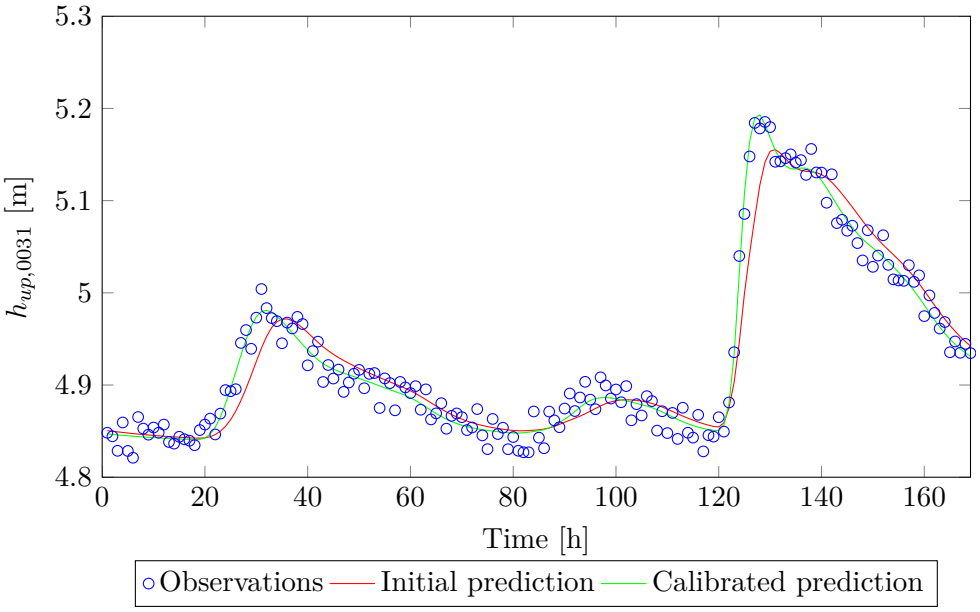

Figure F-17: The upstream water level at location 0031 for scenario FaWcNH1H1 as function of time in the calibration window. The blue dots represent the observational data, the red line the initial prediction and the green line the calibrated prediction.

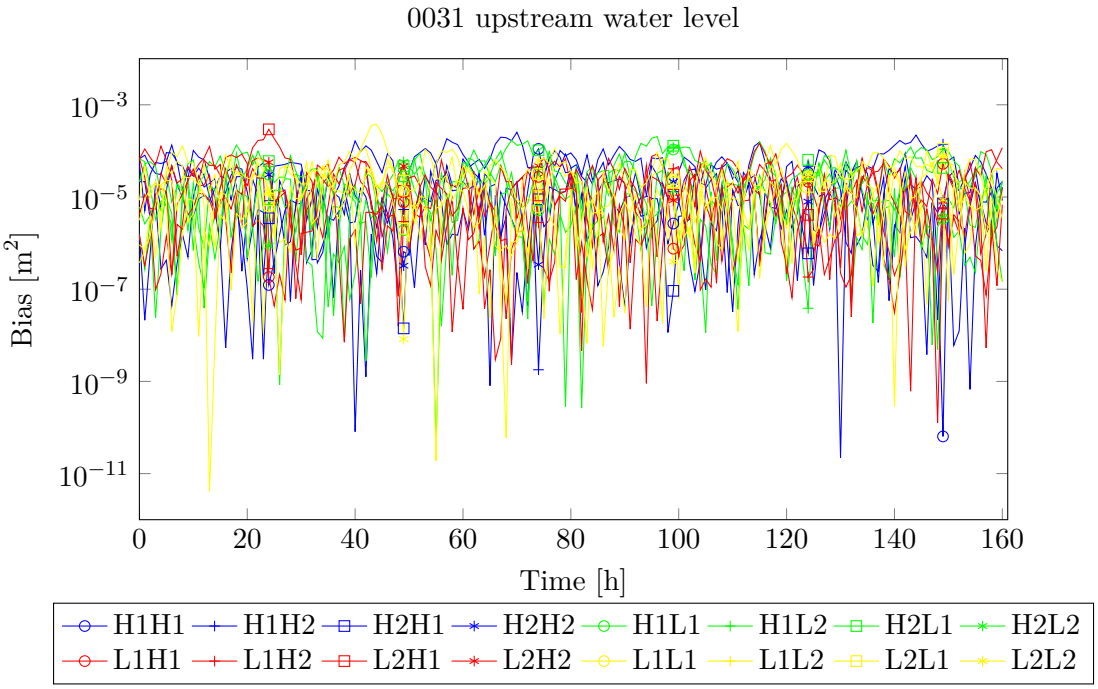

Figure F-18: The bias for the upstream water level at location 0031 for the FaWcN scenarios with different starting points, two actual crest level values and two actual friction values as function of time in the calibration windows (with a time window $T = 2$h).

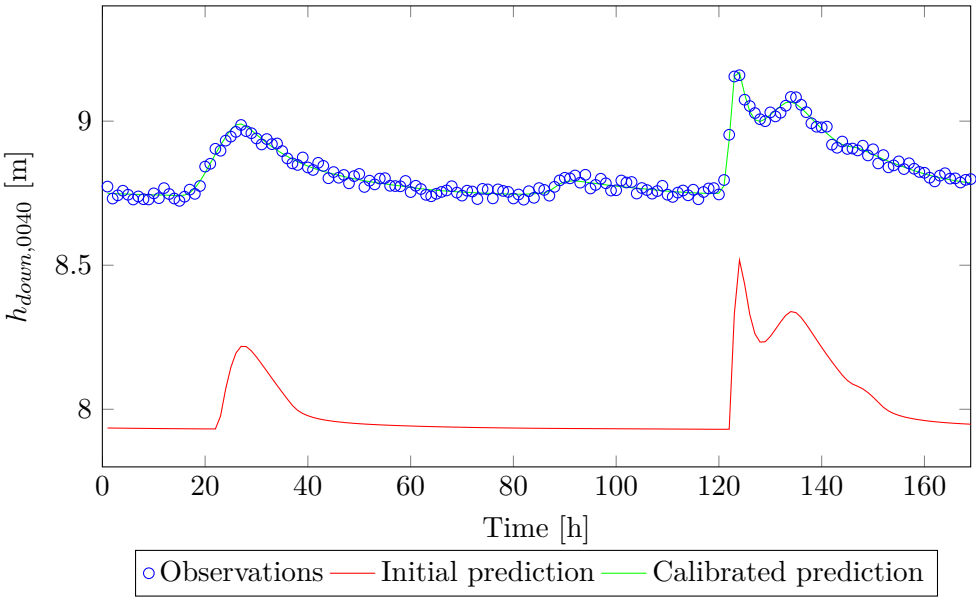

Figure F-19: The downstream water level at location 0040 for scenario FaWcNH1H1 as function of time in the calibration window. The blue dots represent the observational data, the red line the initial prediction and the green line the calibrated prediction.

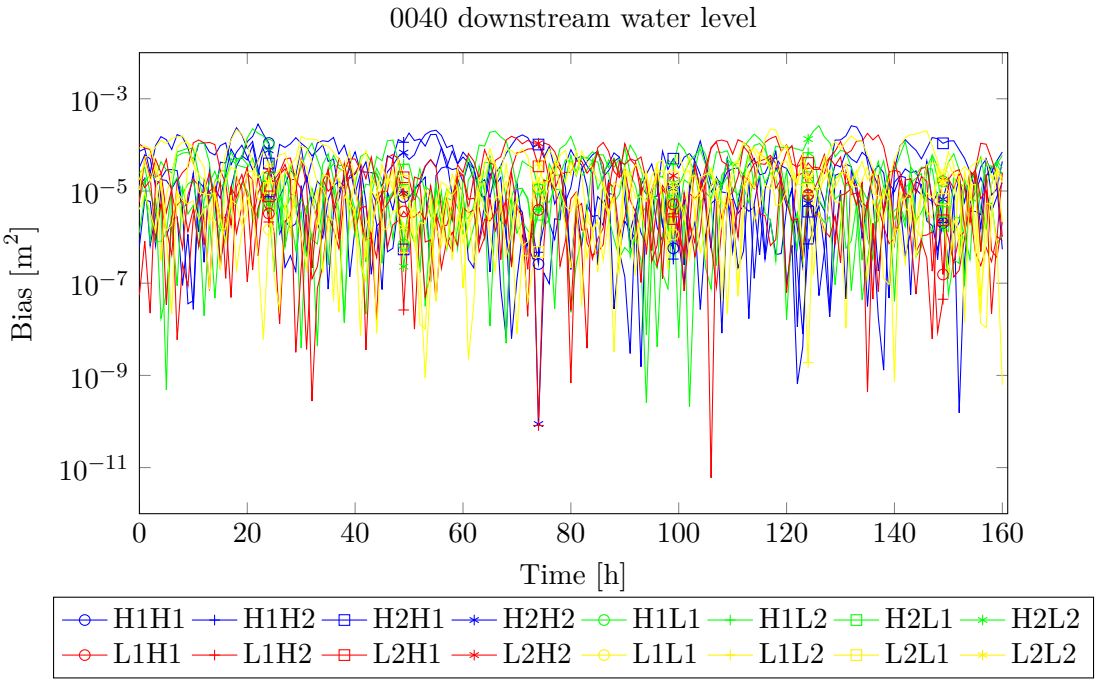

Figure F-20: The bias for the downstream water level at location 0040 for the FaWcN scenarios with different starting points, two actual crest level values and two actual friction values as function of time in the calibration windows (with a time window $T = 2$h).

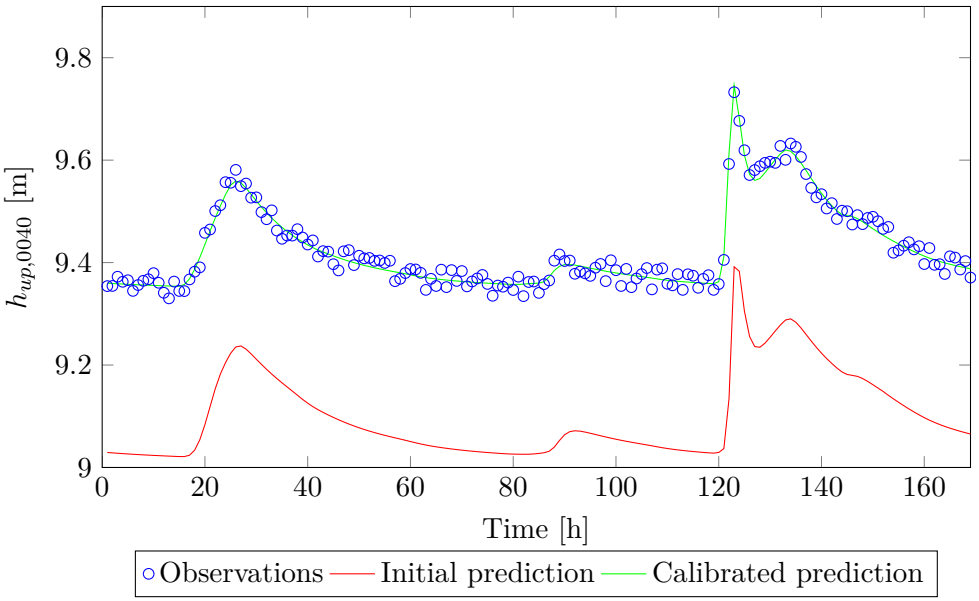

Figure F-21: The upstream water level at location 0040 for scenario FaWcNH1H1 as function of time in the calibration window. The blue dots represent the observational data, the red line the initial prediction and the green line the calibrated prediction.

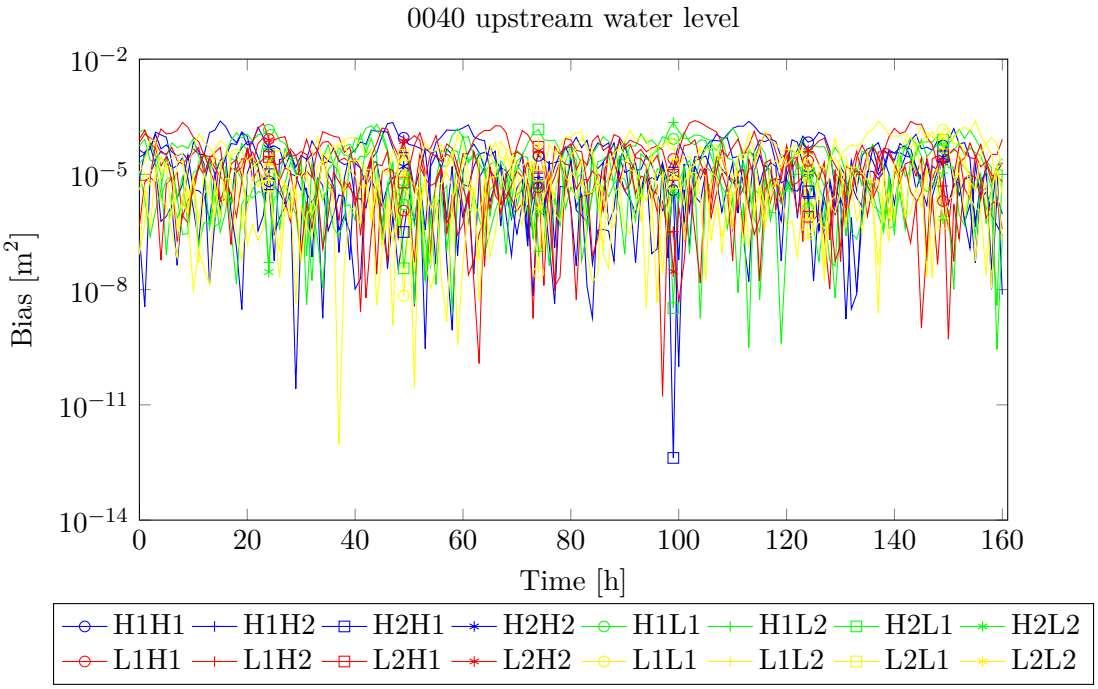

Figure F-22: The bias for the upstream water level at location 0040 for the FaWcN scenarios with different starting points, two actual crest level values and two actual friction values as function of time in the calibration windows (with a time window $T = 2$h).

Bibliography

[1] M. L. Ralston and R. I. Jennrich, "Dud, a derivative-free algorithm for nonlinear least squares," *Technometrics*, vol. 20, pp. 7 – 14.

[2] S. S. Duan, Q. and V. Gupta, "Effective and efficient global optimization for conceptual rainfall-runoff models," *Water Resour. Res.*, vol. 28, pp. 1015 – 1031, 1992.

[3] D. Schwanenberg, A. van Breukelen, and S. Hummel, "Data assimilation for supporting optimum control in large-scale river networks," in *Networking, Sensing and Control (ICNSC), 2011 IEEE International Conference on*, pp. 98 – 103, April 2011.

[4] D. Mulder, "Applying data-assimilation and calibration in the field of urban drainage," Master's thesis, Delft University of Technology, 2014.

[5] S.-Y. Liong and M. Atiquzzaman, "Optimal desing of water distribution network using shuffled complex evolution," *Journal of The Institution of Engineers*, 2004.

[6] Hapuarachchi, "Application of sce-ua method for calibrating the xinanjiang watershed model," *Journal of Lake Science*, 2001.

[7] N. Moosavian and M. R. Jaefarzadeh, "Hydraulic analysis of water distribution network using shuffled complex evolution," *Journal of Fluids*, vol. 2014, 2014.

[8] P. Verschuren and H. Doorewaard, *Designing a Research Project*. Eleven International Publishing, 2010.

[9] F. Clemens, *Hydrodynamic Models in Urban Drainage: Application and Calibration*. PhD thesis, Delft University of Technology, 2001.

[10] U. Eduri and F. Maloberti, "Online calibration of a nyquist-rate analog-to-digital converter using output code-density histograms," *Circuits and Systems I: Regular Papers, IEEE Transactions on*, vol. 51, pp. 15 – 24, Jan 2004.

[11] C. Fleischer, K. Kondak, C. Reinicke, and G. Hommel, "Online calibration of the emg to force relationship," in *Intelligent Robots and Systems, 2004. (IROS 2004). Proceedings. 2004 IEEE/RSJ International Conference on*, vol. 2, pp. 1305 – 1310, Sept 2004.

[12] C. Antoniou, M. Ben-Akiva, and H. Koutsopoulos, "On-line calibration of traffic prediction models," in *Intelligent Transportation Systems, 2004. Proceedings. The 7th International IEEE Conference on*, pp. 82 – 87, Oct 2004.

[13] W. D. Dommel, "Krachtig water - waterbeheerplan 2010 - 2015." http://www.dommel.nl/binaries/content/assets/dommel---website/common/we-0/missie-beleid/waterbeheerplan/wbp.pdf, 2010. Accessed October 30, 2014.

[14] W. D. Dommel, "Beheer van water- en oeverplanten in het gebied van waterschap de dommel." http://www.dommel.nl/binaries/content/assets/dommel---website/producten/veldgids.pdf, 2005. Accessed October 30, 2014.

[15] B. Stegeman, "Model calibration as a tool to identify sewer maintenance," Master's thesis, Delft University of Technology, 2012.

[16] B. Carter, ed., *Op Amps for Everyone (Fourth Edition)*. Boston: Newnes, fourth edition ed., 2013.

[17] I. K. Westerberg, J.-L. Guerrero, P. M. Younger, K. J. Beven, J. Seibert, S. Halldin, J. E. Freer, and C.-Y. Xu, "Calibration of hydrological models using flow-duration curves," *Hydrology and Earth System Sciences*, vol. 15, no. 7, pp. 2205–2227, 2011.

[18] H. R. D. Blasone, R.-S.; Madsen, "Parameter estimation in distributed hydrological modelling: comparison of global and local optimisation techniques," *Nordic Hydrology*, vol. 38, no. 4/5, p. 451, 2007.

[19] T. Beravs, J. Podobnik, and M. Munih, "Three-axial accelerometer calibration using kalman filter covariance matrix for online estimation of optimal sensor orientation," *Instrumentation and Measurement, IEEE Transactions on*, vol. 61, pp. 2501 – 2511, Sept 2012.

[20] P. Hansen, H. Alismail, P. Rander, and B. Browning, "Online continuous stereo extrinsic parameter estimation," in *Computer Vision and Pattern Recognition (CVPR), 2012 IEEE Conference on*, pp. 1059 – 1066, June 2012.

[21] B. Berger, *Modeling and Optimization for Stationary Base Engine Calibration*. PhD thesis, Technical University of Munich, 2012.

[22] P. Van Overloop and R. Van Nooijen, *Diktaat CT5490: Operational Water Management*. Delft University of Technology, 2008.

[23] B. M. Donckels, D. J. De Pauw, P. A. Vanrolleghem, and B. D. Baets, "Performance assessment of the anticipatory approach to optimal experimental design for model discrimination," *Chemometrics and Intelligent Laboratory Systems*, vol. 110, no. 1, pp. 20 – 31, 2012.

[24] B. M. R. Donckels, D. J. W. De Pauw, P. A. Vanrolleghem, and B. De Baets, "A kernel-based method to determine optimal sampling times for the simultaneous estimation of the parameters of rival mathematical models," *Journal of Computational Chemistry*, pp. 2064–2077, 2009.

[25] B. M. R. Donckels, D. J. W. De Pauw, P. A. Vanrolleghem, and B. De Baets, "An ideal point method for the design of compromise experiments to simultaneously estimate the parameters of rival mathematical models," *Chemical Engineering Science*, vol. 65, no. 5, pp. 1705 – 1719, 2010.

[26] B. Dekens, "Gradient-based hybrid model predictive control using time instant optimization for dutch regional water systems," Master's thesis, Delft University of Technology, 2013.

[27] W. Luxemburg and M. Coenders, *Hydrological measurements*. Delft University of Technology, 2010.

[28] S. P. Boyd and L. Vandenberghe, *Convex Optimization*. Cambridge University Press, 2004.

[29] L. SparkNotes, "Calculus bc: Applications of the derivative." http://www.sparknotes.com/math/calcbc1/applicationsofthederivative/section2.rhtml, 2014. Accessed October 30, 2014.

[30] S. J. Qin and T. A. Badgwell, "An overview of nonlinear model predictive control applications," in *Nonlinear Predictive Control*, pp. 369 – 392, Verlag, 2000.

[31] R. Womersley, "Local and global optimization - formulation, methods and applications." http://web.maths.unsw.edu.au/~rsw/, 2008. Accessed October 30, 2014.

[32] OpenDA, "The openda data-assimilation toolbox." http://www.openda.org/, 2014. Accessed October 30, 2014.

[33] A. J. Abebe and D. P. Solomatine, "Application of global optimization to the design of pipe networks," in *Proc. Int. Conf. Hydroinformatics-98*, pp. 989 – 996, 1998.

[34] Q. Duan, S. Sorooshian, and V. K. Gupta, "Optimal use of the sce-ua global optimization method for calibrating watershed models," *Journal of Hydrology*, vol. 158, no. 3 - 4, pp. 265 – 284, 1994.

[35] H. Meshkat Razavi and H. Shariatmadar, "Optimum parameters for tuned mass damper using shuffled complex evolution (sce) algorithm," *Civil Engineering Infrastructures Journal*, pp. 1–18, April 2014.

[36] S. K. P. Cibin, R. and I. Chaubey, "Sensitivity and identifiability of stream flow generation parameters of the swat model," *Hydrol. Process.*, vol. 24, pp. 1133 – 1148.

[37] T. Olsthoorn, *Groundwater Modelling: Calibration and the use of Spreadsheets*. PhD thesis, Delft University of Technology, 1998.

[38] D. Solomatine, "Experiences in using evolutionary and non-evolutionary optimization methods in models calibration," in *Proc. of the iEMSs 3rd Biennial Meeting:*.

[39] Deltares, *SOBEK 3 - Technical reference manual*. Deltares, 2014.

[40] KfW and GIZ, "Water-spreading weirs for the development of degraded dry river valleys - experience from the sahel," tech. rep., German Federal Ministry for Economic Cooperation and Development (BMZ), 2013.

[41] J. Lewin, *Hydraulic gates and valves: in free surface flow and submerged outlets*. Thomas Telford Publishing, 2nd edition, 2001.

[42] P. Malaterre and J.-P. Baume, "Modeling and regulation of irrigation canals: existing applications and ongoing researches," in *Systems, Man, and Cybernetics, 1998. 1998 IEEE International Conference on*, vol. 4, pp. 3850 – 3855, Oct 1998.

[43] G. Stelling and S. Duinmeijer, "A staggered conservative scheme for every froude number in rapidly varied shallow water flows," *Internation Journal Numerical Method in Fluids*, vol. 43, pp. 1329 – 1354, 2003.

[44] G. Stelling and A. Verwey, *Numerical flood simulation*. Encyclopedia of Hydrological Sciences, 2006.

[45] P. Warmerdam and J. Kole, "Modelling rainfall-runoff processes in the hupselse beek research basin," pp. 155 – 161.

[46] C. Brauer, *Modelling rainfall-runoff processes in lowland catchments*. PhD thesis, Delft University of Technology, 2014.

[47] R. Velner, J. Moorman, P. Warmerdam, and J. Kole, "Neerslagafvoerrelaties solide basis voor keuzen in het hoogwaterbehee.," *H2O*, 2008.

[48] R. Velner, B. Van der Wal, and H. De Jonge, "Ontwikkeling van het gebiedsdekkende hoogwatermodel aa en maas (gdhm-am)," tech. rep., Royal Haskoning, 2008.

[49] C. Brauer, P. Kloosterman, R. Teuling, and R. Uijlenhoet, "Simulatie van de overstroming van de hupselse beek met het wageningen model." http://bigfiles.nhv.nu/files/9_brauer_e.a._wur.pdf, 2012. Accessed October 30, 2014.

[50] C. Van Velzen, *A Generic Software Framework for Data Assimilation and Model Calibration*. PhD thesis, Delft University of Technology, 2010.

[51] Vortech, "Vortech." http://www.vortech.nl/, 2014. Accessed October 30, 2014.

[52] J. Post, "Combining field observations and hydrodynamic models in urban drainage," Master's thesis, Delft University of Technology, 2012.

[53] K. N. M. Instituut, "Koninklijk nederlands meteorologisch instituut." http://knmi.nl/, 2010. Accessed October 30, 2014.

[54] B. D. Stem, "Honderden schademeldingen wateroverlast." http://www.bndestem.nl/regio/brabant/honderden-schademeldingen-wateroverlast-1.516349, 2010. Accessed October 30, 2014.

[55] B. Dagblad, "Honderden schademeldingen wateroverlast." http://www.bd.nl/regio/tilburg-en-omgeving/tilburg/honderden-schademeldingen-wateroverlast-1.3366287, 2010. Accessed October 30, 2014.

[56] I. close up, "Aanhoudende regen." http://in-close-up.blogspot.nl/2010_11_01_archive.html, 2010. Accessed October 30, 2014.

[57] Brandweerfotograaf, "Waalwijk/tilburg 13 - 10 - 2010 - waterover-last." http://www.brandweerfotograaf.nl/jt/index.php/uitrukken-2010/389-waalwijk-tilburg-13-11-2010-wateroverlast, 2010. Accessed October 30, 2014.

[58] M. Ertsen, *Irrigation and Drainage*, 2012.

[59] W. L. Price, "Global optimization algorithms for a cad workstation," *J. Optim. Theory Appl.*, vol. 55, pp. 133 – 146, 1987.

[60] M. R. Nelder, J.A., "A simplex method for function minimization," *Comput. J.*, vol. 7, pp. 308 – 313, 1965.

[61] J. H. Holland, "Adaptation in natural and artificial system," *University of Michigan Press*, 1975.

Glossary

List of Acronyms

API	application programming interface
CCE	Competitive Complex Evolution
CSV	Comma-Separated Values
DSS	Decision Support System
DuD	Doesn't Use Derivatives
MPC	Model Predictive Control
OPE	On-line Parameter Estimation
RR	rainfall-runoff
SCE	Shuffled Complex Evolution
SV	De Saint-Venant
TPL	template
TU Delft	Delft University of Technology
W+B	Witteveen+Bos
XML	Extensible Markup Language

List of Definitions

bias	This is considered as a measure for the existence of systematic errors, [9],[15]. The bias is determined by the sum of the variation and the estimation of the errors in the predicted states over a certain time window.

distinctness This refers to the level of how distinctive the shape of the optimisation problem is defined. Usually, an optimisation problem becomes less distinct, when additional parameters are introduced. Eventually, a decrease in distinctness of the optimisation problem can result in longer computation times.

effectiveness This refers to the rate at which the objective function is minimised, i.e. the rate of how accurate the parameters and states are predicted.

efficiency This refers to the computation time required by the OPE tool to obtain a solution that satisfies the stopping criteria.

identifiability This refers to the ability to estimate parameters in terms of model response, [9],[4].

on-line system This refers to a (mathematical) system that simulates and predicts processes in real-time.

robustness This refers to the number of successful approaches of the global minimum, i.e the number of successful approaches of the actual parameter values.

twin experiment This refers to experiments where observations are created artificially by using the model itself. In other words, the outcome of model simulations serves as observational data.

white noise This refers to the noise that is assigned to the observational data. White noise is a random signal with a constant power spectral density, [16]. Noise is presented as a random signal that is uniform distributed in a prescribed interval. The colour of the noise, i.e. white, means that the distribution of the power of the noise is equal for each frequency of occurrence, i.e. the power of the noise is the same regardless of the rate of the observed state.